

# **The Dependence of the Conversion Performance of Different Types of Diesel Catalysts as a Function of Operation Properties**

Vom Fachbereich Chemie  
der Universität Hannover  
zur Erlangung des Grades

Doktor der Naturwissenschaften  
- Dr. rer. nat. -

genehmigte Dissertation

von

Dipl.-Chem. Jörgen Jochheim  
geboren am 21. Juli 1968 in Göteborg, Schweden

1998

Referent: Prof. Dr. D. Hesse

Koreferent: Prof. Dr. G. Rotzoll

Tag der Promotion: 4. Februar 1998

This thesis was written from April 1995 until January 1998 under the supervision of Prof. Dr. D. Hesse whom I would like to thank for giving me the unique opportunity to write a Doctor-Thesis in three different countries on an industry-related subject.

I would like to thank Prof. Dr. G. Rotzoll for being co-reviewer.

I gratefully acknowledge my sponsor

**Johnson Matthey, CSD**

in particular I return thanks to Martyn Twigg, Pelham Hawker, Tony Wilkins, Bob Brisley, and Klaus Schneider of Johnson Matthey CSD and Andy Walker, Steve Bennett, and Paul Millington of Johnson Matthey Technology Centre.

Very special thanks are due to the Johnson Matthey employees at Göteborg and Royston for always making me feel welcome, a little bit Swedish ☺, and all their support: Allan, Anders, Ari, Börje, Karin, Lasse, Lennart, Niels, Pär, Ronny, Steffan (all Sweden: Tack så mycket), Ann, Beverly (at Royston, both especially for their support), Estelle, Miles (at Royston, for a good time in the social club), Jim (at Royston, for all his work during our SAE Paper as well as a good time in the social club and in Cambridge).

This thesis could not have been done without two people:

**Anna-Lena Lindahl (Johnson Matthey, Göteborg)**

**Paul Phillips (Johnson Matthey, Royston)**

Anna-Lena showed me how to control the SCAT reactor, assisted me in case I lost this control, taught me a lot about Sweden and the Swedes, and it were very enjoyable days working with her.

Paul was my contact in Royston. He showed me how to prepare catalysts, answered a lot of my questions, coordinated my stays in England and Sweden, and proof-read the whole thesis, an extra-work for which I am particularly grateful. Certainly working with Paul was as enjoyable as with Anna-Lena.

I would also like to thank Bull Smedler for his support during the initial phase of the project.

Tack så mycket to my sister Sonja Jochheim and her Family for giving me accommodation in Sweden.

Dedicated to Claudia  
- Love knows no distance -

## **Abstract**

Jürgen Jochheim

### **Die Abhängigkeit der Umsatzleistung von verschiedenen Arten von Dieselkatalysatoren als Funktion der Betriebsbedingungen**

In dieser Arbeit wird die Aktivität trägergestützter Edelmetallkatalysatoren für die Nachbehandlung von Dieselabgasen von Personenkraftwagen untersucht. Dies geschieht anhand von Bohrkernproben, die von Wabenkörpern mit unterschiedlichen, katalytisch-aktiven Beschichtungen stammen. Die Bohrkernproben werden mit einem Modellgasreaktor unter Bedingungen untersucht, die denen im realen Dieselabgas nachempfunden sind. Des Weiteren werden die Proben durch BET- und CO-Chemisorptionsmethoden charakterisiert.

Besonderes Gewicht wird bei den Untersuchungen auf den Stickoxidumsatz des Katalysators gelegt.

Es wird festgestellt, daß ein gewisser Umsatz von Stickoxiden und Kohlenwasserstoffen auch auf Katalysatorproben stattfindet, die lediglich mit einem Aluminium- oder Zeolit- Washcoat beschichtet sind und keine Edelmetallkomponente besitzen.

Durch die gezielte Variation von den Eigenschaften Pt Dispersion, Pt Beladung, Washcoat-Beladung und Oberfläche des verwendeten Washcoats eines Pt/Al<sub>2</sub>O<sub>3</sub> Katalysators wird ermittelt, daß ein hoher Umsatz von Stickoxiden unter dieselähnlichen Bedingungen vor allem durch eine hohe Washcoat-Beladung des Katalysators gefördert wird. Darüber hinaus fördert eine hohe Washcoat-Beladung bei gleichbleibender Pt Beladung und gleichbleibender Pt Dispersion die Stabilität eines Pt/Al<sub>2</sub>O<sub>3</sub> Katalysators gegenüber hydrothermalen Alterungen.

Der Einfluß unterschiedlicher Washcoatadditive auf die Umsatzleistung eines Pt/Al<sub>2</sub>O<sub>3</sub> Katalysators und die Alterungsbeständigkeit eines solchen Katalysators wird untersucht. Die Leistung eines Pt/Al<sub>2</sub>O<sub>3</sub> Katalysators hinsichtlich des Stickoxidumsatzes läßt sich insbesondere durch die Zugabe von BaO und geringen Mengen CeO<sub>2</sub> erhöhen.

Es stellt sich heraus, daß der Austausch von Pt durch Ir auf einem Al<sub>2</sub>O<sub>3</sub> Träger zu Katalysatoren führt, die für alle untersuchten Abgaskomponenten sehr schlechte Umsatzleistungen zeigen. Dagegen führt die Addition von Ir zu einem Pt/Al<sub>2</sub>O<sub>3</sub> Katalysator zu einer Steigerung des Kohlenwasserstoff- und Kohlenmonoxidumsatzes dieses Katalysators.

Ein Mechanismus für die Reduktion von Stickoxiden über Pt/Al<sub>2</sub>O<sub>3</sub> Katalysatoren wird aufgestellt, der erklärt, daß bei niedrigen Temperaturen der Katalysator mit einer Schicht aus Kohlenwasserstoffen bedeckt ist, die durch die Oxidation mit Sauerstoff entfernt werden muß, bevor die Reduktion von Stickoxiden stattfinden kann.

Automobilkatalysator, Diesel, Stickoxide

## **Abstract**

Jürgen Jochheim

### **The Dependence of the Conversion Performance of Different Types of Diesel Catalysts as a Function of Operation Properties**

This thesis investigates the activity of supported precious metal catalysts for the aftertreatment of Diesel exhaust from passenger cars. The tested sample cores originate from full-seized monoliths with different, catalytically active layers. The cores are examined in a model gas test reactor under Diesel-like conditions. Further the samples are characterised by BET and CO chemisorption methods. Particular attention is focused on the catalyst's conversion of nitrogen oxides.

It is discovered that samples only carrying alumina- or zeolite washcoat and no precious metal show a certain conversion of nitrogen oxides and hydrocarbons.

By controlled variation of the properties Pt dispersion, Pt load, washcoat load and surface of the washcoat used it is noticed that a high conversion of nitrogen oxides under Diesel-like conditions is achieved by using a catalyst with a high washcoat load. Additionally to this, a high washcoat load at constant Pt load and Pt dispersion enhances the stability of the catalyst against hydrothermal ageing.

The influence of different washcoat additives with regard to the conversion performance of a Pt/Al<sub>2</sub>O<sub>3</sub> and its stability against ageing is investigated. It is possible to increase the performance of a Pt/Al<sub>2</sub>O<sub>3</sub> catalyst particularly by adding BaO and limited amounts of CeO<sub>2</sub>.

The exchange of Pt by Ir on an Al<sub>2</sub>O<sub>3</sub> washcoat results in a catalyst that presents very poor conversion performance for all exhaust gas components examined. On the other hand the addition of Ir to a Pt/Al<sub>2</sub>O<sub>3</sub> catalyst increases the conversion of hydrocarbons and CO by a catalyst.

A mechanism for the reduction of nitrogen oxides by Pt/Al<sub>2</sub>O<sub>3</sub> is presented which proposes that the catalyst is covered by a layer of hydrocarbon that has to be removed by oxygen oxidation before reduction of nitrogen oxides can take place.

Catalytic Converter, Diesel, Nitrogen Oxides

Ich erkläre hiermit an Eides Statt, daß ich die vorliegende Dissertation selbständig verfaßt und die benutzten Hilfsmittel sowie zur Hilfeleistung herangezogenen Institutionen vollständig angegeben habe.

<b>1. Introduction</b>	<b>1</b>
<b>2. Background</b>	<b>4</b>
<b>2.1 Introduction</b>	<b>4</b>
<b>2.2 The Formation of Exhaust Gas Components</b>	<b>6</b>
2.2.1 Combustion Processes inside Diesel Engines	6
2.2.2 Formation of CO <sub>2</sub> and H <sub>2</sub> O	7
2.2.3 Formation of CO	8
2.2.4 Formation of HC	8
2.2.5 Formation of Soot Particles	8
2.2.6 Formation of NO <sub>x</sub>	9
2.2.7 Effect of Operating Conditions on the Formation of Exhaust Gas Components	10
2.2.8 Composition of Diesel Exhaust	10
<b>2.3 Test Procedures</b>	<b>11</b>
2.3.1 Legislative Emission Limits	11
2.3.2 Constant Volume Sampling (CVS)	12
2.3.3 Engine Bench (EB) Testing	14
<b>2.4 Pollutant Control Through Engine Modification</b>	<b>14</b>
2.4.1 The Effect of the Combustion Process	15
2.4.2 The Effect of Injection Timing	15
2.4.3 Exhaust Gas Recirculation (EGR)	16
<b>2.5 Pollutant Control Through Catalysis</b>	<b>16</b>
2.5.1 General Aspects About Catalysis	16
2.5.2 Particle Filters	24
2.5.3 NO <sub>x</sub> Control of Diesel Exhaust in Stationary Systems	25
2.5.4 NO <sub>x</sub> Control of Diesel Exhaust in Vehicles	27
2.5.4.1 Methods using Monoliths	27
2.5.4.1.1 Zeolites	27
2.5.4.1.1.1 Cu/ZSM-5	30
2.5.4.1.1.2 The NO <sub>x</sub> Reduction Mechanism on Cu/ZSM-5	33
2.5.4.1.1.3 Other Metals/Zeolites	37
2.5.4.1.2 Alumina (Al <sub>2</sub> O <sub>3</sub> )	38
2.5.4.1.2.1 Chemical Aspects of Alumina	38
2.5.4.1.2.2 NO <sub>x</sub> Reduction with Alumina	39
2.5.4.1.2.3 Pt/Al <sub>2</sub> O <sub>3</sub>	42
2.5.4.1.2.4 The NO <sub>x</sub> Reduction Mechanism on Pt/Al <sub>2</sub> O <sub>3</sub>	43
2.5.4.1.2.5 Factors Influencing NO <sub>x</sub> Reduction on Pt/Al <sub>2</sub> O <sub>3</sub>	53
2.5.4.1.2.6 Other Metal Ions/Al <sub>2</sub> O <sub>3</sub>	57
2.5.4.1.3 Other Oxides	57
2.5.4.1.4 Perovskites	58
2.5.4.2 Methods using Adsorption	59
2.5.4.3 Other Methods	56



<b>3. Experimental</b>	<b>61</b>
<b>3.1 Catalyst Samples</b>	<b>61</b>
3.1.1 Preparation	61
<b>3.2 Determination of Characteristic Sample Parameters</b>	<b>61</b>
<b>3.3 Synthetic Catalytic Activity Test (SCAT)</b>	<b>62</b>
3.3.1 Standard Light-Off Test (LOT)	64
3.3.2 Temperature Ramps on SCAT Rig	65
3.3.3 Experiments at Constant Temperatures	65
<b>3.4 Temperature Programmed Desorption</b>	<b>66</b>
<b>3.5 Isotope Transient Kinetics (ITK)</b>	<b>67</b>
<b>3.5 Transmission Electron Microscopy (TEM)</b>	<b>69</b>
<b>4. Results and Discussion</b>	<b>70</b>
<b>4.1 The Influence of the Washcoat on the Conversion Performance</b>	<b>70</b>
4.1.1 Al <sub>2</sub> O <sub>3</sub>	70
4.1.1.1 Characterisation of an Al <sub>2</sub> O <sub>3</sub> Washcoat by BET Measurements	70
4.1.1.2 LOTs with Al <sub>2</sub> O <sub>3</sub> Washcoat Only Monoliths	71
4.1.1.3 Temperature Ramps with Al <sub>2</sub> O <sub>3</sub> Washcoat Only Monoliths	79
4.1.1.4 Examination of Al <sub>2</sub> O <sub>3</sub> Washcoat Only Monoliths with TEM and EDX after the LOTs	82
4.1.2 Zeolites	83
4.1.2.1 Characterisation of a Zeolite Containing Washcoat by BET Measurements	83
4.1.2.2 LOTs with Zeolite Containing Washcoat Only Monoliths	85
4.1.2.3 Temperature Ramps with Zeolite Containing Washcoat Only Monoliths	90
4.1.3 Summary	93
<b>4.2 Pt/Al<sub>2</sub>O<sub>3</sub> Catalysts</b>	<b>95</b>
4.2.1 Characterisation of the Pt/Al <sub>2</sub> O <sub>3</sub> Samples by BET and COC Measurements	95
4.2.2 LOT Performance of Pt/Al <sub>2</sub> O <sub>3</sub> Catalysts	99
4.2.2.1 The Influence of Pt Loading	103
4.2.2.2 The Influence of Pt Dispersion	106
4.2.2.3 Examination of Turnover Frequency and Number of Active Sites for CO Oxidation by ITK	107
4.2.2.4 The Influence of the Washcoat Load	109
4.2.2.5 The Influence of the Washcoat Surface Area	110
4.2.3 Summary	113
<b>4.3 Variations of the Pt Support</b>	<b>115</b>
4.3.1 Characterisation of the Samples by BET and COC Measurements	115
4.3.2 LOT Performance of Pt/Al <sub>2</sub> O <sub>3</sub> Catalysts with Additives	117
4.3.3 Temperature Ramps and TPDs with Pt/Al <sub>2</sub> O <sub>3</sub> Catalysts with Additives	122
4.3.4 LOT Performance of Pt/Zeolite Catalysts with Additives	127
4.3.5 Temperature Ramps and TPDs with Pt/Zeolite Catalysts with Additives	130
4.3.6 Summary	134

<b>4. 4 The Influence of Ageing</b>	<b>136</b>
4. 4. 1 <i>The Influence of Ageing on Pt/Al<sub>2</sub>O<sub>3</sub> Samples without Additives</i>	137
4. 4. 1. 1 <i>Characterisation of the Pt/Al<sub>2</sub>O<sub>3</sub> Samples by BET and COC Measurements</i>	137
4. 4. 1. 2 <i>LOT Performance of Aged Pt/Al<sub>2</sub>O<sub>3</sub> Catalysts</i>	139
4. 4. 2 <i>The Influence of Ageing on Pt/Al<sub>2</sub>O<sub>3</sub> Samples with Additives</i>	142
4. 4. 2. 1 <i>Characterisation of the Pt/Al<sub>2</sub>O<sub>3</sub> Samples with Additives by BET and COC Measurements</i>	142
4. 4. 2. 2 <i>LOT Performance of Aged Pt/Al<sub>2</sub>O<sub>3</sub> Catalysts with Additives</i>	144
4. 4. 3 <i>Summary</i>	146
<b>4. 5 Iridium as an Alternative Metal for Pt on Al<sub>2</sub>O<sub>3</sub></b>	<b>147</b>
4. 5. 1 <i>Characterisation of the Ir/Al<sub>2</sub>O<sub>3</sub> Catalyst by BET Measurements</i>	147
4. 5. 2 <i>LOT Performance of Ir/Al<sub>2</sub>O<sub>3</sub> Catalysts</i>	149
4. 5. 2. 1 <i>HC Conversion</i>	149
4. 5. 2. 2 <i>CO Conversion</i>	151
4. 5. 2. 3 <i>NO<sub>x</sub> Conversion</i>	153
4. 5. 3 <i>Summary</i>	156
<b>4. 6 The Influence of the Gasmix</b>	<b>157</b>
4. 6. 1 <i>The Efficiency of CO as Reductant for NO<sub>x</sub></i>	157
4. 6. 2 <i>The Formation of CO during LOTs</i>	159
4. 6. 3 <i>The Influence of the HC:NO<sub>x</sub> Ratio</i>	161
4. 6. 4 <i>The Influence of the Type of HC</i>	163
4. 6. 5 <i>The Influence of the Type of NO<sub>x</sub></i>	168
4. 6. 6 <i>Concentration Variations</i>	170
4. 6. 6. 1 <i>Variation of HC Concentration</i>	170
4. 6. 6. 2 <i>Variation of O<sub>2</sub> Concentration</i>	171
4. 6. 6. 3 <i>Variation of CO Concentration</i>	173
4. 6. 6. 4 <i>Variation of NO<sub>x</sub> Concentration</i>	174
4. 6. 7 <i>Summary</i>	176
<b>4. 7 Advanced Formulation Catalysts</b>	<b>178</b>
<b>5. Concluding Remarks</b>	<b>180</b>
<b>6. Summary</b>	<b>182</b>
<b>Appendix</b>	<b>187</b>
<i>Catalyst Data</i>	187
<i>CV</i>	189
<i>Literature</i>	190

## Abbreviations Sorted Alphabetically

A/F	Air/Fuel
APD	Average Pore Diameter
BSA	BET Surface Area
$c_{in}$	Concentration at the inlet of the reactor
CO	Carbon Monoxide
COC	CO Chemisorption
$c_{out}$	Concentration at the outlet of the reactor
CRT	Continuous Regeneration Trap
CVS	Constant Volume Sampling
DI	Direct Injection
$D_M$	Metal Dispersion
$\Delta_R G^0$	Free Gibbs Enthalpy of Reaction at STP
$\Delta_f H^0$	Enthalpy of Formation under STP
$\Delta_R H^0$	Enthalpy of Reaction at STP
$E_A$	Activation Energy Without Catalyst
$E_A^C$	Activation Energy With Catalyst
ECE	Economic Commission for Europe
EDX	Energy Dispersive X-Ray
ESR	Electron Spin Resonance
EU	European Union
EUDC	Extra Urban Driving Cycle
EXAFS	Electronic X-Ray Adsorption Fourier Spectroscopy
FTP	Federal Test Procedure
HC	Hydrocarbon
HTA	High Temperature Aged
IDI	Indirect Injection
ITK	Isotope Transient Kinetics
JM	Johnson Matthey
k	Rate Constant
$K^T$	Equilibrium Constant at the Temperature T
$\lambda$	Normalised Air/Fuel Ratio
LOT	Light Off Test
$m_A$	Actual Amount of Air per Kilogram of Fuel
$m_{A,St}$	Amount Necessary for Stoichiometric Combustion
MSA	Metal Surface Area
MVEuro2	Motor Vehicle Driving Cycle "Euro2"
$NO_2^{max}$	Maximum $NO_2$ Formation
$NO^{max}$	Maximum NO Conversion
$NO_x^{max}$	Maximum $NO_x$ Conversion

NSCR	Non-Selective Catalytic Reduction
OBD	On Board Diagnostics
p	Partial Pressure
PAH	Polycyclic Aromatic Hydrocarbons
$P_c$	Performance Factor for a Catalyst
PGM	Precious Group Metal
PM	Particle Material
PPS	Platinum Particle Size (Radius)
PSD	Pore Size Distribution
$\theta$	Surface Coverage
$r_{PtP}$	Radius of Platinum Particle
S	Adsorption Site on Surface
SCAT	Synthetic Catalytic Activity Test
SCR	Selective Catalytic Reduction
SFI	Secondary Fuel Injection
SNCR	Selective Non Catalytic Reduction
SO <sub>2</sub> (250)	Conversion of SO <sub>2</sub> at 250°C
SPPV	Single Point Pore Volume
STP	Standard Temperature and Pressure
SV	Space Velocity
T(NO <sup>max</sup> )	Temperature at Maximum NO Conversion
T(NO <sub>x</sub> <sup>max</sup> )	Temperature at Maximum NO <sub>x</sub> Conversion
TAP	Temporary Analysis of Products
TCO(100)	Temperature at 100% CO Conversion
TCO(50)	Temperature at 50% CO Conversion
TCO(80)	Temperature at 80% CO Conversion
TDI	Turbo Direct Injection
THC(100)	Temperature at 100% HC Conversion
THC(50)	Temperature at 50% HC Conversion
T <sub>i</sub>	Inlet Temperature
T <sub>o</sub>	Oven Temperature
TPD	Temperature Programmed Desorption
TWC	Three Way Catalyst
U	Conversion
v	reaction rate
VOF	Volatile Organic Fraction
W(NO <sub>x</sub> )	Width of the NO <sub>x</sub> Conversion Window
Z	Zeolite Anion Site

## 1. Introduction

Throughout the world, environmental pollution is a growing concern in the public opinion. Besides energy and production industry, motor traffic is an important contributor to the pollution of earth's atmosphere<sup>1</sup>. Many countries therefore have enacted laws which require to keep the tailpipe emissions of motor vehicles below certain limits. The current state of the art for the reduction of petrol car tailpipe emissions is the closed loop three-way catalyst (TWC). In contrast to the petrol engine which operates at a stoichiometric air/fuel ratio, the Diesel engine operates at a much higher air/fuel ratio. This results in a significant higher concentration of oxygen in the exhaust gas of a Diesel engine. A high amount of oxygen quickly deactivates certain components on a TWC. Because of this deactivation, a TWC can not be used to reduce the emissions of a Diesel engine. The positive aspect of the high air/fuel ratio is a lower emission of hydrocarbons (HC) and carbon monoxide (CO) from a Diesel engine compared to a petrol engine.

Using an oxidation catalyst, the additional removal of HC and CO from the exhaust of a Diesel engine poses no problems: the high oxygen concentration in the Diesels exhaust gas favours oxidation reactions over the catalyst. The remaining challenges regarding the reduction of tailpipe emissions of Diesel cars are: (1) the removal of soot particles by either trapping or oxidation and (2) the removal of nitrogen oxides by reduction. The removal of nitrogen oxides is one of the major topics of this thesis. The NO<sub>x</sub> content in Diesel engine exhaust can be significantly reduced by engine modifications, e.g. by injection timing or by using exhaust gas recirculation (EGR). However, future NO<sub>x</sub> emission limits can hardly be met by means of an improved combustion process plus EGR alone. This is one of the reasons why world-wide research and development work is ongoing with respect to NO<sub>x</sub> reduction catalysts, also referred to as lean-NO<sub>x</sub> catalysts<sup>24</sup>. The challenge of this development is to achieve a NO<sub>x</sub> decomposition or reduction in the oxidising atmosphere of the Diesel exhaust gas. In principle there are two routes pursued:

1. Selective Catalytic Reduction (SCR)
2. Non-Selective (or Alternative Selective) Catalytic Reduction (NSCR or lean-NO<sub>x</sub>)

Using SCR, high conversion rates can be achieved by adding reducing agents such as ammonia or urea into the exhaust gas before the catalyst. For this method, it is absolutely necessary to maintain a careful stoichiometric control of the ammonia injected, in order to avoid a release of surplus  $\text{NH}_3$  while maintaining sufficient  $\text{NO}_x$  removal<sup>27 32</sup>. This, and the necessity to refill the  $\text{NH}_3$  tank makes the use of this technology especially for passenger car applications unfavourable.

Much attention is given therefore to the lean- $\text{NO}_x$  process using HCs as reducing agents. Three research fields are of particular interest<sup>24</sup>:

1. Choice, characterisation, and improvement of suitable catalyst materials. According to today's status, Cu exchanged zeolites are considered to offer the highest efficiency at high exhaust gas temperature (higher than  $350^\circ\text{C}$ ), where  $\text{NO}_x$  reduction for heavy-duty engines has the highest priority. Precious metal coated zeolites or precious metal coated base metal oxides can be used at low temperatures ( $180^\circ\text{C}$  -  $300^\circ\text{C}$ ) for light-duty passenger car application
2. Determination of the most efficient HC reductant to increase  $\text{NO}_x$  conversion rates. In order to avoid the need to refill the HC tank it is aspired to use Diesel fuel as the source for HC
3. Optimisation of the different parameters affecting the catalysts performance (e.g. space velocity (SV), working temperature range, type of reducing agent enrichment equipment) to enable and to maximise its use with vehicle engines, and their exhaust gas compositions.

A  $\text{Pt}/\text{Al}_2\text{O}_3$  catalyst has been reported<sup>4 9 13 14 19 24 34 56 67 70 72 75-91 93</sup> to be exceptionally active in the reduction of  $\text{NO}_x$  from Diesel exhaust. Additionally the  $\text{Pt}/\text{Al}_2\text{O}_3$  catalyst proved satisfying durability (in contrast to Cu/Zeolite catalysts). This thesis focuses therefore on the characterisation and improvement of precious metal coated base metal oxides or zeolites as catalysts for light-duty passenger car applications.

Practical investigations of automotive catalysts have to be carried out with real exhaust gas on both engine test benches and vehicle chassis dynamometers<sup>24</sup>. Such tests are expensive and therefore not suitable for catalytic activity screening purposes. The screening is performed under laboratory conditions with model gas test reactors. This test procedure is called Synthetic Catalytic Activity Test (SCAT). Most of the results obtained and discussed in this thesis were obtained by SCAT.

The thesis in hand intends to provide a deeper understanding of the processes occurring on a precious metal based Diesel catalyst. These processes are influenced by the composition and the properties of the catalyst. A variation of the composition or the properties of the catalyst will therefore result in a change of the catalyst's overall conversion performance. It is important to realise that an examination of NO<sub>x</sub> reduction can not be performed separately from an examination of HC oxidation because HC and NO<sub>x</sub> removal are closely related.

A thorough literature review on the subject of catalytic detoxification of Diesel exhaust gases, with the main emphasis on NO<sub>x</sub> removal, is given at the beginning of the thesis as background.

The practical part of the thesis starts with an examination of the conversion of Diesel exhaust gas components over pure alumina and zeolite washcoats without precious metal.

After that the influence of some properties of a Pt/Al<sub>2</sub>O<sub>3</sub> catalyst such as Pt dispersion, Pt load, washcoat load, and washcoat surface area on its conversion performance are described. It is discovered that these properties do not only effect the conversion performance but also the stability of the catalyst against ageing.

In the ensuing section, it is attempted to obtain an improvement of conversion performance and ageing stability by adding various components to the catalyst's washcoat. Some additives improve the NO<sub>x</sub> conversion but do not make the catalysts less susceptible against ageing.

The next section deals with the use of Ir instead of Pt on an Al<sub>2</sub>O<sub>3</sub> washcoat. It is shown that an Ir/Al<sub>2</sub>O<sub>3</sub> catalyst has a much poorer conversion performance than a Pt/Al<sub>2</sub>O<sub>3</sub> catalyst. However, adding Ir to the composition of a Pt/Al<sub>2</sub>O<sub>3</sub> catalyst improves the HC and CO conversion performance compared to a Pt/Al<sub>2</sub>O<sub>3</sub> only catalyst.

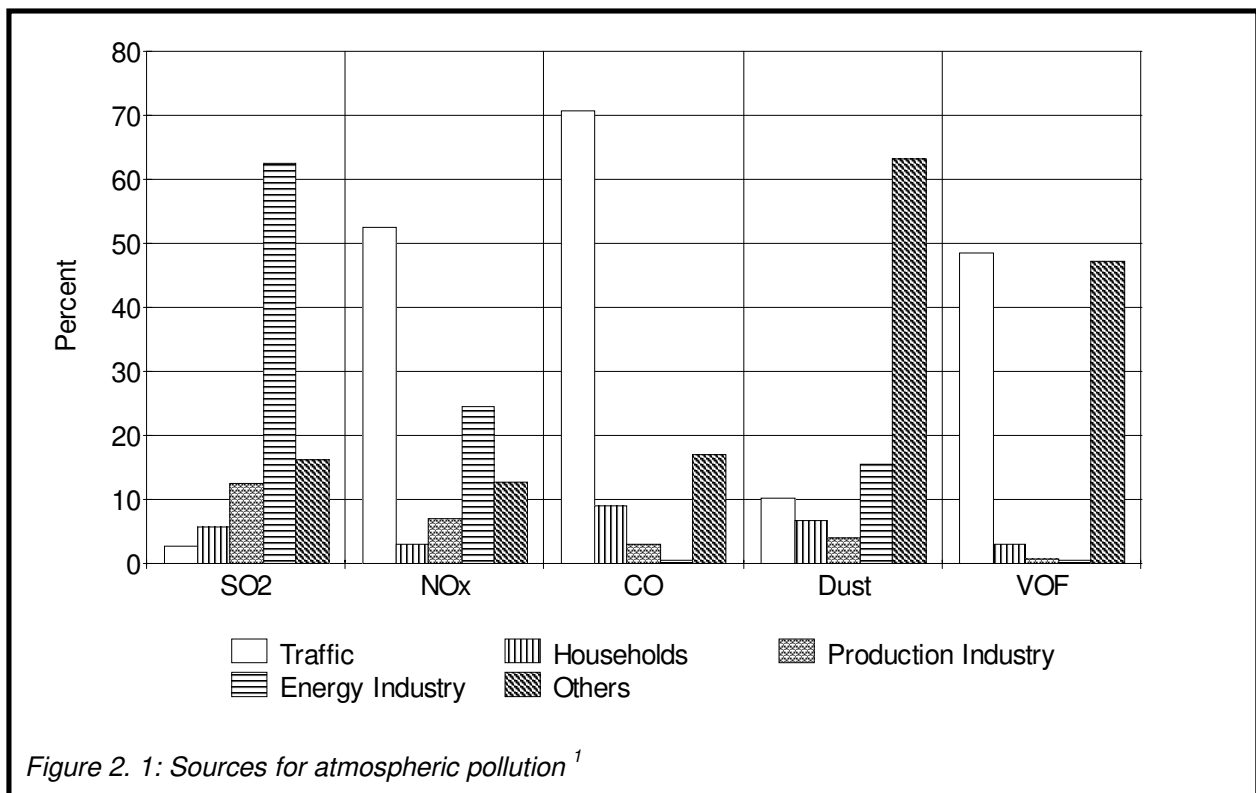
The following section examines the influence of the gas mix on the processes occurring on the Pt/Al<sub>2</sub>O<sub>3</sub> catalyst in more detail. It is concluded that several gas mix components can reduce the catalyst's activity by covering most of the catalyst's surface if their partial pressures are high.

The thesis ends with the presentation of a mechanism for the reduction of NO<sub>x</sub> under oxidising conditions over a Pt/Al<sub>2</sub>O<sub>3</sub> catalyst. The mechanism explains the positive influence of oxygen on the NO<sub>x</sub> conversion observed by many researchers.

## 2. Background

### 2. 1 Introduction

Environmental consciousness in Europe has grown strong in the last decade - so have the problems caused by pollution. The pollution of earth's atmosphere has caused three publicly well known problems: (1) the global warm-up by the so-called greenhouse effect predominantly caused by CO<sub>2</sub>, (2) holes in the ozone layer caused by radicals or volatile compounds able to form such radicals through ultraviolet irradiation, and (3) ozone smog experienced during Summer in many major cities caused by nitrogen oxides. Figure 2. 1 gives an overview over the sources of atmospheric pollution.



As can be seen from Figure 2. 1, traffic is the major origin of NO<sub>x</sub>, CO, and volatile organic fraction (VOF) pollutants in our atmosphere. Since CO<sub>2</sub> is not directly toxic, it is not mentioned in the figure. Nevertheless, traffic is also the major source of CO<sub>2</sub> emitted by fossil fuel combustion. Most western countries as well as India and China



have enacted laws that limit the allowed maximum release of toxic compounds in exhaust gases of motor vehicles<sup>2</sup>.

It is important to differentiate between cars driven by petrol engines and cars driven by Diesel engines. Petrol engines are commonly used in passenger cars and light-duty vehicles. Diesel engines are dominating light and heavy duty applications<sup>3</sup>. In Europe, where several countries offer tax benefits on Diesel fuel, 20 - 25 % of all passenger cars are Diesel driven<sup>4</sup>. In the United States, where there is no fiscal benefit for Diesel, compression ignition engines are rarely used in passenger cars. The growing demand for vehicles with low fuel consumption has favoured the development of so called lean-burn (LB) engines. These engines do not operate at a petrol engine's stoichiometric, normalised air/fuel ratio of  $\lambda = 1$ , but with a much higher oxygen content resulting in  $\lambda > 1,2$ . The normalised air/fuel ratio ( $\lambda$ ) is defined by the actual amount of air per kilogram of fuel ( $m_A$ ) divided by the amount necessary for stoichiometric combustion ( $m_{a,St}$ ):

$$\lambda = \frac{m_A}{m_{A,St}}$$

*Equation 2. 1*

Diesel engines themselves operate at  $\lambda$  up to 2,2. LB and Diesel engines may therefore be combined in a group of engines operating at high air/fuel ratios.

This thesis will entirely discuss Diesel/LB related topics.

The superior fuel-economy and high thermal efficiency of Diesel engines compared to gasoline engines has received much attention, and with concomitant lower carbon dioxide (CO<sub>2</sub>) emissions presents an important ecological aspect<sup>5</sup>. The automobile industry in Europe has agreed to reduce the CO<sub>2</sub> emission of new vehicles to 120 g/km by the year 2005.

The introduction of TDI technology has made the Diesel more popular among customers preferring cars with high power output, while the consumer market for high-mileage vehicles is to be satisfied with the introduction of the so called "3-Liter-Vehicle". It currently seems that this latter vehicle type can only be realised by the use of either a LB or a Diesel engine<sup>6</sup>. Other advantages of the Diesel engine are its lower hydrocarbon (HC) and CO emissions compared to petrol engines. This is

caused by the high air/fuel ratio at which the Diesel operates. On the other hand, this high air/fuel ratio provokes an increased emission of nitrogen oxides, NO and NO<sub>2</sub>, referred to as NO<sub>x</sub>. Furthermore, Diesel engines emit soot particles (PM), polycyclic aromatic HC (PAH), and a volatile organic fraction (VOF). The emissions of NO<sub>x</sub> and PM represent challenges that still have the potential for improvement. Table 2. 1 summarises the pros and cons for Diesel vehicles.

Pro	Con
high fuel-economy	increased emission of NO <sub>x</sub>
high thermal efficiency	emission of PM, PAH, and VOF
low emission of CO	
low emission of HC	
fiscal benefits on Diesel fuel in the EU	

Table 2. 1: Pros and cons for Diesel vehicles

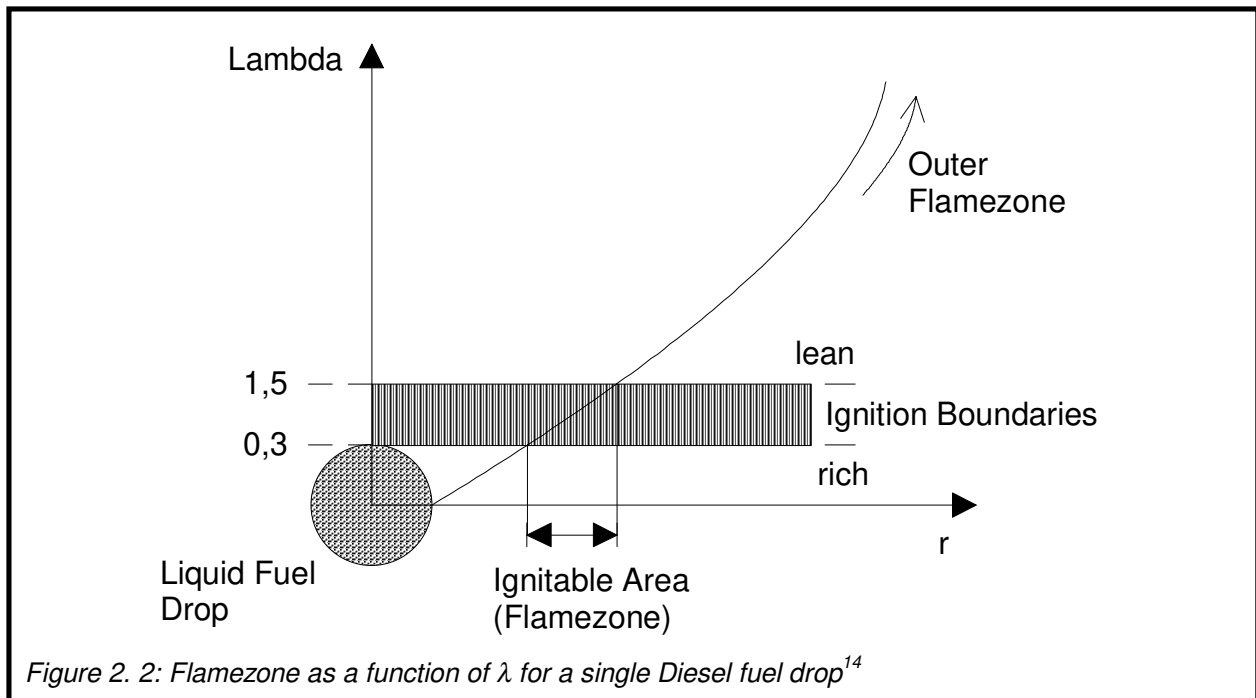
For the control of CO and HC emissions, promising results have been achieved with oxidation catalysts<sup>7 8 9</sup>. Most recently, Johnson Matthey has developed a system that is able to remove particle material from the exhaust of Diesel trucks and buses<sup>3</sup>. Other groups<sup>10 11</sup> have also developed methods which reduce the emission of PM. The major challenge remains the elimination of nitrogen oxides from the exhaust of Diesel/LB engines. This is especially difficult in passenger cars, where free space for methods that may be used on heavy-duty vehicles or stationary systems is not readily available.

## 2. 2 The Formation of Exhaust Gas Components

### 2. 2. 1 Combustion Processes inside Diesel Engines

In the Diesel engine, the temperature of the air inside the piston chamber rises during the compression phase up to 1300 K. This temperature is high enough to trigger self-ignition of the Diesel fuel injected towards the end of the compression phase. The air/fuel mixture is heterogeneous, in contrast to the homogeneous A/F mixture of petrol engines. This heterogeneous mixing implies that areas can be found within the air/Diesel mix with  $\lambda = \infty$  (pure air) and  $\lambda = 0$  (pure Diesel). After the

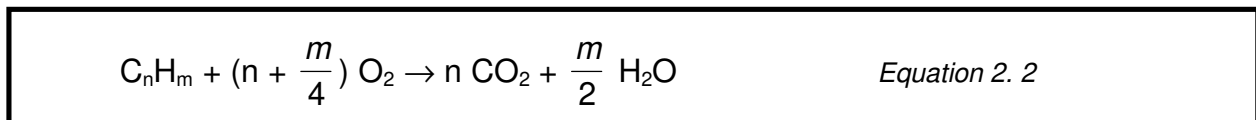
injection of the Diesel fuel into the piston chamber (DI Diesel), the mixture is prepared to become ignitable. This occurs by spraying, turbulences, evaporation, diffusion, and chemical reactions. The time between fuel injection and onset of combustion is called ignition delay. The ignition shall not begin before the compression phase has reached its maximum<sup>12</sup> and starts in those areas where the preparation of the mixture is completed first<sup>13</sup>. The boundaries in which ignition is possible are shown in Figure 2. 2.



Combustion proceeds in a flamezone surrounding the drop. Fuel is diffusing from the inner of the drop into this area, while oxygen is delivered from the outside.

### 2. 2. 2 Formation of $CO_2$ and $H_2O$

In any complete combustion process of fossil fuels,  $CO_2$  and  $H_2O$  are the products. The energy used to propel the vehicle is the enthalpy of formation  $\Delta H_f$ . The reaction equation can be written in a standard expression:



In case of propene ( $C_3H_6$ ) the standard enthalpy of formation is  $\Delta H_f^\ominus(C_3H_6)$ : - 1926,3  $\text{kJ mol}^{-1}$ <sup>15</sup>.

### *2. 2. 3 Formation of CO*

Formation of CO is caused by the incomplete oxidation of HC. This is most likely to occur in the rich area of the flame zone where the partial pressure of oxygen is low.

### *2. 2. 4 Formation of HC*

HC originate in the outer zones of the injection spray, where the fuel has thoroughly mixed with air to produce a non-ignitable mixture<sup>16</sup>.

### *2. 2. 5 Formation of Soot Particles*

The emission of soot particles is a consequence of the heterogeneous air/fuel mixture of Diesel engines. After the ignition of the injected fuel, local rich-mixture areas are heated up. Cracking and dehydration occurs in the centre of the injection stream where  $\lambda = 0$ . The radicals created can not be oxidised completely due to lack of oxygen, and ethyne ( $C_2H_2$ ) is formed. Rapidly, ethyne molecules combine to diethyne and polyethyne. Since polyethyne is formed during the end of the combustion phase, the temperature necessary for oxidation is only available for a little more time. Complete conversion to  $CO_2$  and  $H_2O$  is not possible under these conditions<sup>13</sup>. With ongoing ethyne addition the carbon/hydrogen ratio increases resulting in the formation of soot nuclei with a diameter between 0,001 and 0,01  $\mu m$ . These nuclei consist of parallel plates with a graphite like structure of the carbon atoms<sup>14</sup>. Several of these nuclei aggregate to primary particles which coagulate to grape-like soot agglomerates which in turn continue to grow on the walls of the exhaust system. The typical average diameter of such particles lies between 0,1 and 0,3  $\mu m$ .

Because of its high surface area, soot particles have a high adsorption capability. They adsorb the cancerous polycyclic aromatic HC and the volatile organic fraction. Another important contribution to the particle emission are sulphates. Sulphates are formed by oxidation of  $SO_2$  to  $SO_3$  and subsequent reaction with water to form  $H_2SO_4$  or with base metal oxides from engine wear to form sulphates, respectively. The influence of sulphur is discussed in more detail in chapter 2. 5. 4. 1. 2. 5. The sulphur compounds adsorb on the soot particles and thereby increase the weight of the PM. Since the limitation of the emission of particles from a Diesel engine is

based on the total weight, this weight contribution becomes an issue during legislative test procedures.

### 2. 2. 6 Formation of NO<sub>x</sub>

The amount of nitrogen oxides emitted from an engine depends largely on the engine design and the conditions during combustion. NO<sub>x</sub> concentrations typically vary between 500 and 1000 ppm for Diesel engines<sup>17</sup>. More than 95% of the nitrogen oxides produced in a Diesel engine is nitrogen monoxide, NO. Since the reaction of NO with oxygen to nitrogen dioxide, NO<sub>2</sub>, is exothermic<sup>18</sup>:



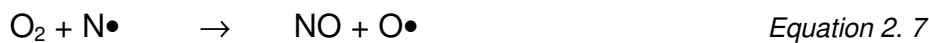
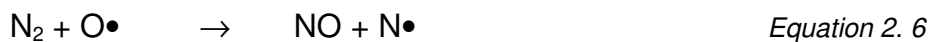
NO<sub>2</sub> is formed in the exhaust only after cooling below 923 K or through catalytic oxidation<sup>19</sup>.

There are two main causes for the formation of nitrogen oxides in Diesel engines<sup>13</sup>:

- thermal NO-formation
- direct NO-formation

#### *Thermic NO-Formation:*

At temperatures above 1573 K and oxygen excess, NO is forming from dissociated N<sub>2</sub> and O<sub>2</sub> molecules. Neuendorf<sup>13</sup> refers to a mechanism proposed by Zeldovic:



The main influence factors for these reactions are temperature, oxygen concentration from O<sub>2</sub> dissociation and residence time.

#### *Direct NO-Formation:*

At high temperatures, molecular N<sub>2</sub> reacts at the flame-front with fuel radicals (CH•).

NO is formed via cyanide compounds:



The compounds marked with \* then form nitrogen monoxide. The main influence factors are the concentration of oxygen from the combustion, and the A/F ratio.

From a health point of view, pure NO does not have any irritating effects. It reacts, however, with haemoglobin to form methaemoglobin, resulting in cyanosis and possible death.

NO<sub>2</sub> is an irritant gas. Inhalation of NO<sub>2</sub> causes pulmonary oedema which can result in death (lethal dose 200 ppm)<sup>20</sup>.

### 2. 2. 7 Effect of Operating Conditions on the Formation of Exhaust Gas Components

At cold start, all of the injected Diesel fuel is emitted if self-ignition is not achieved during the first compression. Part of the injected fuel condenses on the cold chamber walls. The fuel burns only partially at first ignition and appears as a hydrocarbon discharge with white or blue colouring in the exhaust gas.

Since the amount of Diesel fuel injected depends on engine speed, the emissions do not increase during acceleration. For exhaust gas turbo-charged Diesel engines, delayed response of the turbocharger can cause excess fuel to be injected into the cylinder. The result is strong soot emission (black smoke).

During deceleration no problems arise with Diesel engines regarding emissions<sup>16</sup>.

### 2. 2. 8 Composition of Diesel Exhaust

The engine-out values of the gases NO<sub>x</sub>, CO, HC, SO<sub>2</sub>, O<sub>2</sub>, CO<sub>2</sub>, and H<sub>2</sub>O vary from engine to engine. The values given in Table 2. 2 may be interpreted as a rough average. HC levels emitted from Diesel engines are not high enough to effect substantial lean NO<sub>x</sub> conversion. Therefore additional fuel needs to be presented to the catalyst to boost the HC/NO<sub>x</sub> ratio. This can be done either by adjusting the spark timing within the engine, or by directly injecting fuel into the exhaust pipe, upstream of the catalyst<sup>85</sup>. By low or high pressure injection of Diesel fuel ahead of the catalyst some of the injected fuel is converted to more reactive compounds by

cracking<sup>24</sup>. Low molecular weight cracked HCs can double NO<sub>x</sub> conversion efficiency compared to high molecular weight (=uncracked Diesel fuel) species even with a relatively low HC/NO<sub>x</sub> ratio.

Gas	Concentration [ppm]
NO <sub>x</sub>	500
O <sub>2</sub>	160000 (16 vol.-%)
CO <sub>2</sub>	40000 (4 vol.-%)
CO	350
Total HC (based on C <sub>1</sub> )	500
SO <sub>2</sub>	dependant on fuel: 350 ppm S in the fuel result in ~20 ppm in the exhaust gas <sup>22</sup>
H <sub>2</sub> O	60000 (6 vol.-%)

Table 2. 2: Average engine out values<sup>69</sup>

## 2. 3 Test Procedures

### 2. 3. 1 Legislative Emission Limits

Legislations limiting the amounts of CO, HC, NO<sub>x</sub>, and PM that may be released from a Diesel engine were introduced in the United States in 1985<sup>21</sup> and in Europe in 1993<sup>3</sup>. However, the fate of the Diesel/LB engine is currently partially dependent on the joint efforts of the automobile and catalyst industries to meet the stringent legislations coming into effect world-wide at the end of our century. Table 2. 3 summarises current and future European emission limits.

European passenger cars currently must meet emissions standards over the MVEuro2 driving cycle, Figure 2. 3. It reflects urban driving in Part 1, the Economic Commission for Europe (ECE) driving cycle, and high speed driving in Part 2, the extra-urban driving cycle (EUDC). Inlet catalyst temperatures typically peak around 230°C in Part 1 and 440°C in Part 2, depending on engine type and calibration<sup>4</sup>. Over the MVEuro2 drive cycle, SV range from 26000 to 36000 /h with a catalyst volume equivalent to engine displacement.

It shall be pointed out that other countries, such as the United States or Japan, have different driving cycles.

Law	Cycle Type	Implementation		Pollutant [g/km]			
		NTA	ANR	CO	HC	NO <sub>x</sub>	PM
91/441/EEC	EURO 1	current	current	TA:2,72 SL: 3,16	IDI/TA: 0,97 IDI/SL: 1,13 DI/TA:1,358 DI/SL: 1,582	TA: 0,14 SL: 0,18	
94/12/EC	EURO 2	01/01/96	01/01/97	IDI: 1,0 DI: 1,0	IDI: 0,7 DI: 0,9	IDI: 0,08 DI: 0,1	
proposal	EURO 3	year 2000	year 2000	0,64	HC+NO <sub>x</sub> : 0,56 NO <sub>x</sub> : 0,50	0,05	
proposal	EURO 4	year 2005	year 2005	0,50	HC+NO <sub>x</sub> : 0,30 NO <sub>x</sub> : 0,25	0,025	

NTA: New Type Approvals      ANR: All New Registrations  
TA: Type Approval              SL: Series Limit

Table 2. 3: Current and future European emission limits<sup>22</sup>

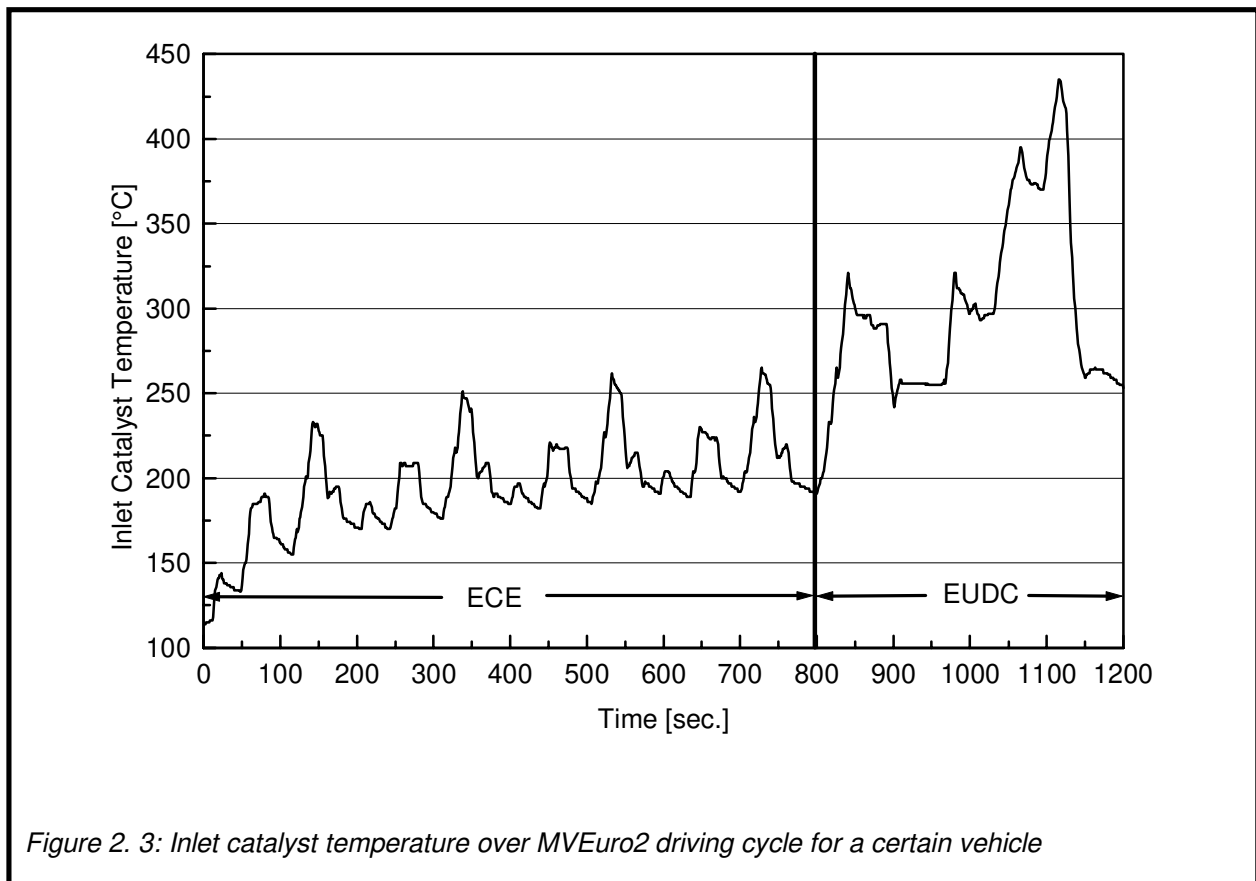


Figure 2. 3: Inlet catalyst temperature over MVEuro2 driving cycle for a certain vehicle

### 2. 3. 2 Constant Volume Sampling (CVS)

CVS is used to measure the emission per kilometre of the gas components in a vehicle's exhaust gas. In order to do so, the vehicle runs on a dynamometer as shown in Figure 2. 4.



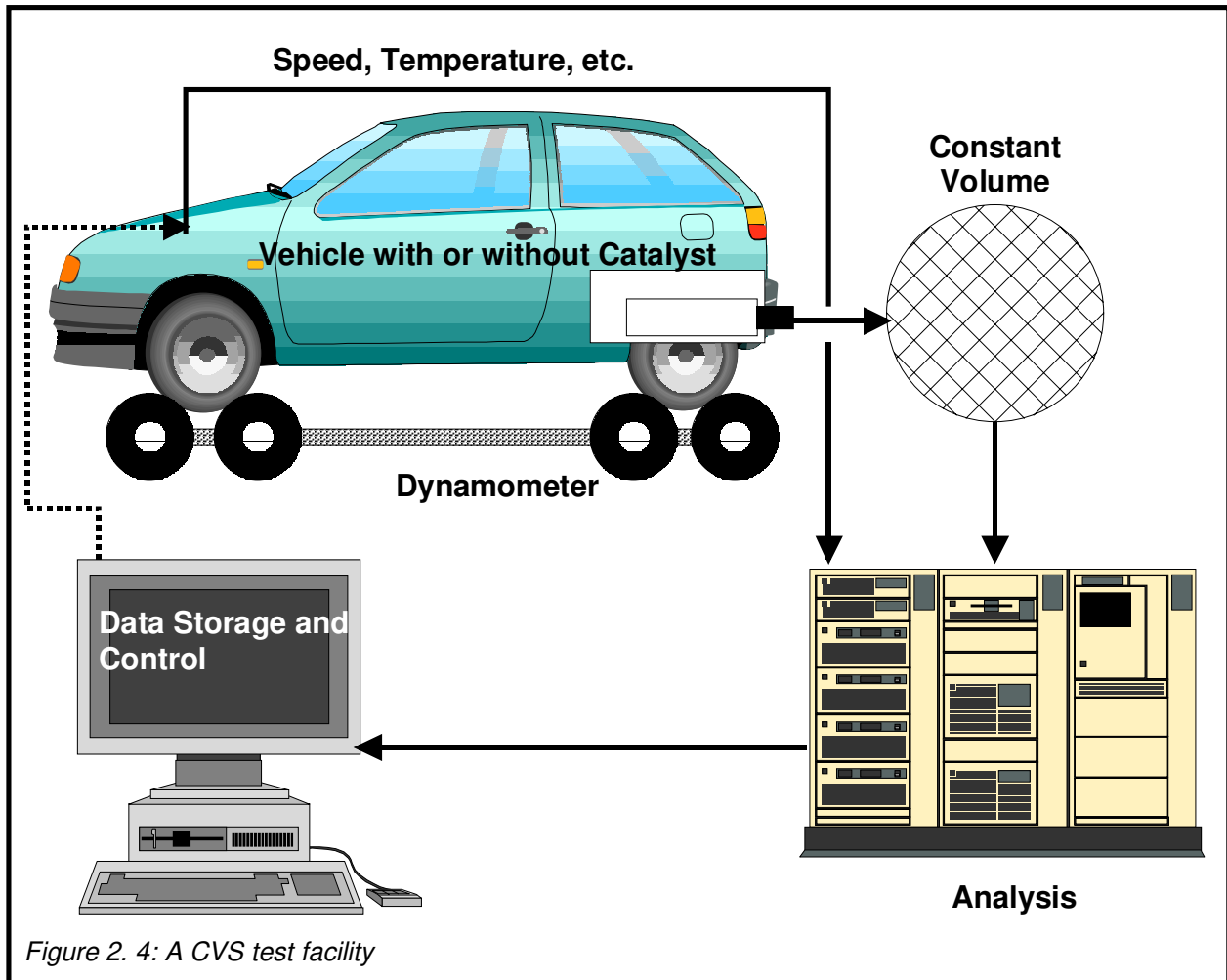


Figure 2. 4: A CVS test facility

The exhaust is collected in a bag with constant volume. At specific time intervals a sample from the bag is taken and analysed. A computer is used to store the data obtained and to control the simulation of the legislative driving cycle, for instance, the MVEuro2 test cycle. If the vehicle tested is catalyst equipped, the catalyst experiences dynamic operation conditions, i.e. frequent changes of exhaust gas temperature, of pressure, of exhaust gas composition, and varying thermal and mechanical stress. While this method of testing is as close to realistic driving conditions as possible, it is also the most expensive. It is uneconomical to apply it for activity screening tests of freshly developed catalyst formulations. This screening can be done by either engine bench testing or synthetic catalytic activity testing (SCAT).

### 2. 3. 3 Engine Bench (EB) Testing

Engine bench testing can be used to test catalysts with realistic Diesel engine emissions. For this set-up only the vehicle's engine is used. A brake is applied to the engine to simulate increasing and decreasing engine loads, Figure 2. 5. The engine load strongly determines the exhaust gas temperature. An increase of the catalyst's operation temperature through an increase of the engine load always coincides with a variation of the exhaust gas composition. NO<sub>x</sub> concentration for instance, rises with increasing engine load. Temperature dependent activity measurements at constant gas compositions can therefore not be performed. This can only be done by SCAT.

This thesis reports only results obtained by SCAT testing. A detailed description of the experimental apparatus is given in the experimental chapter.

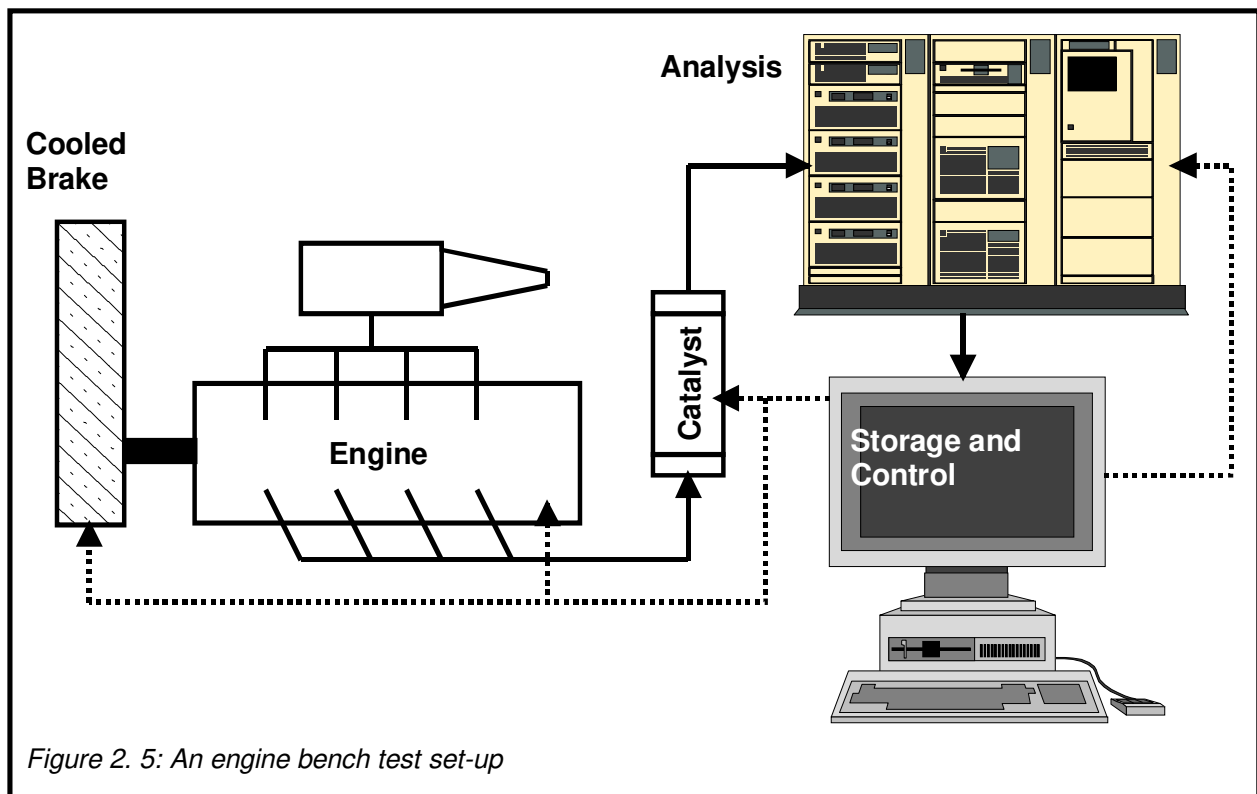


Figure 2. 5: An engine bench test set-up

### 2. 4 Pollutant Control Through Engine Modification

Although this thesis deals only with pollutant control through catalysis, a brief overview about mechanical possibilities to reduce emissions shall be given. Only the

combination of catalytic and mechanical pollutant control will be able to meet future emission limits.

#### *2. 4. 1 The Effect of the Combustion Process*

The combustion inside Diesel engines is predominantly influenced by three factors: the combustion chamber shape, the turbulence in the chamber, and the injection geometry.

In indirect injection (IDI) engines, the fuel is injected into a relatively small pre- or swirl chamber and as ignition begins the mixture is blown into the combustion chamber. The two-stage combustion and the swirl effect imparted to the mixture in IDI engines results in lower emissions of NO<sub>x</sub>, CO, HC, and PM than in direct injection engines described below.

Direct injection engines (DI) operate differently from IDI engines. The fuel is injected near the cylinder wall into a piston bowl or into the turbulent air in the piston bowl. While this method reduces fuel consumption and thereby emission of CO<sub>2</sub> significantly, it has the consequence of higher emissions of CO, HC, and NO<sub>x</sub>.

The use of a turbo charger for a Diesel engine increases its power output. It also increases the heat capacity of the gas, thereby reducing the combustion temperature. A lower combustion temperature always entails a decreased formation of NO<sub>x</sub>. However, the exhaust gas of a turbo charged vehicle has a lower temperature than the exhaust gas of a naturally aspirated vehicle<sup>23</sup>. A lower gas temperature may decrease the activity of a catalyst.

Generally, measures that accelerate combustion (additional sprays, increased turbulence with swirl inlets or with squish flows in the chamber) lower the emission of HC, CO, and PM as well as fuel consumption because of higher combustion temperatures while they increase the NO<sub>x</sub> emissions<sup>16</sup>.

#### *2. 4. 2 The Effect of Injection Timing*

When the fuel is injected earlier during the compression phase, the ignition begins shortly after the compression has reached its maximum. Consequently, the combustion is concentrated to a smaller volume and hence the combustion temperature is higher. This results in a higher NO<sub>x</sub> emission rate but slightly lower HC, CO and particulate emissions. On the other hand, so called post-injection of a

small amount of Diesel fuel after the end of combustion into the expansion stroke can provide the exhaust gas with highly reactive HC compounds necessary for NO<sub>x</sub> reduction by utilisation of a catalyst<sup>24</sup>.

### 2. 4. 3 Exhaust Gas Recirculation (EGR)

EGR is current industrial standard for many Diesel vehicles in order to reduce NO<sub>x</sub> emissions. It makes use of the strong dependence of NO formation on temperature<sup>17</sup>:

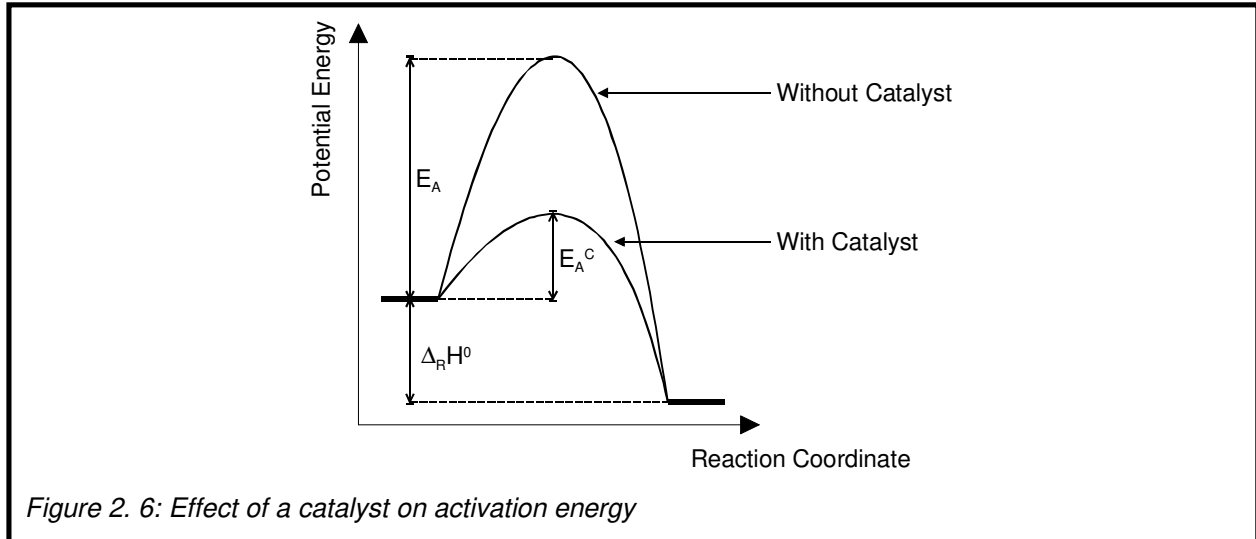
$$\frac{d[NO]}{dt} = \frac{6 \times 10^{16}}{T^{1/2}} \exp\left[\frac{-69,09}{T}\right] [O_2]_e^{0,5} [N_2]_e \frac{mol}{cm^3 s} \quad \text{Equation 2. 11}$$

The index <sub>e</sub> denotes exhaust gas. Since the exhaust gas consists mainly of N<sub>2</sub>, CO<sub>2</sub>, and H<sub>2</sub>O, it acts as a diluent and reduces the oxygen concentration in the engine. This raises the specific heat capacity of the intake charge and consequently reduces the local peak temperatures in the Diesel engine. This in turn decreases the thermal NO formation<sup>13 17</sup>. Unfortunately, although less NO<sub>x</sub> emissions are produced, due to the lower oxygen concentration the complete combustion of HC, CO, and PM is deteriorated and their emissions increase.

## 2. 5 Pollutant Control Through Catalysis

### 2. 5. 1 General Aspects About Catalysis

It is necessary to differentiate between initiator and catalyst. While the former does not create a new reaction path, the latter's effect is based on providing an alternative reaction path with a lower activation energy, Figure 2. 6.



A catalyst is a substance that increases the rate of a chemical reaction, while itself remaining unchanged. Suppose a reaction



has a negative free Gibbs enthalpy of reaction ( $\Delta_R G^0$ ) to proceed to the right. Only in this case is it thermodynamically allowed and its rate can be increased by a catalyst. The catalyst provides a new reaction path where A reacts first with the catalyst (K) and this intermediate then reacts with B to form AB and release K again:



The catalyst does not disturb the equilibrium composition between A + B and AB, it only accelerates the rate at which this equilibrium is attained. A catalyst can not work against thermodynamics; if  $\Delta_R G^0$  for a reaction is close to zero the use of a catalyst will not help to create more product.

Catalysis can be divided into two major groups: homogeneous catalysis and heterogeneous catalysis. In homogeneous catalysis both the catalyst and the reactive compounds are of similar phase, for instance liquid or gaseous. In heterogeneous catalysis, catalyst and reactive compounds are in different phases,

often solid and gaseous, respectively. This thesis deals entirely with heterogeneous catalytic reactions.

A catalysed, heterogeneous, gas-solid reaction comprises 9 steps:

1. Transport of the reactants through the gas phase to a boundary layer by convection
2. Transport of the reactants through the boundary layer to the outer catalyst surface by diffusion
3. Transport of the reactants through the pores of the catalyst to the inner catalyst surface by pore diffusion
4. Adsorption of the reactants on the inner catalyst surface
5. Chemical reaction
6. Desorption of the products from the inner catalyst surface
7. Transport of the products through the pores of the catalyst to the outer catalyst surface by pore diffusion
8. Transport of the products through the boundary layer to the surrounding gas by diffusion
9. Transport of the products through the gas phase by convection

Heterogeneous catalysis normally depends on at least one reactant being adsorbed (usually chemisorbed) and modified to a form in which it readily undergoes reaction.

Two mechanisms are often encountered in heterogeneous catalysis: the Eley-Rideal mechanism and the Langmuir-Hinshelwood mechanism.

In the Eley-Rideal mechanism a gas phase molecule collides with another molecule adsorbed on the surface. The rate of formation ( $v$ ) of product is expected to be proportional to the partial pressure ( $p_B$ ) of the non-adsorbed gas B and the extent of the surface coverage ( $\theta_A$ ) of the adsorbed gas A.

$$v = k p_B \theta_A$$

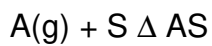
*Equation 2. 15*

The surface coverage is defined as

$$\theta = \frac{\text{number of adsorption sites occupied}}{\text{number of adsorption sites available}}$$

*Equation 2. 16*

The rate constant ( $k$ ) might be much larger than for the uncatalysed gas-phase reaction because the reaction on the surface has a low activation energy and the adsorption itself is often not activated. If the adsorption isotherm for A is known, the rate law can be expressed in terms of its partial pressure  $p_A$ . A well known isotherm is the Langmuir isotherm. This isotherm is based on the assumption that every adsorption site (S) is equivalent and that the ability of a particle to bind there is independent of whether or not nearby sites are occupied. The dynamic equilibrium is:



*Equation 2. 17*

where (g) denotes gas phase and S an adsorption site on the surface. The rate constant for this adsorption is  $k_A$  and for the desorption  $k_D$ . The rate of change of surface coverage due to adsorption is proportional to the pressure  $p_A$  of A and the number of vacant sites  $N(1-\theta)$ , where N is the total number of sites

$$N \frac{d\theta}{dt} = k_A p_A N(1-\theta)$$

*Equation 2. 18*

The rate of change of  $\theta$  due to desorption is proportional to the number of adsorbed species,  $N\theta$

$$N \frac{d\theta}{dt} = k_D N\theta$$

*Equation 2. 19*

At equilibrium both rates are equal

$$k_A p_A N(1-\theta) = k_D N\theta$$

*Equation 2. 20*

Solving for  $\theta$  gives the Langmuir isotherm

$$\theta = \frac{Kp_A}{1 + Kp_A}$$

$$K = \frac{k_A}{k_D}$$

*Equation 2. 21*

For diatomic molecules (like O<sub>2</sub>), the rate of adsorption is proportional to the pressure and to the probability that both atoms will find sites after dissociation

$$N \frac{d\theta}{dt} = k_A p_A \{N(1-\theta)\}^2 \quad \text{Equation 2. 22}$$

The rate of desorption is proportional to the frequency of encounters of atoms on the surface, and therefore second order in the number of atoms present

$$N \frac{d\theta}{dt} = k_D (N\theta)^2 \quad \text{Equation 2. 23}$$

Combination of Equations 2. 22 and 2. 23 leads to

$$\theta = \frac{(Kp_A)^{1/2}}{1 + (Kp_A)^{1/2}} \quad \text{Equation 2. 24}$$

Using Equation 2. 21 in Equation 2. 15 the rate law for the Eley-Rideal mechanism becomes

$$v = \frac{kKp_A p_B}{1 + Kp_A} \quad \text{Equation 2. 25}$$

If A is a diatomic molecule that adsorbs dissociatively, Equation 2. 24 is used instead of 2. 21. According to Equation 2. 25, when the partial pressure of A is high ( $Kp_A \gg 1$ ) there is almost complete surface coverage, and the rate is equal to

$$v = kp_B \quad (\text{for } Kp_A \gg 1) \quad \text{Equation 2. 26}$$

and the rate determining step is the collision of B with the adsorbed atoms or fragments of A. In the case that the pressure of A is low ( $Kp_A \ll 1$ ) the reaction rate equals



$$v = kK_A p_A p_B \quad (\text{for } K_A p_A \ll 1)$$

*Equation 2. 27*

In this case the coverage of the surface is important in the determination of the rate. In the Langmuir-Hinshelwood mechanism of surface catalysed reactions, the reaction takes place by encounters between molecular fragments and atoms adsorbed on the surface. The rate law is therefore second order in the extent of surface coverage

$$v = k\theta_A\theta_B$$

*Equation 2. 28*

Insertion of the appropriate isotherms for A and B then gives the reaction rate in terms of the partial pressures for the reactants. If A and B follow Langmuir isotherms and adsorb without dissociation it follows

$$\theta_A = \frac{K_A p_A}{1 + K_A p_A + K_B p_B}$$

*Equation 2. 29*

$$\theta_B = \frac{K_B p_B}{1 + K_A p_A + K_B p_B}$$

*Equation 2. 30*

and the rate law is

$$v = k \frac{K_A p_A K_B p_B}{(1 + K_A p_A + K_B p_B)^2}$$

*Equation 2. 31*

The activity of a catalyst is dependent on several factors, one of them being strength of adsorption. In order to be active, the catalyst should be extensively covered by adsorbate, which is the case if chemisorption is strong. On the other hand, if the strength of the substrate-adsorbate bond becomes too great, the activity declines either because the other reactant molecules can not react with the adsorbate or because the adsorbate molecules are immobilised on the surface. Many metals are suitable for adsorbing gases and the general order of adsorption strengths

decreases along the series O<sub>2</sub>, CO, H<sub>2</sub>, CO<sub>2</sub>, N<sub>2</sub><sup>15</sup>. An overview of chemisorption abilities is given in Table 2. 4

	O <sub>2</sub>	CO	H <sub>2</sub>	CO <sub>2</sub>	N <sub>2</sub>
Ti, Cr, Mo, Fe	+	+	+	+	+
Ni, Co	+	+	+	+	-
Pd, Pt	+	+	+	-	-
Mn, Cu	+	+	±	-	-
Al, Au	+	+	-	-	-
Li, Na, K	+	-	-	-	-
Mg, Ag, Zn, Pb	+	-	-	-	-

+ Strong Chemisorption; ± Chemisorption; - No Chemisorption

Table 2. 4: Chemisorption abilities of several metals<sup>15</sup>

In automobile exhaust catalysis, the active metal is usually dispersed on a support, the so called washcoat, and this washcoat is used to coat a ceramic or metallic substrate, the monolith. An important aspect in heterogeneous catalysis are the strong metal-support interactions (SMSI) that may occur between active metal and support. To name but a few these are particle size effects, catalyst poisons, promoters, real metal-support interactions, apparent metal-support effects, and metal-support interactions with insulator oxides<sup>25</sup>:

The first manifestation of an influence of the support on the metal is through the average size and size distribution of the metallic particles. The particle shape may also be influenced by the support. This occurs through differences in the interfacial energy where the metal and support connect. The support provides a means of separating small metal particles from each other. This can impart a high thermal stability to allow continuous use at temperatures of at least 770K.

Some supports can retain a trace of a substance which would be toxic (catalyst poison) to the supported metal or they retain a by-product of the reaction which might otherwise inhibit the metal through competitive adsorption.

Promoters could be those which control the acid-base balance of the total system (alkali to control carbon deposition).

Electron movement between metal and support is a real possibility resulting in real metal-support interactions. The magnitude of the interaction is also a function of metal load, as suggested by experiments. There is evidence that certain supports,

especially  $\text{Al}_2\text{O}_3$ , stabilise intermediate oxidation states such as  $\text{Rh}^I$ ,  $\text{Pt}^{III}$  as well as retard reduction because of strong interaction with the metal precursor.

Apparent metal-support interactions manifest in the observation that in the NO-CO reaction on  $\text{Pt}/\text{Al}_2\text{O}_3$  an intermediate isocyanate (-NCO) species resides on the support. This species is not observed if the Pt is absent. The preferred mechanism is that the N atoms migrate from the metal to the support where they react with gaseous CO.

The direct influence of insulator oxide supports upon the geometric or electronic properties of small metal particles is usually negligible. However, highly dispersed metal may differ, especially in its electronic constitution, from bulk metal. Oxidising acid centres of the insulator support can attract electrons from the metal particles.

Summarising, the present evidence suggests three ways in which a support can modify the catalytic properties of a metal particle:

1. the metal and the particle interact to form a compound or there may be a partial encapsulation of the metal by the support
2. there may be a transfer of electrons between the metal and the support
3. the particle size distribution and/or the particle morphology may be altered

A summary of some reactions occurring on a Diesel catalyst is given in Table 2. 5. The free Gibbs enthalpy of reaction as calculated from values given in<sup>15</sup> has been included in Table 2. 5. As mentioned earlier, the removal of HC and CO from Diesel exhaust poses no real problems due to the high oxygen content of the exhaust gas favouring oxidation reactions. Two challenges remain: first, the removal of soot particles. The soot consists predominantly of rather inert carbon particles difficult to oxidise. Second, the removal of nitrogen oxides by reduction. The latter is the major topic of this thesis.

$C_nH_m + (n + m/4) O_2$	$\rightarrow$	$n CO_2 + m/2 H_2O$	Equation 2. 32	$\Delta_R G^0_{Propene} = -1931,57 \text{ kJ mol}^{-1};$ $\Delta_R G^0_{Propane} = -2073,87 \text{ kJ mol}^{-1}$
$C_nH_m + (2n + m/2) NO$	$\rightarrow$	$(n + m/4) N_2 + m/2 H_2O + nCO_2$	Equation 2. 33	$\Delta_R G^0_{Propene} = -2710,52 \text{ kJ mol}^{-1};$ $\Delta_R G^0_{Propane} = -2939,37 \text{ kJ mol}^{-1}$
$C_nH_m + (n + m/4) NO_2$	$\rightarrow$	$1/2(n + m/4) N_2 + m/2 H_2O + nCO_2$	Equation 2. 34	$\Delta_R G^0_{Propene} = -2162,47 \text{ kJ mol}^{-1};$ $\Delta_R G^0_{Propane} = -2330,47 \text{ kJ mol}^{-1}$
$CO + 1/2 O_2$	$\rightarrow$	$CO_2$	Equation 2. 35	$\Delta_R G^0 = -257,19 \text{ kJ mol}^{-1}$
$CO + NO$	$\rightarrow$	$CO_2 + 1/2 N_2$	Equation 2. 36	$\Delta_R G^0 = -343,74 \text{ kJ mol}^{-1}$
$CO + NO_2$	$\rightarrow$	$CO_2 + NO$	Equation 2. 37	$\Delta_R G^0 = -221,95 \text{ kJ mol}^{-1}$
$CO + H_2O$	$\rightarrow$	$CO_2 + H_2$	Equation 2. 38	$\Delta_R G^0 = -28,62 \text{ kJ mol}^{-1}$
$CO + N_2O$	$\rightarrow$	$NO + CO_2 + 1/2 N_2$	Equation 2. 39	$\Delta_R G^0 = -274,84 \text{ kJ mol}^{-1}$
$CO + N_2O$	$\rightarrow$	$N_2 + CO_2$	Equation 2. 40	$\Delta_R G^0 = -361,39 \text{ kJ mol}^{-1}$
$H_2 + 1/2 O_2$	$\rightarrow$	$H_2O$	Equation 2. 41	$\Delta_R G^0 = -228,57 \text{ kJ mol}^{-1}$
$SO_2 + 1/2 O_2$	$\rightarrow$	$SO_3$	Equation 2. 42	$\Delta_R G^0 = -70,87 \text{ kJ mol}^{-1}$
$SO_2 + 3 H_2$	$\rightarrow$	$H_2S + 2 H_2O$	Equation 2. 43	$\Delta_R G^0 = -190,51 \text{ kJ mol}^{-1}$
$NO_2 + 2CO$	$\rightarrow$	$2CO_2 + 1/2 N_2$	Equation 2. 44	$\Delta_R G^0 = -565,69 \text{ kJ mol}^{-1}$
$NO_2 + C$	$\rightarrow$	$NO + CO$	Equation 2. 45	$\Delta_R G^0 = -101,93 \text{ kJ mol}^{-1}$
$NO_2$	$\rightarrow$	$1/2 N_2 + O_2$	Equation 2. 46	$\Delta_R G^0 = -51,31 \text{ kJ mol}^{-1}$
$NO_2 + N$	$\rightarrow$	$N_2O + 1/2 O_2$	Equation 2. 47	$\Delta_R G^0 = -402,67 \text{ kJ mol}^{-1}$
$2NO$	$\rightarrow$	$N_2O + 1/2 O_2$	Equation 2. 48	$\Delta_R G^0 = -68,9 \text{ kJ mol}^{-1}$
$NO + N$	$\rightarrow$	$N_2O$	Equation 2. 49	$\Delta_R G^0 = -437,91 \text{ kJ mol}^{-1}$
$NO + H_2$	$\rightarrow$	$1/2 N_2 + H_2O$	Equation 2. 50	$\Delta_R G^0 = -315,12 \text{ kJ mol}^{-1}$
$NO + 5/2 H_2$	$\rightarrow$	$NH_3 + H_2O$	Equation 2. 51	$\Delta_R G^0 = -331,57 \text{ kJ mol}^{-1}$
$NO$	$\rightarrow$	$1/2 N_2 + 1/2 O_2$	Equation 2. 52	$\Delta_R G^0 = -86,55 \text{ kJ mol}^{-1}$
$NO + 1/2 O_2$	$\rightarrow$	$NO_2$	Equation 2. 53	$\Delta_R G^0 = -35,24 \text{ kJ mol}^{-1}$
$NO + C$	$\rightarrow$	$1/2 N_2 + CO$	Equation 2. 54	$\Delta_R G^0 = -223,72 \text{ kJ mol}^{-1}$
$NO + 1/2 C$	$\rightarrow$	$1/2 N_2 + 1/2 CO_2$	Equation 2. 55	$\Delta_R G^0 = -480,91 \text{ kJ mol}^{-1}$
$N_2O + 1/2 O_2$	$\rightarrow$	$N_2 + O_2$	Equation 2. 56	$\Delta_R G^0 = -104,2 \text{ kJ mol}^{-1}$
$N_2O + NO_2$	$\rightarrow$	$N_2 + O_2 + NO$	Equation 2. 57	$\Delta_R G^0 = -68,96 \text{ kJ mol}^{-1}$
$N_2O$	$\rightarrow$	$N_2 + 1/2 O_2$	Equation 2. 58	$\Delta_R G^0 = -104,2 \text{ kJ mol}^{-1}$
$N_2O$	$\rightarrow$	$1/2 N_2 + NO$	Equation 2. 59	$\Delta_R G^0 = -17,7 \text{ kJ mol}^{-1}$
$NH_3 + CH_4$	$\rightarrow$	$HCN + 3 H_2$	Equation 2. 60	$\Delta_R G^0 = +191,87 \text{ kJ mol}^{-1}$

Table 2. 5: Some reactions occurring on a catalyst

### 2. 5. 2 Particle Filters

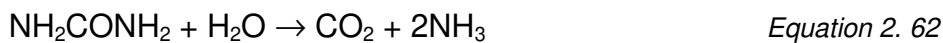
Usually, the PM emissions of a Diesel vehicle are treated by a filter system. This is a rather mechanical approach and should fit better in chapter 2. 4. However, advanced filter systems like the so called "Continuous Regeneration Trap" (CRT) use a combination of particle filter and oxidation catalyst<sup>3</sup>. The major problem of any particle filter is that during the operation the high amount of particles held back in the filter increase the back pressure and thereby reduce the engine's power output. Consequently, the filter needs to be regenerated from time to time by removing the particles. This can be done stationary by heating the filter or by flushing hydrogen over it and burning of the particles. The CRT method uses a combination of an

oxidation catalyst in front (towards the engine) and a filter coupled after the catalyst. The oxidation catalyst removes HC and CO and oxidises NO to NO<sub>2</sub>. NO<sub>2</sub> is a better oxidant than NO and continuously oxidises the soot particles held back on the filter. Currently, the dimensions of the CRT are too big to be applicable for passenger cars. The treatment of PM has not been a topic of this thesis and is therefore discussed no further.

### 2. 5. 3 NO<sub>x</sub> Control of Diesel Exhaust in Stationary Systems

Stationary systems have the advantage that generally enough space is available to apply certain techniques and that they are mainly operated under non-transient conditions.

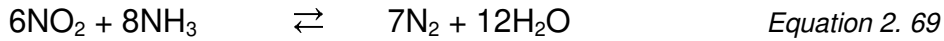
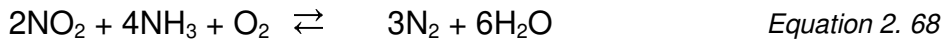
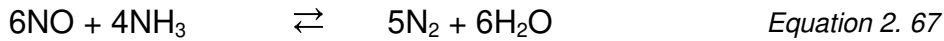
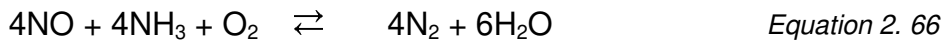
In 1962 a process was developed that used a precious metal and ammonia to selectively remove NO<sub>x</sub> from exhaust gas in the presence of oxygen. This process has been developed to a commercial scale and has the acronym of SCR, Selective Catalytic Reduction<sup>26 27 28</sup>. Instead of NH<sub>3</sub>, ammonia or urea dissolved in water can be used<sup>29</sup>. If urea is used, the process is known as the CARNOX-Process<sup>30</sup>. Urea reacts via<sup>13</sup>



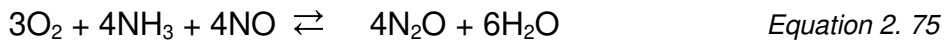
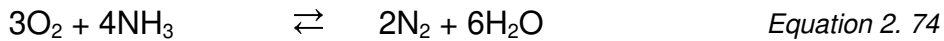
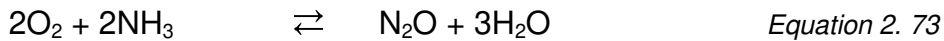
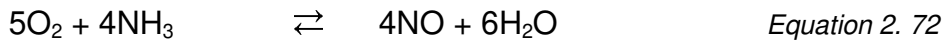
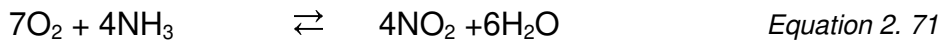
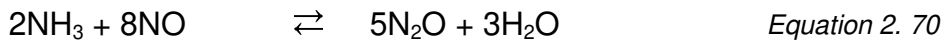
to form carbon dioxide and ammonia. The NH<sub>2</sub>• radical can react directly with nitrogen monoxide



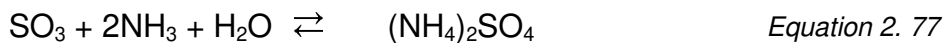
The advantage of using urea is its easy storage compared to ammonia while the disadvantage is the possibility of side reactions if temperature or residence time is too low<sup>29</sup>. During SCR, depending on the active component, different reaction processes can occur<sup>31 29</sup>



At higher temperatures, unwanted side reactions may take place



If  $\text{SO}_2$  oxidation to  $\text{SO}_3$  occurs on the catalyst, the formation of sulphates can also take place



These sulphates can lead to a deactivation of the catalyst by blocking the surface for further reactions.

Another process which is applied to stationary systems, is called Selective Non-Catalytic Reduction, SNCR. In this process, ammonia is injected directly into the flue gas at temperatures between 1100 and 1400 K<sup>31</sup>.

For both methods, SCR and SNCR, it is absolutely necessary to maintain a careful stoichiometric control of the ammonia injected, in order to avoid a release of surplus  $\text{NH}_3$ , while maintaining sufficient  $\text{NO}_x$  removal<sup>27 32</sup>. This, and the complex regulation of ammonia injection, makes the use of ammonia in a mobile system difficult, if not impossible<sup>32 33 34</sup>.

A different approach to de-NO<sub>x</sub>-ing is made by a combined oxidation/absorption method. In this method the flue gas is passed through columns containing HNO<sub>3</sub> and H<sub>2</sub>O<sub>2</sub>. Since the apparatus needed for this method is very complex, this is a rather expensive process<sup>35</sup>.

#### 2. 5. 4 NO<sub>x</sub> Control of Diesel Exhaust in Vehicles

A variety of methods have been proposed to achieve the reduction of NO<sub>x</sub> under Diesel exhaust conditions. They can be divided into methods using monoliths, methods using adsorption, and other methods.

##### 2. 5. 4. 1 Methods using Monoliths

All of these methods use a so-called honeycomb monolith support which predominantly consists of α-cordierite (Mg<sub>2</sub>Al<sub>4</sub>Si<sub>5</sub>O<sub>18</sub>)<sup>36</sup>. Cordierite is a hexagonal framework silicate with zeolite-like channels parallel to the c axis<sup>37</sup>. It has a low dielectric constant, a low coefficient of thermal expansion, and high thermal and chemical resistance<sup>38</sup>. The cordierite support is coated with a so called washcoat which contains the active catalytic material.

The most common types of washcoats are zeolites (ZSM-5, Mordenite, Ferrierite) and alumina (γ-Al<sub>2</sub>O<sub>3</sub>), less common are Perowskites, titania (TiO<sub>2</sub>), and zirconia (ZrO<sub>2</sub>).

##### 2. 5. 4. 1. 1 Zeolites

Zeolites are crystalline aluminosilicates described by the formula<sup>13</sup>



Me is either a single valence alkali-metal (n=1) or a divalent alkaline earth-metal (n=2). The crystal lattices are made up of cubooctahedra, whose corners are alternately occupied by [SiO<sub>4</sub>] and [AlO<sub>4</sub>] tetrahedra. For every Al<sup>3+</sup> in the lattice, an additional positive charge must be present in order to keep charge neutrality<sup>33</sup>. This charge can be either a proton or any other positive metallic or non-metallic ion. Other metals can be exchanged with the initial metal by certain techniques<sup>39-50</sup>.

Zeolites are commonly characterised by their  $\text{SiO}_2/\text{Al}_2\text{O}_3$  molar ratio. The amount of metal ions, ammonium ions, or protons that can be exchanged into the zeolite is determined by this ratio<sup>33</sup>. With increasing  $\text{SiO}_2/\text{Al}_2\text{O}_3$  ratio the amount of exchangeable ions and the acidity of the support decreases.

There is an almost infinite variety of three-dimensional structures in which zeolites can crystallise. These structures are made up of channels, passages, and cavities of molecular dimensions. Because of this, they have a large inner surface area and can act as molecular sieves<sup>13</sup>. Molecules of suitable size can be stored in the cavities. Zeolites also show shape selectivity. There are three types of selectivity<sup>47</sup>: reactant selectivity, product selectivity, and transition-state selectivity.

**Reactant Selectivity:**

This type of selectivity appears if only certain molecules of a reaction mixture are small enough to fit into the channels and reach the interior of the zeolite catalyst. Reactant molecules with larger diameters than the channel openings remain unchanged at the outside.

**Product Selectivity:**

If the products formed in the zeolite structure have a larger diameter, they may not be able to leave the cavities anymore or at least diffuse much slower to the outside. This is called product selectivity. With product selectivity, there is a risk that the catalyst is poisoned by molecules that occupy active catalytic sites and cannot leave anymore.

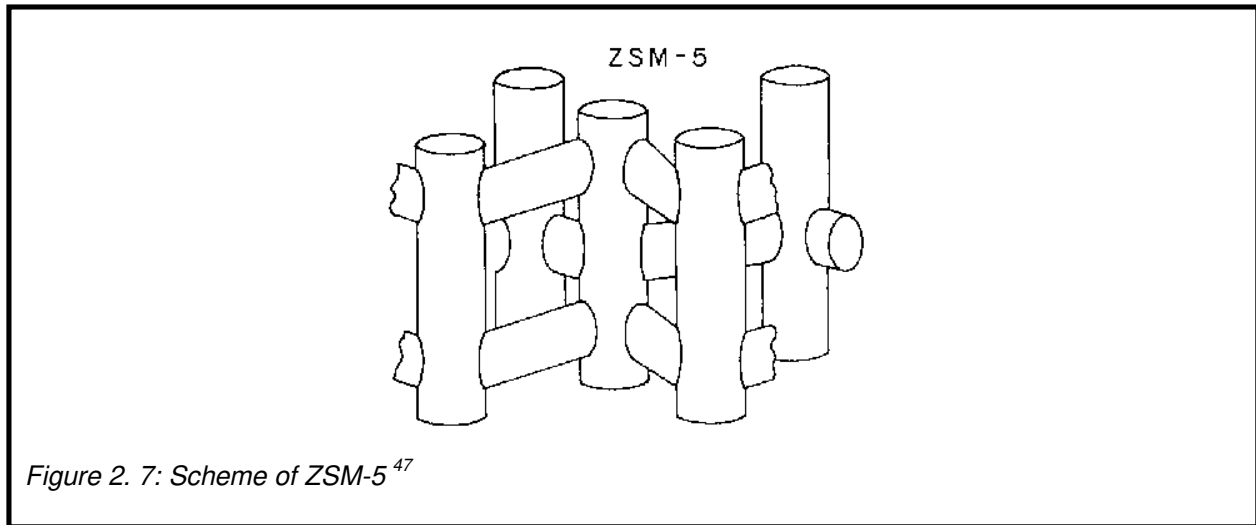
**Transition-State Selectivity:**

Transition-state selectivity is probably the most interesting for any selective reaction. The geometric arrangement of the active sites within the zeolite either promotes or hinders a certain transition-state of a reaction. Ideally, this is a phenomenon that allows to "tailor" a zeolite catalyst so that it only permits one certain reaction.

ZSM zeolites are named after the laboratory in which they were discovered, Zeolite Socony Mobil. In literature, the names Pentasil and MFI are also used instead of ZSM<sup>33</sup>. Among the ZSM zeolites, ZSM-5 is the one which is best characterised and most frequently used. Its structure consists of two types of channels. One is straight with an oval opening of about  $5,2 \times 5,8 \text{ \AA}$ . The second is perpendicular to the former and connects the straight channels with each other, resulting in a "zigzag" shape. Its

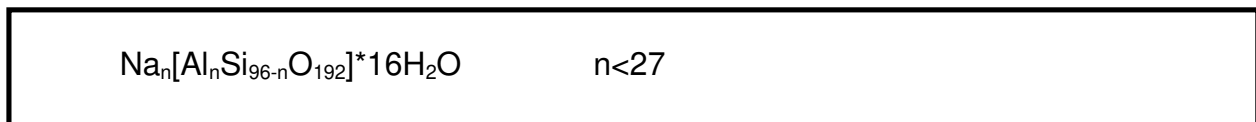


circular cross-section has a diameter of  $5,4 \text{ \AA}$ <sup>47</sup>. The cavities created by these interconnections have diameters of ca.  $9 \text{ \AA}$ . The catalytically active, highly acidic sites are believed to be situated in these cavities<sup>33</sup>.



The acidity of the external ZSM-5 surface plays also an important role in the catalytic properties of this zeolite. As the  $\text{SiO}_2/\text{Al}_2\text{O}_3$  ratio increases, the hydrophilic character decreases while the thermal stability increases. This behaviour contributes to the catalytic performance of ZSM-5-based SCR applications.

The analytical composition of the unit cell of ZSM-5 in the hydrated sodium form has the sum equation<sup>47</sup>



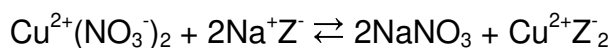
This is the formula of the commercially available ZSM-5. If Na is exchanged by a multivalent transition metal ion, the latter occupies a well defined position within the zeolite structure. Its location determines mainly the catalytic properties of the new ion-exchanged zeolite<sup>33</sup>.

#### 2. 5. 4. 1. 1. 1 Cu/ZSM-5

Iwamoto et al.<sup>48</sup> and Held et al.<sup>31</sup> have independently found that copper exchanged ZSM-5, Cu/ZSM-5, shows selective catalytic reduction of NO under oxidising conditions in the presence of hydrocarbons. Their discovery has triggered intensive investigations on Cu/ZSM-5 in many research groups.

Although no Cu/ZSM-5 catalysts have been used for investigations in this thesis because of reasons discussed later, Cu/ZSM-5 systems are described in detail due to several similarities in reaction mechanisms between this system and the Pt/Al<sub>2</sub>O<sub>3</sub> system.

Great efforts have been made to describe the structure of Cu/ZSM-5, but the results are controversial. It is obvious that the procedure of exchanging copper ions into the zeolite via<sup>33</sup>



*Equation 2. 78*

has a strong influence on the structure of the Cu/ZSM-5. The extent of the exchange is usually calculated by assuming that one Cu<sup>2+</sup> ion replaces two Na<sup>+</sup> ions. Shelef<sup>33</sup> has pointed out that this assumption is misleading, since the two zeolite anion sites (Z<sup>-</sup>) must be very close to each other in order to be neutralised by one Cu<sup>2+</sup> cation. This is only the case in zeolites with low SiO<sub>2</sub>/Al<sub>2</sub>O<sub>3</sub> ratios. Otherwise the second positive charge of the Cu<sup>2+</sup> cation must be compensated by extra lattice oxygen or hydroxyl ions.

When the total amount of Na<sup>+</sup> ions released from the zeolite after exchange was two times that of the Cu<sup>2+</sup> ions prior to exchange, Chajar et al.<sup>41</sup> interpreted this sample as fully exchanged. If the amount of Na<sup>+</sup> was larger than double, the sample was believed to be over exchanged, the surplus copper(II) ions being deposited by precipitation as CuO into the zeolite lattice. However, according to Shelef this would imply that a "100%" exchanged Na/ZSM-5 zeolite would have lost all its Brønsted-acidic sites. Since almost all mechanisms proposed in literature for SCR of NO<sub>x</sub> over Cu/ZSM-5 require the presence of Brønsted-acidic sites, Shelef must be correct by assuming that the so called fully or overexchanged zeolites are merely highly exchanged. Table 2. 6 shows the Cu wt.-% and exchange levels of some Cu/ZSM-5 samples prepared by different researchers

Cu wt--%	Exchange Level [%] <sup>*)</sup>	Type of Zeolite	Reference
5,0	>100	H/ZSM-5	40
1,2	44	Na/ZSM-5	41
2,6	105	Na/ZSM-5	41
3,8	153	Na/ZSM-5	41
2,6	116	Na/ZSM-5	46
3,5	110	H/ZSM-5	46
2,9		Na/ZSM-5	46
1,7	58	H/ZSM-5	46
1,45	-	[Cu/Na/ZSM-5 + H/ZSM-5]	46
3,2	-	-	49

\*) as specified by the author

Table 2. 6: Cu wt.-% and exchange levels

Different values from the same authors are due to different preparation methods. Radtke et al.<sup>50</sup> have discovered that the BET surface area of an ion-exchanged catalyst is nearly identical to the Na/ZSM-5 precursor.

There is much controversy among researchers concerning the oxidation state of the active copper-ions and their chemical environment. Shelef<sup>33</sup> proposes two types of isolated Cu<sup>2+</sup> ions and that there are no clusters of cupric ions. Both ion types are coordinatively unsaturated, one in a square-pyramidal, and one in a square-planar configuration. According to Shelef both ion types are resistant to spontaneous reduction under oxidising conditions even in the presence of reductants and high temperatures.

On the other hand, Grünert et al.<sup>46</sup> have shown by infrared- and electron spin resonance (ESR) spectroscopy and photoluminescence measurements that there is ready interconversion between Cu<sup>2+</sup> and Cu<sup>+</sup> ions. They believe that isolated, irreducible ions are only a minority species in so called overexchanged zeolites. Grünert et al. report that reduced Cu/ZSM-5 catalysts which contained large metallic copper particles showed initially low activity, but upon exposure to the reaction mixture their activity grew. This is explained by dynamic changes of copper dispersion and distribution during the course of the reaction, i.e., the copper dispersion increases by migration of copper ions into the bulk of the zeolite. This is paralleled by the formation of isolated copper ion species. Grünert et al. conclude that in "overexchanged" Cu/ZSM-5 catalysts two types of copper species are present: small clusters with the copper atoms linked by extra lattice oxygen and isolated copper ions in low-symmetry environments. It is suggested that there is a

requirement for an intra zeolite location of the copper ions, so that there can be an interaction between Brønsted-acid and copper sites and that isolated copper ions as well as copper clusters may be necessary for optimal catalytic performance.

The existence of Cu(II) and Cu(I) ions during the course of reaction has been confirmed by Chajar et al.<sup>41</sup> and Spoto et al.<sup>51</sup>. Moretti<sup>52</sup> posits that the active sites are actually pairs of Cu ions rather than single isolated ions. Agreement exists among most researchers<sup>41 33 46 53</sup> that the nature of the copper species is dependent on the type of zeolite and that Cu<sup>+</sup> is stabilised by the zeolite after calcination. Grünert et al.<sup>46</sup> point out that calcined samples are more resistant to reduction of Cu(II) to Cu(I). Nevertheless, reoxidation of the Cu<sup>+</sup> ions restores the catalyst reversibly. This indicates that the equilibrium:



is of major importance for maintaining the active species. Miyamoto et al.<sup>54</sup> have investigated the role of the ZSM-5 framework in stabilising Cu(I) and Cu(II). They also made a suggestion for the location of these ions within the zeolite structure based on molecular dynamics calculations. Cu(II) is assumed to be present in the vicinity of an [AlO<sub>4</sub>]<sup>-</sup> tetrahedron, but because of the extra positive charge two nearby Al sites are needed for Cu(II) to act as a charge compensator simultaneously. This is unlikely in ZSM-5 which is a high silica zeolite. These authors also point out that when the Al content of a zeolite is low, the copper ions are expected to be farther apart from each other, leading to unfavourable coulombic energy and unstable Cu(II).

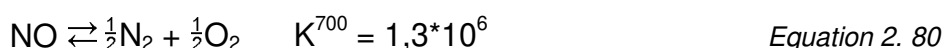
The activity of Cu/ZSM-5 is deteriorated by water vapour at higher temperatures. This fact has led to a decrease in interest for the Cu/ZSM-5 catalyst. According to Grinsted et al.<sup>55</sup> the activity loss is caused by dealumination. The removal of the Al ion from the zeolitic framework will result in the violation of the integrity of the exchanged transition-metal because the exchangeable cations are associated with the Al ions. Thereby, the dealumination can also destroy the Brønsted-acid sites. Ansell et al.<sup>56</sup> make the sintering of Cu and steam-induced dealumination responsible for the activity loss of Cu/ZSM-5. Amiridis et al.<sup>34</sup> continue by stating that

at high temperature and in the presence of water, Al migrates out of the zeolite framework structure. This in turn, leads to a loss in the catalytically active Cu ions bound to the Al sites in the zeolite. Catalyst deactivation becomes even more important if these catalysts are considered for potential applications in Diesel passenger cars where exhaust temperatures can be as high as 973 K, and the exhaust gas contains 10 - 14 % H<sub>2</sub>O and 25 - 50 ppm SO<sub>2</sub>. Adams et al.<sup>4</sup> add that Cu and other base metal modifiers become deactivated by formation of stable surface sulphates. They conclude that Cu zeolite catalysts may be practical for Diesels if sulphur is eliminated from Diesel fuel; a level of 5 ppm SO<sub>2</sub> in Diesel exhaust corresponds to ca. 75 ppm fuel sulphur.

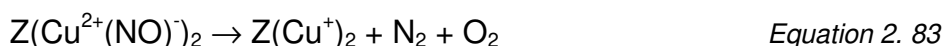
For this reason, Cu/ZSM-5 catalysts have been excluded from further investigation in this thesis.

#### 2. 5. 4. 1. 1. 2 The NO<sub>x</sub> Reduction Mechanism on Cu/ZSM-5

The first question that needs to be answered is: What happens where? There are at least two different types of active sites: Brønsted-acidic sites and the copper ions<sup>33</sup><sup>46</sup>. According to Grünert et al.<sup>46</sup> and Miyamoto et al.<sup>54</sup> the distance between these two sites might also be of importance. The direct decomposition of NO into the elements is favoured by thermodynamics<sup>57</sup>:



Therefore, Iwamoto et al. proposed that the reaction is essentially a decomposition reaction [cited in <sup>45</sup>] with the Cu<sup>+</sup> ions being the active sites:

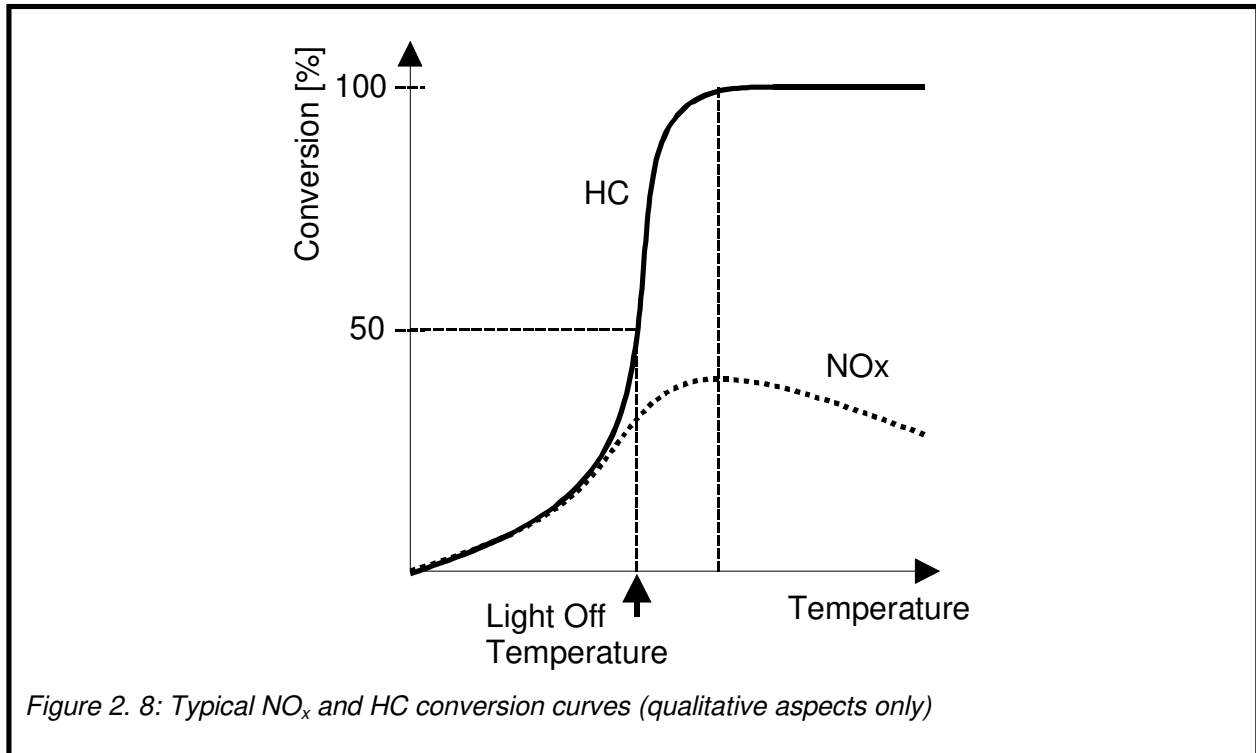


If this was in deed the case, a change of the NO concentration would have to have an effect on its conversion. According to Bennett et al.<sup>45</sup> and Ansell<sup>40</sup> et al. this is not the case under realistic Diesel conditions. Nevertheless, spectroscopic evidence for

the formation of a copper dinitrosyl complex,  $\text{Cu}(\text{NO})_2$ , has been reported<sup>39</sup> and the complex is believed to be an important intermediate. Shelef<sup>33</sup> points out that the mechanism proposed by Iwamoto would require that both copper ions are very close to each other. He states that this is not possible in zeolites with a high silica content. However, Shelef stands almost alone in the literature by postulating that the active sites for NO reduction are well isolated  $\text{Cu}^{2+}$  ions with square-planar co-ordination of oxygen atoms. Grünert et al.<sup>46</sup> have observed some Cu-Cu inter-atomic distances on Cu/ZSM-5 typical of those found in copper oxides. They say, it seems likely that low co-ordinated Cu ions along with Brønsted-acid sites are responsible for hydrocarbon activation, while multinuclear Cu-clusters can provide reactive oxygen and also promote NO activation. Burch et al.<sup>39</sup> suggest that copper ions are the active sites and the role of the zeolite is to provide the correct environment for the reaction. They also rule out the possibility of gas-phase reactions between NO and any molecular or radical hydrocarbon species.

Na/ZSM-5 is not capable of catalysing the decomposition of NO or  $\text{NO}_2$ , although, adsorption of both molecules takes place. Adelman et al.<sup>43</sup> have found that NO adsorption is favoured by co-adsorption of  $\text{NO}_2$ . This leads them to the assumption that NO and  $\text{NO}_2$  do not compete for the same adsorption sites, but have an attractive interaction with each other. They believe that inside the zeolite the molecules are forming a complex with the overall formula  $\text{N}_2\text{O}_3$ . Another important observation they made is that NO is oxidised to  $\text{NO}_2$  over Na/ZSM-5 in the presence of  $\text{O}_2$ . From isotope labelling experiments, Chang and co-workers<sup>109</sup> draw the conclusion that the  $\text{NO}_x$  decomposition activity of Cu/ZSM-5 zeolites is largely due to decomposition of  $\text{NO}_2$  and  $\text{N}_2\text{O}$ , not direct decomposition of NO. Decomposition of NO only becomes significant at high temperatures ( $>350^\circ\text{C}$ ). They point out that the formation of  $\text{N}_2\text{O}$  requires the active metal site to be capable of undergoing a redox cycle. For co-adsorption of NO and  $\text{O}_2$  they suggest the formation of a reaction intermediate which has the characteristic of adsorbed " $\text{N}_2\text{O}_4$ " on  $\text{Cu}^{2+}$ . The decomposition of  $\text{N}_2\text{O}$  over Cu/ZSM-5 has been investigated by Kapteijn et al.<sup>58</sup>. This decomposition comprises the oxidation of a  $\text{Cu}^+$  ion by a  $\text{N}_2\text{O}$  molecule and the subsequent removal of this oxygen ion by either a second  $\text{N}_2\text{O}$  molecule to form  $\text{N}_2$  and  $\text{O}_2$  or by a NO molecule to form  $\text{NO}_2$ .

The dependence of NO conversion on HC partial pressure has been reported by several authors<sup>40 41 45</sup>. It was found that NO conversion shows a nearly first order dependence with respect to propene. Two competing reactions cause the shape of a typical NO<sub>x</sub> conversion curve, shown in Figure 2. 9.



These are the NO reduction by hydrocarbons and the reaction of HC with oxygen to form CO<sub>2</sub> and H<sub>2</sub>O. The latter is favoured at higher temperatures. Certainly, the hydrocarbons consumed by the oxygen can no longer reduce nitrogen oxides. Hydrocarbons, though, have different degrees of selectivity towards promotion of NO reduction versus their consumption by O<sub>2</sub> in the presence of excess oxygen<sup>49</sup>. Selective reductants are: ethylene (C<sub>2</sub>H<sub>4</sub>), propene (C<sub>3</sub>H<sub>6</sub>), propane (C<sub>3</sub>H<sub>8</sub>), and butene (C<sub>4</sub>H<sub>8</sub>). Non-selective reductants are: methane (CH<sub>4</sub>), ethane (C<sub>2</sub>H<sub>6</sub>), CO, and H<sub>2</sub>. At the maximum of the NO<sub>x</sub> conversion curve the oxidation of the hydrocarbon reductant by O<sub>2</sub> starts to dominate over NO reduction, HC is now completely consumed. Cho<sup>49</sup> emphasises that a coincident raise in NO and HC conversion favours the selectivity towards NO reduction. Although the so called light-off temperature of C<sub>3</sub>H<sub>6</sub> is lower, i.e. conversion to O<sub>2</sub> and H<sub>2</sub>O onsets earlier, than that of C<sub>2</sub>H<sub>4</sub>, this is not necessarily an advantage. Most of the reductant has already

been oxidised by the excess oxygen before the temperature is high enough to overcome the activation energy for the NO decomposition. Since the conversion of NO is dependent on the concentration of the hydrocarbon, an early light-off of the hydrocarbon conversion deteriorates the selectivity of NO reduction.

All authors of the current de-NO<sub>x</sub>-ing literature are in agreement, that the presence of oxygen is crucial to the process. Chajar et al.<sup>41</sup> found, that in the absence of oxygen (C<sub>3</sub>H<sub>6</sub>-NO-He mixture) the propene molecule is not a good reductant towards NO. Most authors report, that the optimum oxygen content lies between 2 and 5 vol.-%<sup>39-45 37</sup>. A higher oxygen content favours excessive hydrocarbon oxidation. Burch et al.<sup>39</sup> postulate that the role of oxygen is to prevent over reduction of Cu<sup>+</sup> to inactive Cu<sup>0</sup>. Ansell et al.<sup>40</sup> on the other hand believe that the principal promoting role of oxygen is to activate the NO into the Cu-NO<sub>2</sub> state.

A total contradiction between Burch et al. and Ansell et al. exists in the question whether a carbonaceous deposit of some sort is present on the catalyst. While Burch et al. deny this, Ansell et al. speak strongly for it. Burch did not observe any indication of continued activity for NO reduction after the supply of reductant has been switched of from the model gas mixture. They report that when exposed to NO a pre-coked catalyst shows no reduction activity. Ansell et al. on the other hand, report that a pre-coked catalyst shows high activity in spite of the absence of propene in the gas phase. They state that deposited coke is the active reductant in lean NO<sub>x</sub> catalysis and that this reaction intermediate is long lived. Ansell et al. believe that one function of the zeolite is the facilitation of coke deposition on the Brønsted-acidic sites. The quarrel between the two research groups remains up to now unsolved. Additionally, the work of Grünert et al.<sup>46</sup> highlights a long-lived organo-nitrogen species which they identified by infrared spectroscopy as a nitrile. The nitrile decomposes in the presence of oxygen selectively to N<sub>2</sub> and is their intermediate candidate.

The lean NO<sub>x</sub> mechanism as proposed by Ansell et al.<sup>40</sup> is summarised as follows: NO is activated by an oxygenated copper ion site to a Cu-NO<sub>2</sub> intermediate. The concentration of the Cu-NO<sub>2</sub> intermediate species will be critically dependent on the



presence of adsorbed oxygen on the active copper sites. This "NO<sub>2</sub>" species reacts with adjacent coke present on the ZSM-5. The reactive intermediates need to be in very close proximity in order for the reductive step to occur. When the oxygen atoms on the active copper sites recombine and desorb as O<sub>2</sub>, the reaction probability is reduced as the concentration of the oxygen atoms decreases. There is no indication for any special shape selective role for the zeolite.

Burch et al.<sup>39</sup> have introduced the following mechanism: In the presence of oxygen, the copper ion sites will be found as Cu-O<sub>(Ad)</sub>. To activate this site, the adsorbed oxygen atom must be removed. This is achieved by the reductants. After that, it is a simple matter of statistical probability whether the activated copper site is approached by NO or an oxygen molecule. In the latter case the active site is destroyed until the oxygen is removed again. A small reductant molecule (H<sub>2</sub>, CO) is only able to eliminate a single oxygen atom. This results in a high probability that an adjacent gas-phase oxygen molecule dissociatively adsorbs at the newly created active site and poisons it once more. But, if the reductant is a larger molecule, as for instance C<sub>3</sub>H<sub>6</sub> which can eliminate 9 oxygen atoms, the probability of achieving the initial adsorption of an NO molecule at the activated site is greatly enhanced. The role of the hydrocarbon is therefore to increase the rate of removal of surface oxygen, since the rate of reaction is controlled by surface vacancies. After NO adsorption has occurred the arrival of a second NO molecule results in the formation of a dinitrosyl species which by inversion converts into gaseous N<sub>2</sub>O and O<sub>(Ad)</sub>. The N<sub>2</sub>O is decomposed to N<sub>2</sub> at another copper ion site and the catalytic cycle is complete.

#### *2. 5. 4. 1. 1. 3 Other Metal/Zeolites*

Activity of Pt/ZSM-5 for de-NO<sub>x</sub>-ing has been reported by Hirabayashi et al.<sup>60</sup> and Iwamoto et al.<sup>59</sup>. It has been suggested<sup>34</sup> that Pt exists in these zeolites in the form of fine metallic particles. Since the size of these particles was measured to be larger than the pore size of the supporting ZSM-5 both in the fresh and aged catalyst, their presence is believed to be limited to the external surface of the zeolite. Pt containing zeolites have been found to be the most active among group VIII metals followed by Rh containing catalysts. Pt/ZSM-5 has been found to be more stable than Cu/ZSM-5

even in the presence of water. The former's activity on the other hand, was lower than the latter's. Hirabayashi et al.<sup>60</sup> used platinum and iron in addition to copper with ZSM-5 and Mordenite. Mordenite, Ferrierite, and USY are different types of zeolites which are described in detail by Kripylo et al.<sup>47</sup> and Dyer<sup>61</sup>. Li et al.<sup>44</sup> and Cowan et al.<sup>62</sup> both investigated a Co/ZSM-5 catalyst. Gallium ion-exchanged ZSM-5 catalysts were studied by Yogo et al.<sup>42 63</sup>.

#### 2. 5. 4. 1. 2 Alumina ( $Al_2O_3$ )

##### 2. 5. 4. 1. 2. 1 Chemical Aspects of Alumina

The alumina that is used in adsorption and catalytic processes is usually the  $\gamma$ -form. Actually the term  $\gamma$ - $Al_2O_3$  refers to a single crystalline phase of  $Al_2O_3$ . It has the spinel structure with vacancies. Aluminium ions are placed in  $21\frac{1}{3}$  of the sixteen octahedral and eight tetrahedral gaps<sup>64</sup>.  $\gamma$ -alumina is produced by dehydrogenation of Hydrargillit,  $\gamma$ - $Al(OH)_3$ , or Böhmit,  $\gamma$ - $AlO(OH)$ , at low temperature ( $<720$  K). The  $\gamma$ - $Al_2O_3$  modification is the basis for many so called activated aluminas. By partial dehydration crystal intermediate modifications are prepared ( $\gamma'$ ,  $\delta$ ,  $\zeta$ ,  $\eta$ ,  $\theta$ ,  $\rho$ ,  $\chi$ ). This mixture of microcrystalline forms is falsely also named  $\gamma$ - $Al_2O_3$  in the literature. In this thesis, the terms  $\gamma$ - $Al_2O_3$  and alumina always refer to the activated mixture. Upon calcination above 1300 K  $\gamma$ - $Al_2O_3$  irreversibly changes its modification to  $\alpha$ - $Al_2O_3$ . This modification is more compact and has a smaller BET surface area than the  $\gamma$ -form. It is also called "dead-burned".

$\gamma$ - $Al_2O_3$  is insoluble in water, but soluble in strong acids and bases. It is hygroscopic and has immense importance in adsorption processes. The BET surface area of the alumina is strongly dependent on the dehydrogenation method. The surface is also amphoteric, with acidic and basic sites of different strengths and concentrations<sup>65</sup>. The acidic sites are coordinatively unsaturated  $Al^{3+}$  ions and "acidic" hydroxyl groups. The basic sites are  $O^{2-}$  ions and basic hydroxyls.

Because of its porous structure,  $\gamma$ - $Al_2O_3$  can be impregnated with metal ions. The catalysts are prepared by impregnating the  $\gamma$ - $Al_2O_3$  with solutions of platinum salts, drying, and calcining. The exact preparation methods are usually proprietary.

### 2. 5. 4. 1. 2. 2 NO<sub>x</sub> Reduction with Alumina

Catalytic activity of  $\gamma$ -alumina for NO reduction has been reported in several papers. The observations are summarised in Table 2. 7. Kintaichi et al.<sup>66</sup>, Subramanian et al.<sup>68</sup>, and Hamada et al.<sup>70</sup> contribute the NO<sub>x</sub> reduction activity of Al<sub>2</sub>O<sub>3</sub> to its acidic sites. It is well known that the acidity of  $\gamma$ -Al<sub>2</sub>O<sub>3</sub> is able to activate hydrocarbons by converting them to carbenium ions<sup>47</sup>. Subramanian suggests that these activated hydrocarbons react with NO<sub>2</sub> which has been formed from oxidation of NO. Truex et al.<sup>32</sup> remark that direct NO decomposition over acidic catalysts under oxidising conditions does not take place.

Alumina Surface [m <sup>2</sup> /g]	Nitrogen Oxide	Reducing Agent	HC <sub>1</sub> /NO <sub>x</sub> Ratio	Gas Composition	Maximum Conversion of NO <sub>x</sub> to N <sub>2</sub> + O <sub>2</sub> [%]	Temperature at Maximum NO <sub>x</sub> Conversion [°C]	Reference
285	NO	C <sub>3</sub> H <sub>8</sub>	1:1	Synthetic 10% O <sub>2</sub>	32	500	<sup>66</sup>
285	NO	C <sub>3</sub> H <sub>8</sub>	3:1	Synthetic 10% O <sub>2</sub>	97	500	66
?	NO	C <sub>3</sub> H <sub>8</sub>	1:1	Synthetic 10% O <sub>2</sub>	35	500	<sup>67</sup>
?	NO <sub>2</sub>	C <sub>3</sub> H <sub>8</sub>	1:1	Synthetic 10% O <sub>2</sub>	36	500	67
100	NO	C <sub>3</sub> H <sub>8</sub>	3:1	Synthetic 4% O <sub>2</sub>	80	600	<sup>68</sup>
100	NO	C <sub>3</sub> H <sub>6</sub>	3:1	Synthetic 4% O <sub>2</sub>	95	600	68
100	NO	iso-octane	8:1	Synthetic 4% O <sub>2</sub>	80	600	68
190	NO	C <sub>3</sub> H <sub>6</sub>	3:1	Synthetic 10% O <sub>2</sub>	60	500	<sup>69</sup>
190	NO	CH <sub>3</sub> OH	1:1	Synthetic 10% O <sub>2</sub>	55	350	69
190	NO	CH <sub>3</sub> OH	2:1	Synthetic 10% O <sub>2</sub>	78	400	69
190	NO	C <sub>2</sub> H <sub>5</sub> OH	4:1	Synthetic 10% O <sub>2</sub>	76	350	69
190	NO	(CH <sub>3</sub> ) <sub>2</sub> C O	2:1	Synthetic 10% O <sub>2</sub>	75	400	69
130	NO	CH <sub>3</sub> OH added to exhaust	3:1	Diesel	75	420	69
?	NO	C <sub>3</sub> H <sub>8</sub>	2:1	Synthetic 10% O <sub>2</sub>	50	500	<sup>70</sup>

Table 2. 7: Results of several researchers using Al<sub>2</sub>O<sub>3</sub> as catalyst for NO<sub>x</sub> reduction

It should be pointed out that from the authors point of view some of these values seem unrealistically high. As will be shown in the "Results and Discussions" chapter,

maximum NO<sub>x</sub> conversion values with pure alumina in this thesis did not exceed 60% or 30% in the absence or presence of water, respectively.

It is important to notice that in all cases, NO reduction could be achieved in spite of strongly oxidising environments. On the contrary, oxygen was identified as a promoter of the NO<sub>x</sub> reduction reaction by Sasaki<sup>67</sup>. Hamada<sup>70</sup> adds that NO conversion to N<sub>2</sub> increased with oxygen concentration indicating an oxygen promotional effect. This result, in combination with the observation that NO<sub>2</sub> is reduced more easily than NO over  $\gamma$ -Al<sub>2</sub>O<sub>3</sub> catalysts, led to the speculation that the role of oxygen is to react with NO to form NO<sub>2</sub><sup>68</sup>. However, Hamada<sup>70</sup> states that at elevated temperatures such as 600°C NO was reduced to N<sub>2</sub> by direct reaction with propane even in the absence of O<sub>2</sub>.

It shall be mentioned that Subramanian's<sup>68</sup> group posited a homogeneous gas phase reaction between NO and an unspecified HC resulting in 25% NO conversion at 600°C without catalyst! Nowhere else in literature has a similar observation been reported. On the contrary, without a catalyst Sasaki and co-workers<sup>67</sup> did not observe any conversion of NO using C<sub>3</sub>H<sub>8</sub>. This was also verified by Kintaichi et al.<sup>66</sup>. Kintaichi et al. point out that the selective reduction of NO is closely related to the extent of propane oxidation. Propane is a selective reductant in the sense that it reduces NO in spite of having the opportunity to oxidise immediately to CO<sub>2</sub> and H<sub>2</sub>O because of the large oxygen excess. However, at 600°C, propane was completely oxidised and NO conversion declined. In a gas feed which initially only contained C<sub>3</sub>H<sub>8</sub> and oxygen, propane oxidation was enhanced by adding small amounts of NO or NO<sub>2</sub><sup>67</sup>. NO<sub>2</sub> was more efficient in doing so than NO.

In the absence of oxygen, Sasaki et al.<sup>67</sup> observed almost complete reduction of NO to N<sub>2</sub> or N<sub>2</sub>O by CO at 500°C. The conversion became almost zero in the presence of 10% oxygen. The same observation has been made by them using NO<sub>2</sub> with 88% reduction to N<sub>2</sub> and N<sub>2</sub>O at 600°C. They posit that CO does not serve as a selective NO<sub>x</sub> reductant in an oxidising atmosphere. Further, they concluded that NO<sub>2</sub> is reduced more easily than NO under similar conditions. Subramanian et al.<sup>68</sup> likewise observed no NO conversion when a NO-O<sub>2</sub>-CO-H<sub>2</sub> feed gas mixture was flowed over Al<sub>2</sub>O<sub>3</sub>. Thus, they verify that H<sub>2</sub> and CO are non-selective regarding the reduction of NO over Al<sub>2</sub>O<sub>3</sub>. Sasaki et al.<sup>67</sup> point out that the gas phase oxidation of CO to CO<sub>2</sub> does not occur at temperatures below 600°C.

Subramanian et al.<sup>68</sup> even investigated the effect of feed gas HC concentration and SV on removal of NO from NO-HC-O<sub>2</sub>. They noticed that the NO conversion increases with an increase in HC concentration and a decrease in the SV. C<sub>3</sub>H<sub>8</sub> and C<sub>3</sub>H<sub>6</sub> provided similar levels of NO conversion over the ranges of SV investigated. The HC conversion at a given SV was generally lower when C<sub>3</sub>H<sub>8</sub> was used as a reductant.

Tsuchida et al.<sup>69</sup> studied the effect of alkali and alkali-earth metal in alumina for the reduction of NO by methanol. They realised that all base metal doped aluminas showed less NO conversion efficiency than the pure Al<sub>2</sub>O<sub>3</sub>.

Two compounds significantly deteriorate the NO reduction performance of Al<sub>2</sub>O<sub>3</sub>, namely SO<sub>2</sub> and water. Hamada<sup>70</sup> reports that the treatment of an alumina catalyst with sulphuric acid decreased both NO conversion to N<sub>2</sub> and propane conversion to CO<sub>x</sub>. This effect was attributed to a change in oxidation ability of the catalyst<sup>71</sup>. Based on their finding that alumina was deactivated by Diesel Exhaust, Tsuchida et al.<sup>69</sup> suggested that this deactivation is correlated to the co-existing SO<sub>2</sub> in Diesel exhaust. They assume that the deactivation was caused by the accumulation of sulphur on the surface of the Al<sub>2</sub>O<sub>3</sub>. This accumulation is assumed to be caused by the oxidation of SO<sub>2</sub> to SO<sub>3</sub>. The SO<sub>3</sub> showed a high adsorption ability. Subramanian et al.<sup>68</sup> verify that the addition of SO<sub>2</sub> to the feed gas leads to a decrease in NO conversion over the entire SV range investigated when C<sub>3</sub>H<sub>8</sub> is used as a reductant. Although lower NO conversions are observed in the presence of SO<sub>2</sub>, the activity quickly returns when the SO<sub>2</sub> flow is switched off. They suggest that SO<sub>2</sub> competes with NO for the adsorption sites. When C<sub>3</sub>H<sub>6</sub> is used as a reductant, the addition of SO<sub>2</sub> to the feed gas does not appear to lead to a significant decrease in NO conversion.

The effect of water vapour was closely investigated by Hamada<sup>70</sup>. He found that NO conversion was decreased by the presence of water vapour especially at low temperatures and also observed a decrease in HC conversion. The original activity was resumed after removing the water vapour from the feed gas. This leads him to the assumption that the decrease in NO conversion was not due to catalyst deactivation but due to reaction inhibition. The effect of water vapour is ascribed to its function as a poison for the acid site of alumina responsible for some steps of the overall reaction. Nevertheless, Subramanian et al.<sup>68</sup> and Kintaichi et al.<sup>66</sup> both report

that the decline in activity of  $\text{Al}_2\text{O}_3$  is not as dramatic as for zeolite systems when water is present in the gas mixture. Furthermore, the activity of  $\gamma\text{-Al}_2\text{O}_3$  catalysts shows higher thermostability. The thermostability can be even more enhanced by adding additives like barium or lanthanum, or by using special preparation techniques<sup>72</sup>.

#### 2. 5. 4. 1. 2. 3 Pt/ $\text{Al}_2\text{O}_3$

Since the durability of the Cu/ZSM-5 system is unacceptable for Diesel vehicle applications, an alternative method had to be found to achieve  $\text{NO}_x$  reduction under oxidising conditions. It is well known that platinum is an active catalyst for NO decomposition<sup>73</sup>.

The structure of an ultra-dispersed Pt/ $\text{Al}_2\text{O}_3$  catalyst has been investigated by Nellist et al.<sup>74</sup>. They infer that the Pt configuration is somewhat constrained by the  $\text{Al}_2\text{O}_3$  support surface. They suggest possible configurations with the Pt atoms in sites doubly coordinated by the oxygen ions of the alumina and with Pt-O distances of 0,269 nm. It shall be mentioned that these ultrahigh dispersions are rarely used in automobile catalysts. The electronic properties of such catalysts are influenced by strong metal support interactions (SMSI). Further, it must be questioned whether these platinum particles consisting of one to three Pt atoms are still a metal or rather an oxide.

Vaarkamp et al.<sup>80</sup> studied the structural, electronic, and catalytic properties of Pt/ $\text{Al}_2\text{O}_3$  catalysts after reduction at 300 and 450°C. They observed that the reduction temperature had a significant effect on the local structure around the platinum in Pt/ $\gamma\text{-Al}_2\text{O}_3$  catalysts. From Electronic X-Ray Adsorption Fourier Spectroscopy (EXAFS) studies they inferred that the platinum atoms in the catalyst had more holes in the d-band than did bulk platinum and that the number of holes decreased with increasing reduction temperature. After reduction at 300°C, the average platinum particle contained 11 atoms, resulting in a coordination number of 4,8. This corresponds to a spherical particle. The Pt-Pt distance was 2.76 Å which is equivalent to that of platinum foil. After reduction at 450°C the Pt-Pt distance decreased to 2.72 Å. Reduction at 450°C lowered the Pt-Pt coordination number from 4,8 to 3,8. This decrease indicates either a decrease in the platinum particle size due to a breakup of the particles during high temperature reduction or a change

in the platinum particle morphology from three-dimensional to rafts bringing about a lower number of nearest neighbours for the platinum atoms. After reduction at 300°C, the distance between platinum atoms and the support oxygen atoms is 2,66 Å which is longer than the radii of Pt (metallic, 1,39 Å) and O<sup>2-</sup> (covalent, 0,73 Å). Vaarkamp et al. propose that the long Pt-O distance originates from (neutral) hydrogen atoms located between the metal particles and the support. The spacing of the O atoms in Al<sub>2</sub>O<sub>3</sub> is less than the spacing of the Pt atoms in bulk platinum, and an epitaxial adaptation of the platinum to the alumina therefore requires a shortening of the Pt-Pt distance, as was actually observed.

The activity of Pt/Al<sub>2</sub>O<sub>3</sub> for NO<sub>x</sub> reduction has been investigated intensively by many research groups<sup>4 9 13 14 19 24 34 56 67 70 72 75-93</sup>.

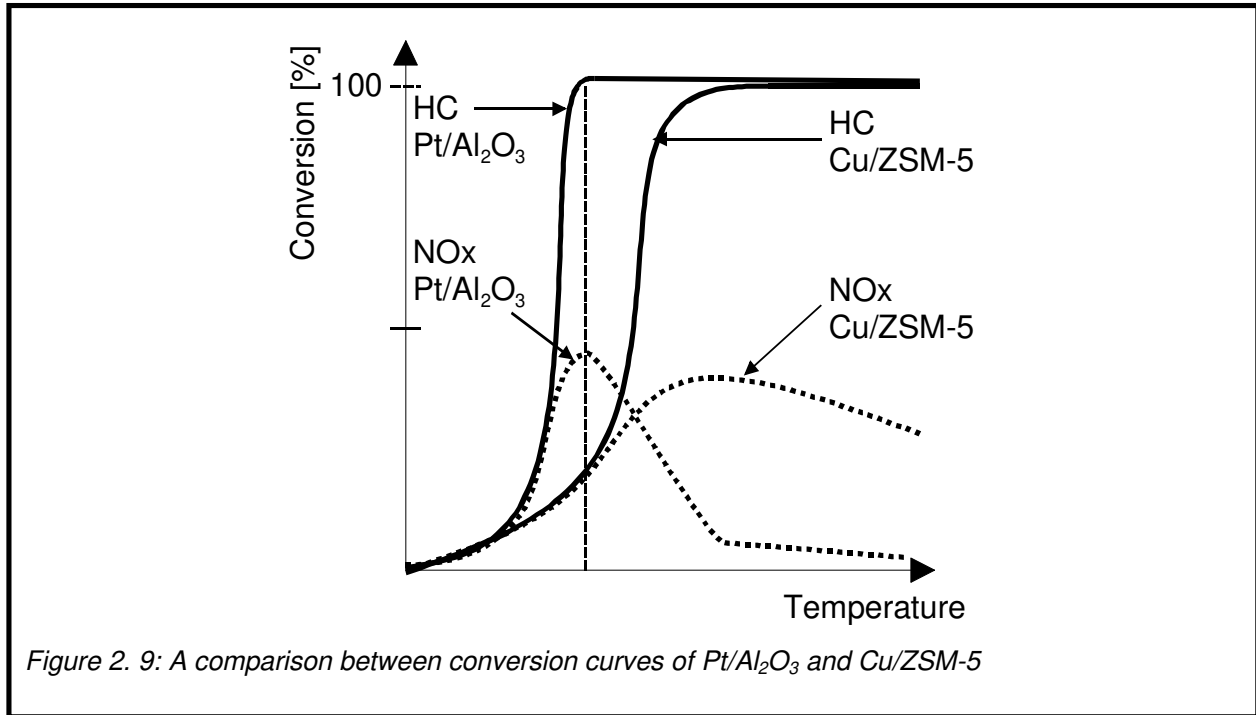
All these groups have observed that Pt/Al<sub>2</sub>O<sub>3</sub> reduces NO<sub>x</sub> from Diesel exhaust gases even in the presence of H<sub>2</sub>O and oxygen. Additionally, the Pt/Al<sub>2</sub>O<sub>3</sub> catalysts proved satisfying durability. This makes this system one of the most interesting for catalyst manufacturers. A remaining challenge is the observation that some of the nitrogen oxides are not converted to N<sub>2</sub> and O<sub>2</sub>, but that N<sub>2</sub>O is also a product. This has long been neglected since the detection of N<sub>2</sub>O with standard NO<sub>x</sub> analysers, based on the chemiluminescence method, is not possible. N<sub>2</sub>O is infamous for being a contributor to the global warming by the green house effect as well as for being an ozone depletion agent.

A direct comparison of the conversions obtained by these groups seems inadequate since there are too many varying parameters of testing as well as catalyst formulations.

#### *2. 5. 4. 1. 2. 4 The NO<sub>x</sub> Reduction Mechanism on Pt/Al<sub>2</sub>O<sub>3</sub>*

The typical conversion curves for HC and NO<sub>x</sub> differ from those of Cu/ZSM-5, Figure 2. 10. Light-off of HC and NO<sub>x</sub> occurs earlier on the Pt/Al<sub>2</sub>O<sub>3</sub> catalyst but 100% HC conversion coincides with maximum NO<sub>x</sub> conversion as observed for the Cu/ZSM-5 system. The Pt/Al<sub>2</sub>O<sub>3</sub> catalyst does not reduce NO<sub>x</sub> very well at higher temperatures. Additionally, the conversion window for the Pt/Al<sub>2</sub>O<sub>3</sub> catalyst is very narrow. These latter issues offer potential for improvement. The NO<sub>x</sub> conversion has four features:

1. temperature where  $\text{NO}_x$  starts to light off
2. temperature of maximum  $\text{NO}_x$  conversion
3. value of maximum  $\text{NO}_x$  conversion
4. width of  $\text{NO}_x$  conversion window



A lot of research groups have tried to investigate the  $\text{NO}_x$  reduction mechanism on  $\text{Pt}/\text{Al}_2\text{O}_3$ . It is widely established that hydrocarbons are involved in this mechanism. Several possibilities have been proposed:

1. oxidation of  $\text{NO}$  to  $\text{NO}_2$  which then reacts with the hydrocarbon
2. formation of an oxidised hydrocarbon intermediate
3. reduction of the metal surface followed by  $\text{NO}$  decomposition on the reduced surface
4. formation of an isocyanate surface species as an intermediate

On a platinum catalyst the kinetics of HC oxidation,  $\text{NO}$  reduction and  $\text{NO}$  oxidation are strongly dependent on the type of HC. Bourges et al.<sup>86</sup> state that these reactions occur at lower temperature with long chain alkanes than with olefins and that these alkanes lead to a higher  $\text{N}_2\text{O}$  selectivity than unsaturated molecules. They found that Pt is very selective for  $\text{N}_2\text{O}$  formation in the presence of decane and have investigated several HCs regarding their selectivities towards  $\text{N}_2\text{O}$  and yield in  $\text{N}_2$ , Table 2. 8.



	N <sub>2</sub> O Selectivity at Maximum NO <sub>x</sub> Conversion [%]	N <sub>2</sub> Yield at the Maximum NO <sub>x</sub> Conversion [%]	Temperature at Maximum NO <sub>x</sub> Conversion [°C]	THC(50) [°C]
n - octane	80	10	220	221
n - decane	73	16	217	218
decaline	75	9	230	222
dodecane	65	10	260	290
ethylene	37	15	305	302
propylene	40	15	311	320
toluene	38	24	295	281
xylene	65	9	288	285

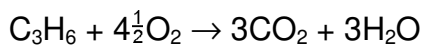
Table 2. 8: N<sub>2</sub>O selectivities of several HCs<sup>86</sup>

Bourges et al.<sup>86</sup> also observed that ethylene is more strongly adsorbed than n-decane and shows inhibiting effects both on HC oxidation and NO reduction. They add that strongly adsorbed HCs induce an inhibiting effect on NO reduction and on HC oxidation. The HC covering of metal surface area is high so that the reaction of NO reduction, HC oxidation, and NO oxidation are shifted to higher temperatures. Moreover, the N<sub>2</sub> selectivity is higher with olefins than with long chain alkanes.

Wahl et al.<sup>90</sup> tested the selectivity of several HCs towards NO reduction against oxidation to CO<sub>2</sub>. They report that n-decane was the most selective reductant tested, succeeding even the selectivity of propene. An increasing number of side chains decreases the selectivity. Except for organic acids, all oxidised HCs showed good selectivity while PAHs were very unselective. According to Adams et al.<sup>4</sup> HC oxidation probably involves parallel competing reactions, the fastest reaction dominates the products. These competing reactions are HC reaction to CO<sub>2</sub> and HC forming an activated complex or site required for NO<sub>x</sub> reduction. The nature of the HC under reaction conditions has been discussed controversially. Zhang et al.<sup>75</sup> merely speak of an activated hydrocarbon, while Obuchi<sup>78</sup> and Sasaki<sup>67</sup> believe that the hydrocarbon is partially oxidised.

There is agreement among Zhang<sup>75</sup>, Sasaki<sup>67</sup>, and Obuchi<sup>78</sup> that the role of oxygen is the activation of the hydrocarbons and the oxidation of NO to NO<sub>2</sub>. Bourges et al.<sup>86</sup> mention that although NO<sub>2</sub> can be formed at low temperatures on platinum, it was not detected by them in the presence of a reductant. They assumed that the sites required for NO oxidation can be blocked by the reductant or that NO<sub>2</sub> adsorbed species are reduced in the presence of CO and HC before their desorption. Thus, the absence of NO<sub>2</sub> in the gas phase does not necessarily mean that it is not present

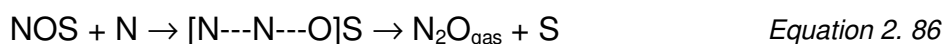
as adsorbed species. They add that NO<sub>2</sub> reduction by HC in the gas phase is negligible. If NO<sub>2</sub> is an intermediate in the NO reduction mechanism, it could participate only as adsorbed species. Burch et al.<sup>76</sup> presume that the activated carbon species present on the catalyst's surface are molecular fragments of propene. This is confirmed by the fact that the iso-propyl-carbenium ion is the smallest stable carbenium ion found in catalytic cracking processes<sup>47</sup>. According to Zhang<sup>75</sup>, Sasaki<sup>67</sup>, and Obuchi<sup>78</sup>, the activated carbon reacts directly with NO or NO<sub>2</sub>. Burch<sup>76</sup> observed that over a completely oxidised catalyst surface most of the NO passed over it adsorbed and desorbed without dissociation. Over a completely reduced surface no molecular NO desorbed, instead N<sub>2</sub> and N<sub>2</sub>O were detected. This led him to the conclusion that reduced platinum sites dissociate NO while oxidised Pt sites do not. Additionally, he stated that over a completely reduced Pt/Al<sub>2</sub>O<sub>3</sub> surface very little of the NO desorbed as N<sub>2</sub>O since excessive NO dissociation took place on the reduced Pt sites leading to N<sub>2</sub> as the principal product. With propene and NO present in his feed gas, Burch draw the conclusion that the HC is either adjacent or at least very close to the platinum particles since he observed CO<sub>2</sub> formation during the decomposition of NO. The latter would imply that the hydrocarbon is situated on the washcoat. Since the alumina washcoat is believed to activate the hydrocarbons this seemed convincing. In 1994, Burch<sup>76</sup> published a mechanism for the reduction of NO by propene over a Pt/Al<sub>2</sub>O<sub>3</sub> catalyst. He assumed that under realistic Diesel conditions, platinum is in the oxidised state (Pt-O). This oxygen is removed by a hydrocarbon adjacent to the Pt-site. The combustion of each propene molecule via



*Equation 2. 84*

removes 9 oxygen atoms from the platinum surface. The combustion of a CO molecule would only generate one active Pt-site. Yet, at least two adjacent active sites are required for the decomposition of NO into the elements. Oxygen and NO compete for the reduced platinum sites. If dissociative reoxidation by O<sub>2</sub> occurs, the reduction by the hydrocarbons has been unsuccessful. But if NO is adsorbed on these activated sites, the dissociation into adsorbed N and O can follow. In a paper dealing with the adsorbate assisted NO decomposition<sup>82</sup> Burch states that the

observed rapid assisted NO decomposition implies that the amount of the Pt surface required to be in the reduced form is very much less than in the case of unassisted NO dissociation. With adsorbate assistance for NO splitting the competition between oxygen (in vast excess) and NO for the reduced Pt sites becomes rather unimportant. After the NO dissociation has taken place on the reduced sites there are two principal ways in which the N-adatoms can be removed<sup>76</sup>: first, by reaction between an adsorbed NO molecule and an adsorbed N atom to form N<sub>2</sub>O. This usually happens at lower temperatures since the mobility of the NO molecules is higher at these temperatures than that of the N atoms. Second, at higher temperatures, the concentration of adsorbed N atoms is higher and their mobility as well. Both factors favour now the N-N recombination to generate molecular N<sub>2</sub>. Burch et al.<sup>82</sup> propose that N<sub>2</sub> and N<sub>2</sub>O are formed from a common intermediate and that Pt is a poor NO<sub>2</sub> decomposition catalyst when HCs are used as reductants. They base this on the fact that the reactions



are calculated to have lower activation energy than the reaction



S denotes an adsorption site. The former reactions are expected to be favoured when undissociated NO is present on the catalyst. N<sub>2</sub>O and N<sub>2</sub> formation may occur at the interface between oxidised and reduced Pt sites with an N atom on the reduced site combining with an NO on a neighbouring oxidised site. Zhang<sup>75</sup> explains the formation of N<sub>2</sub>O which is always observed on Pt/Al<sub>2</sub>O<sub>3</sub> under oxidising conditions by migration of adsorbed NO on the platinum. A (NO)<sub>2</sub>-dimer is produced in this way which leads to the formation of N<sub>2</sub>O and adsorbed oxygen. He also reports that the properties of the support seem to affect the selectivity towards N<sub>2</sub>O. Bourges et al.<sup>86</sup> point out that on a monolith NO reduction to N<sub>2</sub> and N<sub>2</sub>O occurs at the inlet of the monolith while NO oxidation to NO<sub>2</sub> occurs at the outlet. The reason for this is that the concentration of the reductant decreases strongly over the length

of the catalyst. Vice versa, the amount of adsorbed oxygen rises from catalyst inlet to catalyst outlet. With an increase of the temperature<sup>76</sup>, the catalyst turns into an oxidation catalyst which immediately burns off all hydrocarbons. In Burch's<sup>76</sup> opinion the role of the hydrocarbon is to reduce oxidised platinum sites (Pt-O) to activated platinum (Pt<sup>0</sup>) while the direct reduction of NO<sub>x</sub> by propene plays only a minor role in the overall mechanism. However, he pointed out that the carbon on the catalyst's surface is able to break the NO bond and that isolated carbon atoms are very active at binding adsorbed NO molecules which can lead to the formation of CO and adsorbed N.

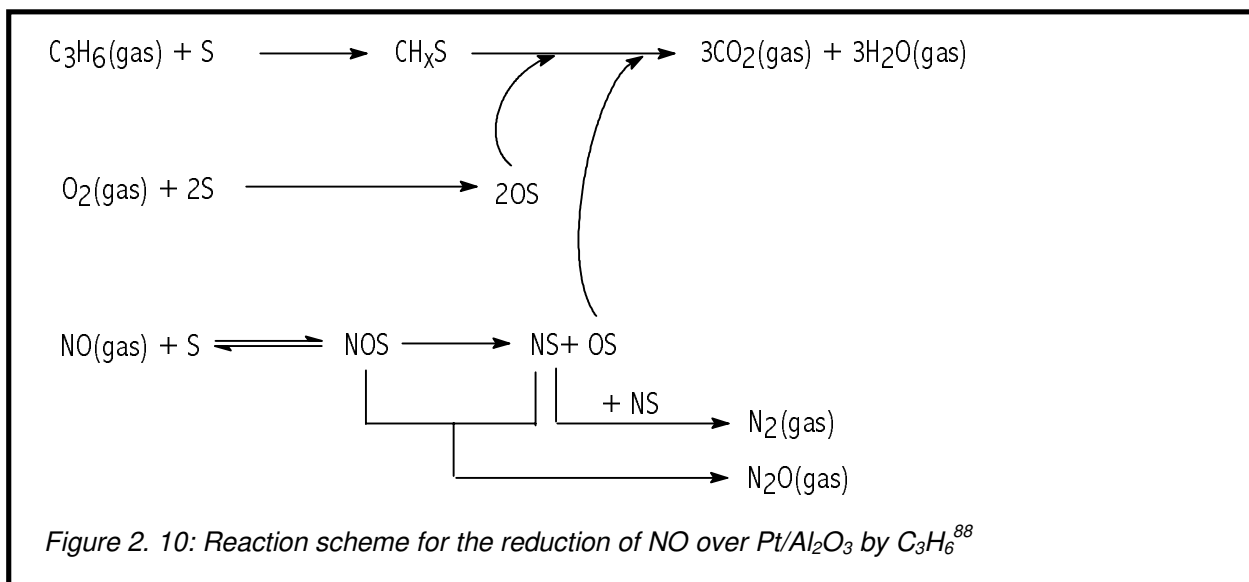
In three later publications, Burch et al.<sup>81 83 88</sup> discussed the differences between alkanes and olefins in the reduction of NO<sub>x</sub> over Pt/Al<sub>2</sub>O<sub>3</sub> under oxidising conditions. They found strong indications that the NO<sub>x</sub> reduction mechanism is different depending on the reductant used. Their different observations for the C<sub>3</sub>H<sub>6</sub>-NO-O<sub>2</sub> and C<sub>3</sub>H<sub>8</sub>-NO-O<sub>2</sub> reactions are summarised in Table 2. 9.

Propene	Propane
Conversion of C <sub>3</sub> H <sub>6</sub> and NO to N <sub>2</sub> and N <sub>2</sub> O both start at the same temperature and increase with increasing temperature until 100% HC conversion is reached	HC light-off occurs at a higher T and is much less steep compared to the C <sub>3</sub> H <sub>6</sub> -NO-O <sub>2</sub> reaction
NO <sub>2</sub> formation begins at the same T as maximum NO <sub>x</sub> conversion	Conversion of NO to NO <sub>2</sub> begins at lower T and occurs well before 100% HC conversion is reached
Maximum NO <sub>x</sub> conversion occurs at 100% HC conversion	Maximum NO <sub>x</sub> conversion is not coincident with 100% HC conversion being reached
	Maximum NO <sub>x</sub> conversion is very much smaller than in the C <sub>3</sub> H <sub>6</sub> -NO-O <sub>2</sub> reaction
HC conversion rate increases strongly with increasing O <sub>2</sub> concentration	HC conversion is inhibited by oxygen at lower O <sub>2</sub> concentrations, but independent of O <sub>2</sub> concentration at higher O <sub>2</sub> concentration
HC conversion is inhibited by NO	HC conversion is only slightly inhibited by NO
HC conversion is zero order in C <sub>3</sub> H <sub>6</sub>	HC conversion is at least 1 <sup>st</sup> order in C <sub>3</sub> H <sub>8</sub>
Kinetics of NO <sub>x</sub> removal are very similar to those of HC oxidation	Kinetics of NO <sub>x</sub> removal are very different from those of HC oxidation

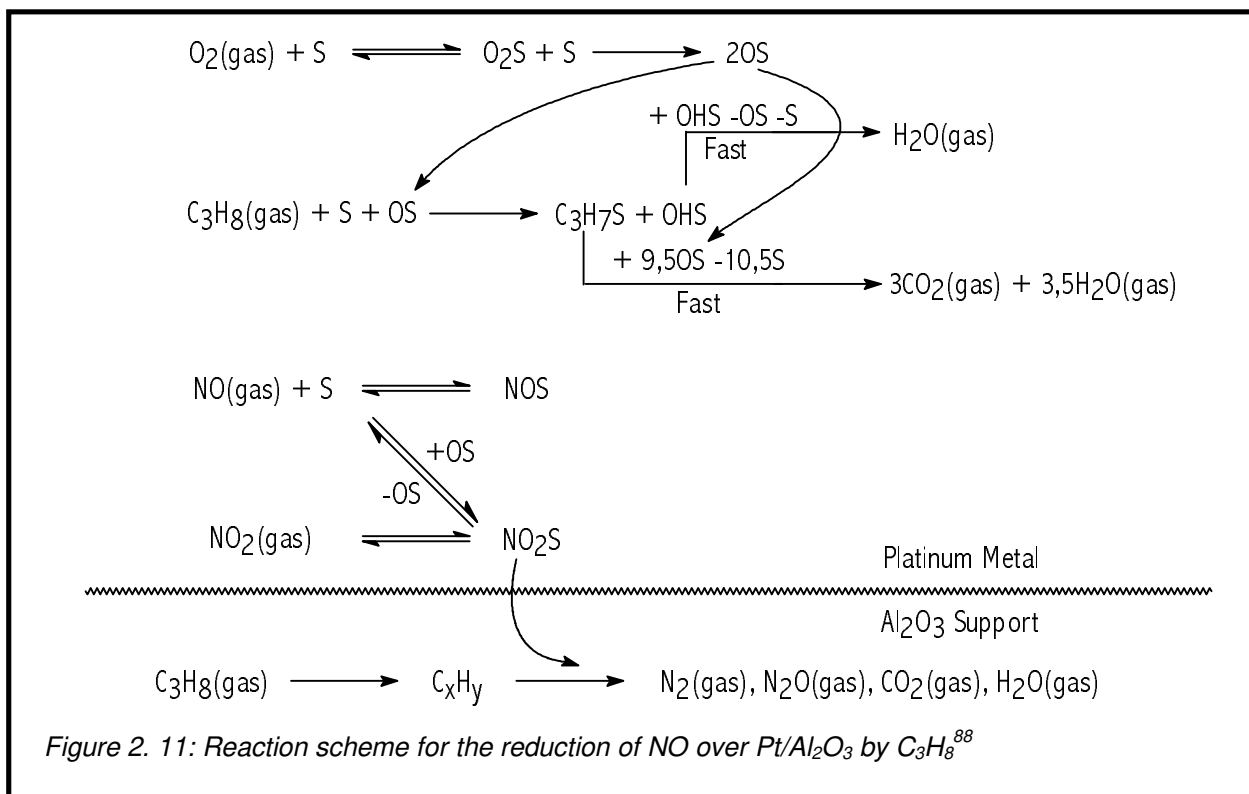
Table 2. 9: Comparison of observations using either propene or propane as reductant for NO over Pt/Al<sub>2</sub>O<sub>3</sub>

Burch et al.<sup>83</sup> describe two different mechanisms for NO reduction over Pt/Al<sub>2</sub>O<sub>3</sub>, one using propene and one using propane. The suggested mechanism for the C<sub>3</sub>H<sub>6</sub>-NO-O<sub>2</sub> reaction differs from the one proposed earlier<sup>76</sup>.

For  $C_3H_6$ , Burch et al.<sup>83</sup> assume that the Pt surface is dominantly covered with  $C_3H_6$  or species derived from  $C_3H_6$ . The double bond of  $C_3H_6$  enables it to interact strongly with the Pt surface resulting in this high coverage. The  $NO_x$  reduction and HC oxidation reactions appear to be linked. At temperatures below the onset of  $C_3H_6$  oxidation the surface is covered with carbonaceous species, which prevent NO from adsorbing on the surface and reacting to form  $N_2$  and  $N_2O$ . Oxidation of these carbonaceous species results in the formation of vacant sites onto which NO can adsorb and react. As the temperature is raised, more and more HC is oxidised. Consequently, the number of vacant sites increases and this in turn raises the rate of  $NO_x$  conversion.  $C_3H_6$  will not react with NO in the absence of  $O_2$  over Pt/ $Al_2O_3$  presumably because surface sites are blocked by carbonaceous species. The oxygen coverage is negligible as long as the HC conversion is below 100%, but predominant as soon as HC is completely consumed. Burch et al.<sup>88</sup> point out that NO competes remarkably well with  $O_2$  for adsorption sites. Especially since in a feed of 5 vol.-%  $O_2$  and 1000 ppm NO, as used by them, there are 100 times more oxygen atoms as  $O_2$  than NO molecules. Nevertheless, they observed that at 240°C the amount of oxygen deposited on the surface from NO is only about ten times smaller than those deposited from  $O_2$ . As soon as HC is completely converted the  $NO_x$  conversion begins to decline<sup>83</sup>. A high oxygen coverage of the surface is not favourable for the dissociation of NO. Yet, NO oxidation to  $NO_2$  requires oxygen to be available. This is the case at temperatures higher than those necessary for complete HC conversion. Hence, the beginning of  $NO_2$  formation coincides with maximum  $NO_x$  conversion and complete HC conversion. A reaction scheme is given in Figure 2. 11. Observe that this mechanism does not require the oxidation of NO to  $NO_2$  and that all reactions occur on the Pt surface. S denotes an adsorption site.



For C<sub>3</sub>H<sub>8</sub>, Burch et al.<sup>83</sup> believe that dissociative adsorption by C-H bond cleavage is the rate determining step for C<sub>3</sub>H<sub>8</sub> adsorption. They postulate that the preferred site for C-H bond activation comprises a combination of a Pt atom carrying a small positive charge in close proximity to an oxygen atom carrying a small negative charge resulting in heterolytic splitting<sup>91</sup>. The resultant adsorbed propyl species presumably reacts rapidly, resulting in no significant surface coverage of the Pt with HC species. The NO<sub>x</sub> reduction and HC oxidation reactions do not appear to be linked and adsorbed oxygen is the predominant surface species. Therefore, oxygen is readily available for the NO oxidation to NO<sub>2</sub> and this occurs already well below complete HC conversion. In another publication<sup>81</sup> they postulate that the rate determining step is the spillover of adsorbed NO<sub>2</sub> onto the Al<sub>2</sub>O<sub>3</sub> support. This NO<sub>2</sub> then reacts with C<sub>3</sub>H<sub>8</sub> derived species deposited on the support, possibly located close to or at the metal-support interface, to give N<sub>2</sub> and N<sub>2</sub>O. The transport of NO<sub>2</sub> to the support occurs predominantly via spillover rather than by gas phase transfer. An interaction between Pt and Al<sub>2</sub>O<sub>3</sub> in this reaction has also been reported by Hamada et al.<sup>70</sup>. This mechanism suggests that the nature of the support is important. They add that another possibility is that NO<sub>2</sub> reacts with the Al<sub>2</sub>O<sub>3</sub> to form a nitrate species which is capable of reacting with the hydrocarbon. A reaction scheme is given in Figure 2. 12. In this case the mechanism requires oxidation of NO to NO<sub>2</sub> and works partly on the platinum and partly on the alumina.



The most important aspect when summarising both reaction mechanisms is that for the C<sub>3</sub>H<sub>6</sub>-NO-O<sub>2</sub> reaction the surface is reduced and covered with carbonaceous species while for the C<sub>3</sub>H<sub>8</sub>-NO-O<sub>2</sub> reaction the surface is oxidised and covered with adsorbed oxygen.

Ansell et al.<sup>56 85</sup> prefer Burch's first mechanism<sup>76</sup> which is consistent with results from their temporary analysis of products (TAP) studies. They point out that at low temperature NO tends to win the competition for reduced Pt sites. With rising temperature the dissociative adsorption of O<sub>2</sub> becomes increasingly rapid, partly because the rate at which molecular NO desorbs from the catalyst increases. This strongly limits the amount of NO adsorption on the catalyst at higher temperature. NO conversion decreases because the NO becomes unable to compete effectively with the oxygen for the reduced Pt sites at high temperature. To them, this also explains why propene is a very good reductant for NO over Pt-based catalysts while propane is not. Propene reduces the Pt sites at significantly lower temperature than does propane, so NO can compete effectively with the oxygen for the reduced Pt sites when propene is the reductant. At high temperatures prevalent during reaction with propane the oxygen wins the competition.

Adams et al.<sup>4</sup> presented kinetic data for the activation energy for NO<sub>x</sub> reduction and C<sub>3</sub>H<sub>6</sub> oxidation. This data is shown in Table 2. 10.

Formulation	Exp. Conditions		NO <sub>x</sub> Reduction		C <sub>3</sub> H <sub>6</sub> Oxidation	
	Length	Flow	E <sub>a</sub>	log A	E <sub>a</sub>	log A
Pt Based	0,5"	vary	36 ± 10	17 ± 5	23 ± 0,1	11 ± 0,1
	1,0"	vary	45 ± 6	22 ± 3		
	2,5 "	vary	28 ± 4	14 ± 2		
	vary	1,2/1,5 l/min	31 ± 9	15 ± 5		
	vary	3 l/min	41 ± 21	20 ± 11		
	vary	6 l/min	30 ± 2	14 ± 1		
Cu Zeolite	0,5"	vary	15 ± 3	6 ± 1	19 ± 3	8 ± 1

Table 2. 10: E<sub>a</sub><sup>o</sup> data obtained from kinetic experiments by Adams et al.<sup>4</sup>

They noticed that NO<sub>x</sub> conversion rates are similar to corresponding HC oxidation rates under lean conditions. According to them it is difficult to determine if this is merely a coincidence or an indication of a common rate determining step in the lean NO<sub>x</sub> reduction mechanism. At maximum NO<sub>x</sub> conversion, they observed that NO<sub>x</sub> conversion drops off relatively sharply once propene reaches 100% conversion. Reasons for that are on the one hand a decrease in lifetime of active sites generated by propene oxidation as temperature increases and on the other hand a decrease in NO surface adsorption as temperature increases. They also noticed that the peak of the NO<sub>x</sub> conversion coincides with a change in the catalyst selectivity from NO<sub>x</sub> reduction to NO oxidation as temperature is increased. Further, at maximum NO<sub>x</sub> conversion CO generation from HC appears to stop. A significant portion of propene is oxidised to CO, instead of CO<sub>2</sub>, while NO<sub>x</sub> reduction is lighting off. When the HC is propane, lean NO<sub>x</sub> conversion is insignificant, and once CO lights off, it achieves 100% conversion very quickly. When propene is used as HC, at ca. 60% CO conversion, CO disappearance slows down over the temperature range where NO<sub>x</sub> lights off and reaches peak conversion the ratio of CO produced to NO consumed increases with temperature and is higher than stoichiometric. According to Adams et al. these observations of CO production suggest that the mechanism(s) of lean NO<sub>x</sub> reduction involves the oxidation of the HC reductant.



#### 2. 5. 4. 1. 2. 5 Factors Influencing NO<sub>x</sub> Reduction on Pt/Al<sub>2</sub>O<sub>3</sub>

The parameters which determine the activity of Pt/Al<sub>2</sub>O<sub>3</sub> are predominantly Pt load, Pt dispersion, gas composition, fuel sulphur level, water content of exhaust gas, SV, and system design. Recently it has been recognised that the support has a major role in the mechanism at least under certain conditions.

Most researchers are in agreement that increasing the platinum load reduces the light-off temperature while increasing the maximum NO<sub>x</sub> conversion simultaneously. In agreement with Burch et al.<sup>76</sup>, Adams et al.<sup>4</sup> found that this was the case. They believe the reasons for this are that the lifetime of active sites generated by propene oxidation decreases as temperature increases, that NO surface adsorption decreases as temperature increases, and that the catalyst selectivity changes from NO<sub>x</sub> reduction to NO oxidation as temperature increases.

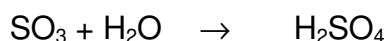
The metal dispersion is defined as

$$D_M = \frac{\text{number of metal atoms on the surface of a metal particle}}{\text{total number of atoms in the metal particle}} \quad \text{Equation 2. 88}$$

While the influence of Pt dispersion on HC and CO oxidation has been thoroughly investigated<sup>92</sup>, the influence of Pt dispersion on NO reduction is discussed controversially. It has been noticed<sup>84</sup> that the HC light-off temperature depends directly on the Pt particle size with a light-off temperature that increases as particle size increases. Ansell et al.<sup>56</sup> report that the activity for NO<sub>x</sub> reduction is not related simply to metal dispersion, some of those catalysts with extremely high metal surface area were rather poor as lean NO<sub>x</sub> catalysts, while some of the more poorly dispersed catalysts were highly active. Tillaart et al.<sup>84</sup> add to this that although platinum particle size is not directly correlated to the lean NO<sub>x</sub> activity, it can influence it indirectly by the hydrocarbon light-off.

As for the pure alumina, sulphur has a major influence on the catalytic performance of a Pt/Al<sub>2</sub>O<sub>3</sub> catalyst. Currently the sulphur level of European Diesel fuels is 500 ppm. Some countries, like Sweden, already use Diesel fuels which have sulphur

levels of only 25 ppm. If such low sulphur level fuels are used the influence of sulphur on the catalytic activity can be neglected. Nevertheless, in order to compete on the world-market the sulphur problem must be addressed. In the exhaust of a Diesel engine sulphur is present as sulphur dioxide, SO<sub>2</sub>. Platinum was found to be a very active catalyst for the oxidation of SO<sub>2</sub><sup>93</sup>. At low temperature the oxidation of SO<sub>2</sub> to SO<sub>3</sub> is kinetically limited. At high temperatures the reaction is thermodynamically hindered. Consequently there is a temperature window of SO<sub>2</sub> oxidation with its maximum at ca. 750 K. Wyatt et al.<sup>8</sup> report that the SO<sub>3</sub> produced reacts with water to form sulphuric acid via:



*Equation 2. 89*

Obuchi et al.<sup>78</sup> presume that there could be a certain synergistic effect between SO<sub>2</sub> and water which contributes to the deterioration of the catalyst. The sulphuric acid can condense or react with the catalyst's support. This is named sulphate storage. The second possibility is that H<sub>2</sub>SO<sub>4</sub> condenses or adsorbs on the particulates of the exhaust. In the latter case the emission of particulate matter (PM) is observed to increase. For this reason, good PM control requires a catalyst that shows minimal oxidation of SO<sub>2</sub>. Beretta et al.<sup>94</sup> state that the SO<sub>2</sub> oxidation kinetics may be indirectly affected by the pore structure of the support since it influences the intraporous concentration gradients of NO and the reductant hydrocarbon. They have observed that the SO<sub>2</sub> conversion turns out to be uniquely controlled by surface area. Catalysts with different pore-size distributions but comparable surface areas yield the same values of SO<sub>2</sub> conversion. For low sulphate emissions the preferred support material should only weakly interact with SO<sub>2</sub>, i.e., it should not adsorb SO<sub>2</sub> strongly neither should it react with SO<sub>3</sub> to form stable washcoat sulphates. One way of reducing the SO<sub>2</sub> oxidation activity on Pt catalysts is thermal deactivation. This method modifies the platinum crystallite size by calcination which results in a loss of surface area. Wyatt et al.<sup>8</sup> have noticed that high temperature calcination causes the platinum crystallite size to increase from ca. 1,5 nm to 40 nm. They admit, though, that this method is a relative unselective means of modifying the SO<sub>2</sub> oxidation activity. Nevertheless, they have observed improved particulate performance after calcination. Another approach is the modification of the supported

platinum by the addition of promoters or selective poisons. Wyatt et al.<sup>8</sup> gained best results by the addition of vanadium which dramatically reduced the storage/release of sulphates relative to that observed for untreated Pt/Al<sub>2</sub>O<sub>3</sub>. They believe that vanadium addition reduces the catalyst's activity for SO<sub>2</sub> oxidation as well as it suppresses the reactivity of the support with sulphuric acid. They claim that the vanadium loading effect is consistent with the model of a surface that involves the formation of a VO<sub>x</sub> surface species which is inert to H<sub>2</sub>SO<sub>4</sub>. It must be remarked yet, that Wyatt et al.<sup>8</sup> did not study the effect of vanadium addition to the NO<sub>x</sub> reduction activity of their catalyst. Interestingly, Zhang et al.<sup>75</sup> have observed that SO<sub>2</sub> addition in a model test gas improved the NO reduction activity of Pt/Al<sub>2</sub>O<sub>3</sub> catalysts and depressed the formation of N<sub>2</sub>O as well. They explained this behaviour by an inhibition effect of SO<sub>2</sub> towards propene (C<sub>3</sub>H<sub>6</sub>) combustion which is a beneficial facilitation of the reaction between NO<sub>x</sub> and propene. The depression of the N<sub>2</sub>O formation is explained by the hypothesis that SO<sub>2</sub> may poison selectively the active sites for N<sub>2</sub>O formation. Another explanation might be that the adsorbed SO<sub>2</sub> retards the mobility of the adsorbed NO molecules on the platinum surface. This NO mobility had been made responsible for the formation of N<sub>2</sub>O in the low temperature regime<sup>76</sup>. If propane (C<sub>3</sub>H<sub>8</sub>) is used as a model reductant gas, Hubbard et al.<sup>9</sup> noticed in contrast to Zhang<sup>75</sup> that the presence of SO<sub>2</sub> promotes the oxidation of this hydrocarbon. This is believed to be caused by new active sites generated by surface sulphates and was verified by Adams et al.<sup>4</sup>. The latter group says that SO<sub>2</sub> inhibits oxidation of reactive HC's, such as propene and other olefins, as well as CO, but enhances oxidation of the saturated HC propane. NO<sub>x</sub> light-off is delayed by SO<sub>2</sub> analogous to propene light-off. SO<sub>2</sub> seems to be quenching an active that is involved in both propene oxidation and NO<sub>x</sub> reduction. For a Pt/Al<sub>2</sub>O<sub>3</sub> catalyst, addition of 20 ppm SO<sub>2</sub> to a synthetic feedgas with oxidising conditions rose THC(50) for propene by 40°C and TCO(50) by 45°C. THC(50) for propane was lowered by 260°C.

For Pt/Al<sub>2</sub>O<sub>3</sub> catalysts two contrasting opinions on the effect of water vapour can be found in literature. While Miyadera et al.<sup>98</sup> report that water vapour has a promoting effect on the NO<sub>x</sub> reduction due to the suppression of undesirable propene over-oxidation Engler et al.<sup>57</sup> state that the NO<sub>x</sub> conversion decreases sharply with the addition of water to the model feed gas. A NO<sub>x</sub> conversion of 55% was nevertheless

observed by them even in the presence of 10 vol.-% of water in the feed. Hamada<sup>70</sup> observed that water vapour did not affect NO reduction by propene but inhibited NO reduction by propane. The inhibition can be ascribed to the inhibition of a reaction step on Al<sub>2</sub>O<sub>3</sub> leading to N<sub>2</sub> formation.

The space velocity (SV) is defined as:

$$SV = \frac{\text{Volume Flow of Exhaust Gas}}{\text{Converter Volume}} \quad \text{Equation 2. 90}$$

Unity exists among researchers<sup>4 31 49 57 68</sup> that an increase in space velocity results in a decrease of NO<sub>x</sub> conversion. Cho<sup>49</sup> states that the temperature of maximum NO<sub>x</sub> conversion is shifted to higher values at higher space velocities. As a matter of fact the whole temperature window for NO<sub>x</sub> conversion is shifted to these higher values. Cho additionally points out that the selective reduction of NO below the maximum NO conversion temperature can be dramatically improved by reducing the space velocity, while the space velocity exerts little effect on the selectivity above this temperature. This was also observed by Adams et al.<sup>4</sup>. They argue that this is consistent with the limited lifetime of an active site at the high temperatures after maximum NO<sub>x</sub> conversion. By waiting a longer time little or no improvement in conversion occurs because active sites have disappeared.

One way of dealing with the problem of the temperature window is to place the converter as close to the engine as possible so it warms up faster and gains its maximum activity more quickly<sup>95</sup>. This is a question of designing the complete exhaust gas aftertreatment system. In order to gain activity also under cold start conditions, electrically heated converters (EHC) have been introduced<sup>96</sup>. Combinations of a short metallic catalytic monolith pre-heater with the standard ceramic monolith catalyst appear to be the most convenient arrangement.

#### 2. 5. 4. 1. 2. 6 Other Metal Ions/ $Al_2O_3$

Several groups have tried other metals than platinum for the impregnation into  $\gamma$ - $Al_2O_3$ <sup>9 21 34 72 77 78 97-104</sup>. Table 2. 8 shows the metal ions used and the corresponding references.

Metal used for Impregnation on $Al_2O_3$	Reference
Ag	97 98 100
Co	97
Pd	9 72 78
Ga	98
In	98
Zn	98
Sn	98
Cu	21 97 99
Rh	34 77 78
Pt-Rh	34 77 78
Ir	78
Ru	78
Pt-Au	78
V	97
Cr	97

Table 2. 8: Metal ions other than Pt used for  $Al_2O_3$  impregnation

The preparation methods and the parameters influencing the catalytic performances of the samples are similar to those of Pt/ $Al_2O_3$ . Rh/ $Al_2O_3$  was found<sup>34</sup> to be the most selective towards the formation of  $N_2$  versus nitrous oxide ( $N_2O$ ). An attempt to form a more active and selective bimetallic Pt-Rh catalyst was not successful.

Under real Diesel exhaust gas conditions, Pt/ $Al_2O_3$  remains the most active and most stable system. The reduction activity of all other systems declines significantly in the presence of  $O_2$ ,  $H_2O$ , and  $SO_2$ . Among these other systems, Ag/ $Al_2O_3$  showed highest activity under real Diesel exhaust conditions.

#### 2. 5. 4. 1. 3 Other Oxides

Teraoka et al.<sup>101</sup> have tested  $SnO_2$  catalysts for NO reduction activity. They observed reduction of NO to  $N_2$  above 500 K with  $C_2H_4$  as reducing agent. Coexisting oxygen promoted the activity. Even treatment with humid air at 1100 K did

not cause a serious decrease. These are surprising results since the surface area of  $\text{SnO}_2$  is by factor 10 smaller than those of ZSM-5 and  $\gamma\text{-Al}_2\text{O}_3$  samples.

De- $\text{NO}_x$ -ing activity is also reported for  $\text{TiO}_2$ ,  $\text{ZrO}_2$ , and sulphuric-acid pre-treated  $\text{Fe}_2\text{O}_3$  by Hamada et al.<sup>70 71</sup>. Hamada<sup>70</sup> reports that Xue et al.<sup>79</sup> state that  $\text{Pt}/\text{SiO}_2$  shows the highest NO oxidation activity to  $\text{NO}_2$  in the row of  $\text{Pt}/\text{SiO}_2$ ,  $\text{Pt}/\text{Al}_2\text{O}_3$ , and  $\text{Pt}/\text{ZrO}_2$ . They also noticed that the exposed Pt atoms did not all have the same activity. For  $\text{SiO}_2$  supported catalysts larger particles seemed to have higher NO oxidation activities than smaller ones and because of this oxidation of NO may be considered structure sensitive on  $\text{Pt}/\text{SiO}_2$  catalysts.  $\text{Pt}/\text{Al}_2\text{O}_3$  showed less structure sensitivity while  $\text{Pt}/\text{ZrO}_2$  was completely structure insensitive. Xue et al.<sup>79</sup> also discovered that from  $\text{Pt}/\text{SiO}_2$  the adsorption of NO and  $\text{SO}_2$  occurs predominantly on the Pt sites and therefore  $\text{SiO}_2$  contributes very little to adsorption on Pt containing catalysts. In contrast to this the  $\text{Al}_2\text{O}_3$  support seemed to govern the desorption characteristics of the Pt loaded samples. They summarise that for  $\text{Al}_2\text{O}_3 / \text{ZrO}_2$  samples the reactant (NO) is probably adsorbed mainly on the support and then migrates to the Pt sites where it is oxidised to form  $\text{NO}_2$ . The product  $\text{NO}_2$  molecules may be held more strongly on  $\text{Al}_2\text{O}_3$  and  $\text{ZrO}_2$  than on  $\text{SiO}_2$ . They remark that  $\text{SiO}_2$  is known to be inert in acidic environment and that this causes little interaction between  $\text{SiO}_2$  and the acidic NO/ $\text{SO}_2$  molecules. On the other hand, the amphoteric  $\text{Al}_2\text{O}_3$  should be more reactive because it has acidic and basic sites. Hubbard et al.<sup>9</sup> report that  $\text{Pt}/\text{ZrO}_2$  and  $\text{Pd}/\text{ZrO}_2$  shows some NO reduction in the presence of oxygen. According to Kintaichi et al.<sup>66</sup>,  $\text{SiO}_2$  and  $\text{SiO}_2\text{-Al}_2\text{O}_3$  mixtures show very low activity for the selective reduction of nitrogen oxides.

#### 2. 5. 4. 1. 4 Perovskites

The compound that has been named perovskite is  $\text{CaTiO}_3$ . Many substances with the general formula  $\text{ABX}_3$  show the same crystal structure. The unit cell is a cube, whose corners are occupied by  $\text{Ca}^{2+}$  ions. Oxygen is located in the centre of each of the six surface sides and  $\text{Ti}^{4+}$  is situated in the centre of the cube<sup>18 64</sup>. Skoglundh et al.<sup>102</sup> have published their results with perovskite phases of the composition  $\text{La}_{1-x}\text{Sr}_x\text{Al}_{1-2y}\text{Cu}_y\text{Ru}_y\text{O}_3$ . They found reduction activity towards NO in model gas tests with  $\text{C}_3\text{H}_6$  and CO as reductants under stoichiometric conditions. Literature on

perowskites for de-NO<sub>x</sub>-ing is very scarce. Perowskites have proven to be of insufficient stability for application under realistic Diesel conditions<sup>30</sup>.

#### *2. 5. 4. 2 Methods using Adsorption*

It is well known that the ability of zeolites to store molecules of suitable size in their cavities can be used to "capture" certain molecules from gas mixtures<sup>61</sup>. Stiles et al.<sup>26</sup> have published their experiments with an adsorbent based on an alkali/alumina support. They claim that their set-up is able to store nitrogen oxides at temperatures of 500 K for 9 hours with high efficiency. The disadvantage of any adsorption method is that the adsorbent must be regenerated. Stiles et al.<sup>26</sup> accomplish this by passing hydrogen through their adsorbent. This makes the process unfavourable for mobile applications.

Miyoshi et al.<sup>103</sup> have presented a system for LB engines that is able of online regeneration without the need for additional reducing agents. The NO<sub>x</sub> storage catalyst usually contains noble metals for reduction and oxidation and a NO<sub>x</sub> storage compound (an alkaline earth oxide like BaO) supported on alumina. During lean burn conditions, NO<sub>x</sub> is being stored on the catalyst. To regenerate the catalyst, short periods of rich conditions are employed during which operation the nitrogen oxides are released and reduced by the hydrocarbons of the exhaust on the noble metal. Because of the low O<sub>2</sub> concentration during the rich phase, the NO<sub>x</sub> reduction is nearly complete. During the lean phase, however, the reduction of NO<sub>x</sub> is negligible. The storage is temperature dependent and very low storage was measured at temperatures above 500°C. Since a Pt-Rh/Al<sub>2</sub>O<sub>3</sub> catalyst with the same noble metal load as the Pt-Rh/BaO/Al<sub>2</sub>O<sub>3</sub> system gave a significantly more pronounced light-off behaviour, Fridell et al.<sup>104</sup> assume that either the dispersion is lower if BaO is present, that BaO partially covers the metal, or that BaO in close vicinity to Pt-Rh inhibits the capacity of the noble metal to catalyse oxidation reactions. They also report that their storage catalyst was completely saturated after 200 seconds and that it was regenerated after 40 seconds completely. They suggest that the storage of NO<sub>x</sub> is possibly preceded by NO oxidation. NO<sub>x</sub> is stored as a nitrate of the storage compound. Their mechanism is described by the following equations

$\text{NO} + \text{S}$	$\rightarrow \text{NOS (l.c.)}$	<i>Equation 2. 91</i>
$\text{O}_2 + 2\text{S}$	$\rightarrow 2\text{OS (l.c.)}$	<i>Equation 2. 92</i>
$\text{NOS} + \text{OS}$	$\rightarrow \text{NO}_2 + 2\text{S (l.c.)}$	<i>Equation 2. 93</i>
$2\text{NO} + 3\text{O} + \text{BaO}$	$\rightarrow \text{Ba(NO}_3)_2 \text{ (l.c.)}$	<i>Equation 2. 94</i>
$2\text{NO}_2 + \text{O} + \text{BaO}$	$\rightarrow \text{Ba(NO}_3)_2 \text{ (l.c.)}$	<i>Equation 2. 95</i>
$\text{Ba(NO}_3)_2$	$\rightarrow 2\text{NO} + 3\text{O} + \text{BaO (r.c.)}$	<i>Equation 2. 96</i>
$\text{Ba(NO}_3)_2$	$\rightarrow 2\text{NO}_2 + \text{O} + \text{BaO (r.c.)}$	<i>Equation 2. 97</i>
$\text{C}_3\text{H}_6 + \text{S}$	$\rightarrow \text{C}_3\text{H}_6\text{S (r.c.)}$	<i>Equation 2. 98</i>
$9\text{NO} + \text{C}_3\text{H}_6$	$\rightarrow 9/2\text{N}_2 + 3\text{CO}_2 + 3\text{H}_2\text{O (r.c.)}$	<i>Equation 2. 99</i>

(l.c.) and (r.c.) denote lean conditions and rich conditions, respectively and S denotes an adsorption site. The formation of  $\text{Ba(NO}_3)_2$  is thermodynamically favoured at high oxygen contents at lower temperature. When switching the oxygen supply off, the decomposition of  $\text{Ba(NO}_3)_2$  is favoured. Aluminium nitrate decomposes at about 150°C. The rate limiting step is assumed to be the decomposition of barium nitrate during the rich phase. Automobiles with these so called  $\text{NO}_x$ -traps have been introduced to the world market by Japanese companies.

#### 2. 5. 4. 3 Other Methods

The subject of de- $\text{NO}_x$ -ing has been investigated so intensively that there is almost an endless amount of ideas. Some researchers even tried to use a plasma burner for de- $\text{NO}_x$ -ing flue gases. Although this sounds like firing cannons on pigeons, the idea of using electric charges for de- $\text{NO}_x$ -ing was already formulated by Haas et al.<sup>105</sup> in 1979. This method has gained new attention in Japan by Tanagawa et al.<sup>106</sup>. Under oxidising conditions the performance is unfortunately not satisfactory. Nevertheless, the observed reduction activity at  $\lambda = 1$  of 98% conversion to  $\text{N}_2$ <sup>107</sup> might justify further investigations.



## 3. Experimental

### 3.1 Catalyst Samples

#### 3.1.1 Preparation

Supported precious group metal (PGM) model catalysts were prepared using standard procedures. The samples were cores drilled from full sized coated cordierite monoliths. They had dimensions of 21 - 25 mm (diameter) by 65 - 76 mm (length), a cell density of 62 cells cm<sup>-2</sup>, and a wall thickness of 0.2 mm. A square shaped cell geometry has been identified to be the best compromise between optimum heat/mass transfer and minimum pressure drop<sup>108</sup>. Sample parameters such as metal species, metal and washcoat load, etc., are given in the results and discussion chapter where appropriate. Further data on the preparation methods can not be given due to proprietary reasons.

#### 3.1.2 Ageing

In order to evaluate the long term performance of certain catalyst formulations, samples of these catalysts were subjected to hydrothermal ageing. This was performed by mounting the sample in a stainless steel reactor. A water saturated air stream (10% H<sub>2</sub>O) was passed through the reactor which was maintained at constant temperature for a designated time. Oven temperatures and ageing times are given in the results and discussion section where appropriate.

### 3.2 Determination of Characteristic Sample Parameters

Characteristic sample parameters were limited to metal dispersion, BET surface area (BSA), and pore size distribution (PSD) measurements. The instrument used was an ASAP 2000 from micromeritics®. BET surface area was specified by using a conventional 5 point method. During the latter experiment, the pore size distribution was simultaneously measured for some samples. Metal dispersion was determined by standard CO chemisorption (COC) techniques. Adsorption stoichiometry was

assumed to be 1:1. In addition, the technique gave the total metal surface area (MSA).

### 3. 3 Synthetic Catalytic Activity Test (SCAT)

The SCATs were conducted on a rig that consisted of three major components: a gas supply, a reactor block, and an analytical train.

The gases used were: O<sub>2</sub>, CO<sub>2</sub>, CO, SO<sub>2</sub>, NO, NO<sub>2</sub>, propene, and decane. Gas supplier and purity of the individual gases are given in Table 3. 1. H<sub>2</sub>O was introduced into the gas feed by pump injection. Gas flows were adjusted with computer controlled mass flow controllers.

Gas	Purity	Supplier
N <sub>2</sub>	≥ 99,998%	Air Liquide
O <sub>2</sub>	≥ 99,95%	Air Liquide
CO <sub>2</sub>	≥ 99,998%	Air Liquide
CO	≥ 99,997%	Air Liquide
SO <sub>2</sub>	15% in N <sub>2</sub>	Air Liquide
NO	≥ 99,97%	Air Liquide
NO <sub>2</sub>	5% in N <sub>2</sub>	AGA Gas AB
propene	≥ 99,998%	Air Liquide
decane	100 ppm in N <sub>2</sub>	Linde Gas UK Ltd

Table 3. 1: Purity and supplier of gases employed

The reactor block comprised a ceramic tube reactor and an oven. The oven temperature was constantly measured by a thermocouple, and could be controlled by the computer. The ceramic material used in the reactor tube was chosen to ensure there was no reaction on the walls of the tube. The samples were mounted in the reactor with fibrefrax paper to ensure a gas tight fit. A thermocouple was placed directly in front of the catalyst sample to measure the inlet temperature of the reactant exhaust gas. This inlet temperature is the temperature given in all figures and discussions throughout this thesis. Reactive gases such as CO, SO<sub>2</sub>, NO, NO<sub>2</sub>, propene, and decane were introduced individually and directly in front of the sample by separated tubes. This separation of gases is particularly important in order to avoid unintended NO<sub>2</sub> formation from reaction between oxygen and NO. It has, however, been reported<sup>109</sup> that homogeneous oxidation of NO by O<sub>2</sub> to form NO<sub>2</sub> is

negligible in a wide temperature range 150-550°C. The major gas stream of N<sub>2</sub>, O<sub>2</sub>, H<sub>2</sub>O, and CO<sub>2</sub> was introduced via a single tube. Behind the water injection, a heating tube was used at a temperature of 250°C to avoid water condensation. Figure 3. 1 shows the complete reactor block.

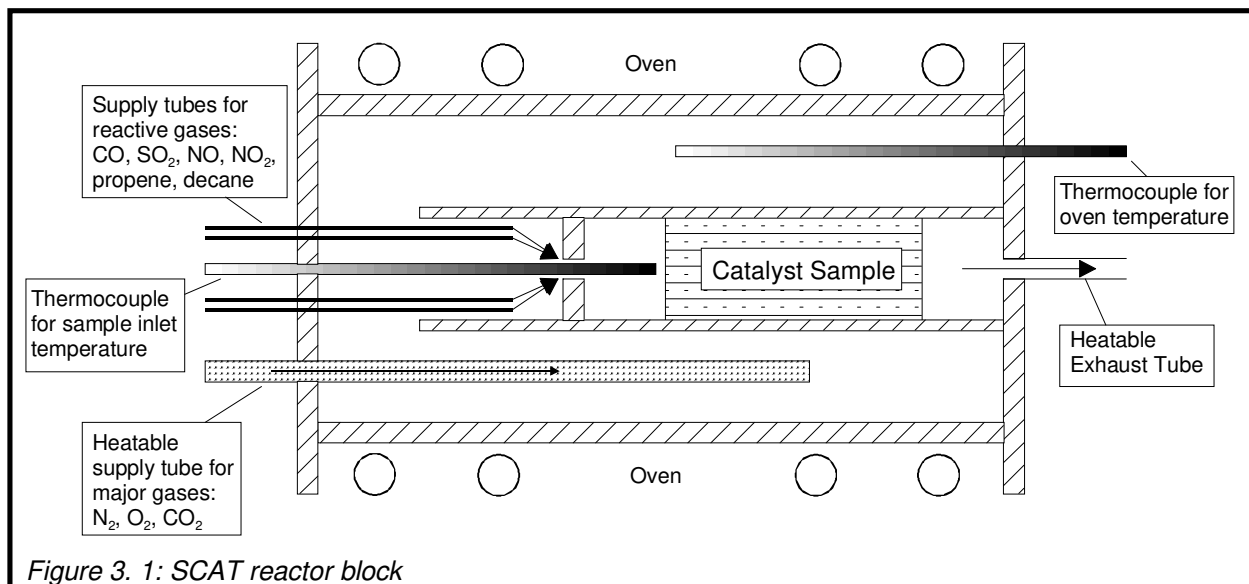


Figure 3. 1: SCAT reactor block

After the catalyst, the product gas mixture was analysed by means of standard analysers as shown in Table 3. 2. To avoid condensation of water vapour in the tube between the reactor block and the analytical train the tube was heatable and held at 160°C.

Gas	Method	Manufacturer
O <sub>2</sub>	Paramagnetic	M&C
CO, CO <sub>2</sub>	NDIR	MAIHAK
SO <sub>2</sub>	Pulsed Fluorescence	Thermoelectron
NO, NO <sub>2</sub> , NO <sub>x</sub>	Chemiluminescence	ECOPHYSICS
Propene, Decane	FID	JUM

Table 3. 2: Analytic equipment used

The accuracy of the analysers is shown in Table 3. 3

Gas	Accuracy
CO <sub>2</sub>	± 0,8%
O <sub>2</sub>	± 0,8%
CO	± 2,5%
SO <sub>2</sub>	± 9,5%
NO	± 2,5%
C <sub>3</sub> H <sub>6</sub>	± 1,9%
H <sub>2</sub> O	± 4,7%

Table 3. 3: Accuracy of analysers

All analysers were calibrated either manually or by computer control at least once a day by standard methods. Analyser data were transferred to the computer and recorded. Simultaneously the computer calculated the conversions of the individual gases by using Equation 3. 1. All data were evaluated with the Microcal™ Origin™ 4.10 program. A LOT with no sample in the reactor revealed no conversion of any gas component. Thus, any gas phase reaction of any of the components can be ruled out safely.

$$U = \frac{C_{in} - C_{out}}{C_{in}}$$

*Equation 3. 1*

### *3. 3. 1 Standard Light-off Test (LOT)*

Standard LOTs were performed in four steps. During the first step the gas concentrations were adjusted by programming the gas flows. A certain time was allowed for the analysers to stabilise at inlet temperatures between 70°C and 90°C. Subsequently the oven temperature was raised at a certain rate to a designated temperature resulting in an increase of the inlet temperature as well. The inlet temperature was usually ~100°C below the oven temperature as shown in Figure 3. 2. In the third step the oven temperature is kept constant for a certain time. It has been observed that during this time the inlet temperature tends to increase further with a non linear rate. Finally the heat is switched off and the oven is cooled as quickly as possible by a fan. During the cooling period, the gas mix was left on and the conversions of this "down-ramp" were also recorded. For fresh catalyst samples, conditioning was done to ensure repeatable evaluations. Conditioning was performed by running LOTs with the samples until the values obtained were similar. This was usually the case after the second LOT. Gas concentrations, heating rates, and maximum temperatures are given in the results and discussions chapter where appropriate.

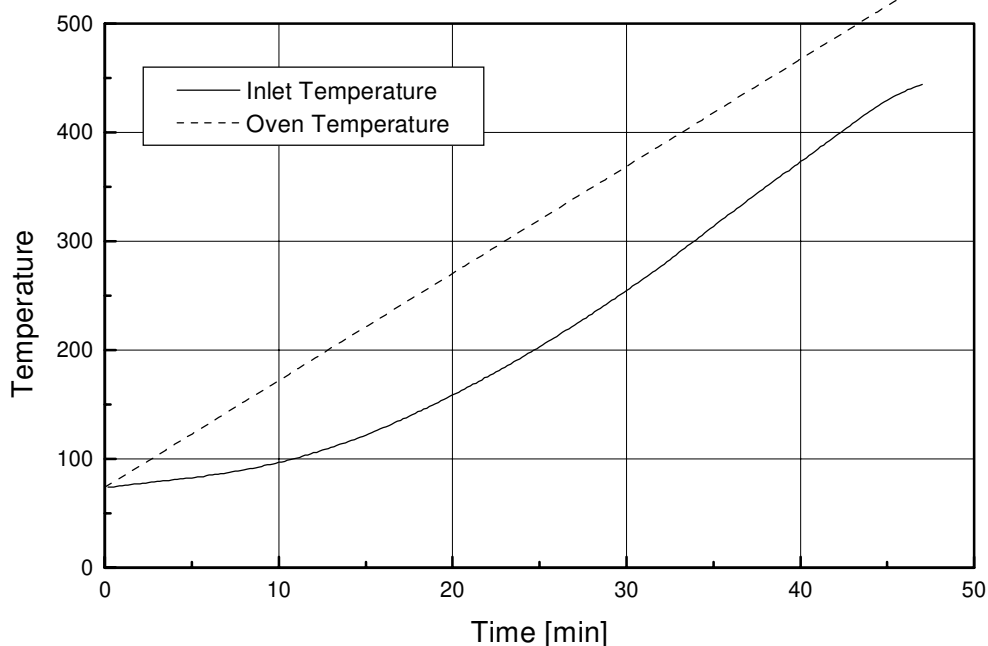


Figure 3. 2: Delay between oven temperature and inlet temperature

### 3. 3. 2 Temperature Ramps on SCAT Rig

Temperature ramps were performed in order to investigate whether any species adsorbed on the catalyst samples during the LOT could be thermally desorbed.

The experiments were done in a similar manner as the standard LOT. Instead of a gas mixture only nitrogen was used as a carrier gas at a flow of 12 000 ml/min. Conditioning was not necessary because all samples had been conditioned during light-off testing. Heating rates and maximum temperatures are given in the results and discussions chapter where appropriate.

### 3. 3. 3 Experiments at Constant Temperatures

These experiments investigated the effect of concentration variations of several gas mix components at constant temperatures.

The catalyst sample was placed in the tube reactor and the oven heated up to the demanded inlet temperature. A certain time was allowed for this temperature to become constant. During this process nitrogen was flushed over the sample. Then the desired gas mix was passed over the sample until all analysers showed stable values. The total flow rate was always 12000 ml/min. After recording these values

the next gas mix was programmed by adjusting the mass flow controllers. This procedure was repeated in a similar manner for all desired gas mixes. The reactor effluent was monitored continuously and recorded on the computer. At the end of each test the oven temperature was ramped to 620°C resulting in an inlet temperature of 550°C. Finally, the oven was cooled down to an inlet temperature of 90°C. Temperatures and gas mixes are given in the results and discussion chapter where appropriate.

### 3. 4 Temperature Programmed Desorption (TPD)

The precision of the temperature ramps on the SCAT rig was limited by the set-up. Above all the distance between the reactor and the analytical train was far to long for a satisfactory desorption temperature resolution. Furthermore, the large reactor volume caused a significant error through its influence on the residence time distribution of the individual gases. Therefore TPD spectra were recorded at Johnson Matthey's Technology Centre in a set-up with all volumes minimised. The distance between the reactor and the analysis apparatus was kept as short as possible. Each experiment involved three steps: sample preparation, SCAT dosing, and the TPD.

#### Sample Preparation:

The catalyst samples were ground to powder, pelletised, crushed and sieved to corn sizes between 250 - 355 µm.

#### SCAT Dosing (performed by Dr. Steve Bennett):

1 g of sample was placed into SCAT rig 1 at JM's Technology Centre at a temperature of 130°C. A gas mix consisting of

O <sub>2</sub>	12,2 vol.-%
CO <sub>2</sub>	4,7 vol.-%
CO	200 ppm
SO <sub>2</sub>	21 ppm
NO	400 ppm
Propene	800 ppm
H <sub>2</sub> O	6,4 vol.-%

in balance nitrogen was passed through the sample, and the total flow rate was 2 l/min. The temperature was raised to 150°C at 5°/min and held constant at 150°C for 10 minutes. Subsequently the temperature was lowered to 130°C within 15 minutes and the H<sub>2</sub>O supply was turned off. Temperature was further reduced to 100°C in the rest of the gas mix for another 15 minutes. After that all gases except N<sub>2</sub> were turned off and the sample cooled as fast as possible to ambient temperature.

TPD (performed by Dr. Paul Millington):

0,3 g of sample was placed into the middle of a quartz tube with quartz wool plugs at both ends. The tube was placed in an oven and helium was passed over the sample at a flow rate of 50 ml/min. The oven temperature was raised from ambient temperature to 1000°C at a heating rate of 20°/min. A mass spectrometer (Fisons GasLab 300) was used to monitor the desorbing species. Together with the data of the mass spectrometer the average temperature of two thermocouples, one placed exactly in front and one placed exactly behind the sample, were recorded by a computer. Properties of the samples tested are given in the results and discussion chapter where appropriate.

### **3. 5 Isotope Transient Kinetics (ITK)**

The isotope transient kinetic technique allows simultaneous measurement of the number of active sites and the turnover frequency of each site of a catalyst sample. In this thesis only the oxidation of CO was investigated by the ITK technique. Theoretically the technique is applicable with any isotopically labelled molecule. A detailed description of the ITK apparatus is given by Biloen<sup>110</sup> and Frost<sup>111</sup>.

The complete rig consisted of the gas feed, a differential pressure transducer, a 4-way switching valve, an oven, and the analysis apparatus. The gas feed included two isotopic feeds of <sup>12</sup>CO and <sup>13</sup>CO plus an additional feed for O<sub>2</sub> and He. Via the 4-way valve the isotopic feeds were routed either to a vent or the reactor. A pressure transducer was used to equalise the pressures between both isotopic feeds. The product gases at the outlet of the reactor were continuously monitored by a mass spectrometer (Fisons GasLab 300). Figure 3. 3 shows the complete ITK rig.

Prior to each experiment the samples were ground to powder, pelletised, crushed and sieved to corn sizes between 250 - 355 µm. Depending on the activity of the

sample, between 0,05 and 0,25 g of sample was placed in a quartz tube and held in place using quartz wool plugs at each end. A thermocouple was placed directly behind the sample to measure the temperature during the reaction. Mass and temperature of the sample as well as the gas flows had to be chosen in such a way as to ensure that differential conditions were maintained, i. e. below 10% conversion. A mixture of 2 ml/min CO, 10 ml/min O<sub>2</sub> and 88 ml/min He was passed over the catalyst at the temperature of interest. He merely served as balance. After a steady state was achieved, the conversion was measured by use of a gas chromatograph (Shimadzu).

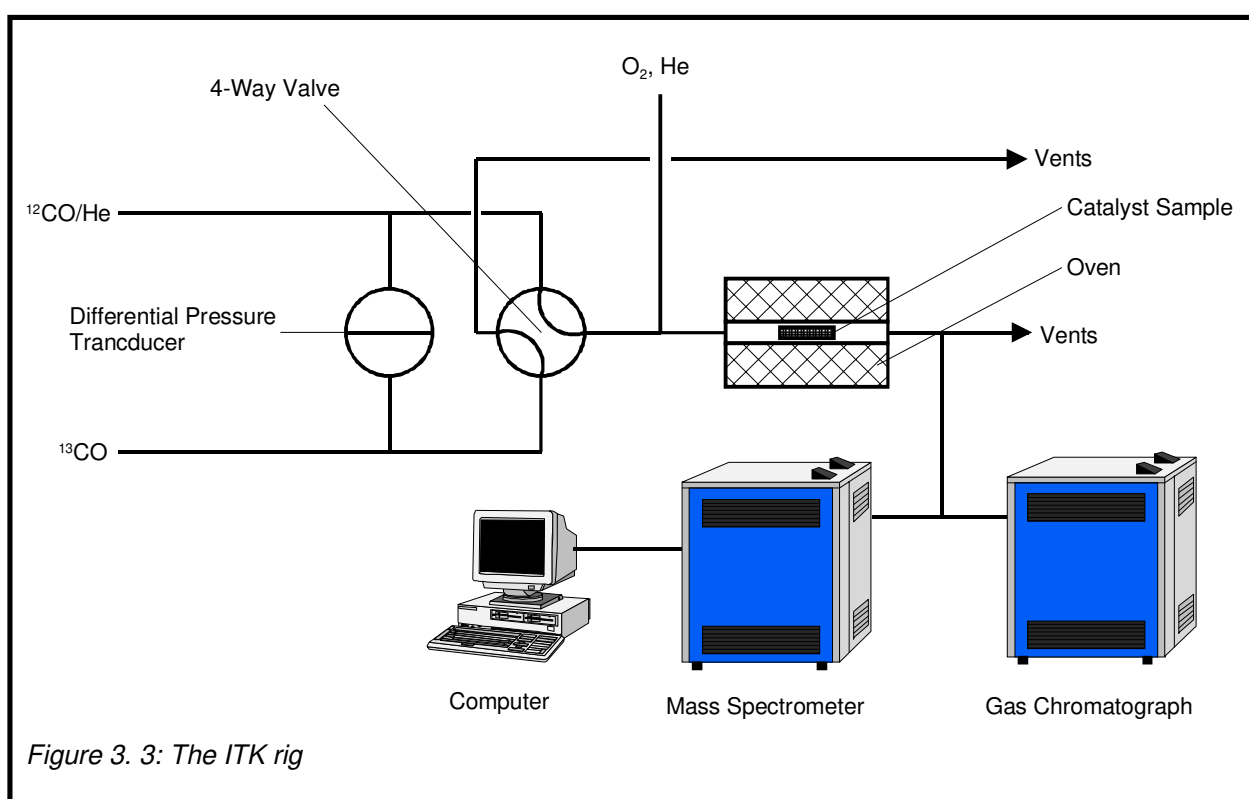


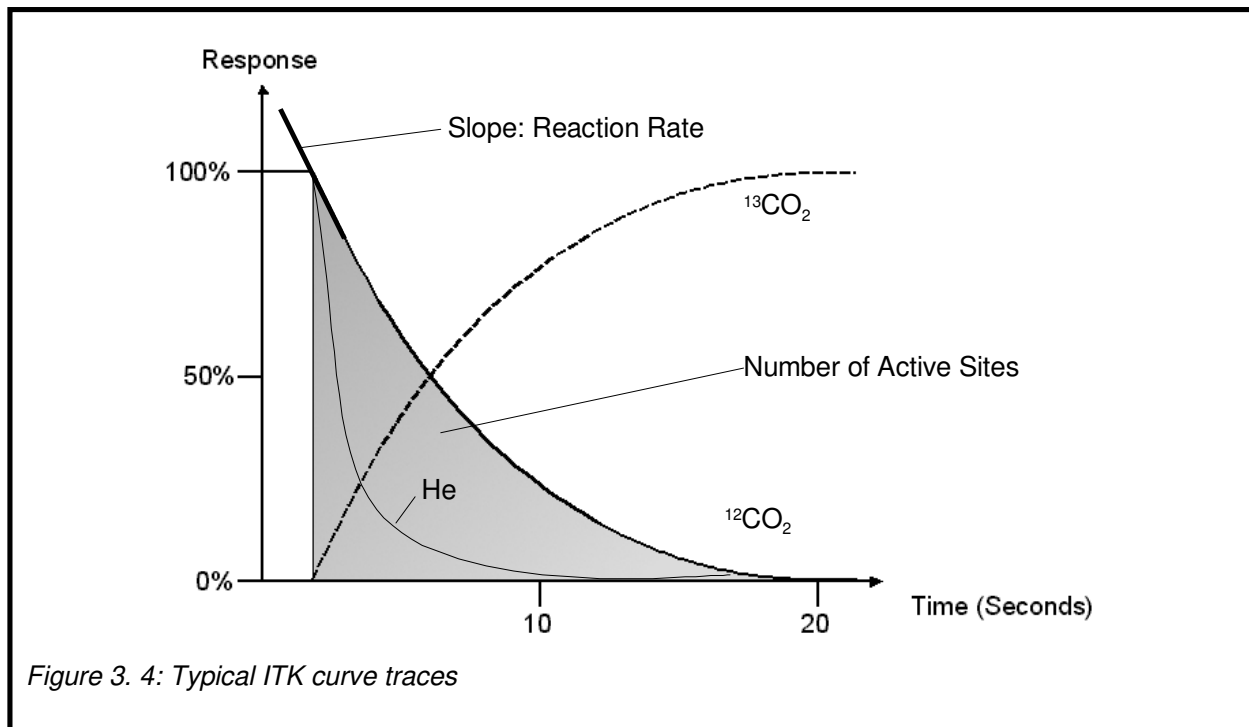
Figure 3. 3: The ITK rig

<sup>13</sup>CO was readied and the pressure of CO and <sup>13</sup>CO equalised using the differential pressure transducer. At a specified time, the CO feed was exchanged for <sup>13</sup>CO. The ensuing transients were then recorded by means of a mass spectrometer. A typical result is shown in Figure 3. 4.

While the He trace decays rapidly, the <sup>12</sup>CO<sub>2</sub> and <sup>13</sup>CO<sub>2</sub> traces mirror each other. From the grey marked area under the <sup>12</sup>CO<sub>2</sub> curve the number of active sites present on the catalyst at the time of the switch can be calculated. The initial slope of this curve represents the specific rate at which the species emerge from the catalyst described by a decay function. The recorded data were evaluated with a proprietary



computer program at JM's Technology Centre. The properties of the samples tested are given in the results and discussion chapter where appropriate.



### 3. 6 Transmission Electron Microscopy (TEM)

Two catalyst samples of formulation PP 41 WCO (one SCAT tested and one fresh) were examined by transmission electron microscopy. The SCAT tested sample featured a visible black residue.

The examination was performed by Mr SBD Spratt.

The black region of the washcoat powder was scraped from the monolith support and the preparation was continued with a proprietary method (TEM6). The sample was examined in a Philips EM400T electron microscope at JM's Technology Centre using the following instrumental conditions:

Voltage [kV]	100
C <sub>2</sub> Aperture [ $\mu\text{m}$ ]	50
Analytical Take-Off Angle	+15°
Mode	Nanoprobe & Microprobe

Typical features were analysed by energy dispersive x-ray (EDX) analysis.

## 4. Results and Discussion

### 4. 1 The Influence of the Washcoat on the Conversion Performance

All automobile catalysts consist of a carrier substrate, active components, and a washcoat to fix the active components on the substrate. Therefore this thesis starts with investigations regarding the washcoat.

#### 4. 1. 1 $Al_2O_3$

##### 4. 1. 1. 1 Characterisation of an $Al_2O_3$ Washcoat by BET Measurements

The BET surface area (BSA), the single point pore volume (SPPV), the average pore diameter (APD), and the pore size distribution (PSD) of a fresh and a hydrothermally aged sample of catalyst PP41 WCO were measured. Ageing was performed at 750°C for 10 hours in a 10% water in air mixture.

#### Observations:

The results are summarised in Table 4. 1 and Figure 4. 1.

Sample	BSA [m <sup>2</sup> /g]	SPPV [cc/g]	APD [Å]
PP 41 WCO fresh	39,8	0,07148	72,0
PP 41 WCO HTA 750°C	31,0	0,060213	57,8

Table 4. 1: Results of BET measurements of catalyst PP 41 WCO fresh and HTA

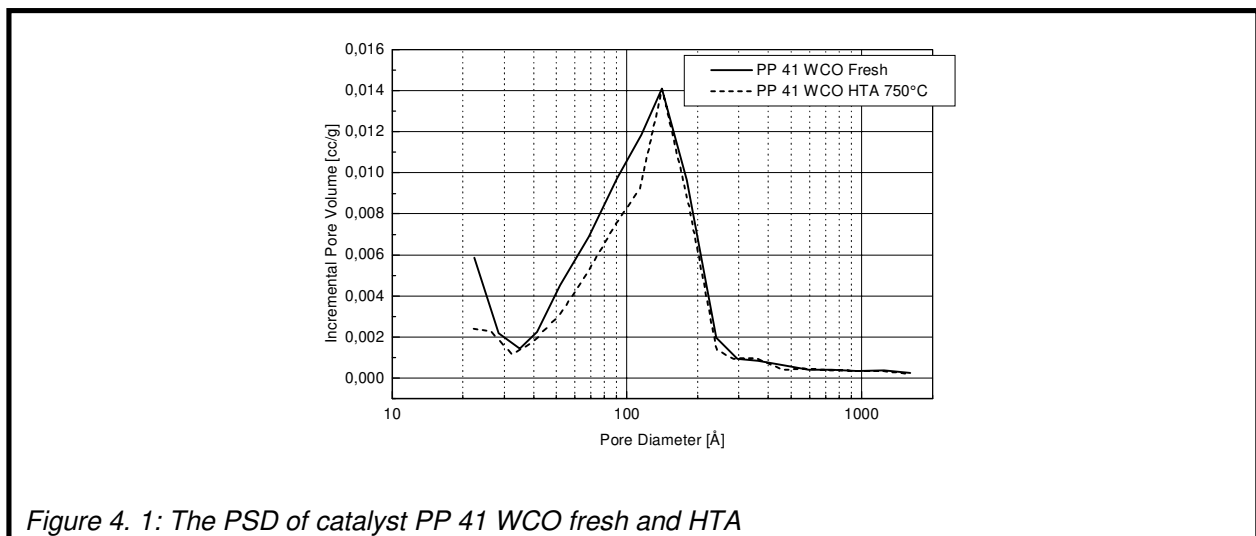


Figure 4. 1: The PSD of catalyst PP 41 WCO fresh and HTA

After ageing, BET surface area, single point pore volume, and average pore diameter are reduced by roughly 20% each. The catalyst has lost a lot of its micropores and some mesopores as well. The number of pores with a diameter larger than 140 Å has not been changed by the ageing process.

**Conclusions:**

The decline of BET surface area and single point pore volume can be explained by the collapse of the micropores. Since the BET surface area is reduced after the ageing one might expect that the average pore diameter would increase. However, the data shows that the reverse is true. The results suggest that the diameters of large diameter pores shrink on ageing because of the thermal treatment or because an oxide layer has build up on the walls of these pores.

*4. 1. 1. 2 LOTs with Al<sub>2</sub>O<sub>3</sub> Washcoat Only Monoliths*

Figures 4. 2 and 4. 3 show the conversion performances for the fresh catalyst PP41 WCO at three different gas mixes specified in Table 4. 2. As discussed in the "Background" chapter, the HC levels emitted from Diesel engines (500 ppm on average) are not high enough to effect substantial lean NO<sub>x</sub> conversion. In order to supply additional reductant to this lean exhaust gas mixture, Diesel fuel may be injected directly into the exhaust pipe, upstream of the catalyst. This method has the synonym Secondary Fuel Injection (SFI). To mimic the increased amount of HC in the gasfeed when using SFI, all LOTs are performed with 800 ppm of HC unless specified differently. After each LOT, a temperature ramp was run to clean of the catalyst of adsorbed species. When the catalyst was removed from the reactor after the six experiments, a black residue was found on top of the washcoat.

LOT 1			LOT 2			LOT 3		
CO <sub>2</sub>	11,9 vol.-%		CO <sub>2</sub>	11,9 vol.-%		CO <sub>2</sub>	11,9 vol.-%	
O <sub>2</sub>	0,3 vol.-% (= λ 0,995)		O <sub>2</sub>	12,1 vol.-% (= λ 2,2)		O <sub>2</sub>	12,1 vol.-% (= λ 2,2)	
CO	401 ppm		CO	398 ppm		CO	400 ppm	
SO <sub>2</sub>	-		SO <sub>2</sub>	-		SO <sub>2</sub>	-	
NO	397 ppm		NO	400 ppm		NO	402 ppm	
C <sub>3</sub> H <sub>6</sub>	800 ppm		C <sub>3</sub> H <sub>6</sub>	800 ppm		C <sub>3</sub> H <sub>6</sub>	796 ppm	
H <sub>2</sub> O	-		H <sub>2</sub> O	-		H <sub>2</sub> O	6,4 vol.-%	
SV	18800 hr <sup>-1</sup>		SV	18800 hr <sup>-1</sup>		SV	18800 hr <sup>-1</sup>	
T <sub>i</sub> <sup>0</sup> → dT/dt → T <sub>i</sub> <sup>max</sup>	80°C → 20°C/min → 720°C		T <sub>i</sub> <sup>0</sup> → dT/dt → T <sub>i</sub> <sup>max</sup>	80°C → 20°C/min → 720°C		T <sub>i</sub> <sup>0</sup> → dT/dt → T <sub>i</sub> <sup>max</sup>	80°C → 20°C/min → 720°C	

Table 4. 2 Gas mix specifications during LOTs shown in Figure 4. 2 and 3

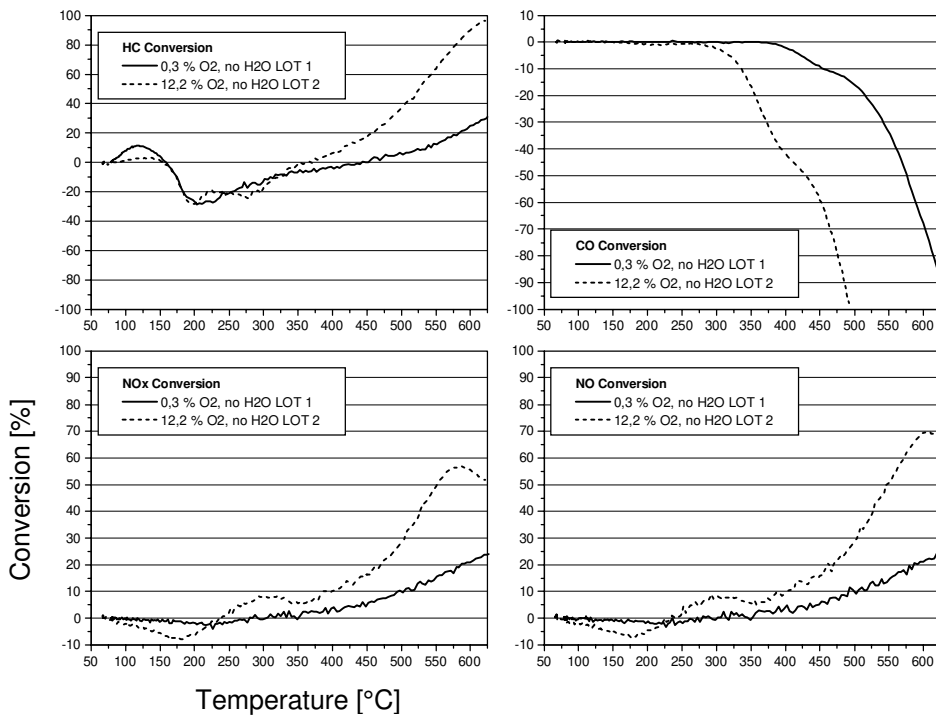


Figure 4. 2: Conversion performances of PP41 WCO

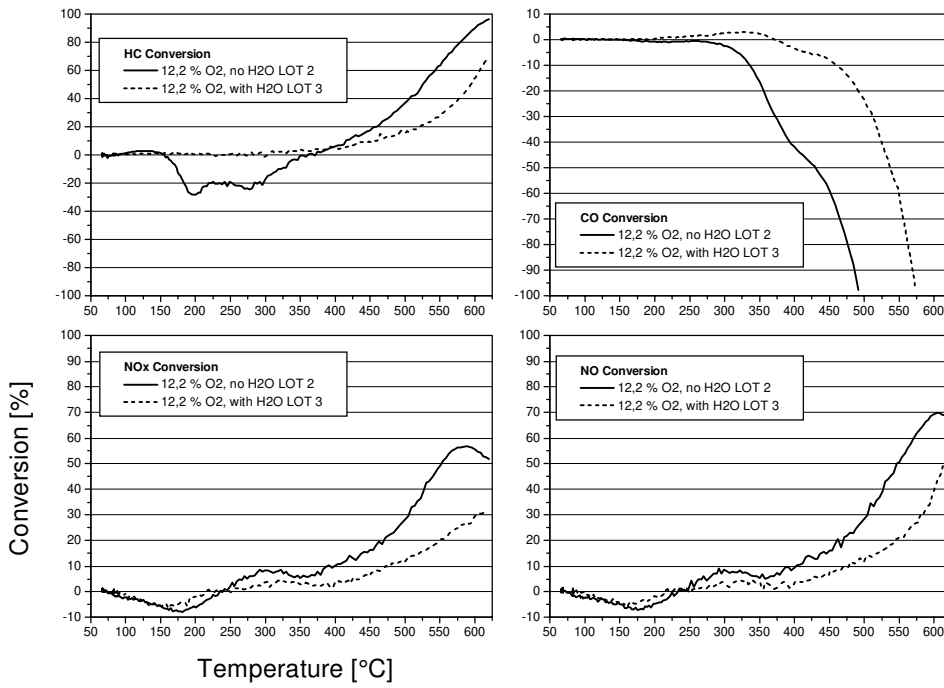


Figure 4. 3: Conversion performance of PP 41 WCO

### Observations made for HC conversion:

Figure 4. 2 shows the influence of oxygen concentration and Figure 4. 3 the influence of water on the catalyst's performance.

During LOT 1 the HC conversion shows a local maximum of 10% at 115°C. At 155°C the conversion has declined to zero and a negative conversion ("formation") of HC is observed. This HC "formation" has a maximum at 205°C (-29%). Subsequently, the "formation" slows down and vanishes at 450°C. Positive conversion is recorded again and has reached roughly 30 % at the end of the test.

During LOT 2 the HC light-off curve has a weak local maximum of 3% positive conversion at low temperature (128°C). The HC light-off curve of LOT 2 exhibits roughly the same amount of HC "formation" (-28%) as observed in LOT 1. The HC "formation" during LOT 2 ends at 360°C. After that positive conversion is recorded which reaches nearly 100% at 625°C at the end of the test.

During LOT 3 neither a local maximum of positive HC conversion nor a negative conversion is observed. Positive HC conversion begins at 305°C and thus earlier than during LOT 1 and LOT 2. At the end of the experiment the HC conversion is 68%.

### Conclusions:

Certainly, the "formation" of HC observed for LOT 1 and LOT 2 is rather a desorption of HC than a formation from C and H. The adsorption of HC probably occurs partly during the time allowed for the analysers to stabilise before the LOT is started. The positive HC conversion observed at temperatures between 80°C and 155°C during LOT 1 and LOT 2 is likely to be caused by the continued adsorption of the HC on the alumina. LOT 2 features a lower positive low-temperature HC conversion than LOT 1. The reason for this is presumably that not all HC stored during LOT 1 was removed by the temperature ramp performed after LOT 1. Hence, the total HC adsorption capability of the Al<sub>2</sub>O<sub>3</sub> washcoat was lower prior to LOT 2.

Judged by the sizes of the negative maxima of the HC conversion curves in Figure 4. 2 it can be concluded that a similar amount of HC is desorbed from the catalyst during LOT 1 and LOT 2 and that no HC desorbs during LOT 3. Based on these three observations it may be postulated that the HC storage capability of the Al<sub>2</sub>O<sub>3</sub> is

independent from the amount of O<sub>2</sub> in the feed gas but reduced by the presence of water.

The activity of Al<sub>2</sub>O<sub>3</sub> for HC conversion at temperatures higher than 360°C over pure alumina is favoured by a high content of oxygen in the feed gas. This is indicated by the earlier onset of the HC conversion during LOT 2 (360°C) than during LOT 1 (450°C) and a higher conversion at the end of LOT 2 (~100% compared to 30% in LOT 1).

With water in the feedgas the HC adsorption capability and the HC oxidation activity of alumina are reduced. Therefore no HC desorption is detected during LOT 3 and the HC conversion measured during this LOT stays behind that measured during LOT 2. The reduction of the HC adsorption and oxidation capability of alumina in the presence of water is probably caused by the loss of acidic and basic sites<sup>65</sup>. Desai et al.<sup>65</sup> explain that the initial contact of water vapour with an alumina surface at 298 K will lead to chemisorption involving dissociation of the water molecule into H<sup>+</sup> and OH<sup>-</sup> ions which attach to the surface sites (Figure 4.4).

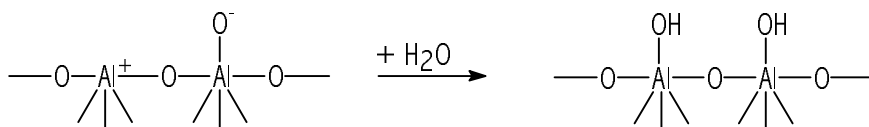


Figure 4. 4: Reaction between water and alumina surface sites

A removal of the chemisorbed water requires vacuum and temperatures above 350°C<sup>65</sup>. Water therefore competes effectively with HC for adsorption sites.

The reduction of the HC adsorption capability is not a totally negative effect: too much HC on the surface "chokes" the onset of the HC oxidation reaction. With less HC on the alumina, HC conversion during LOT 3 can begin at a lower temperature (305°C) than during LOT 2 (360°C), even though water is present. Nevertheless, the presence of water reduces the activity of the catalyst for HC oxidation and therefore the HC conversion at the end of LOT 3 (68%) has not the same magnitude as at the end of LOT 2 (~100%).

#### Observations made for CO conversion:

No CO removal can be observed in LOT 1 and LOT 2. CO formation is observed in all three LOTs. LOT 3 does show positive CO conversion to a very limited extent

between 195°C and 370°C. From 370°C onward, CO formation is detected during LOT 3. In LOT 1 the formation starts at 372°C, in LOT 2 it starts at 255°C. Thus, CO formations for LOT 1 and LOT 2 start 70°C and 105°C earlier, respectively, than the corresponding HC conversions. During LOT 3, CO formation occurs 65°C after the onset of HC conversion. CO<sub>2</sub> formation always coincides with CO formation (not shown).

### Conclusions:

From the observations it may be postulated that in the absence of water CO oxidation over an alumina only catalyst occurs - if it occurs at all - only to a very limited extent. It can not be ruled out that CO oxidation takes place on the alumina at high temperatures. However, due to the high amount of CO generated by incomplete HC combustion at elevated temperatures the small CO conversion can not be detected during LOT 1 and 2. The positive CO conversion during LOT 3 gives evidence that some CO oxidation occurs in the presence of water probably because of the water-gas shift<sup>18</sup>. The formation of CO during LOT 3 starts at a higher temperature (370°C) than during LOT 2 (255°C). Thus, it may be concluded that the presence of water has a twofold effect: (1) it may promote the CO conversion to CO<sub>2</sub> because of a reaction between CO and H<sub>2</sub>O, (2) it inhibits HC oxidation.

The recorded negative CO conversion is caused mainly by the formation of CO resulting from incomplete combustion of HC. CO desorption may contribute to the observed negative conversion but this contribution is probably low.

Since CO and CO<sub>2</sub> formation is observed already while desorption of HC still takes place during LOT 1 and LOT 2, it can be concluded that until the HC desorption ends, the CO and CO<sub>2</sub> amounts recorded originate from the oxidation of the HC stored on the washcoat. This implies that no HC from the gas phase can be adsorbed and converted during this temperature interval. A theory developed by Meyer<sup>110</sup> can give an explanation why adsorption of HC does not take place between 255°C and 360°C: If the coverage of an adsorbent on a surface is high, some adsorption sites which are actually free can not be used for adsorption due to sterical hindrances by already adsorbed molecules. This phenomena has been called the "parking problem". As soon as the HC curve reaches positive values

again, these hindrances have become less significant. HC from the gas phase is adsorbed and can be converted.

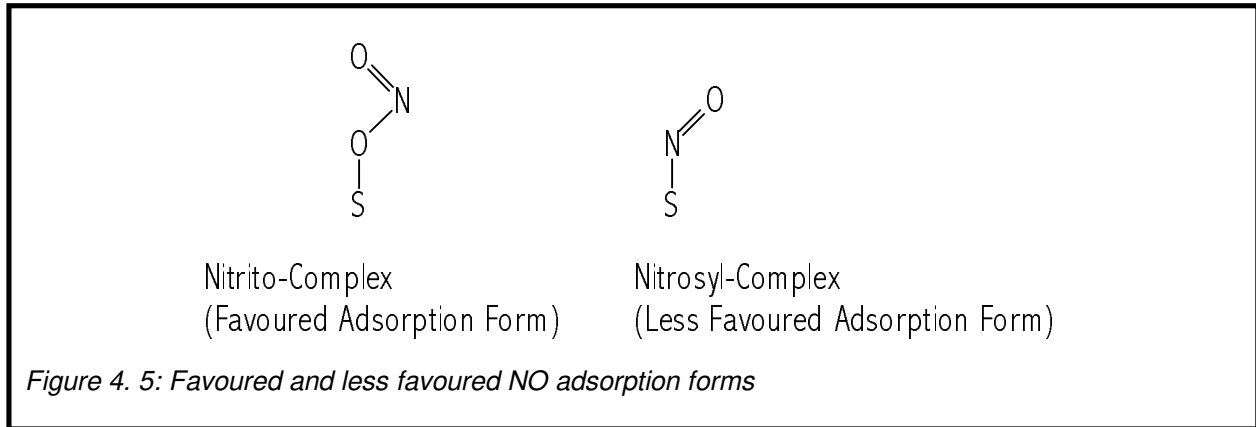
#### Observations made for NO<sub>x</sub> conversion:

The NO<sub>x</sub> light-off curves of LOT 1, 2, and 3 start with negative conversion and have a local maximum (of negative conversion) at 220°C, 180°C, and 160°C respectively. The negative conversion is most pronounced for LOT 2 (-8%). For LOT 1 it is least pronounced (-3%). LOT 1 begins to show positive conversion from 300°C onward while positive conversions for LOT 2 and 3 are recorded already at 235°C. During LOT 1 NO<sub>x</sub> conversion achieves a maximum of 25% at the end of the experiment. The NO<sub>x</sub> light-off curve of LOT 2 exhibits a shoulder at 310°C with roughly 10% conversion and has a maximum of positive conversion at 585°C with 57% conversion. A shoulder is also observed in the NO<sub>x</sub> light-off curve of LOT 3, but it is much smaller (4%) than the one recorded during LOT 2 (10%). NO<sub>2</sub> formation was not detected throughout LOT 1. During LOT 2 and 3 NO<sub>2</sub> formation was recorded from 545°C. At 610°C 63 ppm NO<sub>2</sub> were measured during LOT 2 and 66 ppm NO<sub>2</sub> during LOT 3 in the reactor effluent (not shown).

#### Conclusions:

The direct formation of NO is thermodynamically disallowed at the temperatures investigated. Therefore the observed negative conversions must be a desorption of NO<sub>x</sub>. Since the NO<sub>x</sub> and NO light-off curves during LOT 1, 2, and 3 are similar during the temperature interval of negative NO<sub>x</sub> conversion, it may even be stated that the desorbed species is only NO, not NO<sub>2</sub>. Otherwise there would be more negative NO<sub>x</sub> conversion than negative NO conversion. The adsorption of NO probably takes place during the time which is allowed for the analysers to stabilise at low inlet temperatures, when the feedgas already passes over the catalyst. A high oxygen concentration in the feedgas obviously favours the amount of NO adsorbed on Al<sub>2</sub>O<sub>3</sub>. This can be explained by an adsorbate assisted adsorption. The favoured adsorption form seems to be a nitrito-complex rather than a nitrosyl-complex, Figure 4. 5. The presence of water reduces the NO<sub>x</sub> adsorption capacity of alumina -presumably by poisoning adsorption sites -, but the capacity is still larger than in the absence of oxygen.





The beginning of positive  $\text{NO}_x$  conversion in LOT 1 ( $300^\circ\text{C}$ ) does not coincide with neither the onset of positive HC conversion ( $450^\circ\text{C}$ ) nor with the beginning of CO formation ( $372^\circ\text{C}$ ) and can be divided into two phases. The first phase lasts from  $300^\circ\text{C}$  to  $450^\circ\text{C}$  and the second phase from  $450^\circ\text{C}$  until the end of the experiment. During the second phase the slope of the curve is steeper. This, in combination with the observation that phase 1 ends at the same temperature where positive HC conversion starts, suggests a change in the NO conversion mechanism at  $450^\circ\text{C}$ . During the first phase most of the alumina surface is covered with HC.  $\text{NO}_x$  reduction can only proceed slowly on a few remaining free active sites. When the HC conversion becomes positive, the surface coverage by HC has decreased and hence, a larger number of active alumina sites are available. NO conversion occurs more rapidly, and the slope of the conversion curve becomes steeper.

Similar observations as for LOT 1 are also made for LOT 2 and a change of mechanism can explain the shoulder observed in the  $\text{NO}_x$  conversion curve of LOT 2 as outlined before. Between  $235^\circ\text{C}$  and  $300^\circ\text{C}$  adsorbed  $\text{NO}_x$  is reduced by co-adsorbed, close proximity HC. At  $300^\circ\text{C}$  CO and  $\text{CO}_2$  formations indicate that adsorbed HC is now consumed by oxidation and hence the supply of HC for  $\text{NO}_x$  reduction is decreased. No additional HC is adsorbed from the gas phase until the temperature has reached  $360^\circ\text{C}$  because of the parking problem explained above. The lack of reductant causes the decline of  $\text{NO}_x$  conversion. At  $360^\circ\text{C}$  enough HC has been removed from the  $\text{Al}_2\text{O}_3$  surface either by oxidation or desorption for the sterical hindrance to become less significant. Now HC adsorption from the gas phase takes place again and causes the rise of  $\text{NO}_x$  conversion. At  $585^\circ\text{C}$  HC

consumption by oxidation starts to dominate over the HC-NO<sub>x</sub> reduction reaction. Consequently, NO<sub>x</sub> conversion declines again.

It is proposed that the reason for the decline of NO<sub>x</sub> conversion efficiency in the presence of water during LOT 3 is the competition between water and HC for adsorption sites. Because of this competition less HC is adsorbed and therefore less reductant is available on the alumina surface. The explanation for the shoulder which is observed for LOT 3 is probably the same as that outlined in the conclusion from LOT 2.

NO can react in three ways. The first possibility is that 2 NO molecules are adsorbed, dissociate, and N-N and O-O recombination result in the formation of N<sub>2</sub> and O<sub>2</sub>. It must be kept in mind though that the dissociation of NO over alumina has not been reported in literature. The second possibility is that one adsorbed NO dissociates and the freshly formed N atom combines with an adsorbed but not dissociated NO molecule to form N<sub>2</sub>O. However, since an N<sub>2</sub>O analyser was not available for this thesis this N<sub>2</sub>O formation can not be proven experimentally. The third possibility is that NO reacts directly with adsorbed HC. This third reaction path supports the mechanisms above and is therefore assumed to be correct.

At 540°C it is likely that most of the HC has been removed from the washcoat surface and that adsorbed oxygen is the dominant species on the surface. NO is now easily oxidised to form NO<sub>2</sub>. The amount of NO<sub>2</sub> formed equals the amount which is thermodynamically permitted and is only slightly dependent on the presence or absence of H<sub>2</sub>O.

#### Observations made for NO conversion:

The NO and NO<sub>x</sub> conversion curves of LOT 1 are similar. The same is true for LOT 2 and LOT 3 until the temperature reaches 540°C. After this temperature NO conversion is higher than NO<sub>x</sub> conversion in LOT 2 and LOT 3.

#### Conclusions:

The NO conversion recorded during the LOTs is the sum of reduced NO plus oxidised NO (to form NO<sub>2</sub>). Based on the similarity of the NO and NO<sub>x</sub> conversion curves below 540°C it may be postulated that at these temperatures no NO oxidation takes place: the observed NO conversion is a reduction of NO to either N<sub>2</sub> and O<sub>2</sub> or

N<sub>2</sub>O. Since no N<sub>2</sub>O analyser was available it can not be stated which product was formed. It may be assumed that the oxygen concentration during LOT 1 is too low to cause NO oxidation. During LOT 2 and 3 the oxygen concentration is high enough and NO<sub>2</sub> formation can be observed from 540°C onward. NO reduction continues as well since otherwise the NO<sub>x</sub> conversion curve would drop to zero.

#### 4. 1. 1. 3 Temperature Ramps with Al<sub>2</sub>O<sub>3</sub> Washcoat Only Monoliths

Figure 4. 6 shows the temperature ramp desorption spectra obtained after each of LOT 1, 2, and 3. In all cases the carrier gas was N<sub>2</sub>, the heating rates were 20°C/min, and the maximum inlet temperature was 510°C. The concentration values recorded during these temperature ramps have to be interpreted as qualitative information. The method applied was too crude to give reliable quantitative data regarding the amounts of species desorbed.

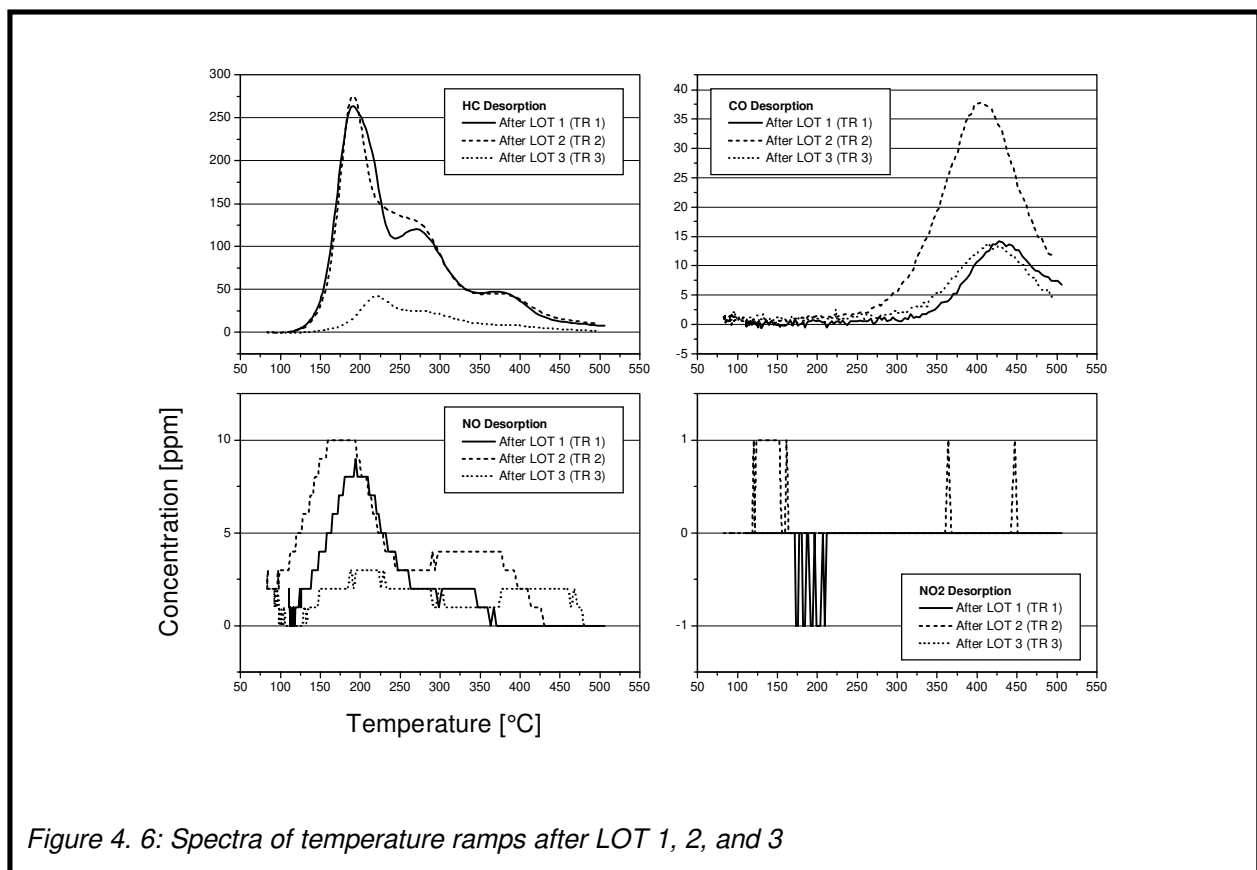


Figure 4. 6: Spectra of temperature ramps after LOT 1, 2, and 3

### Observations made for HC desorption:

Desorption of HC starts at 105°C during TR 1 and 2, and at 135 °C during TR 3.

TR 1 and 2 show their first desorption peaks both at 190°C. The height of the first desorption peak of TR 2 (276 ppm) exceeds the height of the first desorption peak of TR 1 (263 ppm). It must be pointed out again that the peak values are only given to make the comparison of the temperature ramp results easier. They may not represent the true values of the amounts desorbed. The magnitude of the first desorption peak of TR 3 (42 ppm) is roughly 15% of the sizes of the first peaks of TR 1 and 2. At 270°C, TR 1 goes through a local maximum (120 ppm) whereas the desorption curve of TR 2 shows a shoulder (130 ppm). TR 3 displays its first shoulder at 275°C (25 ppm). At 370°C, TR 1 and 2 both show a shoulder of identical height (45 ppm). TR 3 has a second shoulder at 385°C (9 ppm). It may be concluded that the amount of HC desorbed during TR 3 is 20% of that desorbed during TR 1 or TR 2.

### Conclusions:

The observed desorption peaks of TR 1 and TR 2 coincide well with the (negative) peaks observed during the HC formation phase of LOT 1 and 2, respectively. The amounts of HC desorbed during TR 1 and 2 correspond roughly to the amounts of HC desorbed during the LOTs 1 and 2. Obviously the presence or absence of oxygen does not influence the HC storage capacity of pure Al<sub>2</sub>O<sub>3</sub>.

The presence of water on the other hand, reduces HC storage capacity significantly. This leads to the conclusion that water and HC compete for adsorption sites. The shift of the three desorption peak temperatures noticed in TR 3 as compared to TR 1 and 2 also indicates an interaction between H<sub>2</sub>O and the adsorbed HC, which results in HC desorption at higher temperature.

The three distinct desorption temperatures that have been detected during all three temperature ramps can have two reasons. Either the HC is stored on three different sites each with a growing strength of interaction between support and HC, or different types of HC fragments are detected which can not be distinguished due to the analyser measuring total HC content of the reactor effluent.

### Observations made for CO desorption:

Each temperature ramp features a CO desorption peak. The earliest onset of CO desorption is observed during TR 2 at 220°C. This temperature ramp features a desorption peak at 405 °C (38 ppm). The peak is nearly 3 times larger than the desorption peaks of TR 1 and 3. CO desorptions during TR 1 and 3 start both at 280°C. The CO desorption peak heights are identical for both ramps (14 ppm) but the peak of TR 1 is located at 415°C and that of TR 3 at 400°C. Desorption of CO<sub>2</sub> could not be established.

### Conclusions:

The CO detected during the temperature ramps may have two origins. It may be CO that was stored on the washcoat during the preceding LOTs and is desorbing during the ramp. Alternatively it may emanate from a reaction during the temperature ramp between stored HC and co-adsorbed oxygen. Oxygen desorption was not detected during the temperature ramp but it must be mentioned that the measuring range of the oxygen analyser was set to 20 vol.-% and consequently was not very sensitive for ppm amounts of oxygen desorbing.

Since only very little oxygen was present in the gas mix during LOT 1, it may be assumed that not much of this oxygen was stored during the LOT on the washcoat. Hence, the CO detected during TR 1 is likely to originate from CO adsorbed during the preceding LOT 1.

During LOT 2, the concentration of oxygen in the gas mix is probably high enough for significant oxygen adsorption on the washcoat. Some of the CO measured during TR 2 may therefore emerge from a reaction between adsorbed oxygen and co-adsorbed HC. Additionally desorbing CO - pre-adsorbed during LOT 2 - may contribute to the CO detected during TR 2.

Compared to TR 2, less CO is detected during TR 3. Although the oxygen concentration during the preceding LOT 3 was probably high enough for oxygen adsorption to take place, the reaction between the adsorbed oxygen and co-adsorbed HC during the temperature ramp might be retarded by the presence of water. Because of this it may be concluded that the CO detected during TR 3 is mainly CO which was pre-adsorbed during LOT 3.

#### Observations made for NO and NO<sub>2</sub> desorption:

Only very little NO and no NO<sub>2</sub> desorption was measured during all three temperature ramps. In all cases desorption starts at 100°C. TR 2 has a peak at 175°C (10 ppm) and a second peak at 335°C (4 ppm). TR 1 has a maximum at 195°C (9 ppm). NO desorption during TR 3 is insignificant.

#### Conclusions:

Increasing the amount of oxygen in the feedgas of the preceding LOT increases the amount of NO desorbed from the Al<sub>2</sub>O<sub>3</sub> washcoat during the temperature ramp slightly. The reason for this is probably that the adsorption of NO during LOT 2 is assisted by oxygen. The observation that the presence of H<sub>2</sub>O during LOT 3 deteriorates NO adsorption capability leads to the conclusion that water and NO compete for adsorption sites on the alumina washcoat.

#### *4. 1. 1. 4 Examination of Al<sub>2</sub>O<sub>3</sub> Washcoat Only Monoliths with TEM and EDX after the LOTs*

A black residue was found on top of the washcoat on the monolith. The residue was examined by transmission electron microscopy (TEM) and energy dispersive x-ray analysis (EDX). As a reference an untested washcoat sister (a core from the same full sized monolith) was examined in the same manner.

#### Observations:

Figure 4. 7 shows a TEM picture taken from the sample which was tested in the SCAT reactor. A carbon particle is clearly visible in the middle. EDX detected for the same sample Fe, Cr, S, and Si within a variety of particles with the addition of graphitised and amorphous carbon particles. Except for amorphous Si, the examination of the untested sample did not detect any of these elements.

#### Conclusions:

All of the detected elements may contribute to the black residue found on top of the SCAT tested sample. The predominant contributor is carbon. The existence of a carbonaceous layer on top of the washcoat is thereby established. The origin of Fe, Cr, and S is unclear. However, the amounts of these elements were very small and it

may be speculated that they are impurities. The detection of Si is caused by impurities of the  $\text{Al}_2\text{O}_3$ .

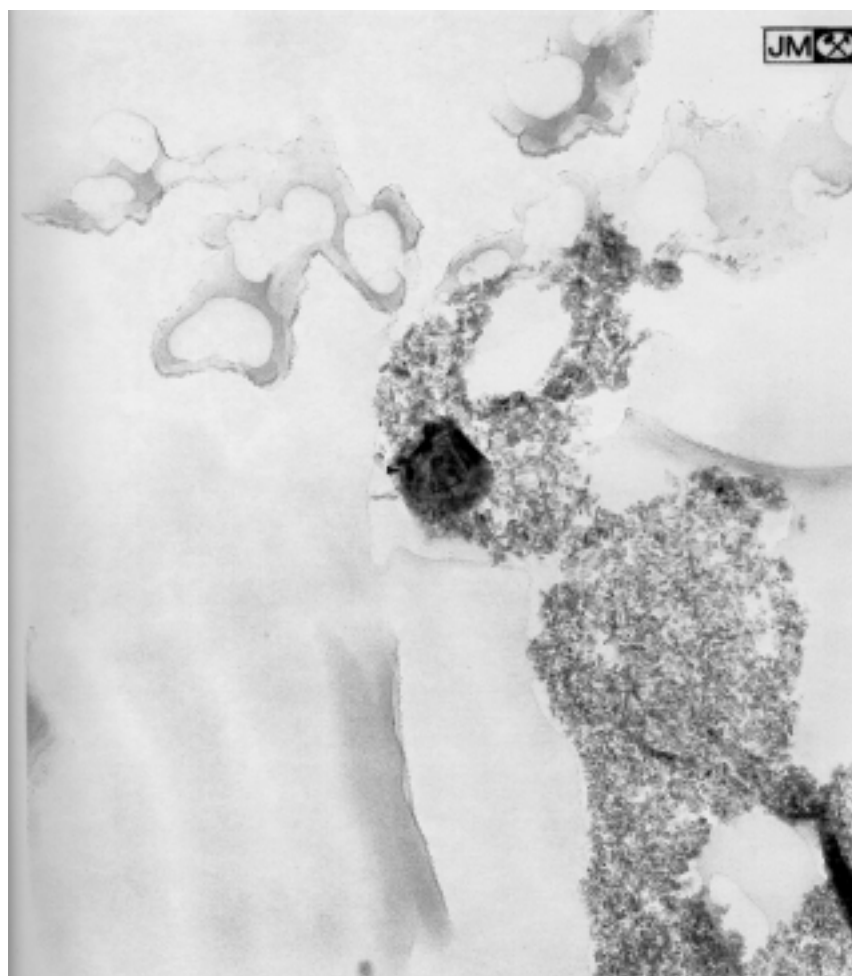


Figure 4. 7: A TEM picture of the SCAT tested  $\text{Al}_2\text{O}_3$  washcoat. Magnification 1:115 000

#### 4. 1. 2 Zeolites

##### 4. 1. 2. 1 Characterisation of a Zeolite Containing Washcoat by BET Measurements

As for the alumina catalyst, the BET surface area, the single point pore volume, average pore diameter, and the pore size distribution of both a fresh and a hydrothermally aged sample of catalyst DEV5 WCO were measured. Ageing was performed at 750°C for 10 hours in a 10% water in air mixture.

Observations:

The results are summarised in Table 4. 3 and in Figure 4. 8.

Sample	BSA [m <sup>2</sup> /g]	SPPV [cc/g]	APD [Å]
DEV5 washcoat only fresh	43,1	0,074620	72,2
DEV5 washcoat only HTA 750°C	35,4	0,073841	62,4

Table 4. 3: Results of BET measurements of catalyst DEV5 WCO fresh and HTA

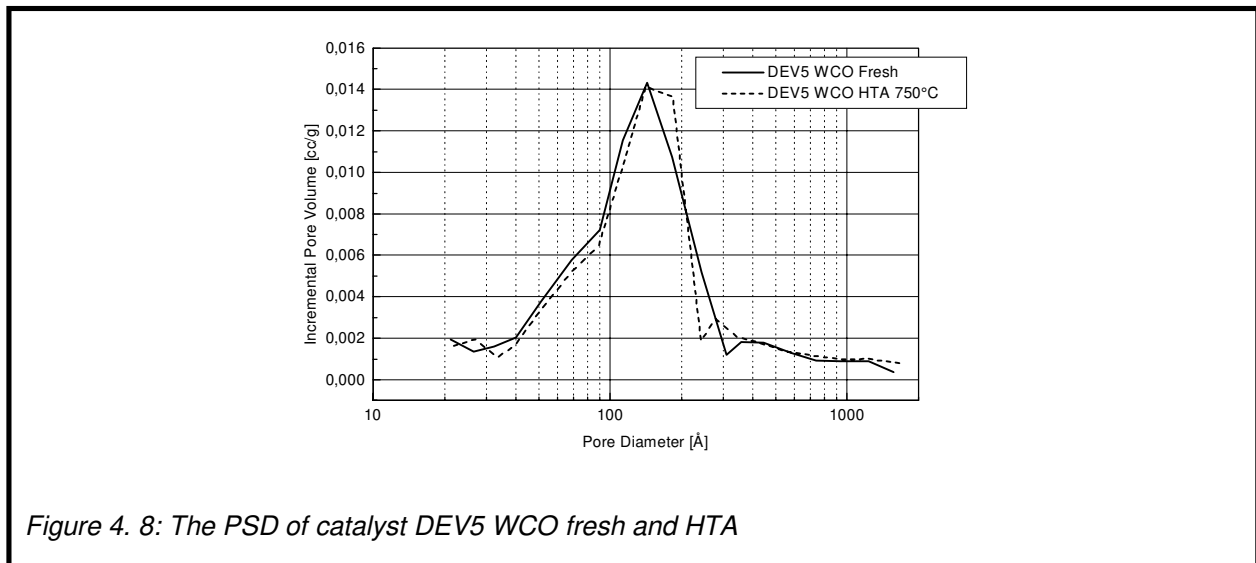


Figure 4. 8: The PSD of catalyst DEV5 WCO fresh and HTA

The ageing process reduces the BET surface area from 43,1 m<sup>2</sup>/g by 18% to 35,1 m<sup>2</sup>/g, the single point pore volume is nearly unchanged, and the average pore diameter is reduced by 14% from 72 Å to 62 Å. Apparently, the pore size distribution of this catalyst has not changed.

Conclusions:

The observations made are quite controversial. The fact that neither the pore size distribution nor the single point pore volume have changed suggests that no pores and no pore-volume is lost due to the ageing. However, the BET surface area has decreased which is usually caused by a collapse of micropores. This sample maintained more of its BET surface area, single point pore volume, average pore diameter and pore size distribution than the alumina sample PP 41 WCO. This is surprising because zeolite-containing washcoats are commonly known to be less stable against ageing than alumina washcoats.



#### 4. 1. 2. 2 LOTs with Zeolite-Containing Washcoat Only Monoliths

Figures 4. 9 and 10 show the conversion performances for the fresh catalyst DEV5 WCO at three different gas mixes specified in Table 4. 4. After each LOT, a temperature ramp was performed to clean of the catalyst from adsorbed species. Again a black residue was found on top of the washcoat when the catalyst was removed from the reactor after the six experiments. By visual judgement it seemed that more residue was left on this zeolite-containing catalyst than on the PP 41 WCO (alumina) catalyst.

LOT 4		LOT 5		LOT 6	
CO <sub>2</sub>	12,0 vol.-%	CO <sub>2</sub>	12,0 vol.-%	CO <sub>2</sub>	12,0 vol.-%
O <sub>2</sub>	0,3 vol.-% (= λ 0,995)	O <sub>2</sub>	12,1 vol.-% (= λ 2,2)	O <sub>2</sub>	12,1 vol.-% (= λ 2,2)
CO	398 ppm	CO	402 ppm	CO	398 ppm
SO <sub>2</sub>	-	SO <sub>2</sub>	-	SO <sub>2</sub>	-
NO	401 ppm	NO	402 ppm	NO	400 ppm
C <sub>3</sub> H <sub>6</sub>	800 ppm	C <sub>3</sub> H <sub>6</sub>	800 ppm	C <sub>3</sub> H <sub>6</sub>	798 ppm
H <sub>2</sub> O	-	H <sub>2</sub> O	-	H <sub>2</sub> O	6,4 vol.-%
SV	18800 hr <sup>-1</sup>	SV	18800 hr <sup>-1</sup>	SV	18800 hr <sup>-1</sup>
T <sub>i</sub> <sup>0</sup> → dT/dt → T <sub>i</sub> <sup>max</sup>	80°C → 20°C/min → 720°C	T <sub>i</sub> <sup>0</sup> → dT/dt → T <sub>i</sub> <sup>max</sup>	80°C → 20°C/min → 720°C	T <sub>i</sub> <sup>0</sup> → dT/dt → T <sub>i</sub> <sup>max</sup>	80°C → 20°C/min → 720°C

Table 4. 4 Gas mix specifications during LOTs shown in Figure 4. 9 and 10

#### Observations made for HC conversion:

Negative conversion is observed for LOT 4, 5, and 6 starting at 145°C, 135°C, and 158°C, and ending at 405°C, 330°C, and 341°C, respectively. Two distinct maxima of negative conversion at 190°C and 275°C are observed for LOT 4 (-71%; -86%) and LOT 5 (-54%; - 72%). LOT 6 features a maximum of negative conversion at 275°C (-49%) and a broad shoulder around 220°C (-40%). At the end of the test LOT 4 achieves a HC conversion of 53% at 670°C, while in LOT 5 and 6 more than 96% HC is converted at 670°C. The slope of positive HC conversion during LOT 6 is less steep than during LOT 5. A small local maximum of positive conversion is noticed at 140°C during LOT 6.

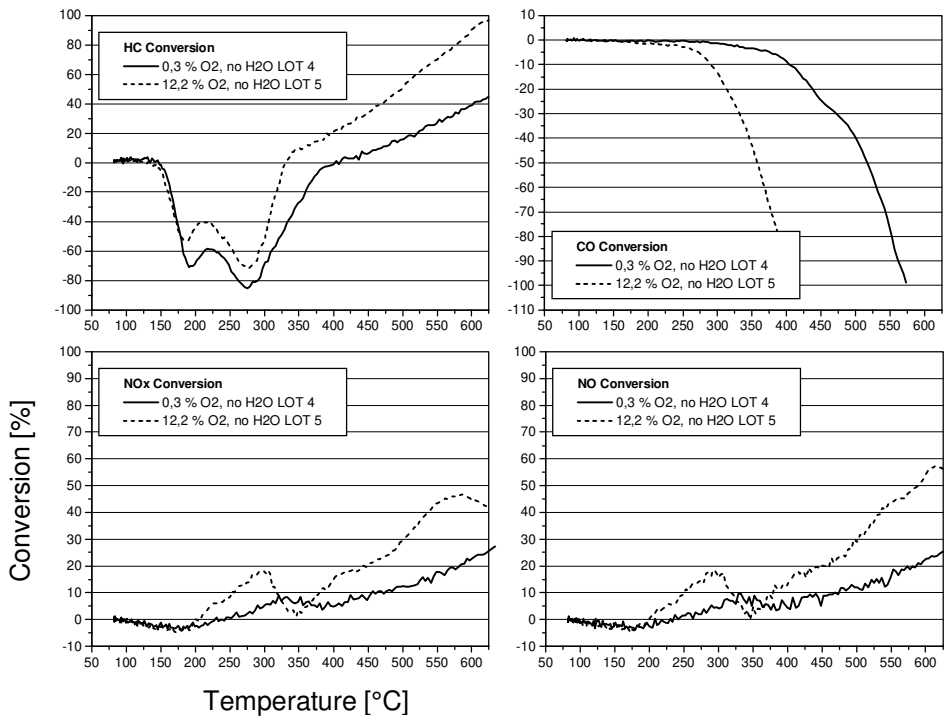


Figure 4. 9: Conversion Performance of DEV5 washcoat only sample

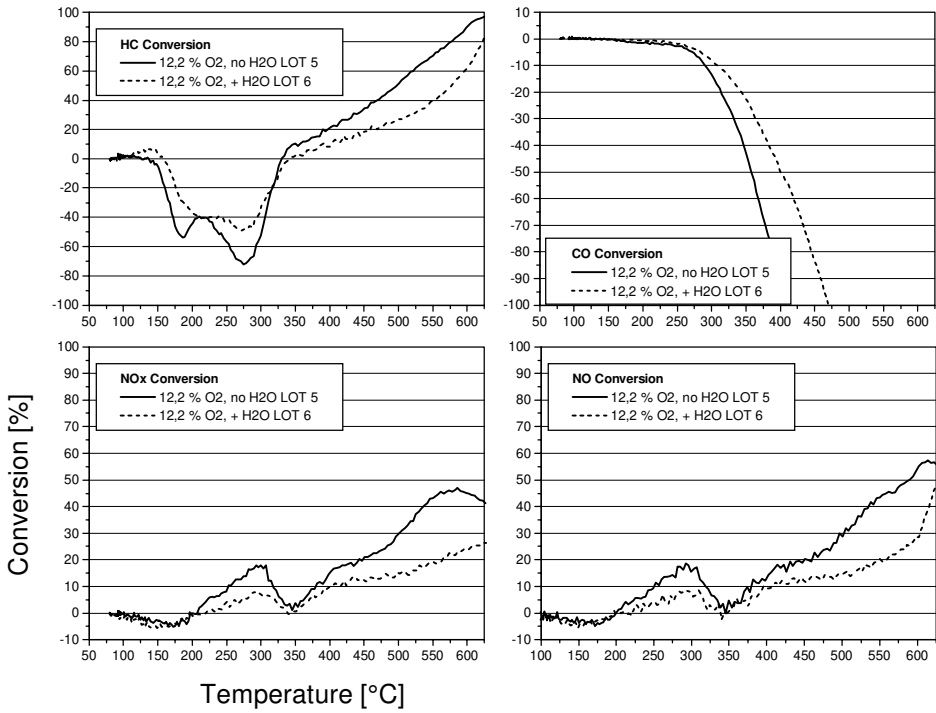


Figure 4. 10: Conversion Performance of DEV5 washcoat only sample

### Conclusions:

Significant "formation" of HC by release during the LOTs was anticipated for this sample since zeolites are well known for their HC storage capability. A high concentration of oxygen in the feed gas apparently reduces the amount of HC released. The co-adsorption of oxygen seems to have a negative effect on the HC storage capacity. Alternatively one could argue that the highly oxidising atmosphere simply oxidises the HC earlier but since CO<sub>2</sub> formation does not start before 300°C during LOT 5 (not shown) this can not be the case. The amount of HC released during the LOT is lower if water is in the gas mix. It was already observed for the alumina washcoat that water competes with the HC molecules for adsorption sites. Obviously this is also the case on a zeolite-containing washcoat.

The maxima observed during the HC desorption phases of LOT 4, 5, and 6 suggest that either two different sites adsorb the HC with increasing adsorption strength, or that two different types of HC fragments are recorded which in turn also adsorb with different heats of adsorption on the zeolite-containing washcoat.

The presence of water in the feed gas reduces the rate at which positive HC conversion can progress. However, at 625°C similar HC conversion is achieved as without water in the feedgas.

The local maximum of positive HC conversion observed during LOT 6 is not caused by a low temperature HC oxidation. There is no CO<sub>2</sub> formation measured during the corresponding interval. Hence, in LOT 6 the positive low-temperature conversion must be storage of HC. The time required for the HC concentration to stabilise prior to the LOT is much longer if a zeolite-containing catalyst is tested in the SCAT reactor. Before the HC concentration achieves stability the zeolite has to be saturated with HC. This happens very slowly on zeolite-containing washcoats compared to alumina washcoats. Possibly the time allowed for this was not long enough prior to LOT 6. Therefore, some storage capability was still available at the beginning of the test.

### Observations made for CO conversion:

CO formation during LOT 4, 5, and 6 starts at 285°C, 155°C, and 220°C respectively and thereby always precedes positive HC conversion which begins at 405°C, 330°C,

and 341°C, respectively. No positive CO conversion is observed on the zeolite-containing washcoat during any of these LOTs.

### Conclusions:

The CO formation is caused predominantly by incomplete HC oxidation. CO desorption may take place but presumably does not contribute significantly to the amount of CO detected. The zeolite-containing washcoat seemingly can not oxidise CO, but as for the Al<sub>2</sub>O<sub>3</sub> catalyst, CO oxidation may not be ruled out completely at high temperatures. The amount of CO oxidised might just not be visible because the high amount of CO formed superposes on the amount of CO oxidised.

A high concentration of oxygen in the feedgas favours HC oxidation and therefore CO formation begins at lower temperatures during LOT 5 (155°C) than during LOT 4 (285°C). The addition of water to the gas mix reduces the activity of the zeolite-containing washcoat to oxidise HC. This is reflected by the higher temperature at which CO formation occurs during LOT 6 (220°C) compared to LOT 5.

Since CO formation always precedes positive HC conversion, the same mechanism of HC conversion can be assumed for the zeolite-containing washcoat as for the Al<sub>2</sub>O<sub>3</sub> washcoat. That is, with increasing temperature the HC stored on the zeolite-containing washcoat is oxidised first and no additional HC is adsorbed because of the parking problem. As HC release ends, the adsorption of HC from the gas phase is no longer sterically impeded and HC from the gas phase is adsorbed and oxidised.

### Observations made for NO<sub>x</sub> conversion:

All three NO<sub>x</sub> light-off curves start with negative conversion. The maxima of these negative NO<sub>x</sub> conversions are of similar size and occur at the same temperature (170°C). Positive NO<sub>x</sub> conversion of LOT 4, 5, and 6 starts at 236°C, 203°C, and 219°C, respectively. Three local maxima of positive conversion are recorded. These maxima are located at 328°C for LOT 4, and at 300°C for LOT 5 and 6. The positive local maximum of LOT 5 is largest in size (18%). Maximum NO<sub>x</sub> conversion during LOT 4 is achieved at 643°C (27%), during LOT 5 at 582°C (46%), and during LOT 6 at 628°C (26%). No NO<sub>2</sub> formation was detected during LOT 4. During LOT 5 and 6 NO<sub>2</sub> formation starts at 560°C.

### Conclusions:

Similar conclusions to those made for the  $\text{Al}_2\text{O}_3$  washcoat are found for the zeolite-containing washcoat. The observed negative conversion is a desorption of NO from the washcoat.  $\text{NO}_2$  is not detected during the desorption interval. The presence of water in the gas mix does not appear to have an influence on the amount of NO desorbed during LOT 6 from the zeolite-containing washcoat. Hence it may be postulated that NO and  $\text{H}_2\text{O}$  do not compete for the same adsorption sites on this washcoat.

A high oxygen concentration in the feedgas improves positive  $\text{NO}_x$  conversion. This is proven with LOT 5 having the earliest onset ( $203^\circ\text{C}$ ) and the highest conversion of  $\text{NO}_x$  (46%). There may be two reasons for the positive effect of oxygen: (1) adsorbed oxygen might assist the adsorption of NO. With more NO being adsorbed, more NO will react with the co-adsorbed HC, (2) the oxygen might "clean" the washcoat partly from HC. This creates active sites on the washcoat for adsorption of NO and thereby favours the reaction of NO with the co-adsorbed HC. The presence of water deteriorates the positive effect of high  $\text{O}_2$  concentration dramatically: the  $\text{NO}_x$  conversion during LOT 6 (26%) equals that of LOT 4 (27%). The reason for this might be a decline of the HC storage capacity of the zeolite-containing washcoat caused by the water. Since there is less HC stored on the washcoat there is less reductant available for  $\text{NO}_x$  reduction. Additionally the water might impede the reaction between  $\text{NO}_x$  and HC and also deter the washcoat from adsorbing NO.

The appearance of the shoulders in all three  $\text{NO}_x$  light-off curves can be explained in a similar way as for LOT 2 of the alumina washcoat. At first, adsorbed  $\text{NO}_x$  is reduced by co-adsorbed HC which is located in close proximity to the  $\text{NO}_x$ . This HC supply starts to decrease at the temperature of the local  $\text{NO}_x$  conversion maximum ( $328^\circ\text{C}$  in case of LOT 4 and  $300^\circ\text{C}$  in case of LOT 5 and 6). HC is now consumed increasingly by desorption and oxidation. During this phase of the LOT, no additional HC is adsorbed from the gas phase because of the parking problem explained previously (page 76). The lack of reductant causes a decline of the  $\text{NO}_x$  conversion curve. At a certain temperature, enough HC has been removed from the washcoats surface for the parking problem to disappear and HC adsorption from the gas phase takes place again. The new supply of reductant causes a second rise of the  $\text{NO}_x$

conversion curve. At high temperatures, i.e. higher than the temperatures where maximum NO<sub>x</sub> conversions occur, HC consumption by oxidation starts to dominate over the HC-NO<sub>x</sub> reduction reaction. Consequently, NO<sub>x</sub> conversion by reduction declines.

Observations made for NO conversion:

The NO conversion curves of all three LOTs are identical to the NO<sub>x</sub> conversion curves until NO<sub>2</sub> formation begins in LOT 5 and 6 (at 560°C).

Conclusions:

The same conclusions as for the Al<sub>2</sub>O<sub>3</sub> washcoat apply. Until the formation of NO<sub>2</sub> starts, NO<sub>x</sub> conversion is only the reduction of NO. During the temperature interval of NO<sub>x</sub> reduction the possibility of the formation of N<sub>2</sub>O can not be excluded since no N<sub>2</sub>O analyser was available. Only during LOT 5 and 6 the oxygen concentration is high enough for NO<sub>2</sub> formation. As soon as NO<sub>2</sub> formation starts, NO conversion is the sum of NO reduction and NO oxidation.

*4. 1. 2. 3 Temperature Ramps with Zeolite-Containing Washcoat Only Monoliths*

Figure 4. 11 shows the temperature ramp desorption spectra obtained after LOT 4, 5, and 6. In all cases the carrier gas was N<sub>2</sub>, the heating rates were 20°C/min, and the maximum inlet temperature was 510°C. The reader shall be reminded that the peak values are only given to make the comparison of the temperature ramp results easier. They may not represent the true values of the amounts desorbed for the same reasons given in chapter 4. 1. 1. 3.

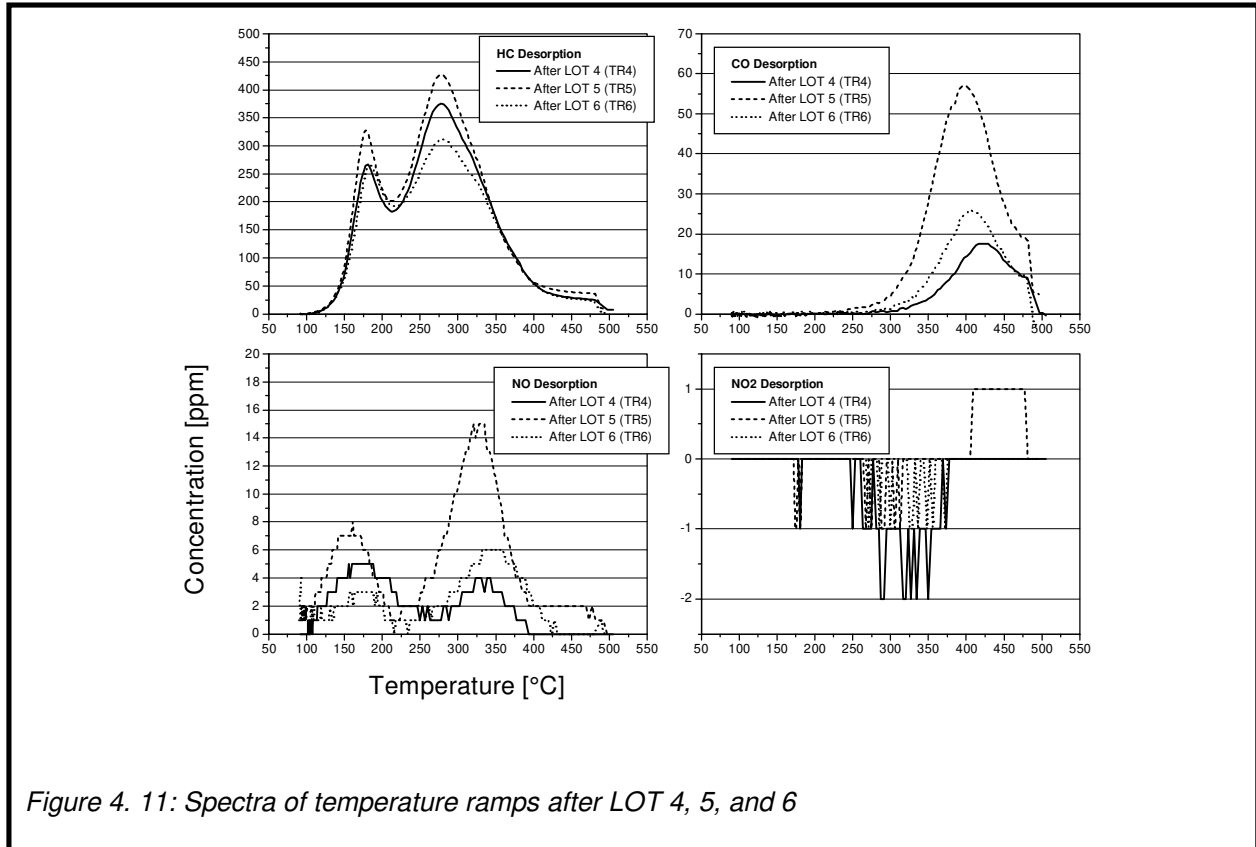


Figure 4. 11: Spectra of temperature ramps after LOT 4, 5, and 6

#### Observations made for HC desorption:

HC desorption starts at 100°C during all three temperature ramps. All three spectra show two HC desorption peaks. The first peak is observed at 180°C. The height of this peak is identical for TR 4 and 6 (264 ppm). In TR 5 the peak is 20% larger (328 ppm). The second peak occurs at 278°C and the intensity declines in the order TR 5 (427 ppm) > TR 4 (376 ppm) > TR 6 (312 ppm).

#### Conclusions:

The positions of the peaks during the temperature ramps coincide well with the positions of the peaks of negative HC conversion observed during the LOTs which occurred at 190°C and 275°C.

The two maxima suggest that two different adsorption sites with increasing interaction strength with the adsorbate exist on the washcoat or that two different species are adsorbed with different adsorption strengths. The high concentration of oxygen in the feedgas during LOT 5 increases the sizes of both desorption peaks in TR 5. It may be speculated that the reason for this is that the oxygen assists the HC

storage on the zeolite-containing washcoat. The presence of water during LOT 6 reduces the adsorption capability of the second HC adsorption site significantly as indicated by the reduced size of peak 2 in TR 6 compared to peak 2 in TR 4 and 5. Depending on whether two different adsorption sites or two different species are the cause for the two peaks in the temperature ramps, the water may either poison the second adsorption site or deter the washcoat from adsorbing the second species. The equipment used for these experiments does not allow to decide between the two possibilities. Since the temperatures where the desorption peaks occur are similar in TR 4, 5, and 6 it may be assumed that the strength of HC adsorption on the zeolite-containing washcoat is not influenced by the presence or absence of oxygen or water. This is in contrast to the observation made in TR 3 for the alumina washcoat where the presence of water shifts the positions of the desorption peaks to higher temperatures compared to TR 1 and 2.

#### Observations made for CO desorption:

CO desorption begins during TR 4 at 270°C. During TR 5 CO desorption is recorded from 205°C onward and at 245°C CO desorption starts in TR 6. Desorption maxima occur during TR 4 at 421°C (18 ppm), during TR 5 at 397°C (57 ppm), and during TR 6 at 403°C (26 ppm). Desorption of CO<sub>2</sub> was not detected.

#### Conclusions:

As concluded from the temperature ramps performed with the Al<sub>2</sub>O<sub>3</sub> washcoat the CO detected during the temperature ramps performed with the zeolite-containing washcoat may have two origins. It may be CO that was stored on the washcoat during the preceding LOTs and is desorbing during the ramps. Alternatively it may emanate from a reaction during the ramps between stored HC and co-adsorbed oxygen. Since the oxygen content of the feedgas during LOT 5 was high and most CO is detected in TR 5, it may be inferred that during TR 5 some of the CO emerges from a reaction between stored HC and co-adsorbed oxygen.



#### Observations made for NO and NO<sub>2</sub> desorption:

The NO desorption spectra show two peaks for each LOT. They are located at 175°C and 332°C in TR 4, 175°C and 346°C in TR 5, and 161°C and 327°C in TR 6. No NO<sub>2</sub> desorption is recorded.

#### Conclusions:

It may be postulated that there are two adsorption sites, each with increasing adsorption strength as observed for HC. If the oxygen concentration during the LOT is high, more NO is desorbed during the TR. The reason for this is probably an assistance of the NO adsorption on the zeolite-containing washcoat by the oxygen. The presence of water during the LOT reduces the amount of NO desorbing from the washcoat during the temperature ramp possibly by poisoning adsorption sites.

#### *4. 1. 3 Summary*

BET measurements indicate that the zeolite-containing washcoat formulation DEV5 WCO presents good stability against hydrothermal ageing. This is noteworthy because zeolite-containing washcoats are commonly known to lose their structural integrity quickly during an ageing treatment.

By TEM and EDX measurements it was established that a carbonaceous deposit is formed on the alumina washcoat during the LOTs. A black residue was also found on the zeolite-containing washcoat after it has been tested in the SCAT rig. It may be assumed that this residue is a similar carbonaceous deposit as the one found on the alumina washcoat.

HC oxidation occurs on both, an alumina and a zeolite-containing washcoat. A high concentration of oxygen strongly favours the activity for HC oxidation. The HC oxidation activity is reduced by the presence of water in the gas mix.

HC is desorbed during the temperature ramps and the LOTs from the alumina and the zeolite-containing washcoat. Most HC is adsorbed on the zeolite-containing washcoat. The concentration of oxygen in the feedgas during the LOT has no influence on the HC storage capacity of the alumina washcoat but it has an influence on the amount of HC stored on the zeolite-containing washcoat: If the oxygen concentration in the gas mix during the LOT is high, the amount of HC stored on the zeolite-containing washcoat is smaller than the amount stored if the oxygen

concentration is low during the LOT. If water is present in the gas mix, the amount of HC adsorbed on both washcoats decreases.

In all LOTs and on both washcoats, CO formation from incomplete HC combustion is observed. The zeolite-containing washcoat is unable to oxidise CO, while the alumina washcoat can achieve CO oxidation to a certain extent because of the "water-gas" equilibrium<sup>18</sup> if water is present in the feedgas.

The alumina and the zeolite-containing washcoat store NO<sub>x</sub> in form of NO. A high O<sub>2</sub> concentration in the feedgas favours NO adsorption while in the presence of water less NO is adsorbed. NO is reduced on both washcoats at temperatures higher than 200°C. During the LOTs, the adsorbed NO reacts first with the HC already adsorbed on the washcoats. Additional HC adsorption from the gas phase does not take place before a certain amount of previously stored HC has been removed from the washcoats by reaction with NO, oxidation of HC, or desorption of HC. This is attributed to the "parking problem" described in literature<sup>110</sup>. N<sub>2</sub>O as a product of the NO<sub>x</sub> reduction reaction can not be ruled out but could not be measured since no N<sub>2</sub>O analyser was available. The reduction of NO is favoured by a high concentration of oxygen in the gas mix and by the absence of water. At temperatures between 200°C and 350°C, the zeolite-containing washcoat reduces more NO<sub>x</sub> than the alumina washcoat. The reason for this is probably that the zeolite stores more HC than the alumina washcoat and therefore more reductant for NO<sub>x</sub> is available on the zeolite-containing washcoat.

NO<sub>2</sub> formation takes place on both washcoats, but only if the content of oxygen in the gas mix is high and at temperatures above 540°C

Several authors<sup>66-70</sup> have reported activity of Al<sub>2</sub>O<sub>3</sub> for NO<sub>x</sub> reduction. The most plausible results are presented by Radtke et al.<sup>112</sup>. Radtke reported 34% NO<sub>x</sub> reduction at 585°C and that CO was the prevailing product of the oxidation of propene. They observed almost no N<sub>2</sub>O formation during the LOT and very little NO<sub>2</sub>. In this thesis, tests performed with an alumina washcoat-only catalyst verified several of Radtke's<sup>112</sup> results. The reason for the higher NO<sub>x</sub> conversion obtained over the alumina washcoat in this thesis (57%) compared with Radtke's 34% is probably the much higher oxygen content (11,9 vol.-%) in the gas mix used in this thesis compared to Radtke's 2 vol.-%. The promoting effect of oxygen for the NO reduction over alumina has been reported elsewhere<sup>66-70</sup>. Most of these researchers

believe that the contribution of oxygen is the oxidation of NO to NO<sub>2</sub> which is subsequently reduced by the hydrocarbon. This can not be confirmed from the results of this thesis because NO<sub>2</sub> formation over the Al<sub>2</sub>O<sub>3</sub> washcoat was only detected at temperatures above 540°C. This thesis presents two explanations why a high O<sub>2</sub> concentration in the gas mix favours NO<sub>x</sub> reduction: (1) adsorbed O atoms may assist the adsorption of NO, (2) the oxygen may "clean" the washcoat partly from HC. This creates active sites on the washcoat for adsorption of NO and thereby favours the reaction of NO with the co-adsorbed HC. The negative influence of water also reported by the above named research groups has once more been established in this thesis. The water presumably reduces the amount of HC reductant on the washcoat because H<sub>2</sub>O and HC compete for adsorption sites. Additionally the water might impede the reaction between NO<sub>x</sub> and HC and also deter the washcoat from adsorbing NO.

## **4. 2 Pt/Al<sub>2</sub>O<sub>3</sub> Catalysts**

Pt has been reported to be active for the reduction of NO<sub>x</sub> even under highly oxidising conditions (refer to "Background" chapter). The influences of four properties of a Pt/Al<sub>2</sub>O<sub>3</sub> catalyst on the conversion performance of this catalyst were extensively examined in this thesis: Pt load, Pt dispersion, washcoat load, and washcoat surface area. A total of 16 different catalyst formulations were coated on cordierite monoliths for this purpose. Four identical cores of each formulation, named a, b, c, d, were prepared in order to perform destructive and non-destructive tests simultaneously. The sample specifications can be found in the "Appendix". Another Pt/Al<sub>2</sub>O<sub>3</sub> sample, named PP 41 38 is included in this section since it is used as a reference in subsequent chapters.

### *4. 2. 1 Characterisation of the Pt/Al<sub>2</sub>O<sub>3</sub> Samples by BET and COC Measurements*

The 16 samples and sample PP 41 38 were examined by BET and CO chemisorption (COC) measurements. The Pt dispersion ( $D_M$ ) and the metal surface area (MSA) were measured by COC. The BET surface area, the single point pore volume, and the average pore diameter were examined by BET measurements.

Sample PP 41 38 was examined in the fresh state and after hydrothermal ageing. Ageing was performed at 750°C for 10 hours in a 10% water in air mixture.

Observations:

The BET and COC data obtained from ASAP 2000 measurements with the fresh and the high temperature aged (HTA) catalyst sample PP 41 38 are given in Table 4. 5 and Figure 4. 12. In Figure 4. 12 the pore size distribution of PP 41 WCO is included for better comparison.

Sample	Measured $D_M$ [%]	MSA [ $m^2/g$ ]	BSA [ $m^2/g$ ]	SPPV [ml/g]	APD [Å]
PP 41 38 fresh	11	0,07	39,2	0,117	114,8
PP 41 38 HTA 750°C	6	0,04	31,5	0,105	133,0

Table 4. 5: Results of BET and COC measurements of catalyst PP 41 38 fresh and HTA

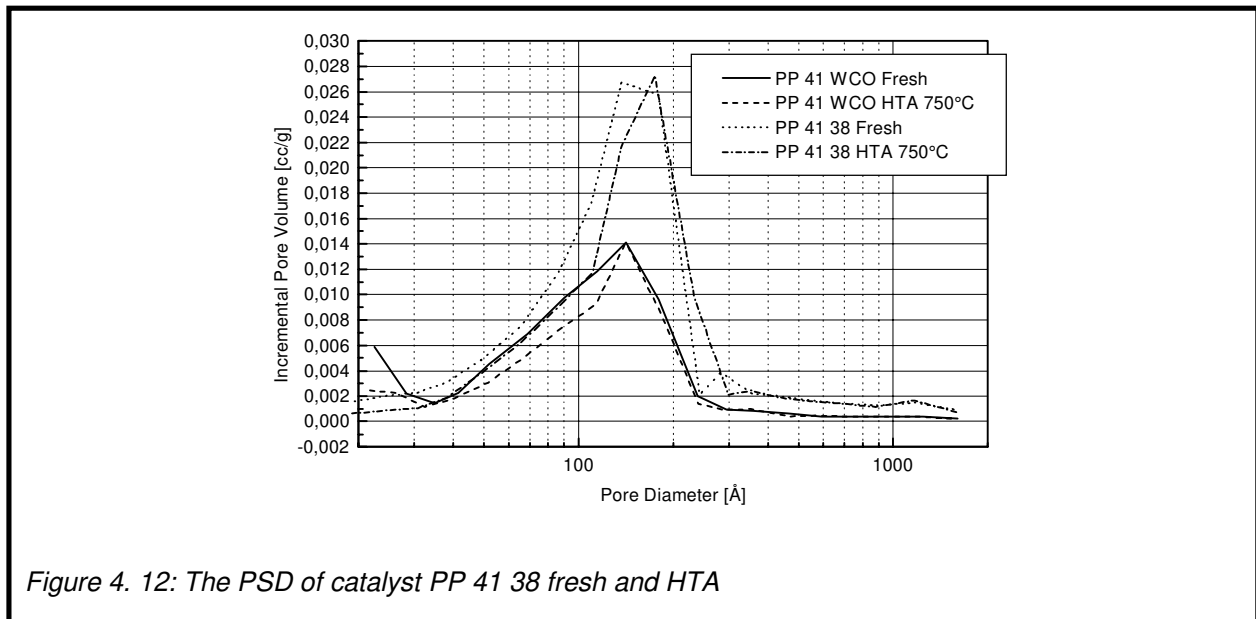


Figure 4. 12: The PSD of catalyst PP 41 38 fresh and HTA

Table 4. 6 shows the BET and COC results of the 16 different catalyst formulations mentioned above.

The measured Pt particle size was calculated from the measured CO dispersion using Equation 4. 1<sup>113</sup>.

$$r_{PtP} = \frac{500}{D_M} \quad \text{Equation 4. 1}$$

Sample	Intended PPS [Å]	Measured PPS [Å]	Measured $D_M$ [%]	MSA [m <sup>2</sup> /g]	BSA [m <sup>2</sup> /g]	SPPV [ml/g]	APD [Å]
4093a	10	19	25,7	0,1396	24,7	0,068	110,4
4094a	50	79	6,4	0,0345	14,7	0,042	113,3
4095a	10	26	19,1	0,2600	21,8	0,060	111,1
4096a	50	80	6,3	0,0851	18,9	0,054	114,3
4097a	10	21	24,0	0,1303	30,3	0,062	81,4
4098a	50	65	7,7	0,0418	26,5	0,062	94,3
4099a	10	11	46,6	0,6337	33,9	0,070	82,4
4100a	50	68	7,3	0,0994	25,8	0,059	91,5
4101a	10	14	34,8	0,1631	36,9	0,103	112,1
4102a	50	74	6,7	0,0315	33,2	0,098	118,2
4103a	10	12	42,7	0,5067	36,1	0,100	110,7
4104a	50	95	5,3	0,0624	33,9	0,100	117,6
4105a	10	18	27,9	0,1311	47,8	0,107	89,5
4106a	50	52	9,6	0,0450	42,1	0,102	96,7
4107a	10	20	25,1	0,2973	54,6	0,123	89,4
4108a	50	95	5,3	0,0626	40,8	0,100	97,6

Table 4. 6: Results of BET and COC measurements of fresh samples

During the ageing of sample PP 41 38, the dispersion is reduced from 11% to 6%, the number of pores with a diameter below 170 Å decreases, the single point pore volume decreases from 0,117 ml/g to 0,105 ml/g, and the average pore diameter increases from 115 Å to 133 Å. For sample PP 41 WCO a decrease in single point pore volume and average pore diameter was found after the ageing procedure.

The addition of Pt to the alumina washcoat does neither reduce nor increase the BET surface area (BSA without Pt: 39,8 m<sup>2</sup>/g; BSA with Pt: 39,2 m<sup>2</sup>/g). The pore size distribution shows that the number of pores with a pore diameter between 70 Å and 240 Å has increased after the Pt was added to the alumina washcoat. single point pore volume and average pore diameter of PP 41 38 are nearly doubled compared to sample PP 41 WCO (SPPV for PP 41 WCO: 0,07 cc/g; SPPV for PP 41 38: 0,12 cc/g; APD for PP 41 WCO: 72 Å; APD for PP 41 38: 115 Å).

Table 4. 6 shows that measured and intended platinum particle sizes (PPS) are close to each other with certain variations. The BET surface area of the samples in Table 4. 6 is strongly related to the Pt particle size. If the Pt particle size changes from small to large, the BET surface area decreases.

If the surface area of the Al<sub>2</sub>O<sub>3</sub> used for the preparation of a sample increases from 140 m<sup>2</sup>/g to 230 m<sup>2</sup>/g, the measured BET surface area increases by 10 m<sup>2</sup>/g on average and the measured average pore diameter is reduced by roughly 20%.

Changing the washcoat load of a sample from 100 to 200 g/l increases the measured BET surface area by 15 m<sup>2</sup>/g on average and doubles the single point pore volume.

### Conclusions:

A decrease of metal dispersion of supported precious metal catalysts during a hydrothermal ageing treatment is well known to occur with many metals on many supports. This process will be discussed in more detail in the chapter "The Influence of Ageing". The collapse of pores with a diameter below 170 Å is probably responsible for the decreased number of these pores after the ageing of sample PP 41 38 as well as for the decrease of the single point pore volume. The two observations that the average pore diameter of sample PP 41 38 has increased from 115 Å to 133 Å during ageing while the average pore diameter of sample PP 41 WCO has decreased from 72 Å to 58 Å during hydrothermal ageing suggest that the presence of Pt on the washcoat widens the pores of the washcoat during the ageing process.

The metal surface area (MSA) measured by COC on sample PP 41 38 is very small (0,07 m<sup>2</sup>/g) compared to the BET surface area measured with sample PP 41 WCO (39,8 m<sup>2</sup>/g). Hence, the addition of Pt to the washcoat does not enlarge the measured total BET surface area of sample PP 41 38 to a noticeable extent. From the observation that the number of pores with a diameter between 70 Å and 240 Å is increased (Figure 4. 12) and the single point pore volume and the average pore diameter are nearly doubled on sample PP 41 38 compared to PP 41 WCO it may be concluded that the addition of Pt to the washcoat causes the pores of the washcoat to widen. Thus, the addition of Pt to an alumina washcoat causes the washcoat pores to widen during the preparation of the Pt/Al<sub>2</sub>O<sub>3</sub> sample as well as during the ageing of this sample.

A comparison between the measured and intended Pt particle size of the samples 4093a - 4108a shows that the specifications of the samples prepared meet the specifications of the samples demanded very well. The decrease of BET surface area with increasing Pt particle size may be explained by postulating that Pt particles of a certain size are able to block washcoat pores. Figure 4. 13 shows that the increase of Pt particle size from sample 4093a to 4094a results in a significant loss

of pores with diameters between 40 Å and 300 Å. These pores can not be reached by the nitrogen gas used in the BET experiments anymore. Hence, the measured BET surface area decreases. This indicates also that reactant gases can not reach the interior of these pores anymore. Any precious metal encapsulated inside such pores is unable to contribute to the catalyst's purpose. Thus it can be postulated that the catalysts with a high Pt particle size will show poorer overall performance during the LOTs.

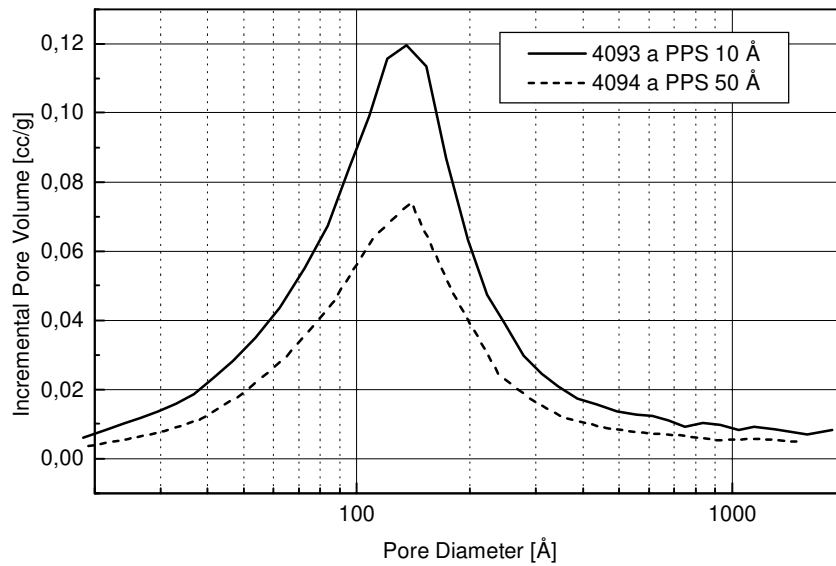


Figure 4. 13: The loss of pore volume due to PPS increase

#### 4. 2. 2 LOT Performance of Pt/Al<sub>2</sub>O<sub>3</sub> Catalysts

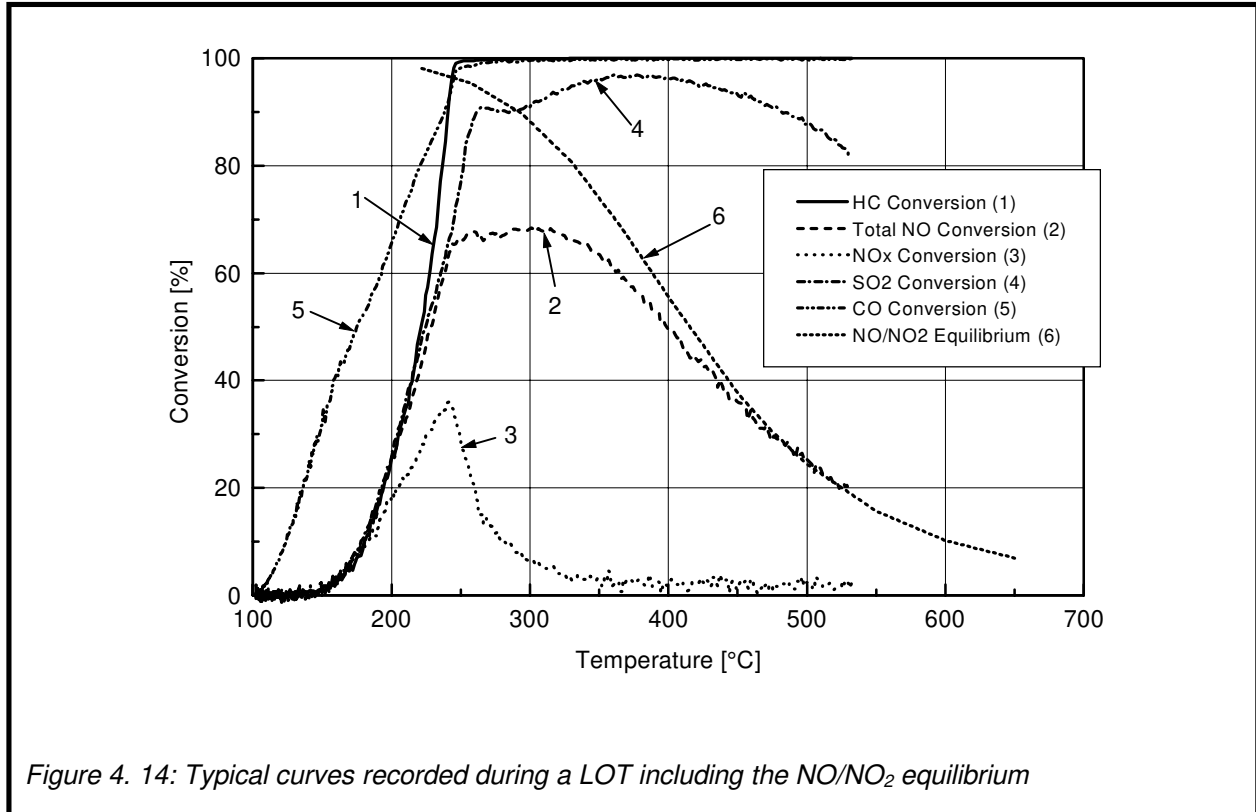
All samples of Table 4. 6 were tested under the same conditions. The concentrations of the gases used in the feedgas are given in Table 4. 7.

CO <sub>2</sub>	4,7 vol.-%
O <sub>2</sub>	12,2 vol.-% (= λ 2,2)
CO	200 ppm
SO <sub>2</sub>	21 ppm
NO	400 ppm
C <sub>3</sub> H <sub>6</sub>	800 ppm
H <sub>2</sub> O	6,4 vol.-%
SV	30000 hr <sup>-1</sup>
T <sub>i</sub> <sup>0</sup> → dT/dt →	80°C →
T <sub>i</sub> <sup>max</sup>	10°C/min →
	530°C

Table 4. 7: Test conditions during LOTs performed in this section

General observations made during LOTs:

Figure 4. 14 shows the curves obtained during a typical LOT. Typical features are the coincident of maximum  $\text{NO}_x$  conversion and total HC conversion, the shape of



the CO conversion curve which rises earlier but is less steep than the HC conversion curve, the decrease of  $\text{SO}_2$  formation at temperatures higher than  $400^\circ\text{C}$ , and the fact that the maximum NO conversion is always higher than the maximum  $\text{NO}_x$  conversion ( $\text{NO}_x^{\text{max}}$ ).

The fact that  $\text{NO}_x^{\text{max}}$  and total HC conversion coincide indicates that HC has a pivotal role in the overall  $\text{NO}_x$  reduction mechanism on a  $\text{Pt}/\text{Al}_2\text{O}_3$  catalyst. At temperatures higher than the temperature where 100% HC conversion is achieved (THC(100)) the extent of  $\text{NO}_x$  reduction is decreasing strongly. At this temperatures there is less HC available on the catalyst's surface because HC is now readily consumed by oxygen. However, since the  $\text{NO}_x$  conversion does not fall to zero immediately, some HC must still be present on the catalyst's surface to react with  $\text{NO}_x$ . This reaction probably takes place in the very first part of the monolith facing the feedgas. Further along the length of the catalyst, the concentration of HC decreases rapidly and no reductant is left to react with  $\text{NO}_x$ .



The different onsets of the CO and the HC conversion curves suggest that the activation energy for the oxidation of CO is lower than the activation energy for the oxidation of HC. However, since the slope of the CO conversion curve is less steep than the slope of the HC conversion curve, the progress of the CO oxidation seems to be inhibited in a certain way. As soon as the activation energy for HC oxidation is overcome, the HC light-off curve rises steeply with no indication of an inhibition. The reason for this different behaviour of CO and HC light-off is discussed in the section 4. 6.

SO<sub>2</sub> is converted by oxidation to SO<sub>3</sub>. At low temperature the oxidation is kinetically limited. At high temperatures it is thermodynamically restricted. Hence there is a temperature window in which the SO<sub>2</sub> conversion reaches a maximum.

The reason for the maximum NO conversion being higher than the maximum NO<sub>x</sub> conversion is that NO conversion is NO<sub>x</sub> reduction on the one hand, and NO oxidation to NO<sub>2</sub> on the other. Although some groups<sup>83</sup> reported that NO<sub>2</sub> formation does not occur before NO<sub>x</sub><sup>max</sup>, this could not be verified in this thesis. In most LOTs NO<sub>2</sub> formation began slightly after the onset of NO<sub>x</sub> reduction. At temperatures higher than 450°C the amount of NO<sub>2</sub> formed equals the NO/NO<sub>2</sub> equilibrium value.

The descriptive values obtained from the LOTs are:

- THC(50), the temperature at which 50% of the HCs are converted to CO or CO<sub>2</sub>
- TCO(80), the temperature at which 80% of the CO are converted to CO<sub>2</sub>
- NO<sub>x</sub><sup>max</sup>, the maximum NO<sub>x</sub> conversion during the test
- T(NO<sub>x</sub><sup>max</sup>), the temperature at which NO<sub>x</sub><sup>max</sup> occurs
- W(NO<sub>x</sub>), the width of the NO<sub>x</sub> conversion window were at least 20% NO<sub>x</sub> is converted by reduction
- NO<sup>max</sup>, the maximum NO conversion during the test
- T(NO<sup>max</sup>), the temperature at which NO<sup>max</sup> occurs
- NO<sub>2</sub><sup>max</sup>, the maximum conversion of NO to NO<sub>2</sub>
- SO<sub>2</sub>(250), SO<sub>2</sub> conversion at 250°C

It is aspired to create a catalyst formulation which has the lowest possible THC(50), TCO(80), and SO<sub>2</sub>(250) values. Maximum NO<sub>x</sub> conversion and the width of the NO<sub>x</sub> conversion window shall be as large as possible. The temperature at which the maximum NO<sub>x</sub> conversion shall be located, depends very much on the engine out values of the vehicle. In general, a low T(NO<sub>x</sub><sup>max</sup>) is endeavoured. The amount of NO oxidised to NO<sub>2</sub> is not scrutinised very well by most researchers. It should be attempted to keep NO<sub>2</sub><sup>max</sup> low since NO<sub>2</sub> is much more dangerous to human health than NO. Combining these values to calculate an overall performance factor P<sub>c</sub> for each catalyst results in the formula

$$P_c = \frac{NO_x^{\max} + W(NO_x)}{THC(50) + TCO(80) + SO_2(250) + NO_2^{\max}} \quad \text{Equation 4. 2}$$

The SO<sub>2</sub> factor may be neglected if low sulphur fuel is used. The NO<sub>2</sub> formation is not yet subjected to a legislative limit and hence can also be neglected. For most purposes a simplified formula can be used

$$P_c = \frac{NO_x^{\max} + W(NO_x)}{THC(50) + TCO(80)} \quad \text{Equation 4. 3}$$

The P<sub>c</sub> factor serves very well to estimate the influence of the four properties of the Pt/Al<sub>2</sub>O<sub>3</sub> catalyst (Pt dispersion, Pt load, washcoat load, and washcoat surface area) on the overall performance of the catalyst. This is done by calculating the average value of all 8 P<sub>c</sub> factors with, for instance, low washcoat load ({15,0 + 9,1 + 14,5 + 17,6 + 14,9 + 19,5 + 16,3 + 16,0} / 8 = **15,4**) and comparing this average value to that obtained from the samples with high washcoat load (**17,6**). A high P<sub>c</sub> factor indicates that the corresponding parameter will favour the overall performance of the catalyst.

Table 4. 8 shows the values obtained for all 16 samples and the P<sub>c</sub> factor calculated with Equation 4. 3.

		4093	4094	4095	4096	4097	4098	4099	4100
THC(50)	°C	231	241	225	227	230	232	212	231
TCO(80)	°C	222	235	201	220	221	228	196	227
NO <sub>x</sub> <sup>max</sup>	%	27,0	21,2	37,6	42,7	27,3	34,8	38,6	38,1
T(NO <sub>x</sub> <sup>max</sup> )	°C	240	261	235	239	253	248	223	243
NO <sup>max</sup>	%	64,0	61,9	64,2	73,2	68,1	61,7	69,1	73,7
T(NO <sup>max</sup> )	°C	305	299	269	252	301	314	241	255
SO <sub>2</sub> (250)	%	54	56	67	60	69	66	83	65
W(NO <sub>x</sub> )	K	41	22	24	36	40	55	28	35
NO <sub>2</sub> <sup>max</sup>	%	63	58	60	68	63	57	67	67
P <sub>c</sub> * 100		15,0	9,1	14,5	17,6	14,9	19,5	16,3	16,0
		4101	4102	4103	4104	4105	4106	4107	4108
THC(50)	°C	217	229	215	228	203	242	222	233
TCO(80)	°C	202	221	196	205	205	237	209	232
NO <sub>x</sub> <sup>max</sup>	%	31,6	26,8	39,8	36,8	38,9	39,4	45	35,9
T(NO <sub>x</sub> <sup>max</sup> )	°C	231	230	222	247	231	255	226	242
NO <sup>max</sup>	%	73,8	66,3	73,1	63,4	78,8	76,4	79	83
T(NO <sup>max</sup> )	°C	255	273	230	264	248	272	246	249
SO <sub>2</sub> (250)	%	86	79	68	44	92	60	89	61
W(NO <sub>x</sub> )	K	57	40	35	31	50	56	30	20
NO <sub>2</sub> <sup>max</sup>	%	70	58	70	59	69	62	81	75
P <sub>c</sub> * 100		21,1	14,8	18,2	15,7	21,8	19,9	17,4	12,0

Table 4. 8: Values obtained from LOTs with samples 4093d - 4108d

#### 4. 2. 2. 1 The Influence of Pt Load, Observations and Conclusions

The average P<sub>c</sub> factors of all samples with low and high Pt load and the average P<sub>c</sub> factors with a reduced weight of the W(NO<sub>x</sub>) factor are given in Table 4. 9.

Equation used	Low Pt Load	High Pt Load
$\overline{P_c} = \frac{(NO_x^{max} + W(NO_x))}{(THC(50) + TCO(80))}$	17,03	15,95
$\overline{P_c} = \frac{(NO_x^{max} + (W(NO_x) / 100))}{(THC(50) + TCO(80))}$	7,01	9,13

Table 4. 9: Average P<sub>c</sub> factors for low and high Pt load, non-weighted and weighted in W(NO<sub>x</sub>)

From the non-weighted values of Table 4. 9 it could be concluded that a high Pt load causes a decline of the average P<sub>c</sub> factor by 6% from 17,03 to 15,95. A closer look at the data reveals that the values of the NO<sub>x</sub> conversion window width are responsible for this conclusion. Reducing the weight of the W(NO<sub>x</sub>) value in Equation 4.3 by factor 100 results in a significant change of the average P<sub>c</sub> factors to 7,01 for low Pt

load samples and 9,13 for high Pt load samples. Now the overall conversion performance of high Pt load samples exceeds that of low Pt load samples by 23%. The reason why  $W(\text{NO}_x)$  is so negatively influenced by a high load of Pt is not very clear. Increasing the Pt load from 40 g/ft<sup>3</sup> to 100 g/ft<sup>3</sup> reduces the average THC(50) value by merely 4°C from 228°C to 224°C. Hence, an argument suggesting that less HC for  $\text{NO}_x$  reduction is available on the high Pt load samples is imprudent. A possible explanation is that the low Pt load samples were the first tested. After these tests repairs had to be performed on the SCAT rig and the ceramic reactor tube was replaced by a different one. This may well have led to a change in the fluid dynamics of the gases. However, except for the  $W(\text{NO}_x)$  value, all other values obtained before and after the repairs are comparable. The dependence of the width of the  $\text{NO}_x$  conversion window on the Pt load is thus not discussed further.

All THC(50) values recorded during tests with low Pt load samples are averaged resulting in a mean THC(50) value of 228°C. The same was done with the THC(50) values of high Pt load samples (224°C) and in a corresponding manner with all other descriptive values obtained during the LOTs. This makes comparison between samples with variation of one property easier and levels out the influences of those properties of the catalyst which are not currently examined, in this case Pt dispersion, washcoat load and washcoat surface area.

As already mentioned, increasing the Pt load reduces the average THC(50) value slightly by 4°C compared to samples with low Pt load. The average TCO(80) value is reduced by 10°C from 221°C to 211°C by using a high Pt load on the catalyst. Catalysts with a high Pt load show a significant increase in average maximum  $\text{NO}_x$  conversion (39,3% compared to 30,8% for low Pt load samples), a reduction of average  $T(\text{NO}_x^{\text{max}})$  values by 10°C (234°C compared to 244°C for low Pt load samples), and surprisingly a reduction of the  $\text{SO}_2(250)$  value (67% compared to 70% for low Pt load samples).

The decrease of the average THC(50)- and TCO(80) values with increasing Pt load was anticipated since more catalytically active material should always result in increased performance, in this case in lower HC respectively CO light-off values.

Obviously this applies to the  $\text{NO}_x$  conversion performance as well. The coincident increase of  $\text{NO}_x^{\text{max}}$  with decreasing  $T(\text{NO}_x^{\text{max}})$  has been reported by Burch et al.<sup>76</sup> and Adams et al.<sup>4</sup>. Adams et al. explain this by the assertion that at higher temperatures

the lifetime of sites active for  $\text{NO}_x$  reduction decreases because of reoxidation. Hence, at lower temperatures more sites active for  $\text{NO}_x$  reduction are available. Their argumentation is not totally conclusive since  $T(\text{NO}_x^{\text{max}})$  usually coincides with total HC conversion ( $\text{THC}(100)$ ). Thus a lower  $T(\text{NO}_x^{\text{max}})$  brings an earlier diminishing of HC along with it. A diminished amount of HC implies less  $\text{NO}_x$  reduction. Consequently a lower HC light-off should be a trade-off against lower  $\text{NO}_x$  conversion. This is, however, not the observation: the light-off temperature of HC is reduced and the maximum  $\text{NO}_x$  conversion is increased by using a higher Pt load on the catalyst. The observations may be explained by postulating that if the Pt load is high, there are more active sites on the catalyst's surface and thus more  $\text{NO}_x$  is reduced.

The fact that HC conversion does not significantly increase by raising the Pt load is remarkable. A possible explanation may be the assumption of a carbonaceous layer which covers most of the catalyst's surface at temperatures below  $\text{THC}(100)$ . This layer retards HC conversion regardless of Pt load.

$\text{SO}_2$  conversion should also increase with increasing Pt load. There is no apparent reason why this is not the case. Beretta et al.<sup>94</sup> propose that the  $\text{SO}_2$  oxidation is indirectly affected by the pore structure of the support since the pore structure influences the intraporous concentration gradients of the gases. However, as shown in Figure 4. 15, the pore size distribution is hardly effected by a change from low to high Pt load and the pore structure is therefore not altered. For now, there is no plausible foundation for  $\text{SO}_2$  oxidation being less severe on high Pt load catalysts.

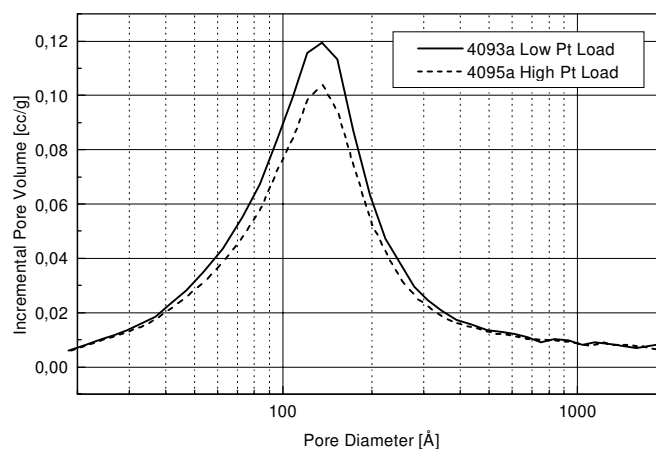


Figure 4. 15: The influence of the Pt load on the PSD

#### 4. 2. 2. 2 *The Influence of Pt Dispersion, Observations and Conclusions*

The average  $P_c$  factor calculated for all samples with high metal dispersion of Table 4.8 is 17,4 and thus 10% larger than the average  $P_c$  factor for samples with low metal dispersion (15,6). The average THC(50) value of the former samples is 219°C and hence 13°C lower than the average THC(50) value of the samples with low Pt dispersion (232°C). The average TCO(80) value of samples with high Pt dispersion is 206°C and thus 20°C lower than the average TCO(80) value of samples with low Pt dispersion (226°C). A high Pt dispersion increases the average maximum  $\text{NO}_x$  conversion from 34,5% to 35,5% compared to samples with low Pt dispersion, while  $T(\text{NO}_x^{\text{max}})$  is lowered by 13°C from 246°C to 233°C which corresponds to the decrease of the average THC(50) value. The average width of the  $\text{NO}_x$  conversion window is increased insignificantly from 37K to 38K by using a high Pt dispersion. The average  $\text{SO}_2(250)$  value and the average  $\text{NO}^{\text{max}}$  value increase from 61% to 76% and from 70% to 71% respectively on samples with high dispersion compared to samples with low Pt dispersion.

A high dispersion of the Pt on the alumina is a benefit for the overall performance of the catalyst. This was already postulated in section 4. 2. 1 based on observations made in BET measurements: washcoat pores can be blocked by large Pt particles. Platinum encapsulated inside these pores can no longer take part in the catalytic reaction and the overall performance of the sample decreases.

From literature<sup>92</sup> it is well known that catalysts with high dispersion of the platinum show an increased activity for the oxidation of HC. This is explained by the large number of metal surface irregularities (steps and kinks) existing on these catalysts. Surface irregularities have high activities in the breaking of C—H and C—C bonds. Consequently their availability is crucial for the conversion of HC. Improved HC conversion on Pt/ $\text{Al}_2\text{O}_3$  catalysts with a high Pt dispersion is also observed in this thesis and can be attributed to the same reason as proposed in literature.

The influence of active metal dispersion on the conversion of CO is less understood. CO oxidation does not require bond breaking of the CO but very well of  $\text{O}_2$ . The dissociation of  $\text{O}_2$  over platinum requires little activation energy and is not structure sensitive. It is likely that the higher number of Pt sites on a sample with a high Pt dispersion is responsible for the lower average TCO(80) values of these samples.

The oxidation of CO over selected Pt/Al<sub>2</sub>O<sub>3</sub> catalyst is investigated more thoroughly in section 4. 2. 2. 3.

Although the average maximum NO<sub>x</sub> conversion achieved by samples with high dispersion of the Pt is slightly larger than that of samples with low dispersion, a closer look at Table 4. 8 discloses that only in 5 of 8 cases a high dispersion results in an increased maximum NO<sub>x</sub> conversion. Ansell et al.<sup>56</sup> report that they found no direct relation between NO<sub>x</sub> conversion and Pt dispersion on the samples they examined. Tillaart et al.<sup>84</sup> state that although NO<sub>x</sub> conversion is not related directly to Pt dispersion, the dispersion influences HC light-off and thereby also the NO<sub>x</sub> conversion. This theory is verified in this thesis with average THC(50) and average T(NO<sub>x</sub><sup>max</sup>) both being lowered by 13°C by the use of high Pt dispersion on the catalysts. Nevertheless, this applies only to the temperature where the maximum occurs, not to the value of the maximum. The magnitude of NO<sub>x</sub><sup>max</sup> is not related to the dispersion of the Pt but it is very closely related to the amount of HC available on the catalyst. This in turn is governed by the temperature necessary for HC oxidation to light off.

Catalysts with high dispersion of the Pt are also more active for SO<sub>2</sub> and NO oxidation. It may be stated in general that on such catalysts more active sites for oxidation reactions are available and hence HC and CO light-off temperatures are decreased while more SO<sub>3</sub> and NO<sub>2</sub> is formed.

#### *4. 2. 2. 3 Examination of Turnover Frequency and Number of Active Sites for CO Oxidation by ITK, Observations and Conclusions*

The CO conversion of samples 4101c - 4108c was examined by measuring the number of sites active for CO oxidation as well as the turnover frequency at two different temperatures. This was done at JM's Technology Centre by the so-called Isotope Transient Kinetics (ITK) Method. The results are shown in Figure 4. 16.

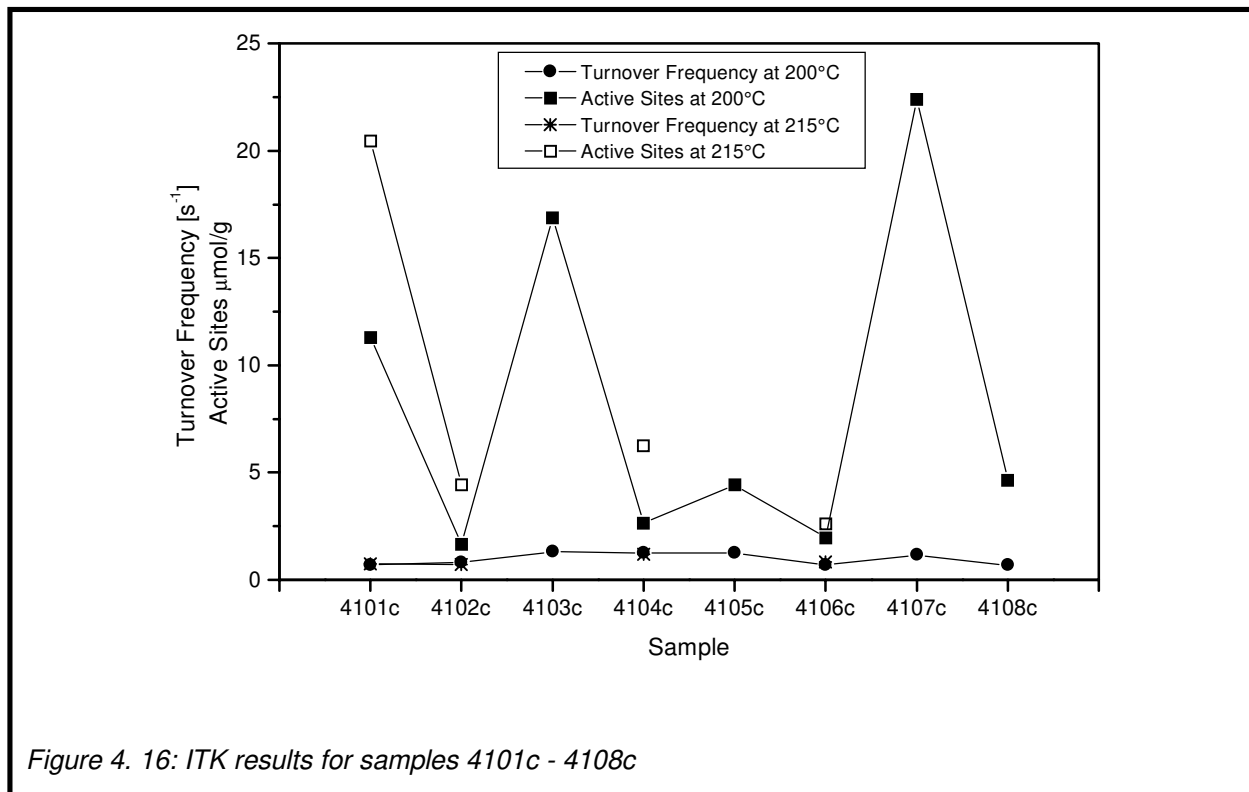


Figure 4. 16: ITK results for samples 4101c - 4108c

#### Observations:

All samples have more or less the same turnover frequencies regardless of dispersion or metal load. Samples with high Pt load and high dispersion (4103c and 4107c) exhibit the highest number of active sites followed by samples with low Pt load but high dispersion (4101c and 4105c). The effect of dispersion is more pronounced than the effect of metal load. A raise in temperature additionally increases the number of active sites.

#### Conclusions:

The results can be explained as follows: It is assumed that the oxidation rate of CO is of negative order in CO. It will be proven in section 4.6 that this is indeed the case. With a high amount of CO present, most of the platinum's active sites are covered by the CO leaving no sites for reaction between CO and O. Catalysts with low Pt load and dispersion are particularly sensitive to this. CO literally chokes its own oxidation. On a catalyst with high Pt load and high dispersion more active sites for O<sub>2</sub> adsorption and dissociation are available resulting in a lower CO light-off. If the Pt load is low but the dispersion is high, there are still more active sites than on a low



load, low dispersion catalyst. At higher temperatures, the adsorption/desorption equilibrium is shifted to desorption. As more CO desorb from the platinum they leave unoccupied sites on which O may adsorb and subsequently react with CO to form CO<sub>2</sub>. The rate limiting factor for CO oxidation is therefore the number of active sites available for O<sub>2</sub> adsorption. Since an adsorption/desorption equilibrium can always be pushed towards adsorption by increasing the partial pressure of the adsorbate according to Equation 2. 17, an increase in the oxygen concentration will result in a decrease of the TCO(80) value. This will be verified in section 4.6.

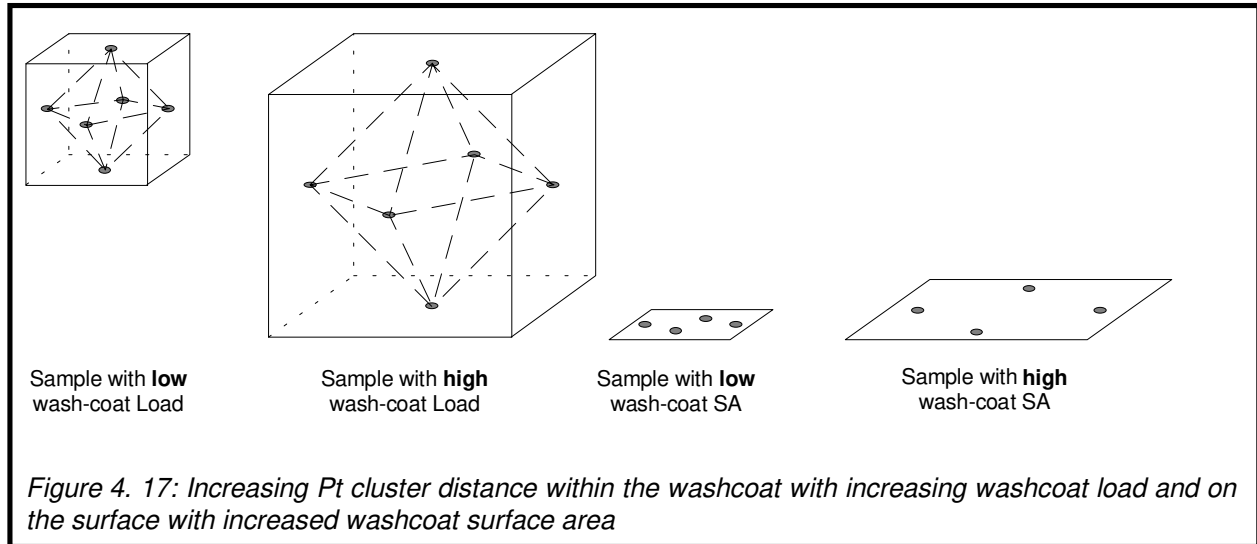
#### *4. 2. 2. 4 The Influence of the Washcoat Load, Observations and Conclusions*

The average P<sub>c</sub> factor (17,6) of all samples of Table 4. 8 with high washcoat load surpasses the average P<sub>c</sub> factor of all samples with low washcoat load (15,4) by 13%. On samples with high washcoat load the average THC(50) and TCO(80) values (224°C and 213°C respectively) are 4°C lower than on samples with low washcoat load (228°C and 217°C respectively). The use of a high washcoat load increases the average maximum NO<sub>x</sub> conversion from 33,4% to 36,8%, the average width of the NO<sub>x</sub> conversion window from 35K to 40K, and reduces the average temperature where the maximum NO<sub>x</sub> conversion occurs from 243°C to 236°C. The average SO<sub>2</sub>(250) and NO<sup>max</sup> values increase by 12% and 6% respectively if high washcoat load samples are used.

The observations suggest that the washcoat load does not influence HC and CO oxidation, while it influences NO<sub>x</sub> conversion, the width of the NO<sub>x</sub> conversion window, and SO<sub>2</sub> oxidation. The influence of the washcoat load on T(NO<sub>x</sub><sup>max</sup>) and NO oxidation is only marginal.

Based on the results obtained from the LOTs with the alumina washcoat-only sample, it was not expected that an increased washcoat load would favour CO oxidation. HC oxidation and NO<sub>x</sub> reduction were observed on the washcoat-only sample but occurred at higher temperature than on the Pt/Al<sub>2</sub>O<sub>3</sub> samples. Therefore it was not expected either that a higher washcoat load would increase the conversion of NO<sub>x</sub> or broaden the width of the NO<sub>x</sub> conversion window in the LOTs with the Pt/Al<sub>2</sub>O<sub>3</sub> samples. Yet, this positive influence of the high washcoat load on NO<sub>x</sub> conversion was observed. Assuming that the metal is distributed evenly, a

higher washcoat load at constant Pt load and dispersion results in an increased distance between Pt clusters within the washcoat, Figure 4. 17. The above results therefore suggest that the distance between these Pt clusters is of importance for the improved overall conversion performance which is dominated by the increased  $\text{NO}_x$  conversion. More evidence for this particularly regarding  $\text{NO}_x$  conversion will be given in the following section.



It was remarked in section 4. 2. 2. 1 that Beretta et al.<sup>94</sup> suggested an influence of the washcoat pores on the  $\text{SO}_2$  oxidation. This is verified by the results obtained in this thesis. A high washcoat load sample features a pore volume twice in magnitude compared to a low washcoat load sample. Apparently, the large pore volume promotes the  $\text{SO}_2$  oxidation.

#### 4. 2. 2. 5 The Influence of the Washcoat Surface Area, Observations and Conclusions

The average  $P_c$  factor (17,2) of the samples with a large washcoat surface area of Table 4. 8 is 9% higher than the average  $P_c$  factor (15,8) of the corresponding samples with low washcoat surface area. Changing the washcoat surface area has only a small influence on the average values of  $\text{THC}(50)$ ,  $\text{TCO}(80)$ , and  $T(\text{NO}_x^{\text{max}})$ . A sample with a high washcoat surface area shows an increased average maximum  $\text{NO}_x$  conversion of 37,3% compared to 32,9% of samples with low washcoat surface areas, and an increased average width of the  $\text{NO}_x$  conversion window of 39K

compared to 36K, respectively. Unfortunately, the use of a washcoat with high surface area also increases the  $\text{SO}_2(250)$  value from 64,3% to 73,1%.

The improved average  $P_c$  factor for samples with high washcoat surface area results from the increase in the maximum  $\text{NO}_x$  conversion and the larger width of the  $\text{NO}_x$  conversion window. If platinum loading and dispersion are kept constant and the metal is distributed evenly, a higher washcoat SA increases the distance between Pt clusters on the washcoat's surface, Figure 4. 17. This, in combination with the increase of  $\text{NO}_x$  conversion on samples with washcoats with high surface areas, gives reason to the assumption that some sort of synergism exists between washcoat and active metal during the  $\text{NO}_x$  reduction reaction. The  $\text{NO}_x^{\text{max}}$  values of all high Pt load samples are shown in Figure 4. 18. In this figure, the distribution of the values with high maximum  $\text{NO}_x$  conversion seems to be at random.

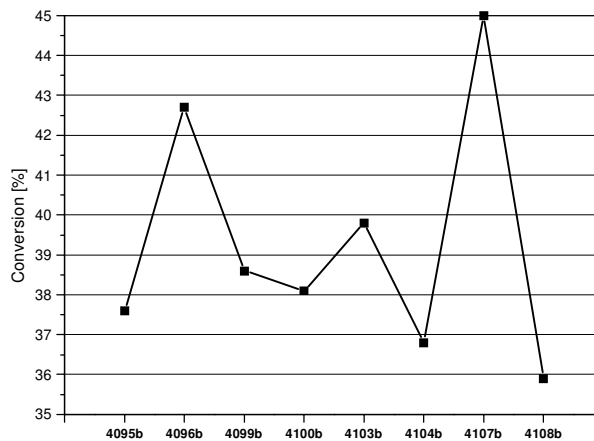
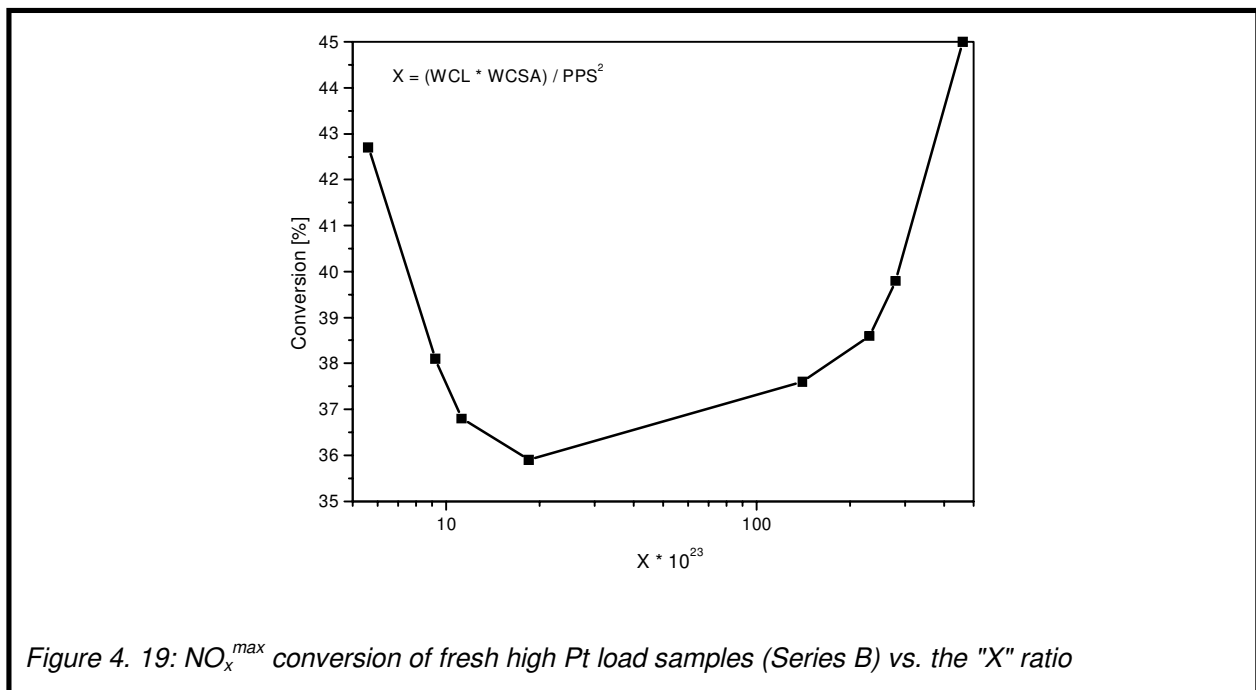


Figure 4. 18:  $\text{NO}_x^{\text{max}}$  conversion of fresh high Pt load samples (lines are drawn to guide the eye)

If the values of maximum  $\text{NO}_x$  conversion are presented as a function of the ratio between total support surface area (i.e. washcoat load times washcoat surface) and active metal surface area (targeted Pt particle size square) a minimum becomes visible, Figure 4. 19. In this context it is important to mention that the reproducibility for the  $\text{NO}_x^{\text{max}}$  values lay at  $\pm 1\%$  conversion.

From Figure 4. 19 it may be concluded that the value of maximum  $\text{NO}_x$  reduction is dependent on a certain ration between the support surface area and the metal surface area. Consequently some sort of interaction between both could be of

importance during the  $\text{NO}_x$  reduction mechanism. One explanation for this interaction is to propose that  $\text{NO}_x$  reduction occurs only on the edge of the metal particle where it meets the washcoat suggesting the spillover of one of the reacting species from the washcoat to the Pt or vice versa. HC might be pre-cracked on the washcoat and reacts as some sort of radical with the NO on the borderline between Pt particle and the washcoat. A similar mechanism has been introduced by Burch et al. with propane as HC<sup>83</sup>. Another conclusion that could be drawn from this observation is that the  $\text{NO}_x$  reduction mechanism on a Pt/ $\text{Al}_2\text{O}_3$  catalyst with low Pt dispersion is different from the  $\text{NO}_x$  reduction mechanism on a catalyst with high Pt dispersion.



This would imply that either very low or very high dispersion of the metal favours  $\text{NO}_x$  conversion. In chapter 4. 2. 2 it was affirmed though that maximum  $\text{NO}_x$  conversion is not related to Pt dispersion directly.

The first theory which suggests that the  $\text{NO}_x$  reduction mechanism on a Pt/ $\text{Al}_2\text{O}_3$  catalyst involves the Pt and the washcoat is the one which is most convincing. The result advises to prepare  $\text{NO}_x$  catalysts in such a way that they do not fall within the area of the minimum.

#### 4. 2. 3 Summary

This section characterises a Pt/Al<sub>2</sub>O<sub>3</sub> catalyst by BET and CO chemisorption measurements and describes the influence of Pt load, Pt dispersion, washcoat load, and washcoat surface area on the conversion performance of this catalyst.

BET measurements reveal that the BET surface area (BSA) of a Pt/Al<sub>2</sub>O<sub>3</sub> catalyst sample does not differ from an alumina washcoat-only sample if the alumina used for both samples is the same. Hence, the addition of Pt to the alumina washcoat does not increase the BET surface area.

Adding Pt to an alumina washcoat does have an influence on the pores of the washcoat as indicated by pore size distribution (PSD) measurements: the addition of Pt causes the washcoat pores to widen during the preparation of the Pt/Al<sub>2</sub>O<sub>3</sub> sample as well as during the ageing of such a sample. The large Pt particles on samples with low Pt dispersion are able to block washcoat pores. This is proven by a lower BET surface area measured on samples with low Pt dispersion. The blocked pores can not be reached by the nitrogen gas used in the BET experiments anymore. Any precious metal encapsulated inside such pores is unable to contribute to the catalyst's purpose. Thus it is postulated that the catalysts with a low Pt dispersion will show poorer overall performance during the LOTs.

During the LOTs, complete conversion of HC coincides with maximum NO<sub>x</sub> conversion, pointing at a pivotal role of HC in the NO<sub>x</sub> reduction mechanism. The progress of CO conversion seems to be restricted in a certain way during the LOT. In contradiction to most research groups<sup>85</sup>, NO<sub>2</sub> formation was observed before maximum NO<sub>x</sub> conversion was achieved.

For easier comparison of the overall performance of catalyst samples with different formulations, the P<sub>c</sub> factor is introduced, Equation 4. 3.

The overall performance of samples with a high load of Pt exceeds the performance of samples with low Pt load by 23 %. It is remarked that the average temperature where 50% of the HC are converted is not significantly reduced by increasing the Pt load. This is explained by a carbonaceous layer on top of the whole catalyst which impedes HC oxidation regardless of Pt load.

High dispersion of Pt on a catalyst increases the P<sub>c</sub> factor by 10%. This result confirms the theory made from BET observations, that large Pt particles can block pores, disabling Pt enclosed in these pores to take part in the catalytic process. ITK

measurements reveal that a high dispersion benefits CO oxidation. The rate limiting factor for CO oxidation is identified as the number of active sites available for O<sub>2</sub> adsorption and dissociation. This is based on the assumption that the oxidation rate of CO is of negative order in CO, i.e. if the concentration of CO in the feedgas is high, CO can "choke" its own oxidation. A catalyst with high dispersion of the Pt features more active sites for O<sub>2</sub> adsorption, the CO oxidation can more readily progress and the TCO(80) value is lower. No direct relation between maximum NO<sub>x</sub> conversion and Pt dispersion is observed. Yet, a high Pt dispersion decreases the temperature at which NO<sub>x</sub><sup>max</sup> occurs since it decreases the THC(100) value which coincides with T(NO<sub>x</sub><sup>max</sup>). SO<sub>2</sub> oxidation increases with higher Pt dispersion for the same reason as for CO oxidation; more active sites for oxidation are available.

An increase of the washcoat load does not influence the HC or CO oxidation, but raises maximum NO<sub>x</sub> conversion by 9% and broadens the width of the conversion window by 12%. The average P<sub>c</sub> factor of samples with high washcoat load is 13% larger than the average P<sub>c</sub> factor of samples with low washcoat load. It is suggested that the distance between the Pt clusters is of importance for the improved NO<sub>x</sub> conversion.

The surface area of the washcoat used on the samples has no significant influence on the HC and CO conversion. Using a washcoat with a higher surface area increases the average P<sub>c</sub> factor by 9%, the maximum NO<sub>x</sub> conversion by 12%, and the SO<sub>2</sub> oxidation by 12%. Presenting the values of NO<sub>x</sub><sup>max</sup> of high Pt load samples as a function of the ratio between total support area (washcoat load times washcoat surface area) and active metal area results in a curve with a minimum. This plot is interpreted as an indication for some sort of interaction between the washcoat and the Pt in the NO<sub>x</sub> reduction mechanism. It is asserted, that NO<sub>x</sub> reduction occurs on the edge of the metal particles with the spillover of reactive species from the washcoat. This mechanism has also been proposed in literature<sup>83</sup> where propane was used as HC. The result also advises to prepare de-NO<sub>x</sub> catalysts in such a way that they do not fall into the area of the minimum.

### 4. 3 Variations of the Support Material

In section 4. 1 the contribution of the pure washcoat to the conversion was examined. A relation between washcoat load/surface area and NO<sub>x</sub> conversion was established in section 4. 2. The first part of this section describes the influence of additives to the alumina washcoat on the conversion performance of a Pt/Al<sub>2</sub>O<sub>3</sub> catalyst. The second part investigates whether zeolite-containing washcoats supporting Pt feature improved conversion performance compared to the alumina variants.

#### 4. 3. 1 Characterisation of the Samples by BET and COC Measurements

Table 4.10 summarises the results of ASAP2000 measurements with samples composed of alumina and zeolite/alumina (called non-zeolite-containing and zeolite-containing respectively in the text below) washcoats with additives to the washcoat. All these samples contain Pt as active component. More detailed information about the samples is given in the "Appendix".

Sample	Washcoat	Additive	Measured D <sub>M</sub> [%]	MSA [m <sup>2</sup> /g]	BSA [m <sup>2</sup> /g]	SPPV [ml/g]	APD [Å]
PP41	Al <sub>2</sub> O <sub>3</sub>	none	16,9	0,0984	36,5	0,0988	108,1
PP325	Al <sub>2</sub> O <sub>3</sub>	5 wt.-% SiO <sub>2</sub>	13,3	0,0700	51,1	0,1066	83,4
PP422	Al <sub>2</sub> O <sub>3</sub>	3 wt.-% BaO	17,8	0,0929	42,3	0,0885	83,8
PP428	Al <sub>2</sub> O <sub>3</sub>	3 wt.-% La <sub>2</sub> O <sub>3</sub>	15,7	0,0775	37,1	0,1036	111,7
RD704	Al <sub>2</sub> O <sub>3</sub>	none	28,1	0,2682	37,8	0,0959	102,5
PP500	Al <sub>2</sub> O <sub>3</sub>	20 wt.-% SiO <sub>2</sub>	15,2	0,0819	46,0	0,1158	91,8
PP452	Al <sub>2</sub> O <sub>3</sub> /Zeolite	2 wt.-% CeO <sub>2</sub>	12,3	0,0589	64,5	0,1096	67,6
PP454	Al <sub>2</sub> O <sub>3</sub> /Zeolite	20 wt.-% CeO <sub>2</sub>	38,7/17,7	0,1967	61,5	0,0964	63,0
RD763	Al <sub>2</sub> O <sub>3</sub> /Zeolite	MnO <sub>2</sub>	42,1	0,2311	49,6	0,0948	76,5

4. 10: Results of BET and COC measurements

Sample RD704 is a Pt/Al<sub>2</sub>O<sub>3</sub> sample without additives which has been prepared in a different, proprietary manner and features a higher Pt load than the rest of the samples.

### Observations:

All non-zeolite-containing samples present a similar dispersion of Pt except for sample RD704. Among the zeolite-containing samples, the dispersions of samples PP454 and RD763 differ significantly from sample PP452.

Since the alumina washcoats used for the non-zeolite-containing samples vary widely in surface area (compare "Appendix"), the measured BET surface areas of these samples also show strong fluctuations. The BET surface areas of the zeolite-containing samples are larger than the BET surface areas of the non-zeolite-containing samples except for the zeolite-containing sample RD763 which has a similar BET surface area (49,6 m<sup>2</sup>/g) as the BET surface area of the non-zeolite-containing sample PP325 (51,1 m<sup>2</sup>/g).

Single point pore volumes (SPPVs) are similar for all samples, no matter whether zeolite is in the washcoat or not. The average pore diameters (APDs) of the zeolite-containing samples are lower than those of the samples without zeolite.

### Conclusions:

The reason for the higher Pt dispersion of sample RD704 compared to the other non-zeolite-containing samples is the different process by which sample RD704 was prepared. It may be proposed that the higher dispersion of sample RD704 will result in improved HC and CO conversion compared to the other non-zeolite-containing samples.

The high dispersion values of samples PP454 and RD763 are not caused by the process by which these samples were prepared. It is speculated that the reason for the high dispersion is rather the addition of ceria (CeO<sub>2</sub>) and manganese (MnO<sub>2</sub>) to the zeolite-containing washcoat. During the sample preparation process some of the MnO<sub>2</sub> is reduced to metallic Mn. A similar process seems to take place on the ceria containing sample. Both processes invoke an increased amount of CO adsorbed during the CO chemisorption measurement which is interpreted by the computer of the CO chemisorption-measuring equipment as a higher Pt dispersion. The dispersion of sample PP454 was therefore measured again, this time with hydrogen instead of CO. Now the dispersion was 17,7 %. This is more comparable with the dispersion of sample PP452. The dispersion value of sample PP452 was not altered by the ceria, probably because the wt.-% of ceria added to this sample was only one



tenth of that of sample PP454. A hydrogen chemisorption experiment with sample RD763 did not give a plausible result.

The addition of manganese to the zeolite-containing washcoat does not only influence the measured dispersion but also the measured BET surface area of sample RD763. It can be speculated that the BET surface area of sample RD763 (49,6 m<sup>2</sup>/g) is lower than the BET surface area of the other two zeolite-containing samples (BSA of PP452: 64,5 m<sup>2</sup>/g; BSA of PP454: 61,5 m<sup>2</sup>/g) because the Mn blocks pores of the washcoat in a similar way as large Pt particles do as observed in section 4. 2. 1.

All zeolite-containing samples feature lower average pore diameters than the non-zeolite-containing samples. Lower average pore diameters result in higher BET surface areas.

#### 4. 3. 2 LOT Performance of Pt/Al<sub>2</sub>O<sub>3</sub> Catalysts with Additives

All non-zeolite-containing samples of Table 4. 10 were tested under the same conditions. The concentrations of the gases used in the feedgas are given in Table 4. 11.

CO <sub>2</sub>	4,7 vol.-%
O <sub>2</sub>	12,2 vol.-% (= λ 2,2)
CO	200 ppm
SO <sub>2</sub>	21 ppm
NO	400 ppm
C <sub>3</sub> H <sub>6</sub>	800 ppm
H <sub>2</sub> O	6,4 vol.-%
SV	18000 hr <sup>-1</sup>
T <sub>i</sub> <sup>0</sup> → dT/dt →	80°C →
T <sub>i</sub> <sup>max</sup>	10°C/min →
	530°C

Table 4. 11: Test conditions during LOTs performed in this chapter

#### Observations:

Table 4. 12 shows the descriptive values obtained from LOTs with the non-zeolite-containing samples of Table 4. 10 and the P<sub>c</sub> factor calculated with Equation 4. 3.

		PP41 F	RD704 F	PP325 F	PP500 F	PP422 F	PP428 F
THC(50)	°C	240	224	239	231	235	232
TCO(80)	°C	206	160	225	193	214	215
NO <sub>x</sub> <sup>max</sup>	%	44,1	42	37,8	39,5	46,8	45,8
T(NO <sub>x</sub> <sup>max</sup> )	°C	252	235	250	246	247	246
NO <sup>max</sup>	%	72	80	79	68	75	69
T(NO <sup>max</sup> )	°C	252	237	259	248	271	267
SO <sub>2</sub> (250)	%	62	100	53	70	84	90
W(NO <sub>x</sub> )	K	28	34	26	31	53	54
NO <sub>2</sub> <sup>max</sup>	%	72	68	79	65	67	58
P <sub>c</sub>		16,2	19,8	13,8	16,6	22,2	22,3

Table 4. 12: Values obtained from LOTs with alumina based samples ("F" denotes fresh catalysts)

In this set of experiments, sample PP41 may serve as a reference for a Pt/Al<sub>2</sub>O<sub>3</sub> catalyst without additives prepared in a conventional manner. The maximum NO<sub>x</sub> conversion of this sample is high (44,1%) compared to the Pt/Al<sub>2</sub>O<sub>3</sub> samples examined in section 4. 2. 2 (21,2% in case of sample 4094 whose properties are comparable to PP41).

Sample RD 704 shows a lower THC(50) value (224°C), a much lower TCO(80) value (160°C) and a similar maximum NO<sub>x</sub> conversion (42,1%) compared to sample PP41 (THC(50): 240°C; TCO(80): 206°C; NO<sub>x</sub><sup>max</sup>: 44,1%). Additionally the NO<sub>x</sub> conversion window of sample RD704 is 6K broader (34K compared to 28K) and the overall P<sub>c</sub> factor is 18% larger (19,8 compared to 16,2) than the P<sub>c</sub> factor of sample PP41. Sample RD704 is the only sample that shows 100% SO<sub>2</sub> conversion at 250°C.

The P<sub>c</sub> factor of sample PP325 is 15% smaller than that of PP41 (13,8 compared to 16,2). Although the THC(50) value of PP325 is similar to that of PP41 (239°C and 240°C respectively), the TCO(80) value of PP325 is significantly higher (225°C) than that of PP41 (206°C), and the NO<sub>x</sub><sup>max</sup> value of PP325 (37,8%) is 14% lower than that of PP41 (44,1%). The conversion of SO<sub>2</sub> at 250°C is lowest on sample PP325 (53%) compared to all other samples of Table 4. 12.

Sample PP500 has a similar P<sub>c</sub> factor as sample PP41 (16,6 and 16,2 respectively). THC(50) (231°C) and TCO(80) (193°C) occur 9°C and 13°C earlier respectively than

on sample PP41 (THC(50): 240°C; TCO(80): 206°C). The maximum NO<sub>x</sub> conversion of PP500 (39,5%) is 10% lower than that of PP41 (44,1%). The HC and CO conversion curves of this catalyst shall be taken as an example for an observation made during a lot of LOTs, Figure 4. 20.

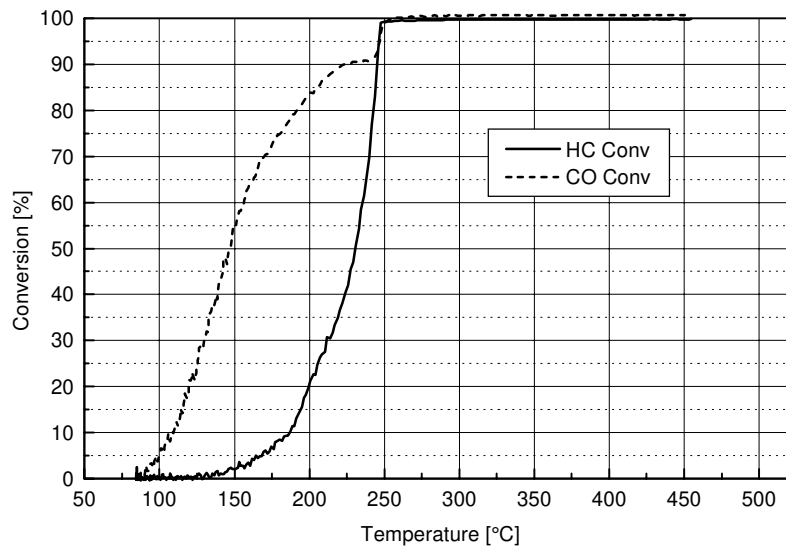


Figure 4. 20: HC and CO light-off curves of sample PP500

The CO light-off curve rises steeply initially. At the temperature where HC conversion begins, the slope of the CO conversion curve becomes less steep and comes to complete stagnation as soon as the CO conversion reaches 90%. The slope of the CO conversion curve rises steeply again when HC conversion also exceeds 90% conversion.

Samples PP422 and PP 428 feature the highest  $P_c$  factors of the alumina containing samples (22,2 and 22,3 respectively). They have the highest maximum NO<sub>x</sub> conversion values (PP422: 46,8%; PP428: 45,8%) and the broadest NO<sub>x</sub> conversion windows (PP422: 53K; PP428: 54K) of all samples in Table 4. 12. The THC(50) and TCO(80) values of both samples are similar (THC(50) PP422: 235°C; THC(50) PP428: 232°C; TCO(80) PP422: 214°C; TCO(80) PP428: 215°C) with the THC(50) values being slightly lower and TCO(80) being slightly higher than those of PP41

(THC(50): 240°C; TCO(80): 206), respectively. Samples PP422 and PP 428 have a very high SO<sub>2</sub> conversion, though not 100% at 250°C.

### Conclusions:

The reason why the maximum NO<sub>x</sub> conversion of sample PP41 is much higher than that of the samples in section 4. 2. 2 is the lower space velocity (SV) applied during the LOTs in this section. It is well established that a decrease of SV results in an increase of NO<sub>x</sub> conversion<sup>49</sup>.

The lower THC(50) and TCO(80) values of sample RD704 compared to PP41 can be explained by the high dispersion of the Pt and the higher Pt load on sample RD704. It was established in section 4. 2. 2. 2 that a high metal dispersion reduces THC(50) and TCO(80). Additionally, the Pt load of RD 704 is nearly twice as high as that of PP41. In section 4. 2. 2. 1 and 4. 2. 2. 3, a high Pt load was proven to reduce TCO(80).

Congruent with the results of section 4. 2. 2. 2, the high dispersion of sample RD704 does not cause a higher maximum NO<sub>x</sub> conversion compared to the NO<sub>x</sub><sup>max</sup> of sample PP41. It was established in section 4. 2. 2. 2 that the maximum NO<sub>x</sub> conversion and the Pt dispersion are not directly related with each other. Hence, a high Pt dispersion does not necessarily cause a high maximum NO<sub>x</sub> conversion. The Pt dispersion does, however, influence the temperature at which the maximum NO<sub>x</sub> conversion is located. This was also proven in section 4. 2. 2. 2. The maximum NO<sub>x</sub> conversion of samples with high Pt dispersion is located at lower temperatures than the maximum NO<sub>x</sub> conversion of samples with low Pt dispersion. Sample RD704 which has the highest Pt dispersion among the samples of Table 4. 12 (28,1%) features the lowest T(NO<sub>x</sub><sup>max</sup>) value.

The P<sub>c</sub> factor of RD704 (19,8) which is larger than the P<sub>c</sub> factor of sample PP41 (16,2). This is caused by the lower THC(50) and TCO(80) values of sample RD704. The high SO<sub>2</sub>(250) value of sample RD704 is presumably caused by the high Pt dispersion of this sample. It was established in section 4. 2. 2. 2 that a high Pt dispersion favours the SO<sub>2</sub> oxidation on the catalyst.

The lower  $P_c$  factor of sample PP325 (13,8) compared to the  $P_c$  factor of sample PP41 (16,2) is caused by a lower maximum  $\text{NO}_x$  conversion and a narrower  $\text{NO}_x$  conversion window of sample PP325.

Judged by a comparison of  $P_c$  factors, PP325 is the poorest catalyst of all samples in Table 4. 12.

From the similar  $\text{THC}(50)$  values of PP325 and PP41 it can be concluded that using an alumina washcoat which contains 5 wt.-%  $\text{SiO}_2$  does not change the  $\text{THC}(50)$  value.

Yet it appears that the washcoat used for sample PP325 causes an increase of the  $\text{TCO}(80)$  value. This is, however, not confirmed by sample PP500. Sample PP500 has 4 times more (20 wt.-%) silica in the  $\text{Al}_2\text{O}_3$  washcoat than sample PP325 (5 wt.-%) but has a lower  $\text{TCO}(80)$  value  $193^\circ\text{C}$  than sample PP325 ( $\text{TCO}(80)$ :  $25^\circ\text{C}$ ) and even PP41 ( $\text{TCO}(80)$ :  $206^\circ\text{C}$ ). The main difference between samples PP325 and PP41 (apart from the  $\text{SiO}_2$  in the alumina of PP325) is that PP325's washcoat has a surface area of  $320 \text{ m}^2/\text{g}$  while the surface area of the washcoat of sample PP41 is  $160 \text{ m}^2/\text{g}$ . In section 4. 2. 2. 5 it was shown that an increase of the surface area of the washcoat does not increase the  $\text{TCO}(80)$  value. There is no reason why sample PP325 should behave differently. Hence, there is currently no plausible explanation why the  $\text{TCO}(80)$  value of sample PP325 is higher than the  $\text{TCO}(80)$  value of sample PP41. In this context the reader shall be reminded that the values of washcoat surface areas given in this thesis were obtained from the product declarations of the washcoat manufacturer. They must not be mixed up with the BET surface areas of the complete samples (washcoat + precious metal coated cordierite block) which were measured in this thesis.

From the observation that the  $\text{NO}_x^{\text{max}}$  value of PP325 (37,8%) is lower than that of PP41 (44,1%) it may be concluded that the silica in the washcoat of this sample has a negative influence on the  $\text{NO}_x$  conversion. Xue et al.<sup>79</sup> state that  $\text{SiO}_2$  is known to be inert in an acidic environment and therefore does not interact well with the acidic  $\text{NO}$  molecules. This is confirmed by the decreased  $\text{NO}_x$  conversion of sample PP325 and should be verified by sample PP500 also having a lower  $\text{NO}_x^{\text{max}}$  value than sample PP41.

The assumption made above that sample PP500 should show a lower maximum NO<sub>x</sub> conversion than sample PP41 because the washcoat of PP500 contains SiO<sub>2</sub> is verified. The maximum NO<sub>x</sub> conversion of sample PP500 is 39,5% compared to PP41's 44,1%.

In spite of having less maximum NO<sub>x</sub> conversion, the low TCO(80) value of PP500 (193°C) results in a P<sub>c</sub> factor for PP500 (16,6) similar to the P<sub>c</sub> factor of sample PP41 (16,2).

As can be seen in Figure 4. 20, the CO conversion is retarded with the onset of HC conversion. From the shape of the CO light-off curve the conclusion may be drawn that HC and CO conversion influence each other. These observations are discussed in more detail in section 4. 6.

The high P<sub>c</sub> factors of catalysts PP422 (22,3) and PP428 (22,3) are caused predominantly by their broad NO<sub>x</sub> conversion windows (W(NO<sub>x</sub>) of PP422: 53K; W(NO<sub>x</sub>) of PP428: 54K). Sample PP422 contained BaO and PP428 contained La<sub>2</sub>O<sub>3</sub> in the washcoat. Although these are two different metal oxides, the performances of these samples hardly deviate from each other. The incorporation of La<sub>2</sub>O<sub>3</sub> and BaO in PP422 and PP428 respectively gives a catalyst that performs with a wider NO<sub>x</sub> conversion window without deteriorating the conversion performance for other gases. However, both samples show very high SO<sub>2</sub> conversions which may lead to the formation of sulphates and add to the weight of the particulates during engine bench and dynamometer tests.

#### *4. 3. 3 Temperature Ramps and TPDs with Pt/Al<sub>2</sub>O<sub>3</sub> Catalysts with Additives*

Figure 4. 21 shows the temperature ramp desorption spectra of samples PP41, RD704, PP422, and PP500. These ramps were performed directly after the LOT of each individual catalyst was completed. In all cases the carrier gas was N<sub>2</sub>, the heating rates were 20°C/min, and the maximum inlet temperature was 500°C. The reader shall be reminded that the concentration values recorded during these temperature ramps have to be interpreted as qualitative information. The peak values are only given to make the comparison of the temperature ramp and TPD results easier. They may not represent the true values of the amounts desorbed.

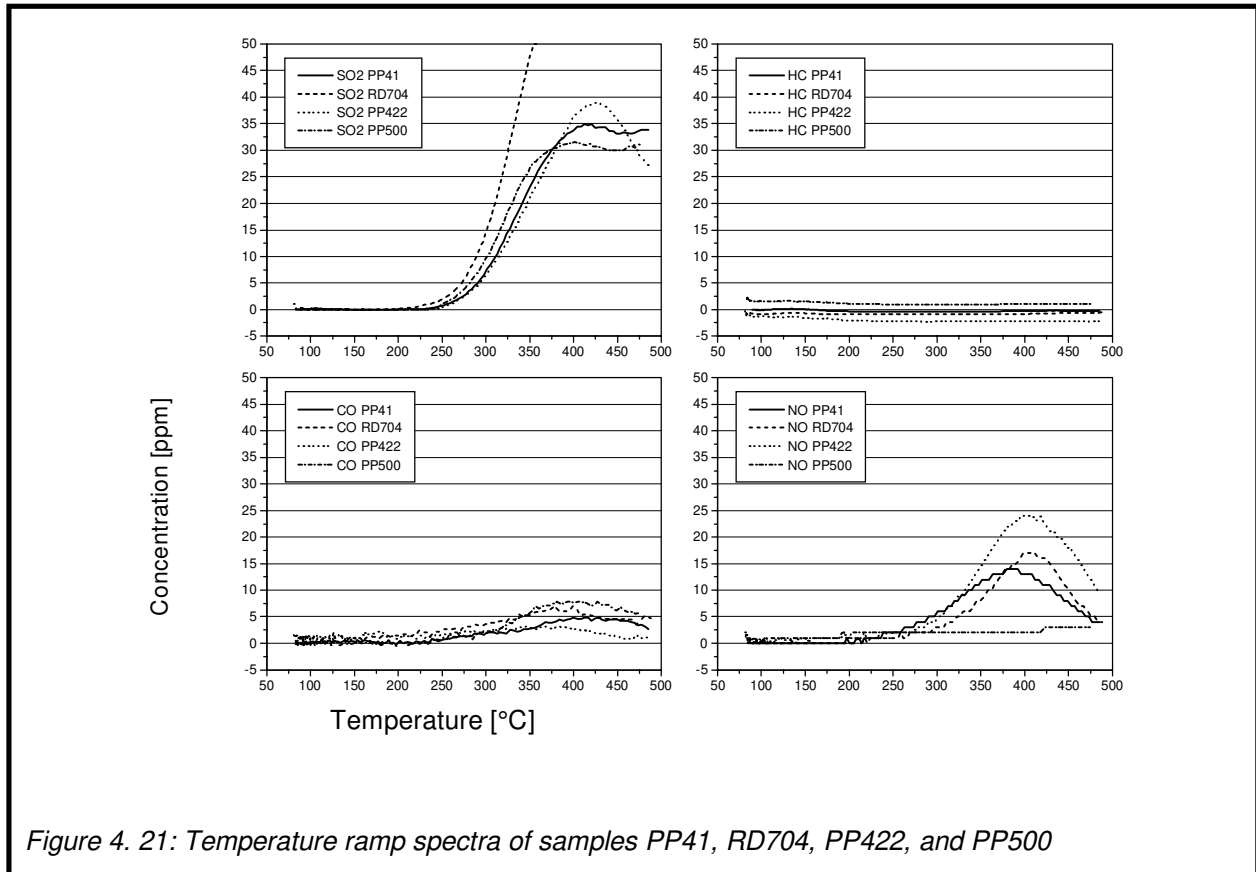


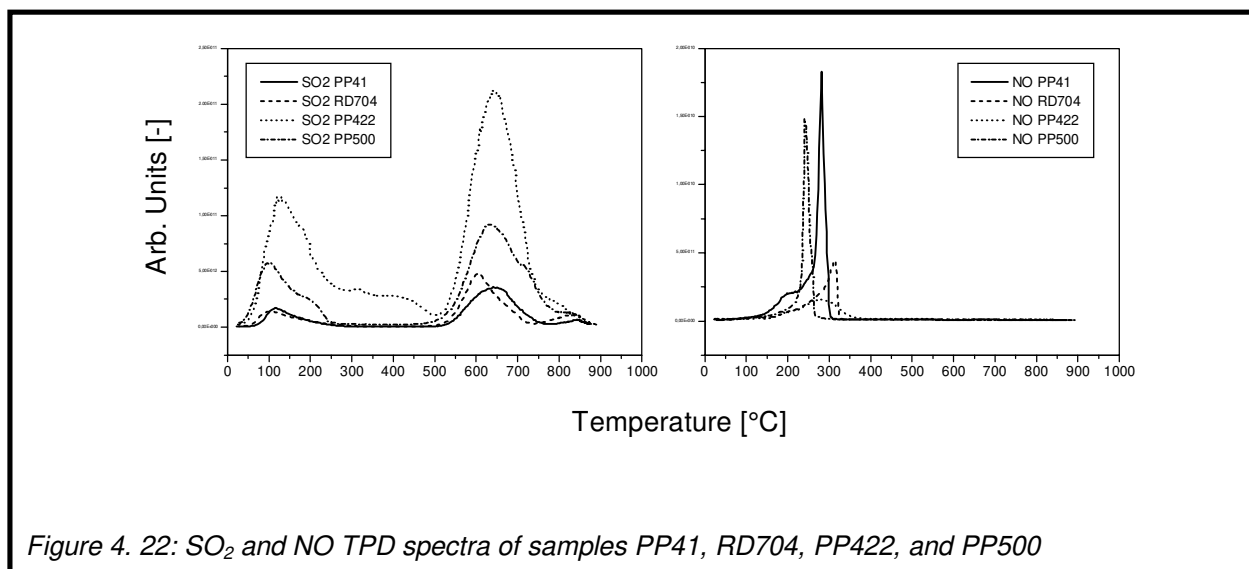
Figure 4. 21: Temperature ramp spectra of samples PP41, RD704, PP422, and PP500

#### Observations:

All four samples desorb  $\text{SO}_2$  and NO. None of them desorb HC and only very little CO is detected compared to the peak heights of the  $\text{SO}_2$  desorption curves. Sample RD704 has the earliest onset ( $193^\circ$ ) of  $\text{SO}_2$  desorption and shows the highest desorption peak which exceeded the measuring range of the analyser. All other samples show similar onsets of  $\text{SO}_2$  desorption (between  $220^\circ\text{C}$  and  $236^\circ\text{C}$ ). The heights of the  $\text{SO}_2$  desorption peaks are in descending order: RD704 (beyond scale), PP422 (39ppm), PP41 (35ppm), PP 500 (32 ppm). The highest NO desorption peak is featured by sample PP422 (24 ppm) followed by RD704 (17 ppm) and PP41 (14 ppm). In comparison with the latter three samples, PP500 shows significantly less NO desorption. The beginning of NO desorption is for all samples similar (approximately  $260^\circ\text{C}$ ).

The precision of the temperature ramps on the SCAT rig was limited by the set-up. Above all the distance between the reactor and the analytical train was far to long for a satisfactory desorption temperature resolution. Furthermore, the large reactor

volume caused a significant error through its influence on the residence time distribution of the individual gases. Therefore temperature programmed desorption (TPD) spectra were recorded at Johnson Matthey's Technology Centre in a set-up with all volumes minimised. The distance between the reactor and the analysis apparatus was kept as short as possible. The results are shown in Figure 4. 22.



It shall be mentioned that the samples were prepared for the TPD by loading them with the gases in a SCAT rig by a certain procedure and then removing them from the SCAT rig and transferring them to the TPD rig. Thus the TPD was not performed immediately after the SCAT dosing. It was assumed that any desorption of species during the transfer would be insignificant. Further details are given in the "Experimental" chapter. The analytical apparatus used to measure the effluent gases during the TPDs could not distinguish between CO the N<sub>2</sub> carrier gas. Therefore no CO data could be obtained.

The HC desorption spectra obtained by TPD are not shown here. However, they confirm the observation made with the SCAT rig temperature ramp that no HC desorbs from the non-zeolite-containing samples examined.

All the samples desorb SO<sub>2</sub> and NO during the TPD. The TPD-spectra of all the samples feature two SO<sub>2</sub> desorption peaks and one NO desorption peak. Sample PP422 has the highest desorption peaks (first peak 1,17; second peak 2,12) followed by PP500 (first peak 0,57; second peak 0,92). The SO<sub>2</sub> desorption peaks of



PP41 are of similar size to RD704 and low compared to the other samples. These observations are in contrast to the results of the temperature ramps on the SCAT rig. The lowest desorption temperature of NO from the TPD experiments is found for sample PP500 (240°C), followed by PP422 (278°C), PP41 (282°C), and RD704 (314°C). These temperatures are significantly different from those found with the temperature ramps on the SCAT rig: PP500 (~475°C), PP422 (403°C), PP41 (385°C), and RD704 (405°C).

### Conclusions:

The data in Figure 4. 21 suggest that the method used to prepare sample RD704 makes this sample especially susceptible for SO<sub>2</sub> adsorption. It may be speculated that this is caused by the high Pt dispersion or the high Pt load of this catalyst sample. All other samples have a lower Pt dispersion and a lower Pt load and desorb less SO<sub>2</sub>. The SO<sub>2</sub> traces recorded for samples RD704 and PP41 are in close agreement to the results of Xue et al.<sup>79</sup>. They report that almost no SO<sub>2</sub> desorbs from alumina only samples (i.e. samples without precious metal) proving that SO<sub>2</sub> is stored on the metal. Raising the Pt load of their catalyst samples resulted in a higher amount of SO<sub>2</sub> desorption during TPD. Based on the results of Xue et al.<sup>79</sup> it may be concluded that the high amount of SO<sub>2</sub> desorbing from sample RD704 is caused in part by the high Pt load of this sample. It can not be stated whether the high Pt dispersion of sample RD704 is another reason for the high SO<sub>2</sub> desorption. However, it is speculated that this is the case.

The fact that most NO desorbs from sample PP422 during the temperature ramp is not surprising since this sample contains BaO which is known to store NO<sup>104</sup>. The storage of NO may well cause the broader NO<sub>x</sub> conversion window observed for this sample during the LOT (compare Table 4. 12) because the NO is held longer on the catalyst's surface and thus has more time to react. A similar broadening of the NO<sub>x</sub> conversion window was found for sample PP428 where the La<sub>2</sub>O<sub>3</sub> may act as the NO storage component and thus widens the conversion window (the desorption curve is not included in Figure 4. 21, but is similar to that of PP422). The NO desorption curve of sample PP500 in Figure 4. 21 suggests that the high content of silica in the alumina washcoat of this sample causes a decline of NO adsorption. The weak interaction of SiO<sub>2</sub> with NO (already described in section 4. 3. 2) can be used to

explain the low maximum  $\text{NO}_x$  conversions of the  $\text{SiO}_2$  containing samples of Table 4. 12.

It is surprising that no HC desorption was detected from any of the Pt containing samples during the SCAT rig temperature ramps because significant HC desorption was detected from alumina washcoat only samples (see section 4. 1. 1. 3). However, the fact that no HC desorption was detected does not necessarily mean that no HC is stored on these samples: Both, temperature ramp and TPD experiments confirm that HC does not desorb from the tested non-zeolite-containing samples. Yet, as shown in Figure 4. 23,  $\text{CO}_2$  was detected during the TPD runs with all samples. It is very unlikely that  $\text{CO}_2$  is stored on the washcoat during the SCAT dosing. Hence, the  $\text{CO}_2$  formation must result from the reaction of adsorbed  $\text{O}_2$  and co-adsorbed HC or CO. The  $\text{CO}_2$  formation may be interpreted as an indirect proof for HC adsorption on the samples.

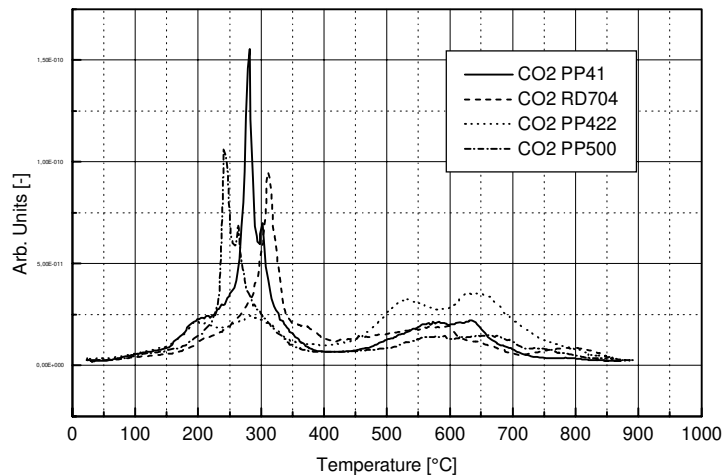


Figure 4. 23:  $\text{CO}_2$  formation during TPD runs

The desorption spectra obtained by TPD were very different from those obtained with the SCAT rig temperature ramps. The discrepancies between the results of the SCAT rig temperature ramps and the TPD experiments can have their origins in the SCAT dosing performed prior to the TPD runs. The maximum temperature during the dosing did not exceed  $150^\circ\text{C}$  while the SCAT rig temperature ramps were performed after LOTs which had a maximum (sample inlet) temperature of  $530^\circ\text{C}$ . Thus, under SCAT conditions, reactions between the reactant gases, the support, and the Pt may occur which might not occur during the SCAT dosing performed prior to the TPD

runs. Hence, SCAT rig temperature ramps and TPDs may show different desorption spectra.

During the TPD, the BaO- containing samples desorbed most SO<sub>2</sub>. The first of the two desorption peaks observed for all samples is attributed to desorption of SO<sub>2</sub> from the surface of the washcoat since the adsorption strength of SO<sub>2</sub> on alumina is assumed to be weak. The second peak is assigned to the desorption of SO<sub>2</sub> from the platinum since it is assumed that the SO<sub>2</sub> interacts more strongly with the Pt than with the washcoat components.

Although sample PP422 was expected to release the most NO compared to the other samples during the TPD, this is clearly not the case. This may be explained with a poisoning of the NO storing BaO by SO<sub>2</sub>. BaO is able to form BaSO<sub>4</sub>. Based on the high amount of SO<sub>2</sub> desorbing from sample PP422 during the TPD, it may be concluded that sample PP 422 has lost a lot of its NO storing capacity by the formation of BaSO<sub>4</sub>.

In the NO-TPD spectrum (Figure 4. 22), the NO desorption peak of sample PP500 is located at the lowest temperature (240°C) compared to the NO desorption peaks of the other tested samples. This low desorption temperature gives evidence that this sample adsorbs NO only weakly. Based on the results of Xue et al.<sup>79</sup> it may be assumed that the weak interaction is caused by the SiO<sub>2</sub> contained in the washcoat of sample PP500. The weak interaction of NO with the SiO<sub>2</sub>-containing washcoat can be used to explain the low maximum NO<sub>x</sub> conversions of the SiO<sub>2</sub> containing samples (pp325 and PP500) of Table 4. 12 and the low amount of NO desorbed during the SCAT rig temperature ramp.

#### *4. 3. 4 LOT Performance of Pt/Zeolite-Containing Catalysts with Additives*

The test conditions and the gas concentrations applied in the LOTs of this section were identical to those described in Table 4. 11.

##### Observations:

Table 4. 13 shows the values obtained with the zeolite-containing samples of Table 4. 10 and the P<sub>c</sub> factor calculated with Equation 4. 3.

		PP452	PP454	RD763
THC(50)	°C	233	234	238
TCO(80)	°C	238	235	233
NO <sub>x</sub> <sup>max</sup>	%	52,7	30,5	40,4
T(NO <sub>x</sub> <sup>max</sup> )	°C	239	238	245
NO <sup>max</sup>	%	62	49	61
T(NO <sup>max</sup> )	°C	277	270	267
SO <sub>2</sub> (250)	%	94	96	89
W(NO <sub>x</sub> )	K	69	18	38
NO <sub>2</sub> <sup>max</sup>	%	54	50	61
P <sub>c</sub>		25,8	10,3	16,6

Table 4. 13: Values obtained from LOTs with zeolite-containing samples with SO<sub>2</sub> in the feedgas

Sample PP41 may serve as a reference for the values shown in Table 4. 13.

Sample PP452 has the highest P<sub>c</sub> factor (25,8) of the three catalysts tested. It also has the highest NO<sub>x</sub><sup>max</sup> value (52,7%) and the broadest conversion window (69K), followed by RD763. The lowest P<sub>c</sub> factor (10,3) and narrowest NO<sub>x</sub> conversion window (18K) was recorded for sample PP454. All catalysts have a similar HC and CO conversion performance (THC(50) between 233°C and 238°C; TCO(80) between 238°C and 233°C) and enhance SO<sub>2</sub> oxidation significantly (all SO<sub>2</sub>(250) values around 90%). Compared to the non-zeolite-containing samples the TCO(80) values of the zeolite-containing samples are relatively high (TCO(80) of PP41: 206°C) while the THC(50) values are akin (THC(50) of PP41: 240°C).

After each LOT a temperature ramp was performed. Directly after the temperature ramp another LOT without SO<sub>2</sub> in the feedgas was performed. The temperature ramps are discussed in the following section, while the results of the LOT without SO<sub>2</sub> in the feedgas are summarised in Table 4. 14.

If SO<sub>2</sub> is not in the gasmix the P<sub>c</sub> factors of samples PP452, PP454, and RD763 rise from 25,8 to 27,3, from 10,3 to 18,8, and from 16,6 to 26,4 respectively. The presence or absence of SO<sub>2</sub> in the gas mix does not have a significant influence on the THC(50) and TCO(80) values of sample PP454 (THC(50) with SO<sub>2</sub>: 234°C; THC(50) without SO<sub>2</sub>: 237°C; TCO(80) with SO<sub>2</sub>: 235°C; TCO(80) without SO<sub>2</sub>: 235°C). The THC(50) and TCO(80) values of RD763 are much lower in the absence of SO<sub>2</sub> (THC(50) with SO<sub>2</sub>: 238°C; THC(50) without SO<sub>2</sub>: 224°C; TCO(80) with SO<sub>2</sub>:

233°C; TCO(80) without SO<sub>2</sub> 206°C). The NO<sub>x</sub><sup>max</sup> values of PP454 and RD763 are greatly enhanced (from 30,5% to 41,5% and from 40,4% to 51,6%, respectively) and the NO<sub>x</sub> conversion window is broader (18K compared to 47K and 38K compared to 54K, respectively) if SO<sub>2</sub> is not in the gas mix. SO<sub>2</sub> absence improves the NO<sub>x</sub> conversion of sample PP452 only slightly (from 52,7% to 54,1%).

		PP452	PP454	RD763
THC(50)	°C	226	237	224
TCO(80)	°C	232	235	206
NO <sub>x</sub> <sup>max</sup>	%	54,1	41,5	51,6
T(NO <sub>x</sub> <sup>max</sup> )	°C	232	239	234
NO <sup>max</sup>	%	64	51	79
T(NO <sup>max</sup> )	°C	267	310	258
SO <sub>2</sub> (250)	%	0	0	0
W(NO <sub>x</sub> )	K	71	47	54
NO <sub>2</sub> <sup>max</sup>	%	54	50	70
P <sub>c</sub>		27,3	18,8	24,6

Table 4. 14: Values obtained from LOTs with zeolite-containing samples without SO<sub>2</sub> in the feedgas

### Conclusions:

The high P<sub>c</sub> factor of sample PP452 (25,8 with SO<sub>2</sub>; 27,3 without SO<sub>2</sub>) is caused by its high maximum NO<sub>x</sub> conversion and the broad conversion window. Many mechanisms proposed for lean NO<sub>x</sub> reduction suggest that a limiting factor for the NO dissociation is an inhibition of this dissociation because of co-adsorbed oxygen<sup>56</sup>  
<sup>76 85</sup>. Lööf et al.<sup>77</sup> reported that this effect is much less pronounced when ceria is added to an Al<sub>2</sub>O<sub>3</sub> washcoat. They explain this by a spillover of oxygen from the noble metal to the ceria. Overall a lower activation energy for NO dissociation results. The comparatively high NO<sub>x</sub><sup>max</sup> value of sample PP452 verifies Lööf's results. Yet, the positive effect of ceria can not be increased indefinitely by using a higher amount of ceria in the zeolite-containing washcoat as proven by the lower NO<sub>x</sub><sup>max</sup> value of PP454. With a high amount of ceria in the zeolite-containing washcoat (20 wt.-% in PP454 compared to 2 wt.-% in PP452) not only the maximum NO<sub>x</sub> conversion is significantly decreased (from 52,7% (PP452) to 30,5% (PP454)), but also the width of the conversion window shrinks considerably (from 69K (PP452) to 18K (PP454)). The high amount of ceria in the washcoat of sample PP454 does not effect the conversion performance of the sample for any other gas mix component.

This may be interpreted as proof that ceria influences only the NO<sub>x</sub> conversion by enhancing NO decomposition up to a certain weight percentage of CeO<sub>2</sub>. A cognate effect is linked to the manganese added to the washcoat of sample RD763. However, the addition of MnO<sub>2</sub> to the washcoat has a positive effect on the NO<sub>x</sub> conversion congruent to ceria addition only if SO<sub>2</sub> is absent from the gas mix. The reason for this is that MnO<sub>2</sub> reacts easily with SO<sub>2</sub> to form MnSO<sub>4</sub>.

Based on a comparison of the THC(50) and TCO(80) values of the zeolite-containing samples with the corresponding values of sample PP41 (THC(50) of PP41:240°C; TCO(80) of PP41: 206°C), it may be stated that the use of zeolite-containing washcoats does neither enhance nor reduce the temperature of HC light-off while it seems to deteriorate CO conversion. The reason for the high TCO(80) values of the zeolite-containing samples compared to those of PP41 is probably that the zeolite-containing washcoat stores a lot more HC which is released even at higher temperatures during the LOT. Consequently HC and CO compete for a longer time for oxidation sites than on the non-zeolite-containing since on the latter less HC is stored on the washcoat.

Two conclusions can be drawn from a comparison of the LOTs with- and the LOTs without SO<sub>2</sub> in the gas mix: (1) the presence of SO<sub>2</sub> in the gas mix does not reduce the P<sub>c</sub> factor of sample PP452 significantly (25,8 with SO<sub>2</sub>; 27,3 without SO<sub>2</sub>) although slight improvements in all descriptive values are recorded if SO<sub>2</sub> is absent. (2) Although the performances of samples PP454 and RD763 are reduced by SO<sub>2</sub>, they can be regenerated by a simple temperature treatment.

#### *4. 3. 5 Temperature Ramps and TPDs with Pt/Zeolite-Containing Catalysts with Additives*

Figure 4. 24 shows the temperature ramp desorption spectra of samples PP452, PP454, and RD763. These ramps were performed directly after the LOT with SO<sub>2</sub> in the gas mix was completed. The carrier gas was N<sub>2</sub>, the heating rates were 20°C/min, and the maximum inlet temperature was 500°C. Figure 4. 25 shows the results of the TPD runs. The reader shall be reminded that the concentration values recorded during these temperature ramps have to be interpreted as qualitative

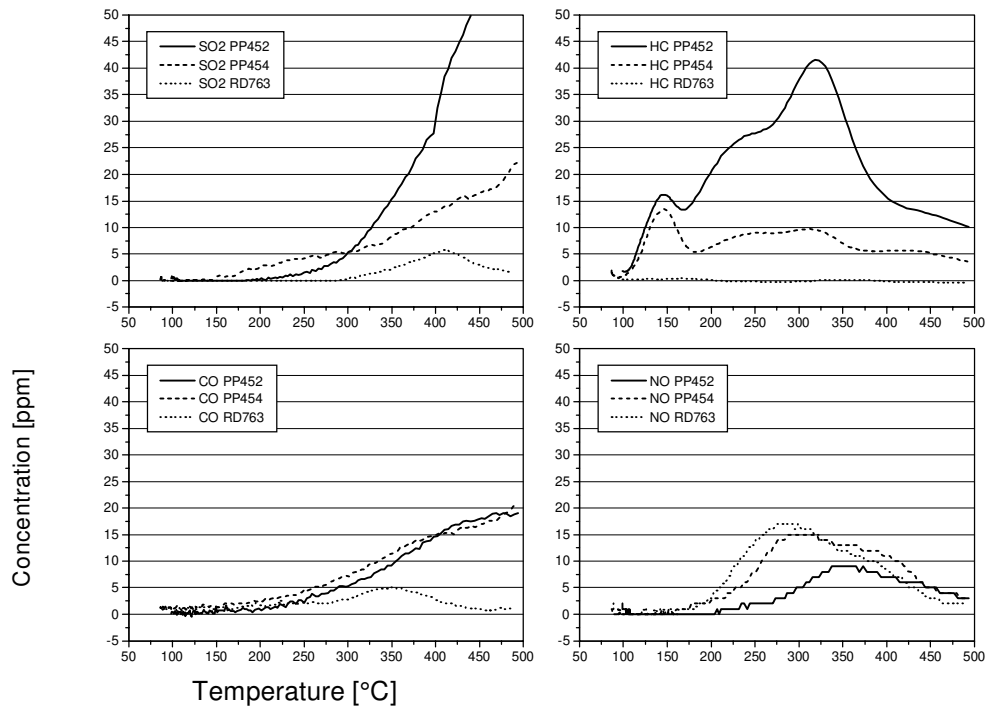


Figure 4. 24: Temperature ramp spectra of samples PP452, PP454, and RD763

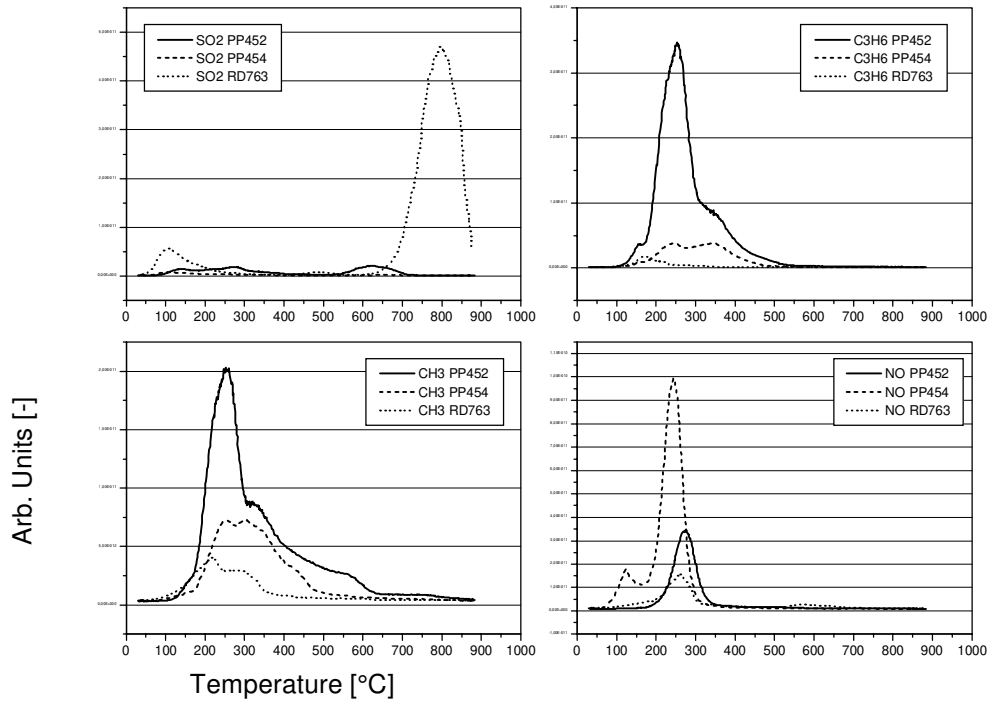


Figure 4. 25: TPD spectra of samples PP452, PP454, and RD763

information. The peak values are only given to make the comparison of the temperature ramp and TPD results easier. They may not represent the true values of the amounts desorbed.

#### Observations:

During the SCAT rig temperature ramps sample PP452 featured the highest SO<sub>2</sub> desorption peak (exceeded measuring range) followed by PP454 (22 ppm at test end). The SO<sub>2</sub> desorption peak of sample RD763 is small (6 ppm) compared to the other samples. The same order of peak heights applies to HC desorption. For sample PP 452 three peaks are recorded: #1 at 145°C (16 ppm), #2 at 247°C (28 ppm), #3 at 319°C (42 ppm). The same number of peaks is recorded for sample PP 454: #1 at 145°C (13 ppm), #2 at 247°C (9 ppm), #3 at 319°C (10 ppm). No HC is detected during the temperature ramp performed with sample RD 763. In contrast to the non-zeolite-containing samples, the magnitude of CO desorption peaks of samples PP452 and PP454 is significant (20 ppm for both samples at test end). During the SCAT rig temperature ramps the most NO desorbs from sample RD763 (17 ppm) ensued by PP454 (15 ppm).

The observations made during the TPD runs for SO<sub>2</sub> and NO desorption are different from the results of the SCAT rig temperature ramps. During the TPDs most SO<sub>2</sub> desorbs from RD763 while the quantities of SO<sub>2</sub> desorbing from the other two samples seems to be negligible (therefore no value is given here). Sample PP454 has the highest NO desorption peak (9,9) followed by PP452 (3,5) and RD763 (1,6). The observations made for propene desorption are similar to those of the SCAT rig temperature ramps: sample PP 452 features the highest propene desorption peak (3,5) followed by sample PP454 (0,38). The propene desorption peak of sample RD763 is smallest (0,17). The same order of peak height is observed for CH<sub>3</sub> desorption.

#### Conclusions:

The order of SO<sub>2</sub> desorption during the SCAT rig temperature ramps was not expected. It was assumed that most SO<sub>2</sub> would desorb from RD763. This assumption was based on the hypothesis that the MnO<sub>2</sub> of the washcoat of RD763 would react



with  $\text{SO}_2$  to form  $\text{MnSO}_4$  which would decompose to  $\text{MnO}_2$  and  $\text{SO}_2$  at higher temperature. Indication for such a mechanism is given by the detection of  $\text{SO}_2$  during the TPD at temperatures above  $700^\circ\text{C}$ .

The shapes of the HC desorption curves in Figure 4. 24 differs strongly from the shape of the HC desorption curve recorded with a washcoat-only zeolite-containing sample, Figure 4. 11. Based on this difference, it is speculated that the presence of the ceria and/or the platinum influence the shape of the curve. The HC desorption spectra (Figure 4.24) obtained from the SCAT rig temperature ramp give two informations: (1) increasing the weight percentage of the ceria in the washcoat from 2 to 20 wt.-% reduces the HC storage capacity. This explains why the  $\text{NO}_x$  conversion performance of PP454 during the LOTs stays behind that of PP452: less HC is stored on PP454 and available for  $\text{NO}_x$  reduction. (2) The addition of  $\text{MnO}_2$  to the washcoat (sample RD763) apparently inhibits HC storage completely. The inhibition of HC storage by  $\text{MnO}_2$  on sample RD763 is confirmed by the TPD spectra: Figure 4. 25 shows only a very small propene desorption peak compared to the peaks of the other two samples. However, - as speculated for the non-zeolite-containing samples - the fact that no HC desorption was detected from RD763 does not necessarily mean that no HC is stored on this sample:  $\text{CO}_2$  is detected during all TPD runs, as shown in Figure 4. 26. The formation of  $\text{CO}_2$  on sample RD763 during the TPD may be interpreted as an indirect proof for the presence of HC on the sample. It may be hypothesised that the adsorbed HC reacts with co-adsorbed oxygen during the TPD to form  $\text{CO}_2$ . Thus no HC desorption is observed, only  $\text{CO}_2$ . A reaction between stored HC and co-adsorbed oxygen during the SCAT rig temperature ramp may also be the reason for the CO detected during the temperature ramps of samples PP452 and PP 454. It must be admitted that the temperature ramps feature only a small CO peak for sample RD763 (compare Figure 4. 24). This conflicts with the hypothesis that enough HC is present on sample RD763 to cause the  $\text{CO}_2$  desorption peak observed in the TPD run unless it is proposed that all HC is converted completely to  $\text{CO}_2$ . A complete conversion of HC to  $\text{CO}_2$  under temperature ramp conditions (no extra-oxygen in the feedgas) is, however, unlikely.

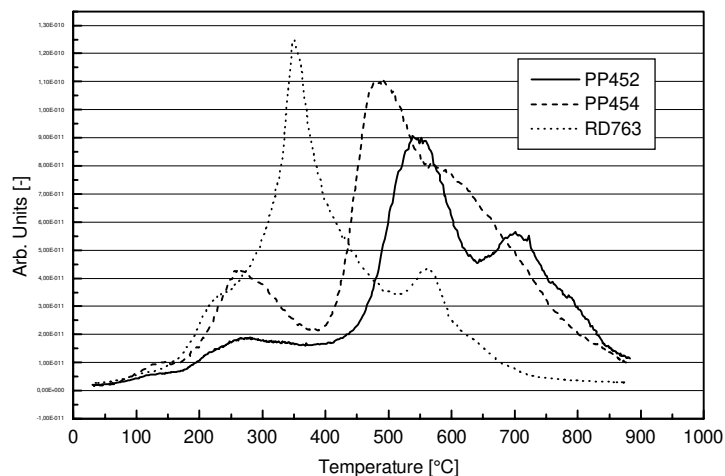


Figure 4. 26: CO<sub>2</sub> formation during TPD runs

The three HC desorption detected during the SCAT rig temperature ramps of samples PP452 and PP454 can have two reasons: (1) the HC is stored on three different sites each with a growing strength of interaction between support and HC. (2) different types of HC fragments are detected which can not be distinguished due to the HC-analyser measuring total HC content of the reactor effluent. The detection of CH<sub>3</sub> during the TPD runs with samples PP452 and PP454 proofs that at least two species desorb from the samples during the SCAT rig temperature ramps.

NO release from sample PP452 and PP454 was not expected to be significant since under the prevalent conditions CeO<sub>2</sub> should enhance NO dissociation according to Lööf et al. [78] resulting in the formation of N<sub>2</sub> and O<sub>2</sub>. This is in agreement with the results of the SCAT rig temperature ramps but not the TPD spectra.

As for the alumina based samples the discrepancies between the results of the SCAT rig temperature ramps and the TPD experiments probably have their origin in the preparation of the samples performed prior to the experiments.

#### 4. 3. 6. Summary

In this chapter it is shown that CO dispersion measurements may be misleading if additives are in the washcoat (in this thesis CeO<sub>2</sub> and MnO<sub>2</sub>) which can be reduced during the preparation process resulting in metallic atoms other than Pt. These other

metallic atoms also chemisorb CO. This effect becomes significant if the mass percentage of the additive is high.

The shapes of the CO light-off curves of the samples tested deliver evidence that CO conversion is retarded by the onset of HC conversion.

It is verified that a high Pt dispersion favours early HC and CO light-off while it has no influence on the magnitude of maximum NO<sub>x</sub> conversion. All three results are congruent with the results of section 4.2.

The use of a washcoat with silica in the alumina reduces NO<sub>x</sub> conversion. It is postulated that the reason for the decline in NO<sub>x</sub> conversion performance is that the silica does not interact very well with the acidic NO molecules<sup>79</sup>.

The incorporation of BaO or La<sub>2</sub>O<sub>3</sub> in an Al<sub>2</sub>O<sub>3</sub> washcoat gives a catalyst that performs with a wider NO<sub>x</sub> conversion window without deteriorating the conversion performance for other gases. Yet, the addition also favours SO<sub>2</sub> oxidation.

During temperature desorption experiments with non-zeolite-containing samples all samples release SO<sub>2</sub>. A high Pt dispersion makes a sample particularly susceptible for SO<sub>2</sub> adsorption which results in the conclusion that SO<sub>2</sub> is predominantly adsorbed on the Pt of a Pt/Al<sub>2</sub>O<sub>3</sub> catalyst.

During temperature ramps performed on the SCAT rig, most NO desorbs from samples which contain BaO and La<sub>2</sub>O<sub>3</sub> as NO<sub>x</sub> storage components. This NO storage is identified as the reason for the broad NO<sub>x</sub> conversion windows featured by these samples.

The interaction of the washcoat with NO is decreased if the alumina contains SiO<sub>2</sub>. This is verified by low amounts of NO desorbing during SCAT rig temperature ramps from samples with alumina/silica washcoats. The weak interaction of the silica-containing washcoat with NO is assumed to be the reason why samples with such a washcoat show comparatively poor NO<sub>x</sub> conversion performance.

HC desorption is not detected from non-zeolite-containing samples during SCAT rig temperature ramps, yet TPD studies revealed the formation of CO<sub>2</sub> indicating the oxidation of adsorbed HC by co-adsorbed oxygen during the temperature ramp.

During the TPD runs much less NO is desorbed from the BaO containing sample than during the SCAT rig temperature ramps. This is attributed to the poisoning of the NO storing BaO by SO<sub>2</sub>.

Different results of the desorption experiments done with the SCAT rig on the one hand and TPD studies performed at JM's Technology Centre on the other are explained with the different gas-dosing procedures applied.

Zeolite containing samples feature higher  $P_c$  factors than non-zeolite-containing samples. The overall conversion performance of the zeolite-containing sample PP452 is unaffected by the presence or absence of  $SO_2$  in the feedgas. Although the conversion performances of the other two zeolite-containing samples tested are reduced by presence of  $SO_2$ , the performances can be regenerated by a simple temperature treatment.

The addition of a small amount of ceria (2 wt.-%) to a zeolite-containing washcoat increases  $NO_x$  conversion without affecting other conversion performances. The addition of manganese instead of  $CeO_2$  has a cognate effect only if  $SO_2$  is not in the feedgas. Adding a high amount of ceria (20 wt.-%) to the zeolite-containing washcoat causes a decrease of the  $NO_x$  conversion. Hence,  $NO_x$  conversion performance can not be improved indefinitely by adding ceria.

The continuous release of HC from the zeolite is speculated to be the reason why the TCO(80) values of zeolite-containing samples are higher than the TCO(80) values of non-zeolite-containing samples.

SCAT rig temperature ramps with zeolite-containing samples show desorption of  $SO_2$  and NO from all samples.

Increasing the weight percentage of ceria in a zeolite-containing washcoat reduces its HC storage capacity. This is the reason why a sample with a high amount of ceria in its washcoat stays behind a sample with a low amount of ceria in its washcoat in  $NO_x$  conversion performance.

A sample with  $MnO_2$  added to its zeolite-containing washcoat does not show HC desorption but  $CO_2$  formation is recorded and is attributed to the oxidation of adsorbed HC by co-adsorbed oxygen.

#### **4. 4 The Influence of Ageing**

Freshly made catalysts can perform very well even under harsh conditions. However, if these conditions are maintained for a longer time, the activity of the catalyst decreases in most cases. Because of this, legislative test procedures have

been introduced which test catalysts after a certain time of operation. For example, one of these tests requires that a catalyst still shows a certain conversion performance after it was used in a car for 160000 kilometres. A test like this takes approximately 1 ½ years and is vastly expensive. For development purposes, a long time of catalyst operation is therefore simulated by heating the catalyst to a high temperature in certain gas atmospheres, usually 10% water in air. Some of these fast ageing procedures also add SO<sub>2</sub> to the gas. A disadvantage of this method is that the influence of soot accumulation can not be mimicked.

The first part of this section examines aged Pt/Al<sub>2</sub>O<sub>3</sub> catalysts regarding their performance after a severe ageing treatment. The second part investigates, whether the washcoat additives described in 4. 3. 2 and 4. 3. 3 can help to maintain the conversion performance of a Pt/Al<sub>2</sub>O<sub>3</sub> catalyst after ageing.

#### 4. 4. 1 The Influence of Ageing on Pt/Al<sub>2</sub>O<sub>3</sub> Samples without Additives

The samples of this section were aged at 800°C for 24 hours in a 10% water in air atmosphere. This treatment can be classified as very severe.

##### 4. 4. 1. 1 Characterisation of the Pt/Al<sub>2</sub>O<sub>3</sub> Samples by BET and COC Measurements

The BET and COC data obtained from ASAP 2000 measurements with the aged samples of Table 4. 6 are given in Table 4. 15.

Sample	Measured D <sub>M</sub> [%]	MSA [m <sup>2</sup> /g]	BSA [m <sup>2</sup> /g]	SPPV [ml/g]	APD [Å]
4093a	1,8	0,0096	15,9	0,050	125,1
4094a	1,0	0,0057	17,6	0,054	123,4
4095a	1,0	0,115	18,2	0,055	121,0
4096a	1,0	0,0141	16,4	0,051	123,1
4097a	2,7	0,145	18,1	0,053	117,5
4098a	3,0	0,0164	18,6	0,055	119,3
4099a	1,4	0,0194	20,3	0,059	116,7
4100a	1,6	0,0222	22,0	0,065	118,5
4101a	6,4	0,0300	30,7	0,099	129,6
4102a	5,8	0,0273	30,1	0,097	129,2
4103a	2,5	0,0301	29,0	0,094	129,7
4104a	2,1	0,0254	27,3	0,088	128,6
4105a	4,8	0,0226	39,2	0,116	118,1
4106a	5,3	0,0250	39,6	0,123	123,9
4107a	2,2	0,0264	33,9	0,101	118,4
4108a	2,6	0,0313	33,7	0,100	119,2

Table 4. 15: Results of BET and COC measurements of aged samples

### Observations:

The Pt dispersion on all samples has decreased compared to the fresh samples (compare Table 4. 6). Samples with a low washcoat load (4093 - 4100) loose more of their Pt dispersion than their high washcoat load counterparts (4101 - 4108). The reverse trend applies to Pt load: samples with low Pt load (4093, 4094, 4097, 4098, 4101, 4102, 4105, 4106) maintain more dispersion than samples with high Pt load (4095, 4096, 4099, 4100, 403, 4104, 4107, 4108).

The BET surface area of all samples has decreased as well (compare Table 4. 6). The influence of the dispersion on the BET surface area noticed for the fresh samples (compare section 4. 2. 1) is not observed anymore: samples which had a low Pt dispersion before ageing (all samples with even numbers in Table 4. 15) do no longer have a significantly smaller BET surface area than samples which had a high dispersion before ageing (all samples with odd numbers in Table 4. 15).

The ratio of the single point pore volumes of corresponding low and high washcoat load aged samples (for instance 4093 and 4101) is similar to the ratio measured for corresponding fresh samples with low and high washcoat load.

The average pore diameter is similar for all aged samples of Table 4. 15. Figure 4. 27 shows the pore size distribution for the fresh and aged sample 4093 as a representative for all other samples.

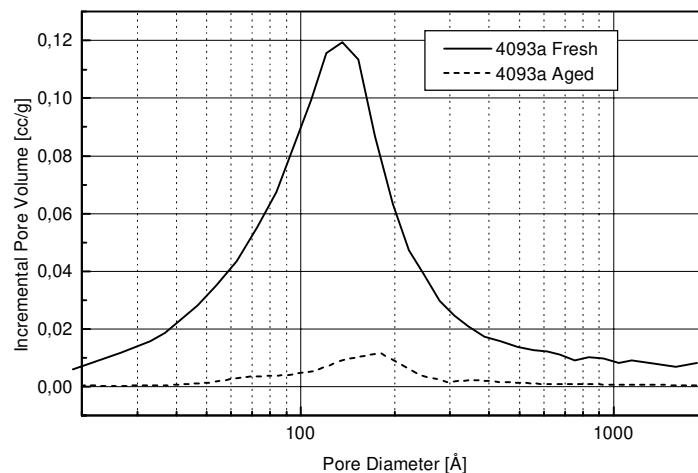


Figure 4. 27: The PSD of catalyst 4093 fresh and after ageing

### Conclusions:

The Pt dispersion is reduced more if the Pt clusters are closer to each other (compare Figure 4. 17). If washcoat load, surface area, and Pt dispersion are kept constant while Pt load is increased, this results a reduced distance between individual Pt clusters, assuming that the metal is distributed evenly. This reduced distance between the Pt clusters increases the decline of Pt dispersion upon ageing. In order to make the Pt dispersion of a catalyst less sensitive towards ageing, the Pt clusters must be kept apart from each other for a certain distance. This can be done by using a large amount of washcoat (i.e. a high washcoat load) or a washcoat with a high surface area (compare sections 4. 2. 2. 4 and 4. 2. 2. 5).

The changes of the pore size distribution indicate a major loss of pore structure of the Al<sub>2</sub>O<sub>3</sub> washcoat. The percentage loss of BET surface area is similar for all aged samples. The loss is caused by the collapse of pores. This pore collapse also causes encapsulation of Pt which can no longer contribute to the catalytic reaction. This encapsulation of Pt is another reason why metal surface area is reduced through the ageing procedure besides the decrease of Pt dispersion.

#### *4. 4. 1. 2 LOT Performance of Aged Pt/Al<sub>2</sub>O<sub>3</sub> Catalysts*

All samples of Table 4. 15 were tested under similar conditions. The concentrations of the gases used in the feedgas are given in Table 4. 7. The descriptive values obtained during the LOTs as well as the P<sub>c</sub> factor calculated with Equation 4. 3 are summarised in Table 4. 16.

### Observations:

High Pt load samples have an average P<sub>c</sub> factor of 4,1. This is 41% larger than the average P<sub>c</sub> factor of low Pt load samples (2,4). The average P<sub>c</sub> factor of samples with a high washcoat load is 3,6 and thus 19% larger than the average P<sub>c</sub> factor of low washcoat load samples 2,9.

Only one sample with low washcoat load (sample 4100) has a maximum NO<sub>x</sub> conversion exceeding 20% (20,8%) and has therefore a small W(NO<sub>x</sub>) value (10K). Samples 4103, 4104, and 4108 with high Pt load and high washcoat load have very broad NO<sub>x</sub> conversion windows (55K, 70K, and 53K, respectively).

		4093	4094	4095	4096	4097	4098	4099	4100
THC(50)	°C	308	302	297	272	328	317	290	282
TCO(80)	°C	314	307	294	269	331	315	290	275
NO <sub>x</sub> <sup>max</sup>	%	12,6	16,5	18,4	15,8	12,3	14,9	16,9	20,8
T(NO <sub>x</sub> <sup>max</sup> )	°C	313	313	268	281	318	294	302	290
NO <sup>max</sup>	%	34,5	44,6	52,2	53,8	42,6	47,2	49,1	59,7
T(NO <sup>max</sup> )	°C	358	333	333	302	370	349	320	303
SO <sub>2</sub> (250)	%	18	23,7	47,5	30,4	17,9	34,5	43,9	37,8
W(NO <sub>x</sub> )	K	0	0	0	0	0	0	0	10
NO <sub>2</sub> <sup>max</sup>	%	63	58	60	68	63	57	67	67
P <sub>c</sub>		2,0	2,7	3,1	2,9	1,9	2,4	2,9	5,5
		4101	4102	4103	4104	4105	4106	4107	4108
THC(50)	°C	316	316	276	271	326	319	287	273
TCO(80)	°C	320	321	273	285	321	314	276	264
NO <sub>x</sub> <sup>max</sup>	%	16,1	16,2	25,9	28,8	17	17,3	18,1	28,6
T(NO <sub>x</sub> <sup>max</sup> )	°C	311	310	281	274	336	305	293	283
NO <sup>max</sup>	%	40,1	41,2	60,9	50,6	40,5	45,5	49,7	58
T(NO <sup>max</sup> )	°C	347	348	305	329	350	334	325	298
SO <sub>2</sub> (250)	%	15,8	29,8	53,1	40	14,3	27,5	15,8	43,2
W(NO <sub>x</sub> )	K	1	0	55	70	0	0	0	53
NO <sub>2</sub> <sup>max</sup>	%	70	58	70	59	69	62	81	75
P <sub>c</sub>		2,7	2,5	14,7	17,8	2,6	2,7	3,2	15,2

Table 4. 16: Values obtained from LOTs with aged samples 4093d - 4108d

### Conclusions:

The high P<sub>c</sub> factors of samples with a high Pt load (4095, 4096, 4099, 4100, 4103, 4104, 4107, 4108) are caused by the lower TCO(80) and THC(50) values of these samples compared to the samples with low Pt load (4093, 4094, 4097, 4098, 4101, 4102, 4105, 4106). The high P<sub>c</sub> factors of samples with a high washcoat load (4101 - 4108) are caused by the high maximum NO<sub>x</sub> conversions of these samples compared to samples with a low washcoat load (4093 - 4100). Thus it may be concluded that a high Pt load helps to maintain oxidation activity of the catalyst after ageing, while a high washcoat load helps to maintain a better NO<sub>x</sub> conversion efficiency of the same catalyst after ageing. Therefore, samples with a high Pt load and a high washcoat load feature the highest P<sub>c</sub> factors in Table 4. 16.

The positive effect of a high Pt load seems to contradict the results of the previous section 4. 4. 1. 1. In section 4. 4. 1. 1 it was concluded that the Pt dispersion of samples with high Pt load declines more than on samples with low Pt load. Yet, a high Pt dispersion was identified in section 4. 2. 2. 2 to reduce the values of THC(50) and TCO(80) compared to a low Pt dispersion. The observation in this section is that although the samples with high Pt load loose more Pt dispersion



during ageing, they feature lower values of THC(50) and TCO(80) than samples with low Pt load. Based on this observation it must be assumed that the Pt dispersion of aged samples does not influence the values of THC(50) and TCO(80). It is postulated that the reason for the positive effect of high Pt load is that a high Pt load ensures enough metal surface area with at least some active sites for reaction on the catalyst after the ageing process.

The reason for the positive effect of high washcoat load is probably that a high washcoat load impedes the sintering of the Pt particles: If Pt Load, Pt dispersion, and washcoat surface area are kept constant, an increase in washcoat load results in an increase of the distance between Pt particles on the washcoat (assuming that the metal is distributed evenly, compare section 4. 2. 2. 4).

The importance of the distance between Pt particles for the sintering process may be explained with a thermoconductivity phenomena. This hypothesis assumes that the heat distribution throughout the samples is not even. Figure 4. 28a shows six Pt clusters on an alumina support. If the washcoat is heated, the Pt cluster closest to the heat source will begin sintering first, driven by the trend to minimise its surface energy. The other clusters stay unaffected since alumina is a poor heat conductor and heat is necessary to initiate the sintering process. When the Pt clusters are closer to each other, Figure 4. 28b, so that some of the migrating Pt atoms originating from the first cluster reach the second cluster, heat is transferred by these energy rich Pt atoms from the first to the second cluster. The second cluster responds by sintering, again driven by the trend to minimise its surface energy. A high washcoat load at constant Pt load and constant Pt dispersion keeps the Pt clusters farther apart from each other and the migrating, energy-rich Pt atoms do not reach adjacent clusters.

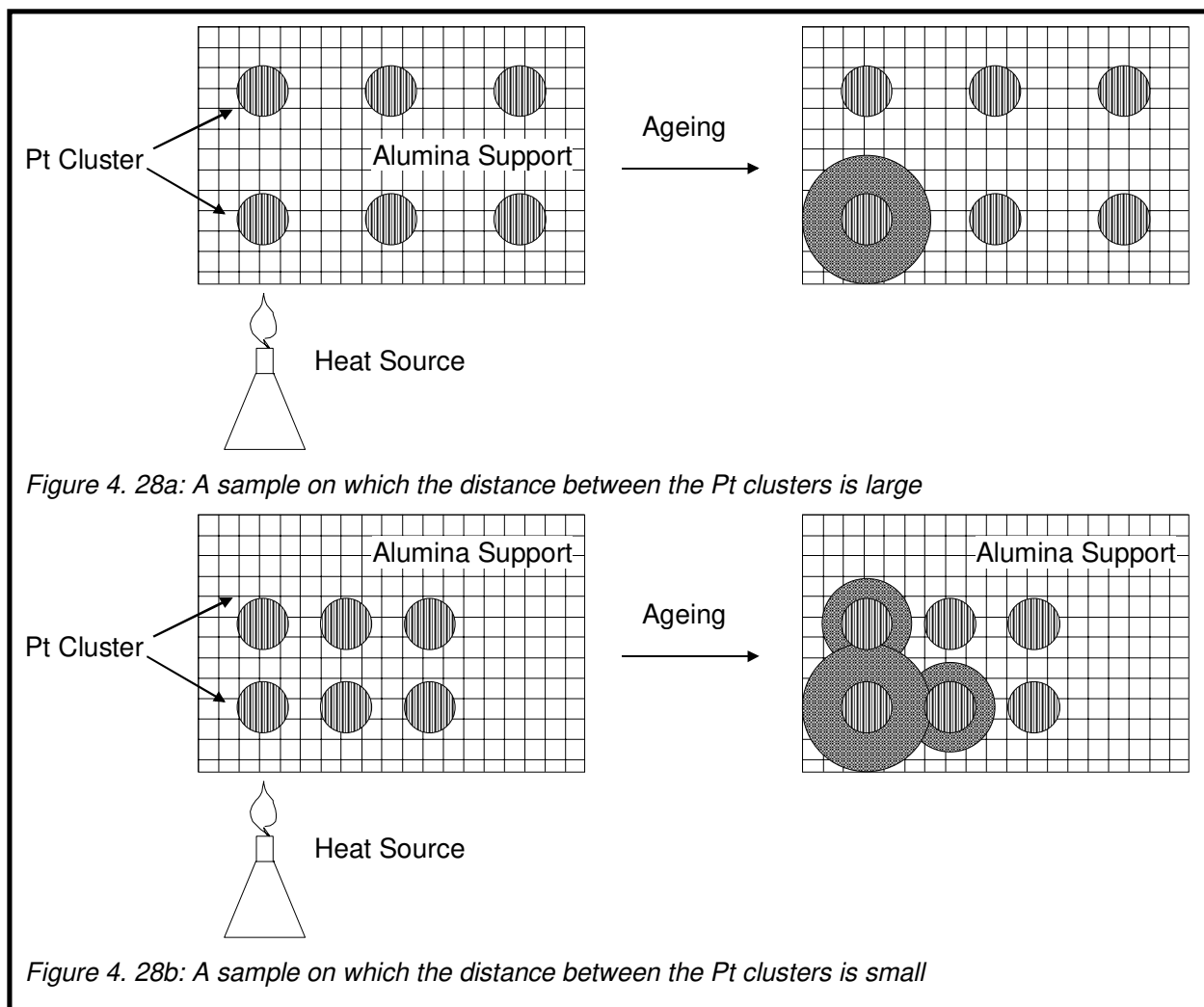


Figure 4. 28a: A sample on which the distance between the Pt clusters is large

Figure 4. 28b: A sample on which the distance between the Pt clusters is small

#### 4. 4. 2 The Influence of Ageing on $Pt/Al_2O_3$ Samples with Additives

In the last section it was established that the washcoat of a  $Pt/Al_2O_3$  catalyst may contribute to maintain catalytic activity during an ageing procedure by keeping the Pt clusters at a certain distance from each other and thus impeding sintering of the Pt. The experiments of the following chapter describe how the catalyst's conversion performance after ageing can be maintained by the use of the additives of section 4. 3. 2. The samples were aged for ten hours in a 10% water in air atmosphere at 650°C and another set of identical samples at 750°C.

##### 4. 4. 2. 1 Characterisation of the $Pt/Al_2O_3$ Samples with Additives by BET and COC Measurements

Table 4.17 summarises the results of ASAP2000 measurements from alumina samples with additives. The numbers 650 and 750 denote samples aged at 650°C

and 750°C, respectively. For easier comparison the results of the fresh samples are also included.

Sample	Measured $D_M$ [%]	MSA [ $m^2/g$ ]	BSA [ $m^2/g$ ]	SPPV [ml/g]	APD [Å]
PP41 fresh	16,9	0,0984	36,5	0,0988	108,1
PP41 650	4,7	0,0272	32,3	0,0934	115,6
PP41 750	4,0	0,0232	28,4	0,0847	119,3
PP325 fresh	13,3	0,0700	51,1	0,1066	83,4
PP325 650	5,3	0,0279	59,2	0,1386	93,7
PP325 750	2,8	0,0145	41,0	0,1020	99,5
PP422 fresh	17,8	0,0929	42,3	0,0885	83,8
PP422 650	3,2	0,0168	29,6	0,0732	98,9
PP422 750	5,5	0,0288	30,1	0,0820	108,9
PP428 fresh	15,7	0,0775	37,1	0,1036	111,7
PP428 650	5,0	0,0247	28,7	0,0968	135,2
PP428 750	7,8	0,0386	19,2	0,0705	146,8
RD704 fresh	28,1	0,2682	37,8	0,0959	102,5
RD704 650	4,2	0,0398	27,8	0,0813	116,9
RD704 750	2,6	0,0252	29,0	0,0886	122,0
PP500 fresh	15,2	0,0819	46,0	0,1158	91,8
PP500 650	2,4	0,0131	38,5	0,0959	99,7
PP500 750	1,8	0,0097	39,5	0,1022	103,6

Table 4. 17: Results of BET and COC measurements

#### Observations:

The dispersion of all samples is reduced during the ageing procedure. For samples PP422 and PP428 the decline is not linear with increasing temperature (17,8% → 3,2% → 5,5% and 15,7% → 5,0% → 7,8%, respectively).

Generally, the samples loose BET surface area during the ageing. The increase of BET surface area of sample PP325 (51,1  $m^2/g$  → 59,2  $m^2/g$ ) during the ageing is assumed to be an experimental error. BET surface areas which do not differ more than 2  $m^2/g$  from each other may be regarded as equal.

The average pore diameters increase linearly with increasing ageing temperature.

#### Conclusions:

According to the BET and COC measurements, no particular additive helps to maintain the Pt dispersion or the BET surface area. Pt dispersion and BET surface area decrease on all samples to a similar extend during the ageing procedure.

There is no plausible explanation for the non-linear decline of Pt dispersion with increasing ageing temperature observed for PP422 and PP428. However, the differences are small and may be neglected considering the reproducibility.

The theory of section 4. 2. 1 that Pt crystals widen the pores of the washcoat during the ageing process was verified by the increase of the average pore diameters with increasing ageing temperature found for all catalyst samples.

#### 4. 4. 2. 2 LOT Performance of Aged Pt/Al<sub>2</sub>O<sub>3</sub> Catalysts with Additives

All aged samples of Table 4. 17 were tested under the same conditions. The concentrations of the gases used in the feedgas are given in Table 4. 18.

CO <sub>2</sub>	4,7 vol.-%
O <sub>2</sub>	12,2 vol.-% (= λ 2,2)
CO	200 ppm
SO <sub>2</sub>	21 ppm
NO	400 ppm
C <sub>3</sub> H <sub>6</sub>	800 ppm
H <sub>2</sub> O	6,4 vol.-%
SV	18000 hr <sup>-1</sup>
T <sub>i</sub> <sup>0</sup> → dT/dt →	80°C →
T <sub>i</sub> <sup>max</sup>	10°C/min →
	530°C

Table 4. 18: Test conditions during LOTs performed in this chapter

Table 4. 19 shows the descriptive values obtained during the LOTs and the P<sub>c</sub> factor calculated with equation 4.3. The weight of the width was reduced by factor 100.

#### Observations:

The P<sub>c</sub> factors of all samples have decreased after ageing. Samples RD704 and PP422 maintain their P<sub>c</sub> factors best while the P<sub>c</sub> factor of PP500 declines most (from 9,4 to 4,6). The weight of the width of the NO<sub>x</sub> conversion window had to be reduced in Equation 4. 3 since otherwise the P<sub>c</sub> factors would give a false impression of the actual performance of the aged samples.

The THC(50) values of all samples increase with increasing ageing temperature. The TCO(80) values of samples PP500, PP422, and PP428 increase as well with increasing ageing temperature. The samples PP41 650, RD704 650, and PP325 650 all have higher TCO(80) values (244°C, 237°C, 261°C, respectively) than their fresh

counterparts (206°C, 160°C, 225°C). However, all of these samples have in common that the TCO(80) value of the samples aged at 650°C is higher than that of the samples aged at 750°C (232°C, 227°C, 240°C, respectively).

NO<sub>x</sub><sup>max</sup> and SO<sub>2</sub>(250) values decline on all samples with increasing ageing temperature, while the NO<sub>x</sub> conversion windows become wider. Sample RD704 features the smallest decline of maximum NO<sub>x</sub> conversion.

	PP41 F	PP41 650	PP41 750	RD704 F	RD704 650	RD704 750	PP325 F	PP325 650	PP325 750
THC(50)	240	246	268	224	257	259	239	264	273
TCO(80)	206	244	232	160	237	227	225	261	240
NO <sub>x</sub> <sup>max</sup>	44,1	37,6	33	42	39,1	40,4	37,8	35,9	35,1
T(NO <sub>x</sub> <sup>max</sup> )	252	259	281	235	272	277	250	275	289
NO <sub>x</sub> <sup>max</sup>	72	71	64	80	71	72	79	71	70
T(NO <sub>x</sub> <sup>max</sup> )	252	259	289	237	279	282	259	285	295
SO <sub>2</sub> (250)	62	51	20	100	53	33	53	38	24
W(NO <sub>x</sub> )	28	26	56	34	43	48	26	37	48
NO <sub>2</sub> <sup>max</sup>	72	66	59	68	64	65	79	64	62
P <sub>c</sub>	10,0	7,7	6,7	9,8	8,0	8,4	8,2	6,9	6,9
	PP500 F	PP500 650	PP500 750	PP422 F	PP422 650	PP422 750	PP428 F	PP428 650	PP428 750
THC(50)	231	264	284	235	238	228	232	258	266
TCO(80)	193	271	325	214	211	260	215	251	280
NO <sub>x</sub> <sup>max</sup>	39,5	37,6	27,3	46,8	39,9	40,6	45,8	41,5	35,6
T(NO <sub>x</sub> <sup>max</sup> )	246	277	279	247	263	277	246	277	282
NO <sub>x</sub> <sup>max</sup>	68	68	48	75	78	72	69	79	64
T(NO <sub>x</sub> <sup>max</sup> )	248	295	339	271	273	285	267	285	289
SO <sub>2</sub> (250)	70	40	19	84	64	36	90	61	47
W(NO <sub>x</sub> )	31	43	55	53	51	62	54	38	54
NO <sub>2</sub> <sup>max</sup>	65	62	45	67	71	61	58	73	56
P <sub>c</sub>	9,4	7,1	4,6	10,5	9,0	8,4	10,4	8,2	6,6

Table 4. 19: Values obtained from LOTs with aged Pt/Al<sub>2</sub>O<sub>3</sub> samples with additives

### Conclusions:

Among the samples tested, RD704 and PP422 are most resistant against ageing and PP500 is least resistant judged on the basis of the corresponding P<sub>c</sub> factors. Hence the preparation procedure used for RD704 or the addition of BaO (PP422) help to maintain conversion performance after ageing.

HC and NO<sub>x</sub> conversion activity are maintained best by samples PP422 and RD704, respectively.

There is no logical explanation why samples PP41 750, RD704 750, and PP325 750 have lower TCO(80) values than their counterparts aged at 650°C. Neither the

measured Pt dispersions nor differences in Pt load can be brought into a plausible relation with this observation.

A decline of SO<sub>2</sub> oxidation with increasing temperature was expected since it was established in section 4. 4. 1. 2 that sites active for oxidation are lost during the ageing process.

The broadening of the NO<sub>x</sub> conversion windows after ageing may be explained by the raise of the THC(50) values: on the aged catalysts HC is not as readily oxidised as on the fresh ones. Thus, it is available for NO<sub>x</sub> reduction for a longer time which increases the width of the conversion window.

It must be kept in mind that the ageing procedure used in this section is not as severe as that of the previous section. Therefore, the maximum NO<sub>x</sub> conversion of all samples are reduced during ageing but still exceed 20% in all cases.

#### *4. 4. 3 Summary*

This section examines aged Pt/Al<sub>2</sub>O<sub>3</sub> catalysts regarding their performance after a severe ageing treatment and whether washcoat additives can help to maintain the conversion performance of a Pt/Al<sub>2</sub>O<sub>3</sub> catalyst after ageing.

Samples of Pt/Al<sub>2</sub>O<sub>3</sub> catalysts loose Pt dispersion during hydrothermal ageing. The Pt dispersion is reduced more if the Pt clusters are closer to each other. Therefore, in order to make the Pt dispersion of a catalyst less sensitive towards ageing, the Pt clusters must be kept apart from each other for a certain distance. This can be achieved by using a high washcoat load on the sample or a washcoat with a high surface area.

The BET surface area of Pt/Al<sub>2</sub>O<sub>3</sub> samples decreases as well during the ageing process. This loss of BET surface area is assigned to a loss of pore structure in the Al<sub>2</sub>O<sub>3</sub> washcoat. It is speculated that the collapse of pores may cause an encapsulation of Pt. This encapsulation reduces the metal surface area additionally besides the loss of dispersion.

A high Pt load helps to maintain oxidation activity of the catalyst after ageing, while a high washcoat load helps to maintain a better NO<sub>x</sub> conversion efficiency of the same catalyst after ageing. Therefore, samples with a high Pt load and a high washcoat load feature high P<sub>c</sub> factors. It is postulated that a high washcoat load impedes the sintering of Pt particles. This is explained by thermoconductivity phenomena, based

on the increased distance between Pt particles on samples with high washcoat load as compared to the distance between Pt particles on catalysts with low washcoat load.

None of the additives examined help exceptionally well to preserve the Pt dispersion or the BET surface area during an ageing treatment of the samples tested. It is established that the pores of Pt/Al<sub>2</sub>O<sub>3</sub> catalysts widen during ageing.

Two samples, one prepared by a different preparation method (RD704) than the other samples and another containing BaO (PP422) maintain most of their overall conversion performance during ageing.

#### **4. 5 Iridium as an Alternative Metal for Pt on Al<sub>2</sub>O<sub>3</sub>**

The platinum metal group of the periodic table of the elements includes ruthenium, rhodium, palladium, osmium, iridium, and platinum. Ruthenium and osmium form very toxic oxides and can therefore not be used as an active metal in an exhaust gas aftertreatment system. The use of palladium, rhodium and platinum for this purpose is widespread. Very little information is available from literature on the performance of iridium. Because of this, the conversion performance of various catalyst formulations including iridium is examined in this chapter. The samples descriptions are given in the appendix.

##### *4. 5. 1 Characterisation of the Ir/Al<sub>2</sub>O<sub>3</sub> Catalyst by BET Measurements*

Two variations of formulation DEV1 (refer to "Appendix") were prepared. One core was fired at 600°C and another one fired at 800°C. These cores are now given the descriptions DEV1600 and DEV1800, respectively. The BET surface area of both cores was measured and the results are shown together with those of PP 41 38 and PP41 WCO in Table 4. 20. The pore size distributions of all four samples are displayed in Figure 4. 29. A CO chemisorption experiment was not performed since the stoichiometry of Ir/CO is not well defined under the prevalent conditions.

Sample	BSA [m <sup>2</sup> /g]	SPPV [cc/g]	APD [Å]
PP 41 WCO fresh	39,8	0,071	72,0
PP 41 38 fresh	39,2	0,117	114,8
DEV1600 (Ir/Al <sub>2</sub> O <sub>3</sub> )	47,0	0,084	71,4
DEV1800 (Ir/Al <sub>2</sub> O <sub>3</sub> )	37,1	0,070	56,7

Table 4. 20: Results of BET measurements

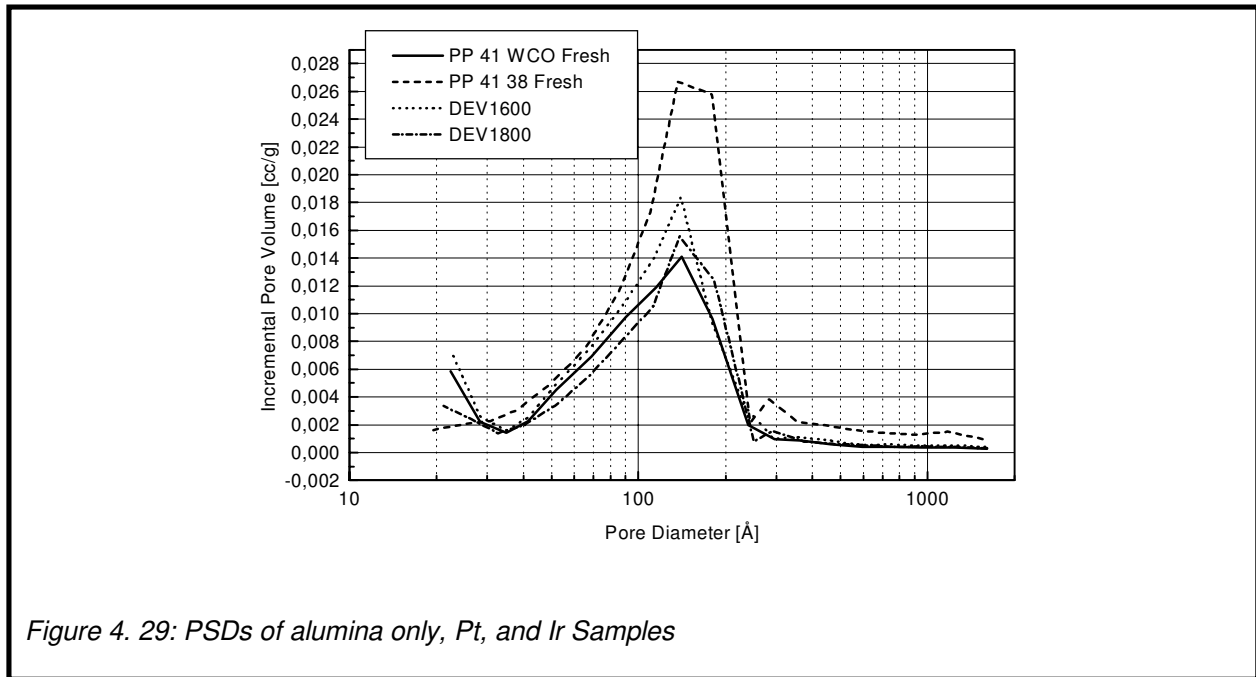


Figure 4. 29: PSDs of alumina only, Pt, and Ir Samples

### Observations:

The BET surface area of DEV1600 is 47,0 m<sup>2</sup>/g and thus 16% larger than that of the alumina only sample (39,8 m<sup>2</sup>/g) while the average pore diameter, single point pore volume, and the pore size distribution of sample DEV1600 is similar to those of sample PP 41 WCO.

Firing the Ir/Al<sub>2</sub>O<sub>3</sub> sample at 800°C results in a matching BET surface area (37,1 m<sup>2</sup>/g) compared to sample PP 41 WCO while the average pore diameter of DEV1800 (56,7 Å) is lower than that of PP41 WCO (72,0 Å).

### Conclusions:

As opposed to Pt, iridium does not widen the pores of the Al<sub>2</sub>O<sub>3</sub> washcoat. This is clearly verified by the average pore diameter values and the pore size distribution plots. It appears as if the addition of Ir to the washcoat results in an increase of the BET surface area. A close look at the pore size distribution plot suggests that



sample DEV1600 has more micropores than PP41 WCO and much more than PP 41 38. The amount of these micropores dominates the BET surface area of any sample. Firing the sample at a higher temperature results in a significant loss of these pores and consequently the BET surface area declines.

#### 4. 5. 2 LOT Performance of Ir/Al<sub>2</sub>O<sub>3</sub> Catalysts

This section examines the conversion performance of Ir containing samples during LOTs at two different oxygen concentrations. The test at lower O<sub>2</sub> concentration was always performed first and the test conditions are given in table 4. 21.

CO <sub>2</sub>	12,0 vol.-%
O <sub>2</sub> and	12,2 vol.-% (= λ 2,2) 0,3 vol.-% (= λ 0,995)
CO	400 ppm
SO <sub>2</sub>	0 ppm
NO	400 ppm
C <sub>3</sub> H <sub>6</sub>	800 ppm
H <sub>2</sub> O	6,4 vol.-%
SV	18000 hr <sup>-1</sup>
T <sub>i</sub> <sup>0</sup> → dT/dt → T <sub>i</sub> <sup>max</sup>	80°C → 20°C/min → 530°C

Table 4. 21: Test conditions during LOTs performed in this chapter

#### 4. 5. 2. 1 HC Conversion

Figure 4. 30a features the HC light-off curves of all Ir samples tested at λ = 0,995 (under-stoichiometric conditions) and sample PP 41 38 for comparison, Figure 4. 30b shows the HC light-off curves of the same samples at λ = 2,2 (highly oxidising conditions).

#### Observations:

In Figure 4. 30a, best performance is presented by sample DEV4 (Ir/Al<sub>2</sub>O<sub>3</sub> containing BaO) followed by PP 41 38 (Pt/Al<sub>2</sub>O<sub>3</sub>) and DEV3 (Pt/Ir/Al<sub>2</sub>O<sub>3</sub>). DEV1800 (Ir/Al<sub>2</sub>O<sub>3</sub> fired at 800°C) is the poorest HC oxidation catalyst under these conditions. Sample DEV3 has the lowest THC(50) value (223°C) in Figure 4. 30b, closely followed by the Pt/Al<sub>2</sub>O<sub>3</sub> reference (239°C). Samples DEV1800, DEV 1600, and DEV4 reach THC(50) at 326°C, 357°C, and 378°C, respectively.

Conclusions:

At under-stoichiometric conditions, the BaO containing Ir/Al<sub>2</sub>O<sub>3</sub> sample DEV4 shows the best HC conversion. Presumably the oxygen of the BaO enhances HC oxidation. The addition of Ir to a Pt/Al<sub>2</sub>O<sub>3</sub> catalyst (sample DEV3) delays the onset of HC oxidation at under-stoichiometric conditions but enhances the conversion at higher temperatures compared to a Pt/Al<sub>2</sub>O<sub>3</sub> sample without Ir (PP 41 38).

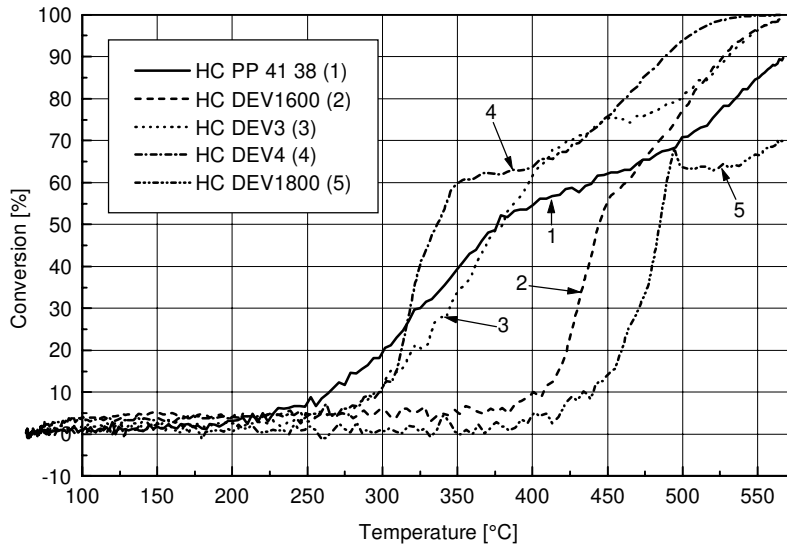


Figure 4. 30a: HC light-off curves of Pt and Ir samples at  $\lambda = 0,995$

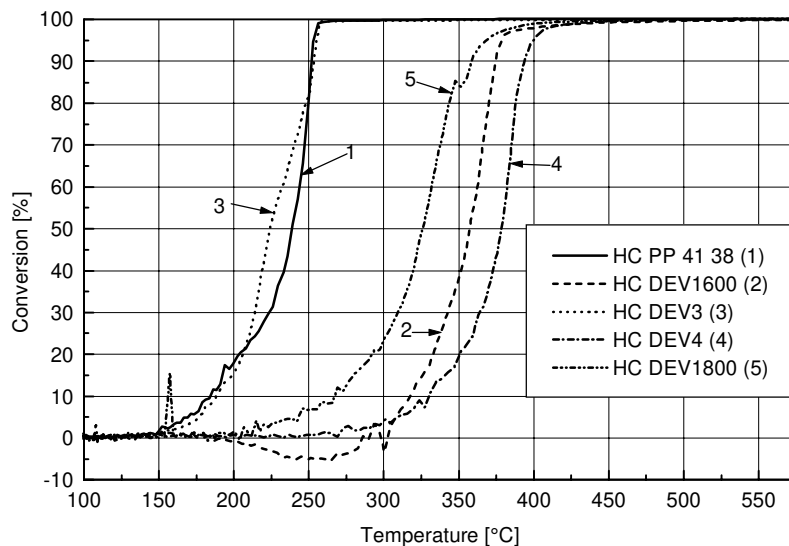


Figure 4. 30b: HC light-off curves of Pt and Ir samples at  $\lambda = 2,2$

The Ir/Al<sub>2</sub>O<sub>3</sub> samples DEV1600 and DEV1800 are very poor HC conversion catalysts at  $\lambda = 0,995$ .

Under oxidising conditions, the HC conversion performance of a Pt/Al<sub>2</sub>O<sub>3</sub> catalyst can be enhanced by the addition of Ir. Firing an Ir/Al<sub>2</sub>O<sub>3</sub> catalyst at 800°C during its preparation reduces the THC(50) value (325°C) of this sample (DEV1800) compared to a sample fired at 600°C (DEV1600, THC(50): 357°C) while the addition of BaO (DEV4) results in an increase of this value (378°C).

#### 4. 5. 2. 2 CO Conversion

Figure 4. 31a features the CO light-off curves of all Ir samples tested at  $\lambda = 0,995$  and sample PP 41 38 for comparison, Figure 4. 31b shows the CO light-off curves of the same samples at  $\lambda = 2,2$ .

#### Observations:

When the oxygen concentration in the feedgas is low, all samples show negative CO conversion at elevated temperatures. Sample PP 41 38, which has the earliest onset (~250°C) of HC conversion under these conditions, presents a local CO-conversion maximum at 189°C. Maximum positive CO conversion of this sample (87%) stays behind that of sample DEV4 (97%). Sample DEV1600 shows only very little positive CO conversion (38%) and DEV1800 none.

When the oxygen concentration in the feedgas is high, samples DEV3 has the lowest TCO(80) value (211°C) followed by PP 41 38 (235°C). Under these conditions, sample DEV1800 shows a much better CO conversion (TCO(80): 313°C) than DEV1600 (TCO(80): 381°C) whose performance is similar to that of DEV4 (TCO(80): 389°C).

#### Conclusions:

As already explained for the washcoat only samples of section 4. 1, the negative conversion of CO observed at under-stoichiometric conditions is a formation of this compound caused by incomplete HC combustion. The local CO conversion maximum of sample PP 41 38 coincides with the start of HC conversion on this sample (around 190°C). Evidently, CO formation begins with the onset of HC

conversion. At temperatures above 400°C the CO formation from incomplete HC combustion dominates the CO conversion.

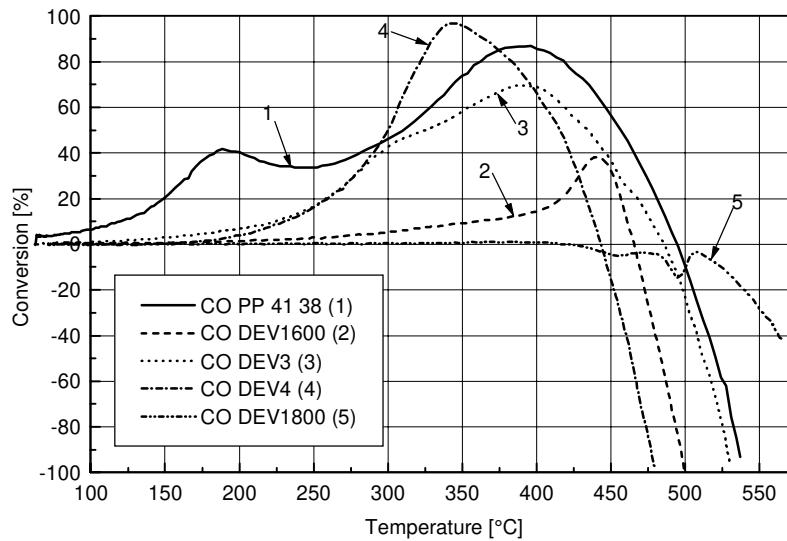


Figure 4. 31a: CO light-off curves of Pt and Ir samples at  $\lambda = 0,995$

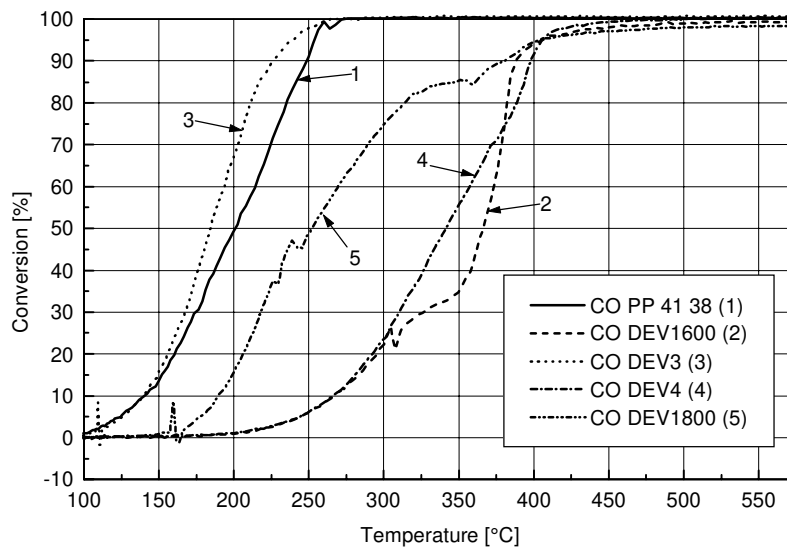


Figure 4. 31b: CO light-off curves of Pt and Ir samples at  $\lambda = 2,2$

CO can not be oxidised as rapidly as it is formed anymore. Additionally, this observation proofs that CO and HC compete for oxidation sites at under-stoichiometric conditions, with HC being the winner at higher temperatures. This probably has to do with an increase of CO desorption at these temperatures. CO is not on the catalyst long enough for being oxidised to CO<sub>2</sub>. The presence of BaO

helps to convert more CO, but only up to a certain temperature (345°C). As already noticed for HC conversion performance, the Ir/Al<sub>2</sub>O<sub>3</sub> samples are also very poor CO conversion catalysts.

Under highly oxidising conditions, the addition of Ir to a Pt/Al<sub>2</sub>O<sub>3</sub> catalyst reduces the TCO(80) value but not the onset of CO conversion. This points to the conclusion that the Ir lowers the activation energy for CO conversion over this catalyst. Further investigations on this method to reduce TCO(80) are strongly recommended. The high amount of oxygen also seems to have a positive influence on the conversion performance of the Ir/Al<sub>2</sub>O<sub>3</sub> catalyst fired at 800°C while it deteriorates the performance of the BaO containing sample.

#### 4. 5. 2. 3 NO<sub>x</sub> Conversion

Figure 4. 32a features the NO<sub>x</sub> conversion curves of all Ir samples tested at  $\lambda = 0,995$  and sample PP 41 38 for comparison, Figure 4. 32b shows the NO<sub>x</sub> conversion curves of the same samples at  $\lambda = 2,2$ .

##### Observations:

From 400°C onward, all samples show a NO<sub>x</sub> conversion larger than 70% if the O<sub>2</sub> concentration in the feedgas is low. DEV4 achieves this level of conversion already at 350°C, but shows a release of NO at temperatures between 148°C and 288°C. Sample DEV1800 also shows some release of NO and NO<sub>2</sub> and achieves 85% NO<sub>x</sub> conversion at temperatures above 500°C.

If the concentration of oxygen in the gas mix is high, PP 41 38 shows the largest NO<sub>x</sub><sup>max</sup> value (66,7%), nearly matched by sample DEV3 (63,9%). Both samples release NO<sub>x</sub> between 285°C to 500°C. Sample DEV4 shows NO<sub>x</sub> release before and after its maximum NO<sub>x</sub> conversion at 428°C (29,6%). Sample DEV1800 exceeds DEV1600 only slightly in NO<sub>x</sub> conversion performance. Both samples do not reach 20% NO<sub>x</sub> conversion.

##### Conclusions:

The shapes of the NO<sub>x</sub> conversions curves obtained at low oxygen conditions are very interesting. Based on an adsorption/dissociation mechanism for the NO<sub>x</sub> reduction one might expect that the NO<sub>x</sub> conversion is high, but that the conversion

would begin at a much lower temperature. Such a theory would assume that under the prevalent conditions only a few Pt sites are occupied by oxygen. The rest of these sites can adsorb NO, which dissociates and two adsorbed nitrogen atoms and two adsorbed oxygen atoms recombine to form N<sub>2</sub> and O<sub>2</sub>.

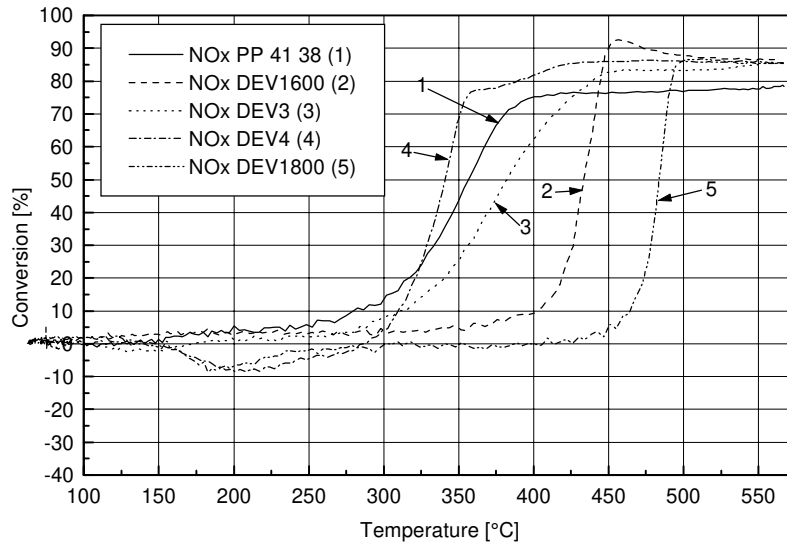


Figure 4. 32a: NO<sub>x</sub> light-off curves of Pt and Ir samples at  $\lambda = 0,995$

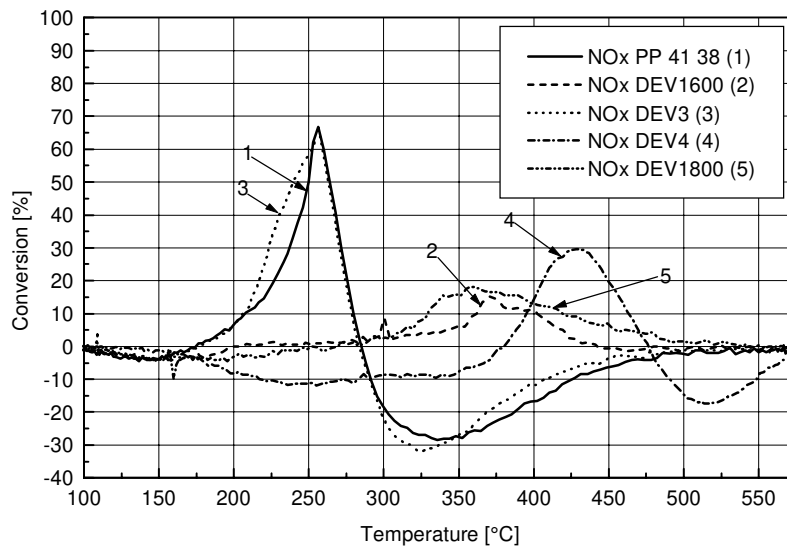


Figure 4. 32b: NO<sub>x</sub> light-off curves of Pt and Ir samples at  $\lambda = 2,2$

A mechanism like this can only take place at moderately low temperatures, since at elevated temperatures NO would desorb before it can dissociate. However, NO<sub>x</sub> conversion does not begin at temperatures below 300°C. It is postulated that the

reason for this is a blocking of sites active for  $\text{NO}_x$  conversion by HC. The onset of  $\text{NO}_x$  conversion coincides in all cases with the begin of HC conversion. It is speculated that BaO enhances HC oxidation under low oxygen conditions and hence, sample DEV4 is the first to reach a high level of  $\text{NO}_x$  conversion. Sample DEV4 also desorbs  $\text{NO}_x$  before conversion starts. This proves that on this catalyst, the NO storage sites (provided by BaO) are unable to dissociate NO as long as HC conversion does not take place. It could also indicate, that the sites storing  $\text{NO}_x$  are different from the ones reducing it and that no NO dissociation takes place on the storing sites.

Another interesting observation is that the  $\text{NO}_x$  conversions of all samples approach constant values which are smaller than 90%  $\text{NO}_x$  conversion. The reason for this is not very clear. Surely, there is no lack of reductant on the catalyst surface. Since HC has lit off at these temperatures there should also be enough free active sites available. The conclusion may be drawn that these constant  $\text{NO}_x$  conversion values are caused by transport limitations on the catalyst. A spillover of HC from the washcoat to the active metal sites was already discussed in chapter 4. 2. 2. 5. and has found new evidence here.

The shapes of the  $\text{NO}_x$  conversion curves at high oxygen concentration also present a new feature, the release of  $\text{NO}_x$  from samples PP 41 38 and DEV3. Since this result was so surprising the reproducibility of this phenomena was well established. In all cases the desorption occurred. The effect occurs only if the concentration of oxygen in the feedgas is high (12,2 vol.-%). The reason for this phenomena is the absence of  $\text{SO}_2$  in the feedgas as proven by LOTs with and without  $\text{SO}_2$ , Figure 4. 33.

Consequently the absence of  $\text{SO}_2$  has a positive effect, namely an increase of  $\text{NO}_x^{\text{max}}$  and  $W(\text{NO}_x)$ , but also a negative effect and that is the desorption of  $\text{NO}_x$  at higher temperatures. This observation also suggests, that  $\text{SO}_2$  and NO compete for adsorption sites. If  $\text{SO}_2$  is absent,  $\text{NO}_x$  is stored on sites otherwise occupied by  $\text{SO}_2$ . Nevertheless, both samples have comparatively high maximum  $\text{NO}_x$  conversions and broad conversion windows. The  $P_c$  factor for sample PP 41 38 and DEV3 is 25,2 and 27,1, respectively. Thus, the addition of Ir to a Pt/ $\text{Al}_2\text{O}_3$  formulation has a very positive effect on the overall performance of the catalyst. A release of  $\text{NO}_x$  from DEV4 was expected since this sample contains the NO storing BaO. A maximum

conversion of 29,6% at 428°C does not make this sample a top-candidate for vehicle application. The two Ir/Al<sub>2</sub>O<sub>3</sub> samples are even less suitable.

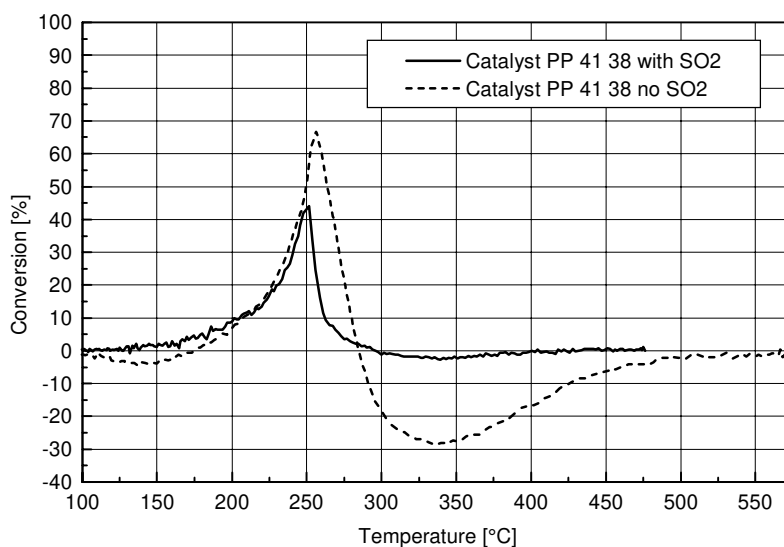


Figure 4. 33: LOTs with PP 41 38 with and without SO<sub>2</sub>

#### 4. 5. 3 Summary

Since very little information in literature is available on the performance of Ir as a catalyst for NO<sub>x</sub> reduction under oxidising conditions, this chapter investigates Ir closely.

Differently from Pt, the addition of iridium to an Al<sub>2</sub>O<sub>3</sub> washcoat does not widen the pores of this washcoat. The BET surface area is increased because of an increased number of micropores.

The conversion performances of various catalyst formulations including Ir are examined at two different oxygen levels:  $\lambda = 0,995$  (under-stoichiometric) and  $\lambda = 2,2$  (highly oxidising).

At under-stoichiometric conditions an Ir/BaO-Al<sub>2</sub>O<sub>3</sub> sample shows the best HC conversion while plain Ir/Al<sub>2</sub>O<sub>3</sub> samples perform very poorly. All samples tested under these conditions form CO at high temperatures, beginning with the onset of HC conversion. At temperatures above 400°C the CO formation dominates the CO conversion. While the Ir/BaO-Al<sub>2</sub>O<sub>3</sub> sample has the highest positive CO conversion, Ir/Al<sub>2</sub>O<sub>3</sub> does not convert very much CO. Beginning at 400°C, all samples show a



NO<sub>x</sub> conversion larger than 70% and approach constant values of this conversion. This is explained with transport limitations on the catalyst. From the shapes of the NO<sub>x</sub> conversion curves the conclusion is drawn that HC blocks sites active for NO<sub>x</sub> reduction until HC conversion begins. NO storage sites on the Ir/BaO-Al<sub>2</sub>O<sub>3</sub> sample are unable to dissociate NO as long as HC conversion does not take place.

Under highly oxidising conditions, the addition of Ir to a Pt/Al<sub>2</sub>O<sub>3</sub> catalyst reduced the THC(50) and the TCO(80) value compared to a plain Pt/Al<sub>2</sub>O<sub>3</sub> catalyst. With a high oxygen concentration in the feedgas the Ir/BaO-Al<sub>2</sub>O<sub>3</sub> and the plain Ir/Al<sub>2</sub>O<sub>3</sub> samples feature very high THC(50) and TCO(80) values. The NO<sub>x</sub> conversion curves show a release of NO<sub>x</sub> from the Pt/Al<sub>2</sub>O<sub>3</sub> sample and the Ir/Pt/Al<sub>2</sub>O<sub>3</sub> sample under these conditions. It is established that SO<sub>2</sub> and NO compete for adsorption sites and that in the absence of SO<sub>2</sub>, NO<sub>x</sub> is stored on sites otherwise occupied by SO<sub>2</sub>. Judged by overall conversion performance, the Ir/Pt/Al<sub>2</sub>O<sub>3</sub> sample performs best while a plain Ir/Al<sub>2</sub>O<sub>3</sub> sample is a very poor catalyst under highly oxidising conditions. The poor conversion performance of the Ir/Al<sub>2</sub>O<sub>3</sub> sample is in agreement with the results of Obuchi et al. [79].

#### **4. 6 The Influence of the Gas mix**

It was established in the last chapter that the gas mix can have a significant influence on the observed conversion performance of the catalyst. This chapter looks at various gas mixes and discusses how they influence the catalyst's conversion performance.

##### *4. 6. 1 The Efficiency of CO as Reductant for NO<sub>x</sub>*

This section investigates, whether CO contributes at all to the reduction of NO<sub>x</sub>. Cho<sup>49</sup> has classified CO as an unselective reagent for NO<sub>x</sub> reduction: instead of reacting with NO via Equation 2. 36, it is oxidised to CO<sub>2</sub>. Two LOTs were performed with sample 4100. The sample was picked as a random representative of a Pt/Al<sub>2</sub>O<sub>3</sub> catalyst without additives. LOT 1, done for comparison, used a standard gas mix. LOT 2 used a similar mix without CO<sub>2</sub>, SO<sub>2</sub>, and C<sub>3</sub>H<sub>6</sub>. The concentrations of the gases used in the feedgas are given in Table 4. 22.

LOT 1		LOT 2	
CO <sub>2</sub>	4,7 vol.-%	CO <sub>2</sub>	0 vol.-%
O <sub>2</sub>	12,2 vol.-% (= λ 2,2)	O <sub>2</sub>	12,2 vol.-% (= λ 2,2)
CO	200 ppm	CO	200 ppm
SO <sub>2</sub>	21 ppm	SO <sub>2</sub>	0 ppm
NO	400 ppm	NO	400 ppm
C <sub>3</sub> H <sub>6</sub>	800 ppm	C <sub>3</sub> H <sub>6</sub>	0 ppm
H <sub>2</sub> O	6,4 vol.-%	H <sub>2</sub> O	6,4 vol.-%
SV	30000 hr <sup>-1</sup>	SV	30000 hr <sup>-1</sup>
T <sub>i</sub> <sup>0</sup> → dT/dt →	80°C →	T <sub>i</sub> <sup>0</sup> → dT/dt →	80°C →
T <sub>i</sub> <sup>max</sup>	10°C/min →	T <sub>i</sub> <sup>max</sup>	10°C/min →
	550°C		550°C

Table 4. 22 Gas mix specifications during LOTs shown in Figure 4. 34

### Observations:

The CO and NO<sub>x</sub> light-off curves obtained are presented in Figure 4. 34. Without propene in the feedgas the maximum NO<sub>x</sub> conversion decreases from 38,1% at 243°C to 6,5% at 175°C. Maximum NO<sub>x</sub> conversion coincides in both LOTs with complete CO conversion. In LOT 2 the CO light-off curve is much steeper than in LOT 1 and achieves 80% conversion at 154°C. LOT 1 achieves 80% conversion at 227°C.

### Conclusions:

Since positive NO<sub>x</sub> conversion is observed, it may be concluded that CO does reduce NO<sub>x</sub>. However, the NO<sub>x</sub> conversion by CO is very small compared to the NO<sub>x</sub> conversion by propene. From the different slopes of the CO conversion curves and the different TCO(80) values observed during LOT 1 and LOT 2, it can be concluded that CO must compete with C<sub>3</sub>H<sub>6</sub> for oxidation sites. Additionally, the HC molecules may block some of these sites which contributes to the delay of the CO conversion in LOT 1.

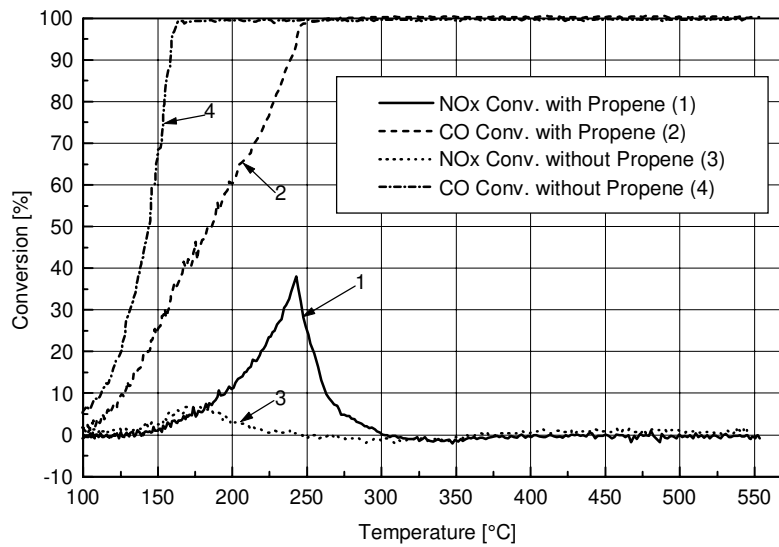


Figure 4. 34: The CO and NO<sub>x</sub> light-off curves obtained from LOT 1 and LOT 2

#### 4. 6. 2 The Formation of CO during LOTs

In the last section and in section 4. 3. 2 it was observed that the conversion of CO is influenced by HC. In section 4. 3. 2. this assumption was based on the observation that with the onset of HC conversion the conversion of CO is retarded on sample PP500 (fresh). In order to study this in more detail, a LOT without CO (LOT 3) and a LOT with CO (LOT 4) in the gas mix were performed with a fresh sample of formulation PP500. The concentrations of the gases used in the feedgas are given in Table 4. 23, the light-off curves obtained are shown in Figure 4. 35.

#### Observations:

The HC and NO<sub>x</sub> light-off curves are similar in both LOTs within the limits of reproducibility.

Although CO is not in the feedgas, CO is detected at the reactor outlet. The onsets of CO formation and HC conversion during LOT 4 coincide. The CO concentration has its maximum at a temperature (240°C) where HC conversion is 75%. The CO concentration has declined to zero, when HC conversion reaches 100% (255°C)

LOT 3			LOT 4		
CO <sub>2</sub>	4,7 vol.-%		CO <sub>2</sub>	4,7 vol.-%	
O <sub>2</sub>	12,2 vol.-% (= λ 2,2)		O <sub>2</sub>	12,2 vol.-% (= λ 2,2)	
CO	0 ppm		CO	200 ppm	
SO <sub>2</sub>	21 ppm		SO <sub>2</sub>	21 ppm	
NO	400 ppm		NO	400 ppm	
C <sub>3</sub> H <sub>6</sub>	800 ppm		C <sub>3</sub> H <sub>6</sub>	800 ppm	
H <sub>2</sub> O	6,4 vol.-%		H <sub>2</sub> O	6,4 vol.-%	
SV	18000 hr <sup>-1</sup>		SV	18000 hr <sup>-1</sup>	
T <sub>i</sub> <sup>0</sup> → dT/dt →	80°C →		T <sub>i</sub> <sup>0</sup> → dT/dt →	80°C →	
T <sub>i</sub> <sup>max</sup>	10°C/min →		T <sub>i</sub> <sup>max</sup>	10°C/min →	
	450°C			450°C	

Table 4. 23 Gas mix specifications during LOTs shown in Figure 4. 35

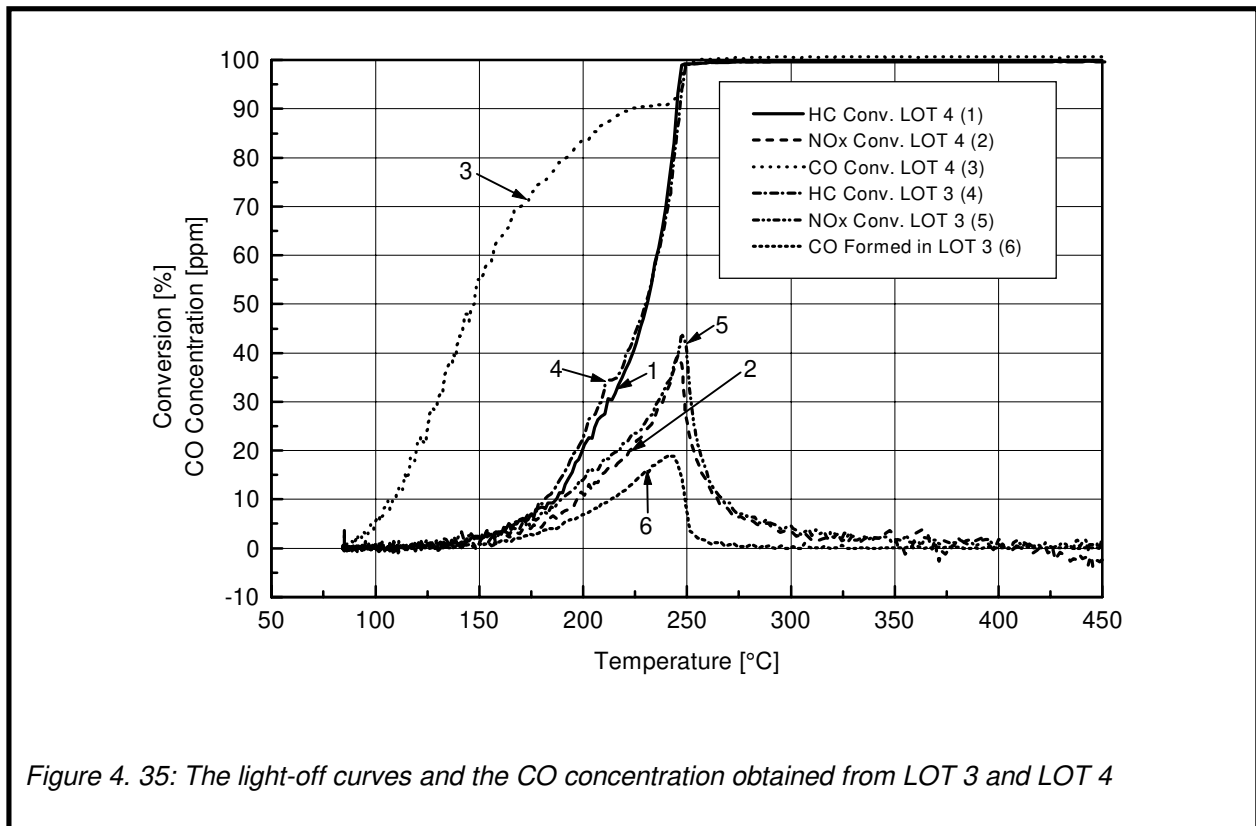


Figure 4. 35: The light-off curves and the CO concentration obtained from LOT 3 and LOT 4

### Conclusions:

The CO formed during LOT 3 can only originate from incomplete HC combustion which is proven by the coincidence of CO formation and the onset of HC light-off. There are two possible explanations why the CO concentration measured during LOT 3 goes down at 240°C. The first is that from this temperature onward all HC is converted directly to CO<sub>2</sub> and consequently no new CO is formed. In this case, however, the maximum of CO concentration should correspond with 100% HC

conversion which is not the case. The second is that the oxidation of the CO formed does not begin before the CO maximum. This is surprising since usually CO conversion (on fresh catalysts) begins at much lower temperatures than 240°C. It was established in section 4. 6. 1 that CO and HC compete for oxidation sites. From the results of section 4. 6. 1 and the observations made in this section it can be concluded that HC succeeds more often in occupying free adsorption sites than CO. Only if HC is completely converted, CO conversion can readily progress. A carbonaceous layer which covers a the active surface may inhibit the adsorption of CO additionally.

#### 4. 6. 3 The Influence of the HC:NO<sub>x</sub> Ratio

Since it was established in the two previous sections that the presence of HC has a negative effect on CO conversion, the high HC:NO<sub>x</sub> ratio of 6:1 (based on C<sub>1</sub>) was reduced to 2:1. With this ratio the conversion performance of sample PP500 (fresh) was tested (LOT 5) and compared with the results of LOT 4 (of section 4. 6. 2). The concentrations of the gases used in the feedgas are given in Table 4. 24, the light-off curves obtained are shown in Figure 4. 36.

LOT 4 (HC:NO <sub>x</sub> = 6:1)		LOT 5 (HC:NO <sub>x</sub> = 2:1)	
CO <sub>2</sub>	4,7 vol.-%	CO <sub>2</sub>	4,7 vol.-%
O <sub>2</sub>	12,2 vol.-% (= λ 2,2)	O <sub>2</sub>	12,2 vol.-% (= λ 2,2)
CO	200 ppm	CO	200 ppm
SO <sub>2</sub>	21 ppm	SO <sub>2</sub>	21 ppm
NO	400 ppm	NO	150 ppm
C <sub>3</sub> H <sub>6</sub>	800 ppm	C <sub>3</sub> H <sub>6</sub>	100 ppm
H <sub>2</sub> O	6,4 vol.-%	H <sub>2</sub> O	6,4 vol.-%
SV	18000 hr <sup>-1</sup>	SV	18000 hr <sup>-1</sup>
T <sub>i</sub> <sup>0</sup> → dT/dt →	80°C →	T <sub>i</sub> <sup>0</sup> → dT/dt →	80°C →
T <sub>i</sub> <sup>max</sup>	10°C/min →	T <sub>i</sub> <sup>max</sup>	10°C/min →
	450°C		450°C

Table 4. 24 Gas mix specifications during LOTs shown in Figure 4. 36

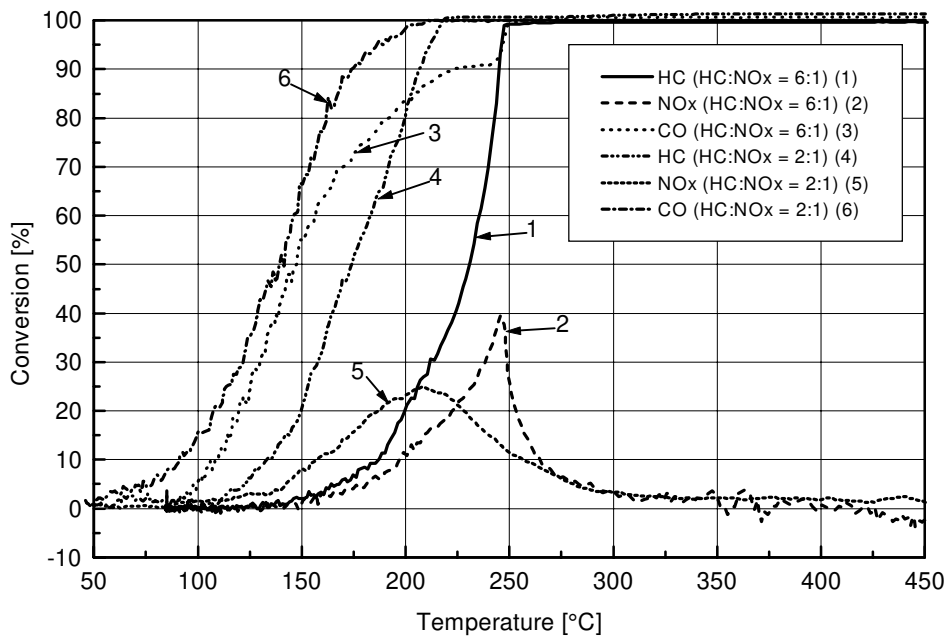


Figure 4. 36: The light-off curves and the CO concentration obtained from LOT 3 and LOT 5

#### Observations:

The NO<sub>x</sub> conversion during LOT 4 (HC:NO<sub>x</sub> = 6:1) achieves a maximum of 39,5 % and has a window width of 31K. THC(50) and TCO(80) occur at 231°C and 193°C, respectively. The P<sub>c</sub> factor calculated with Equation 4. 3 is 16,6.

If the HC:NO<sub>x</sub> ratio is low (LOT 5), the P<sub>c</sub> factor equals 19,6, maximum NO<sub>x</sub> conversion is 24,9%, and the conversion window width is 41K. THC(50) and TCO(80) occur at 174°C and 162°C respectively. Under these conditions, the CO conversion curve seems to be less influenced (based on visual judgement) by the HC conversion and T(NO<sub>x</sub><sup>max</sup>) is reduced from 246°C to 208°C.

#### Conclusion:

Reducing the HC:NO<sub>x</sub> ratio from 6:1 to 2:1 increases the P<sub>c</sub> factor by 15%. This is due to a broader NO<sub>x</sub> conversion window and lower THC(50) and TCO(80) values in LOT 5. From these observations and the results of the two previous sections the conclusion can be drawn that CO experiences less competition from HC for oxidation sites on the catalyst if the HC:NO<sub>x</sub> ratio is 2:1 than if the HC:NO<sub>x</sub> ratio is 6:1.

It is remarkable that the HC light-off occurs earlier in LOT 5 than in LOT 4. It is postulated that a high amount of HC causes a slow-down of its own oxidation. This will be examined more closely in section 4. 6. 6. 1.

The lower maximum NO<sub>x</sub> conversion in LOT 5 compared to LOT 4 is related to the lower amount of reductant available in LOT 5.

#### 4. 6. 4 The Influence of the Type of HC

Wahl et al.<sup>90</sup> tested the selectivity of several HCs towards NO reduction and report that n-decane was the most selective reductant tested. Bourges et al.<sup>86</sup> state that HC and NO oxidation and NO reduction are strongly dependent on the type of reductant and that these reactions occur at lower temperature with long chain alkanes than with olefins.

In this section, it is examined whether the conversion efficiency of a Pt/Al<sub>2</sub>O<sub>3</sub> catalyst for NO<sub>x</sub> changes by changing the HC from propene to n-decane. In order to examine the influence of dispersion on the conversion of HC, samples 4107 (sample with high Pt dispersion) and 4108 (sample with low Pt dispersion) were chosen for these experiments. The decane was used as a gas, and in order to keep the experimental costs acceptable, the test conditions had to be altered. A HC:NO<sub>x</sub> ratio of 6:1 was maintained, but the concentrations were set very low. The concentrations of the gases used in the feedgas are given in Table 4. 25, the light-off curves obtained are shown in Figure 4. 37 and 4. 38.

LOTs Using Propene		LOTs Using n-Decane	
CO <sub>2</sub>	4,7 vol.-%	CO <sub>2</sub>	4,7 vol.-%
O <sub>2</sub>	11,9 vol.-% (= λ 2,1)	O <sub>2</sub>	11,9 vol.-% (= λ 2,1)
CO	25 ppm	CO	25 ppm
SO <sub>2</sub>	0 ppm	SO <sub>2</sub>	0 ppm
NO	50 ppm	NO	50 ppm
C <sub>3</sub> H <sub>6</sub>	90 ppm	C <sub>10</sub> H <sub>22</sub>	30 ppm (=90 ppm C <sub>3</sub> )
H <sub>2</sub> O	6,4 vol.-%	H <sub>2</sub> O	6,4 vol.-%
SV	30000 hr <sup>-1</sup>	SV	30000 hr <sup>-1</sup>
T <sub>i</sub> <sup>0</sup> → dT/dt →	90°C →	T <sub>i</sub> <sup>0</sup> → dT/dt →	90°C →
T <sub>i</sub> <sup>max</sup>	20°C/min →	T <sub>i</sub> <sup>max</sup>	20°C/min →
	425°C		425°C

Table 4. 25 Gas mix specifications during LOTs shown in Figure 4. 37 and 4. 38

### Observations:

With decane as HC, CO conversion is complete at 100°C on both samples. Maximum NO<sub>x</sub> conversion of sample 4107 (38%) is twice as high than that of sample 4108 (20%). Both NO<sub>x</sub> conversion maxima occur at roughly 185°C. During the LOT sample 4107 releases four times as much NO<sub>x</sub> (-80% conversion) at 350°C than sample 4108 (-20% conversion). Sample 4107 converts 50% decane at 137°C while sample 4108 reaches 50% decane conversion at 142°C.

With propene as HC sample 4107 achieves 80% CO conversion at 100°C and sample 4108 achieves 80% CO conversion at 125°C. The samples have maximum NO<sub>x</sub> conversions of 53% (4107) and 48% (4108), respectively. Both maxima occur at 185°C. Sample 4107 releases nearly 3 times more NO<sub>x</sub> (-60% conversion) at 350°C than sample 4108 (~-20% conversion). 50% propene conversion occurs on sample 4107 and 4108 at 166°C and 170°C, respectively.

### Conclusions:

Due to the high Pt-load on both samples and the low concentration of CO in the feedgas, a good CO conversion performance was expected from both samples. The fact that total CO conversion is achieved earlier if decane is used as HC was not expected. It was postulated that decane would tend to block sites active for CO oxidation due to its size. Propene on the other hand should not block these active sites and allow rapid CO light-off. Yet, the opposite is true and the reasons are probably the same as for the HC conversion results (see below).

The CO conversions observed with propene as HC show the same influence of the catalyst's metal dispersion on the TCO(80) values observed in earlier tests with higher C<sub>3</sub>H<sub>6</sub>, CO, and NO concentrations (compare chapter 4. 2. 2. 3): using a catalyst with a high Pt dispersion reduces TCO(80) compared to catalysts with low Pt dispersion. The lower CO light-off of samples with high metal dispersion is attributed to the increased number of the active sites.

The early HC light-off with decane in the feed gas was surprising. It was expected that the LOTs with propene as HC would show lower THC(50) values than the LOTs with decane as HC since decane was assumed to block active sites on the catalyst<sup>5</sup>.



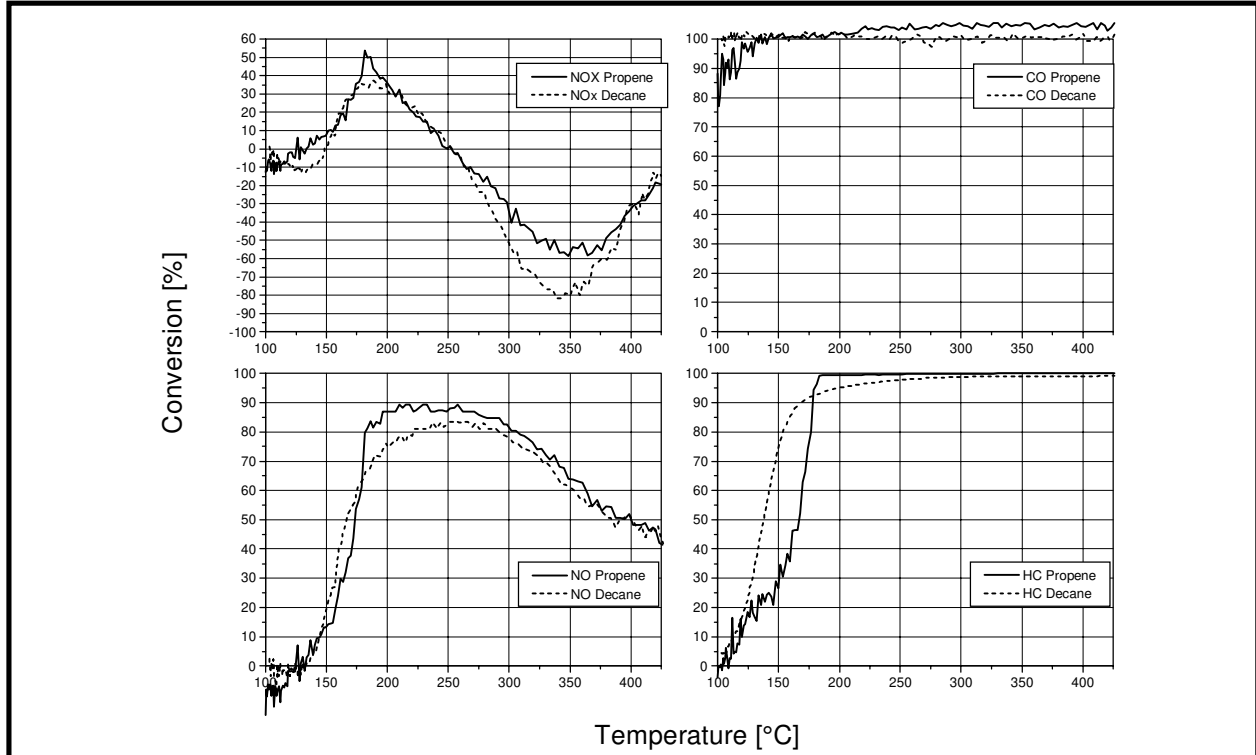


Figure 4. 37: The light-off curves obtained using sample 4107

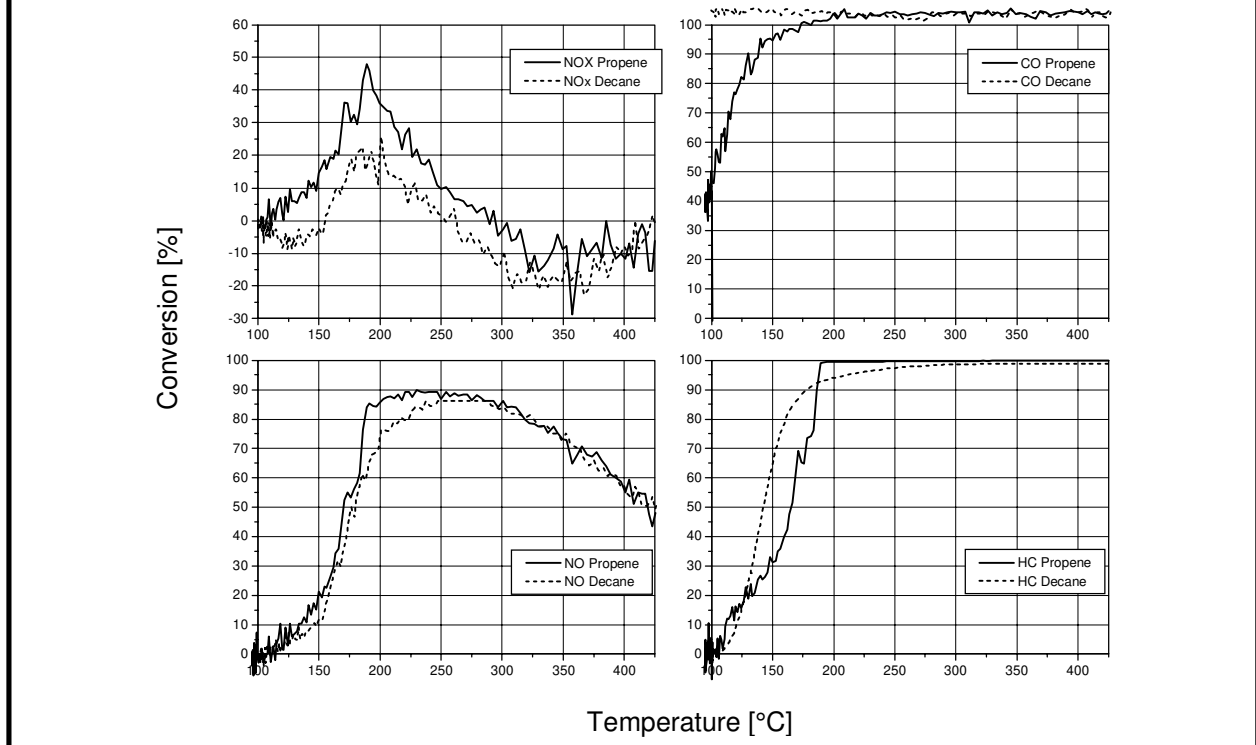


Figure 4. 38: The light-off curves obtained using sample 4108

However, the observations are opposite to the expectations: an inhibition effect through the formation of a decane layer on top of the catalyst as previously postulated does not seem to exist. The observations are explained with the speculation that decane requires a lower activation energy for oxidation than propene. The enthalpies of reaction for propene and decane combustion were calculated with  $-1926,3 \text{ kJ mol}^{-1}$  and approximately  $-6325 \text{ kJ mol}^{-1}$ , respectively. Because of this the catalyst itself will - in theory - warm up faster if decane is used as HC than with propene. It is further speculated that decane oxidation does not proceed directly: cracking reactions which break down the long chained (decane) molecule into smaller fragments are assumed to occur prior to oxidation reactions. In an attempt to find an explanation for the observed light-off succession of propene and decane the following hypothesis is postulated: while the breaking of a single C-C bond may take place on acidic sites of the washcoat's alumina, the dissociation of the double bonds of propene may require active sites on the platinum. The Pt sites are therefore occupied for a longer time by HC species if propene is used as HC and thus, the overall rate of oxidation of the resulting carbon species may be lower. This presupposes that, at the prevalent temperatures, the carbon species can only be oxidised on the platinum. If decane is used as HC, the active sites of the platinum may be unencumbered from pre-cracking processes. They oxidise decane fragments spilling over from the washcoat directly and hence, light-off of decane occurs at lower temperature.

The differences in decane light-off performance for the sample with high Pt dispersion (4107) compared to the sample with low Pt dispersion (4108) lie almost within error margins. In earlier tests with 800 ppm  $\text{C}_3\text{H}_6$  and 400 ppm NO, samples with higher dispersion of the Pt always showed significantly lower THC(50) values than samples with low Pt dispersion. It is postulated that in the tests with 800 ppm HC in the gasfeed the HC concentration was high enough to build a carbonaceous layer on the catalyst's surface. Consequently free sites for HC oxidation were rare but more numerous on a catalyst with high Pt dispersion which resulted in lower THC(50) values of these catalysts. The difference between those results and the results in this section may be due to the low concentrations of HC which had to be chosen in the experiments of this section for economical and set-up reasons. Because the concentration of the HC in the gas mixes of the LOTs in this section is

only 90ppm (based on C<sub>3</sub>) blocking of active sites by a carbonaceous layer may not be a notable issue. Hence both samples have similar THC(50) value regardless of their dispersion. This explains correspondingly the similar propene light-off values of samples 4107 and 4108.

A comparison between Figures 4. 37 and 4. 38, show that the Pt dispersion of the tested samples has an important influence on the maximum NO<sub>x</sub> conversion as well as on the amount of NO<sub>x</sub> which is released during the LOT from the catalyst at higher temperature. Based on the observation that the sample with high Pt dispersion (4107) releases more NO<sub>x</sub> than the sample with low Pt dispersion (4108) it can be concluded that a large number of surface Pt-atoms is necessary to store a lot of NO<sub>x</sub>. Hence it may be speculated that the adsorption of NO<sub>x</sub> occurs predominantly on the platinum and not on the washcoat.

A relation between dispersion and NO<sub>x</sub> conversion could not be established in earlier tests (compare section 4. 2. 2. 2), i.e. a high Pt dispersion did not necessarily result in high NO<sub>x</sub> conversion. However, the much higher NO<sub>x</sub> and HC concentrations of the tests in section 4. 2. 2. 2 might have blurred the actual influence of dispersion. Based on the large amount of NO<sub>x</sub> desorbing from both samples during the LOTs performed with decane as HC, it may be speculated that a significant amount of the NO<sub>x</sub> conversion observed during these LOTs is actually a removal of NO<sub>x</sub> by adsorption. As assumed previously, the Pt particles are less encumbered by HC fragments during the LOTs performed with decane. Therefore more NO<sub>x</sub> can be stored during the low temperature phase of the decane LOT than in the propene LOT and be released during the high temperature phase. Implying that most NO<sub>x</sub> conversion during the decane LOTs is in fact NO<sub>x</sub> adsorption on the surface Pt atoms, the lower NO<sub>x</sub> conversion of sample 4108 compared to sample 4107 can be explained by the lower dispersion of sample 4108. It is assumed that NO<sub>x</sub> is stored mainly in the form of NO on the catalyst and desorbs as NO as well. Under LOT conditions the desorbed NO is oxidised to NO<sub>2</sub> on a Pt-site further up the catalyst's length. At temperatures above 350°C, approximately 80% of the total amount of NO<sub>x</sub> detected is NO<sub>2</sub>.

Since the propene fragments are present on the catalyst's surface for a longer time, as discussed previously, the NO<sub>x</sub> has more time to react with the fragments and hence, maximum NO<sub>x</sub> conversions during the LOTs with propene are higher.

#### 4. 6. 5 The Influence of the Type of NO<sub>x</sub>

Several groups<sup>66 67 78</sup> claim that NO<sub>2</sub> is more easily reduced than NO. This is investigated in the subsequent section. Two LOTs were performed with sample 4107 (for sample specifications refer to "Appendix"), one with NO and another one with NO<sub>2</sub> instead for NO. The concentrations of the gases used are given in Table 4. 26, the light-off curves obtained are shown in Figure 4. 39.

##### Observations:

In the LOT with NO, the NO<sub>x</sub> conversion achieves a maximum of 43,3% and the width of the conversion window is 47K. Some NO<sub>x</sub> is released at temperatures above 293°C. TCO(80) lies at 137°C and THC(50) at 187°C. The NO conversion curve approaches the NO/NO<sub>2</sub> equilibrium (not included in Figure 4. 39) at temperatures higher than 375°C.

In the LOT using NO<sub>2</sub> instead of NO, the NO<sub>x</sub> conversion is negative at the beginning and decreases to a local maximum of negative conversion of -27,7% at 131°C. Then the slope of the curve becomes positive and achieves NO<sub>x</sub><sup>max</sup> at 217°C with 20,4%. NO<sub>x</sub> conversion declines again below zero and stays negative from 244°C to the end of the test. The CO light-off curve approaches 80% conversion at 112°C. The THC(50) value is identical to that of the NO LOT. Negative NO conversion is recorded from the beginning of the test until 214°C, and from 345°C to the end of the LOT.

LOT Using NO		LOT Using NO <sub>2</sub>	
CO <sub>2</sub>	4,7 vol.-%	CO <sub>2</sub>	4,7 vol.-%
O <sub>2</sub>	12,2 vol.-% (= λ 2,2)	O <sub>2</sub>	12,2 vol.-% (= λ 2,2)
CO	80 ppm	CO	80 ppm
SO <sub>2</sub>	0 ppm	SO <sub>2</sub>	0 ppm
NO	150 ppm	NO <sub>2</sub>	150 ppm
C <sub>3</sub> H <sub>6</sub>	300 ppm	C <sub>3</sub> H <sub>6</sub>	300 ppm
H <sub>2</sub> O	6,4 vol.-%	H <sub>2</sub> O	6,4 vol.-%
SV	30000 hr <sup>-1</sup>	SV	30000 hr <sup>-1</sup>
T <sub>i</sub> <sup>0</sup> → dT/dt →	90°C →	T <sub>i</sub> <sup>0</sup> → dT/dt →	90°C →
T <sub>i</sub> <sup>max</sup>	20°C/min →	T <sub>i</sub> <sup>max</sup>	20°C/min →
	425°C		425°C

Table 4. 26 Gas mix specifications during LOTs shown in Figure 4. 39

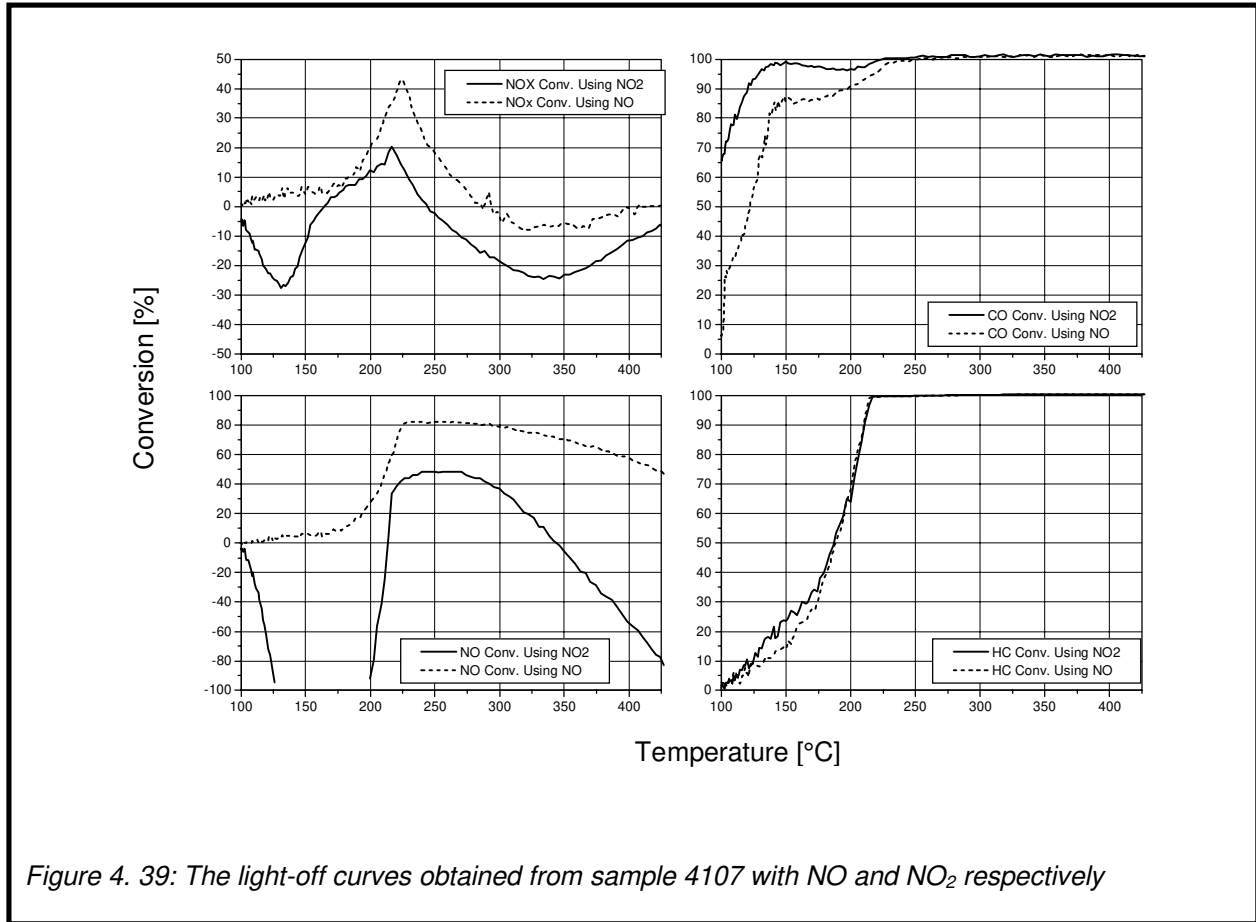


Figure 4. 39: The light-off curves obtained from sample 4107 with NO and NO<sub>2</sub> respectively

**Conclusions:**

The use of NO<sub>2</sub> instead of NO does not result in an increase of NO<sub>x</sub> conversion. This is clearly established by the NO<sub>x</sub> conversion curves. Although NO<sub>2</sub> is known to be a better oxidant than NO, the HC light-off is not influenced by a change from one nitrogen oxide to the other. The use of NO<sub>2</sub> has a significant influence on the CO conversion. It can be assumed that the high NO formation at the beginning of the LOT with NO<sub>2</sub> is caused by a reaction between NO<sub>2</sub> and CO



This results in an earlier light-off of CO (TCO(80): 112°C compared to 137°C in the LOT using NO) and a significant formation of NO during the LOT. From 131°C onward, NO<sub>x</sub> conversion during the LOT using NO<sub>2</sub> progresses, and causes the positive slope of the curve. However, at the same time the reaction of Equation 4. 4 continues, which is probably the reason why the NO conversion is negative until

214°C. When the temperature of total HC conversion is achieved (215°C), the NO<sub>x</sub> conversion declines again and quickly falls below zero. This is attributed to release of stored NO<sub>x</sub> from the catalyst.

At temperatures higher than 345°C, the NO conversion of the LOT using NO<sub>2</sub> falls below zero. At this temperatures, the NO/NO<sub>2</sub> equilibrium is shifted to NO and hence, all NO<sub>2</sub> supplied from the feed gas immediately converts to NO and O<sub>2</sub>. It must be mentioned that the initial concentrations in the NO<sub>x</sub> analyser for NO and NO<sub>2</sub> are set to zero ppm and 150 ppm at the beginning of the LOTs, respectively. Because of these settings, the NO formed from NO<sub>2</sub> decomposition at temperatures above 345°C is interpreted as a formation (negative conversion).

#### *4. 6. 6 Concentration Variations*

These experiments scrutinised the effect of concentration variations of several gas mix components at constant temperatures on the conversion of these gases. In all cases a fresh sample PP 41 38 was used as catalyst.

##### *4. 6. 6. 1 Variation of HC Concentration*

NO<sub>x</sub> and O<sub>2</sub> concentrations were constant at 400 ppm and 12 vol.-% respectively. HC concentration was increased in the following steps: 133, 267, 400, 533, 667, 800 ppm. After the value at 800 ppm was taken, the concentration was decreased to 133 ppm. This was to ensure that the decrease in HC conversion was not due to HC blocking. The inlet temperatures at which the conversions were measured were 178°C and 194°C. The resulting values are shown in Figure 4. 40.

#### Observations:

Propene conversion decreases exponentially with increasing propene content in the feedgas. This is the case for both temperatures studied.

#### Conclusions:

In the reaction rate equation for propene oxidation propene must be of negative order. It appears that for HC oxidation sufficient oxidised Pt atoms must be in close proximity in order for oxidation to occur. As a petrol car can be choked by too much

petrol injected, HC oxidation can be choked by too much HC in the feedgas. This "choking" takes place regardless of the test temperature.

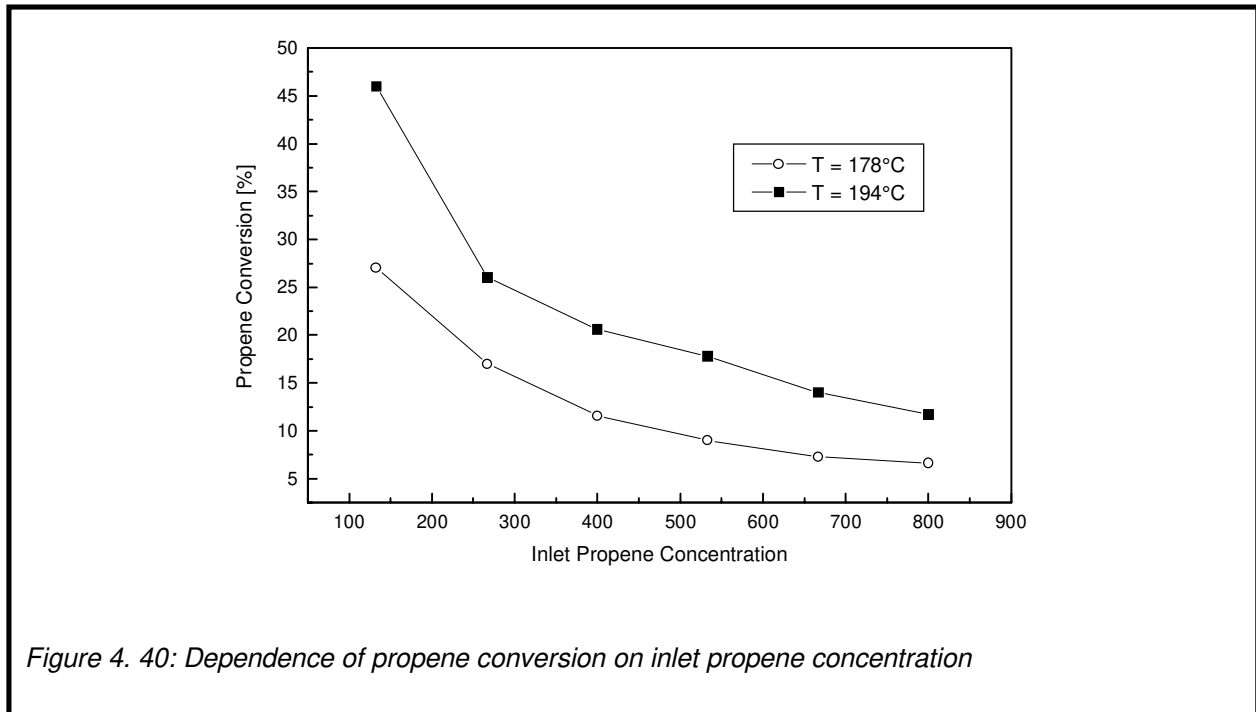


Figure 4. 40: Dependence of propene conversion on inlet propene concentration

#### 4. 6. 6. 2 Variation of O<sub>2</sub> Concentration

NO<sub>x</sub> and HC concentrations were constant at 400 ppm and 800 ppm respectively. Oxygen concentration was decreased in the following steps: 12, 10, 8, 6, 4, 2 vol.-%. After the 2 vol.-% value the concentration was increased to 12 vol.-% in order to check for reproducibility. The inlet temperatures at which the conversions were measured were 194°C and 222°C. The resulting values for T = 194°C are shown in Figure 4. 41, those for 222°C in Figure 4. 42.

#### Observations:

At 194°C, Propene and NO<sub>x</sub> conversion increase linearly with increasing oxygen concentration.

At 222°C propene conversion decreases drastically when the oxygen concentration goes below 8 vol.-%. Maximum NO<sub>x</sub> conversion was measured at an oxygen concentration of 6 vol.-%. At concentrations below 6 vol.-% the decline in NO<sub>x</sub> conversion is more dramatic than at concentrations above 6 vol.-%.

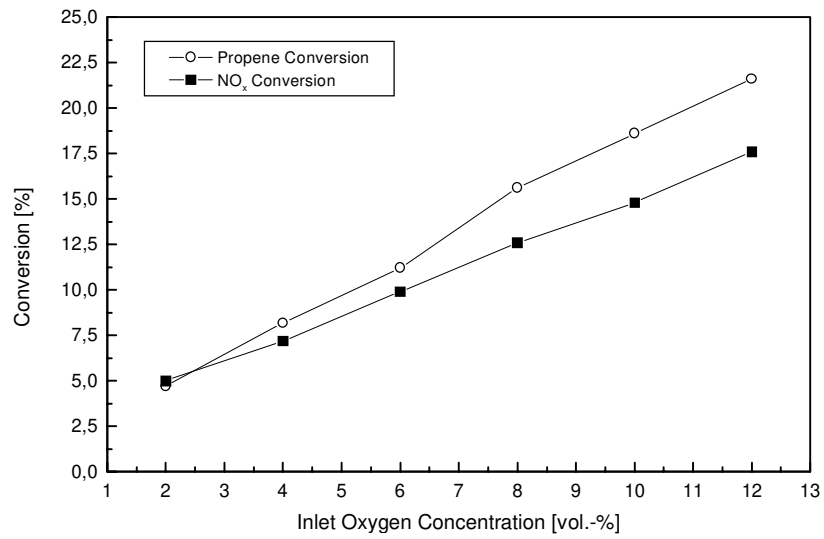


Figure 4. 41: Dependence of propene and NO<sub>x</sub> conversion on inlet O<sub>2</sub> concentration @ 194°C

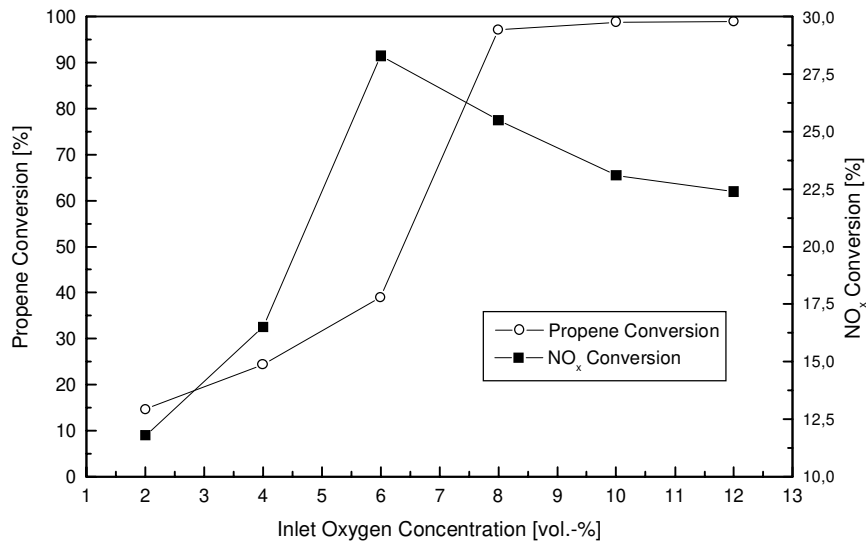


Figure 4. 42: Dependence of propene and NO<sub>x</sub> conversion on inlet O<sub>2</sub> concentration @ 222°C

**Conclusions:**

While increase of propene conversion with increasing oxygen content was expected, increasing NO<sub>x</sub> conversion was not. Possibly the HC blocks the catalyst from NO<sub>x</sub> molecules and the oxygen must at least partially remove this HC layer. After that NO<sub>x</sub> can adsorb on the platinum and react. This result is in contrast to the theory that HC



must reduce oxidised platinum sites before  $\text{NO}_x$  reduction can take place<sup>76</sup>. It seems that under low oxygen concentrations this mechanism is the other way round.

The steep decrease of propene conversions at oxygen concentrations below 8 vol.-% can be explained as follows: At oxygen concentrations higher than 8 vol.-% the HC had lit off. Reducing the oxygen concentration chokes the catalyst with (non-oxidised) propene and the catalyst "lights down". The high presence of reductant under these conditions explains the coincidence of maximum of  $\text{NO}_x$  conversion.

The strong decline of  $\text{NO}_x$  conversion at oxygen concentrations smaller than 6 vol.-% is probably caused by the formation of a blocking HC layer on top of the catalyst. This formation does not occur at oxygen concentrations higher than 6 vol.-%.

#### *4. 6. 6. 3 Variation of CO Concentration*

$\text{NO}_x$ , HC, and  $\text{O}_2$  concentrations were constant at 400 ppm, 800 ppm, and 12 vol.-% respectively. CO concentration was increased in the following steps: 50, 100, 150, 200, 300, 400 ppm. After the value at 400 ppm was taken, the concentration was decreased to 50 ppm. This was to ensure that the decrease in CO conversion was not due to CO blocking. The inlet temperature at which the conversions were measured was 170°C. The resulting values for CO conversion are shown in Figure 4. 43, those for propene and  $\text{NO}_x$  conversion in Figure 4. 44.

#### Observations:

CO conversion decreases linearly with increasing CO concentration while propene and  $\text{NO}_x$  conversion decrease exponentially. The exponential decrease is more pronounced for  $\text{NO}_x$  conversion.

#### Conclusions:

As for propene the rate for CO oxidation is of negative order in CO. With a high amount of CO present in the gas mix most of the platinum sites are covered with CO leaving no sites for reaction between CO and O. The rate limiting factor for CO oxidation is the number of sites available for  $\text{O}_2$  adsorption/dissociation. This was already established in section 4. 2. 2. 3 and is verified here once more.

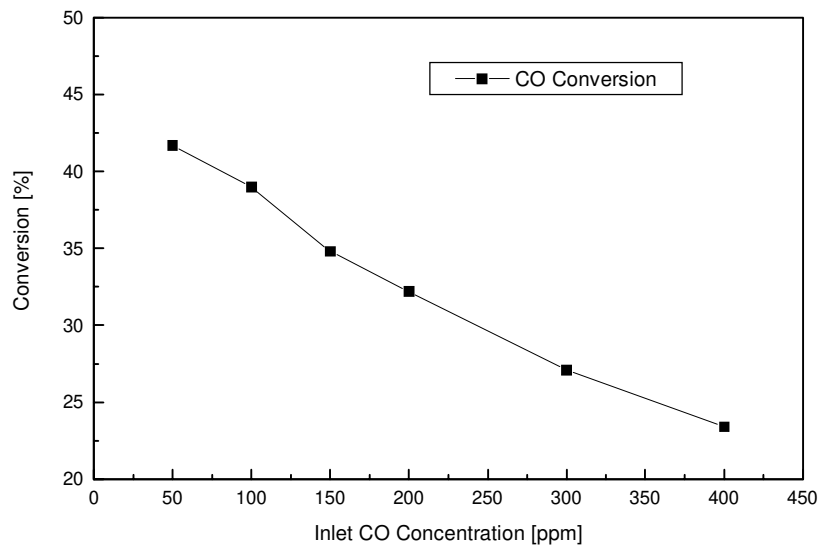


Figure 4. 43: Dependence of CO conversion on inlet CO concentration

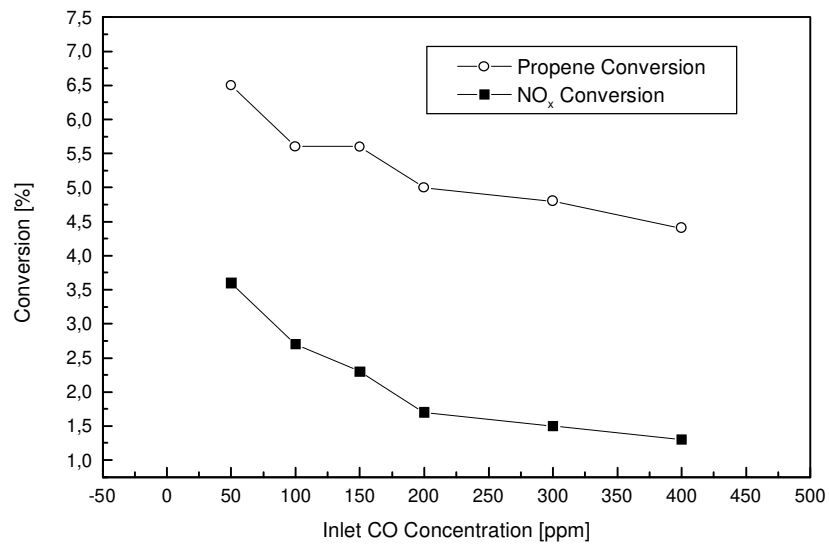


Figure 4. 44: Dependence of propene and NO<sub>x</sub> conversion on inlet CO concentration

The same CO-poisoning effect is responsible for the decrease of propene and NO<sub>x</sub> conversion with increasing CO concentration.

#### 4. 6. 6. 4 Variation of NO<sub>x</sub> Concentration

HC and O<sub>2</sub> concentrations were constant at 800 ppm and 12 vol.-% respectively. NO<sub>x</sub> concentration was increased in the following steps: 50, 100, 200, 300, 400, 500,

600, 700 ppm. After the value at 700 ppm was taken, the concentration was decreased to 50 ppm. This was to ensure that the decrease in  $\text{NO}_x$  conversion was not due to  $\text{NO}_x$  blocking. The inlet temperatures at which the conversions were measured were 170°C and 200°C. The resulting values are shown in Figure 4. 45.

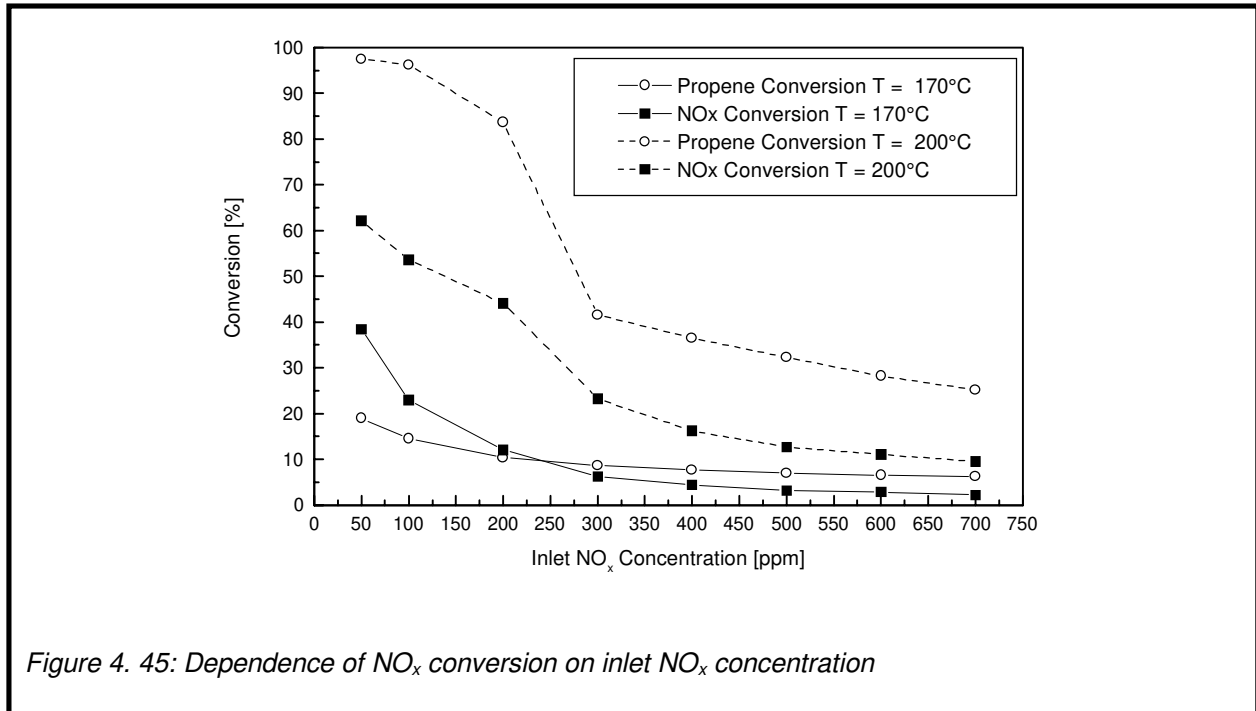


Figure 4. 45: Dependence of  $\text{NO}_x$  conversion on inlet  $\text{NO}_x$  concentration

#### Observations:

At 170°C,  $\text{NO}_x$  and propene conversion decrease exponentially with increasing  $\text{NO}_x$  concentration. At very low  $\text{NO}_x$  concentrations  $\text{NO}_x$  conversion exceeds propene conversion. At very high  $\text{NO}_x$  concentrations  $\text{NO}_x$  conversion declines to nearly zero percent. If the  $\text{NO}_x$  concentration is higher than 200 ppm at 200°C,  $\text{NO}_x$  and propene conversion show a drastic decrease. At concentrations above 300 ppm the decrease of propene is linear while that of  $\text{NO}_x$  seems to be exponential.

#### Conclusions:

The conclusions from the CO concentration variation experiments apply to the observations made in this section for  $\text{NO}_x$ : at high  $\text{NO}_x$  concentrations in the gasfeed, the catalyst "poisons" itself due to dense  $\text{NO}_x$  coverage. This leaves no sites for either  $\text{NO}_x$  dissociation or reaction with the reductant: *"Islands of  $\text{NO}_x$  in an ocean of propene can only react on the coastline."*

This experiment shows that HC light-off can be choked not only by HC but also by  $\text{NO}_x$ . This "NO<sub>x</sub>-choking" implies that at if the concentration of  $\text{NO}_x$  exceeds 100 ppm, the adsorption of  $\text{NO}_x$  is favoured to the adsorption of propene.

#### 4. 6. 7 Summary

This section examines the influence of gas mix variations on the catalyst's conversion performance.

By a LOT performed without HC in the gasfeed, it is established that CO reduces  $\text{NO}_x$ . However, only to a very limited extent. Based on the observation that CO conversion occurs later if HC is present in the gas mix than if HC is absent, it is postulated that CO and HC compete for active oxidation sites.

During a LOT performed without CO in the feedgas, CO is detected at the outlet of the catalyst. It is assumed that this CO originates from incomplete HC combustion. It is observed that the oxidation of the formed CO does not begin before HC conversion has reached 75%. Based on this observation it is concluded that CO and HC compete for oxidation and that propene may block active sites from CO adsorption.

The competition between HC and CO for active sites is verified by experiments with a reduced HC: $\text{NO}_x$  ratio. Reducing the HC: $\text{NO}_x$  ratio from 6:1 to 2:1 increases the  $P_c$  factor by 15%. This is ascribed to CO experiencing less competition from HC for active sites which is proven by lower TCO(80) values recorded at a low HC: $\text{NO}_x$  ratio. Since the THC(50) values was reduced as well as the TCO(80) value in the LOTs with low HC: $\text{NO}_x$  ratio, it is postulated that a high amount of HC inhibits its own oxidation.

Further tests in this section investigate how the use of n-decane as a HC instead of propene changes the conversion efficiency of a Pt/ $\text{Al}_2\text{O}_3$  catalyst. As opposed to the expectations<sup>5</sup>, the use of decane as HC results in THC(50) and TCO(80) values which are lower than the corresponding values obtained from LOTs with propene. In order to explain the observed light-off succession of propene and decane it is

postulated that the breaking of a single C-C bond of decane may take place on acidic sites of the washcoat's alumina, the dissociation of the double bonds of propene may require active sites on the platinum. The Pt sites are therefore occupied for a longer time by HC species if propene is used as HC and thus, the overall rate of oxidation of the resulting carbon species may be lower. A blocking of the catalyst's surface anticipated by the long chained decane is not observed. This is explained with the low concentrations of HCs used in these tests for economical reasons.

Maximum  $\text{NO}_x$  conversion is lower if decane is used in the LOT. The reason for this is assumed to be that in the propene LOTs, the propene fragments remain on the catalyst's surface for a longer time than the decane fragments during the decane LOTs. Hence, the  $\text{NO}_x$  has more time to react with the propene fragments and maximum  $\text{NO}_x$  conversions during the LOTs with propene are higher.

Based on LOTs performed with  $\text{NO}_2$  instead of  $\text{NO}$  it can be stated that the use of  $\text{NO}_2$  reduces  $\text{NO}_x$  conversion efficiency compared to the use of  $\text{NO}$ . From the observation of lower TCO(80) values in LOTs performed with  $\text{NO}_2$  compared to the TCO(80) values obtained in LOTs with  $\text{NO}$ , it is proposed that  $\text{NO}_2$  reacts with  $\text{CO}$  at low temperatures and forms  $\text{CO}_2$  and  $\text{NO}$ . The THC(50) value remains uninfluenced by a change from  $\text{NO}$  to  $\text{NO}_2$ .

Experiments in which the gasmixes over a  $\text{Pt}/\text{Al}_2\text{O}_3$  catalyst were varied at constant (inlet) temperatures resulted in the following conclusions:

1. The rate for propene oxidation must be of negative order in propene. The catalyst can get choked by too much propene in the gas mix.
2. At a temperature below HC light-off, oxygen concentration must be high enough in order to avoid choking of the catalyst by HC. Reducing  $\text{O}_2$  concentration at a temperature above HC light-off can choke the HC conversion as well.
3.  $\text{NO}_x$  conversion increases at temperatures below HC light-off with increasing oxygen concentration in the feedgas. Based on this observation it is concluded that oxygen "cleans" the catalyst's surface from HC deposits before  $\text{NO}_x$  conversion can progress. This is in contrast to a mechanism proposed by Burch et al.<sup>76</sup> and Ansell et al.<sup>56 85</sup>.

4. As for propene, the rate for CO oxidation must be of negative order in CO. It is postulated that at high CO concentrations the catalyst is covered with CO leaving no place for oxygen adsorption and consecutive CO oxidation. It is assumed that the rate limiting factor for CO oxidation is the number of sites available for O<sub>2</sub> adsorption/dissociation. This is in agreement with the results of section 4. 2. 2. 3.
5. The observations made for increasing CO concentrations are made for increasing NO<sub>x</sub> concentrations as well: at high NO<sub>x</sub> concentrations in the gasfeed, the catalyst "poisons" itself due to dense NO<sub>x</sub> coverage. This leaves no sites for either NO<sub>x</sub> dissociation or reaction with the reductant. At temperatures above HC light-off an increase in NO<sub>x</sub> concentration above a certain value can choke the HC conversion.

#### 4. 7 Advanced Formulation Catalysts

A final highlight shall close this results and discussion chapter. Since Pt/Al<sub>2</sub>O<sub>3</sub> catalysts have been well scrutinised not only in this thesis but also by many other researchers, it may be stated that the prospects of this system to achieve NO<sub>x</sub> conversions above 70% under oxidising conditions are not too good. The major problem is the availability of enough HC reductant: the HC has to be present on the catalyst's surface at a temperature higher than the activation energy for NO<sub>x</sub> conversion and simultaneously must not block the catalyst's surface against other reactants, particularly NO<sub>x</sub> and CO. This challenge can only be achieved by creating a multifunctional catalyst that divides the location of NO<sub>x</sub> reduction sites from the oxidation sites. An excellent progress has been made with a catalytic formulation named JJ1. The NO<sub>x</sub> conversion curve is shown in Figure 4. 46 together with the NO<sub>x</sub> conversion curve of PP 41 38 for comparison. The test conditions were similar to those in Table 4. 21 ( $\lambda = 2,2$ ).

Sample JJ1 features a P<sub>c</sub> factor of 38,1, 36% larger than that of PP 41 38. This is caused by a maximum NO<sub>x</sub> conversion of 80,5% and a conversion window width of 89K. A current setback is that this conversion can only be achieved if SO<sub>2</sub> is not in the gas mix. Nevertheless, NO<sub>x</sub> conversion obtained with sample JJ1 suggests to investigate these multifunctional catalysts closely.

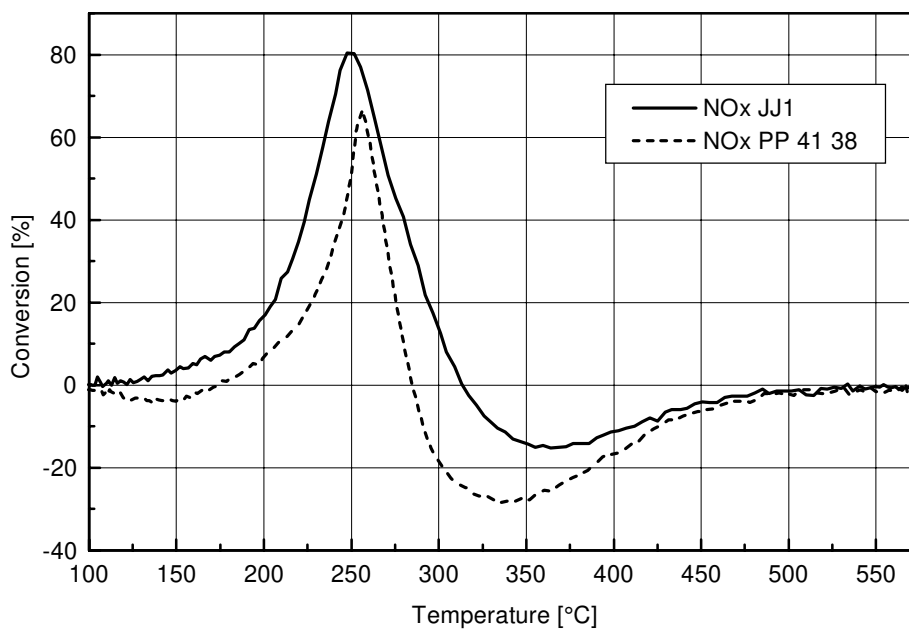


Figure 4. 46: NO<sub>x</sub> conversion curves for samples PP 41 38 and JJ1

## 5. Concluding Remarks

Four main mechanisms for the catalysed reduction of  $\text{NO}_x$  under oxidising conditions by a  $\text{Pt}/\text{Al}_2\text{O}_3$  catalyst have been proposed:

1. the oxidation of  $\text{NO}$  to  $\text{NO}_2$  which then reacts with the  $\text{HC}$ <sup>114-116</sup>
2. the formation of an oxidised  $\text{HC}$  intermediate<sup>67 78</sup>
3. reduction of the metal surface followed by  $\text{NO}$  dissociation on the reduced surface<sup>76</sup>, possibly with  $\text{NO}$  dissociation being assisted by other adsorbed species<sup>82</sup>
4. the formation of an isocyanate surface species as an intermediate<sup>117</sup>

Among these, number 3 is the one which is most widely accepted. Mechanism 3 presupposes that under oxidising conditions  $\text{Pt}$  is in the oxidised state ( $\text{Pt-O}$ ). The role of the  $\text{HC}$  is to remove the oxygen by an oxidation reaction.  $\text{NO}$  adsorbs on the freshly reduced  $\text{Pt}$  site and dissociates if another reduced  $\text{Pt}$  site is in close proximity (to adsorb the oxygen of  $\text{NO}$ ). Subsequently the adsorbed  $\text{N}$  atom combines with another adsorbed  $\text{N}$  atom to form  $\text{N}_2$ . The oxygen is believed to remain on the surface until removed in a new catalytic cycle by the  $\text{HC}$  reductant. On pre-oxidised  $\text{Pt}/\text{Al}_2\text{O}_3$  samples Burch et al.<sup>76</sup> observed no  $\text{NO}$  dissociation, rather  $\text{NO}_2$  formation. The weakness of this mechanism is that it does not explain why an increasing oxygen concentration has a promoting effect on the  $\text{NO}_x$  reduction at temperatures below  $\sim 200^\circ\text{C}$  as observed by many researchers<sup>67 75 78</sup> and in this thesis.

The results obtained in this thesis lead to the following conclusions:

At temperatures below  $\text{HC}$  light-off, the surface of the  $\text{Pt}/\text{Al}_2\text{O}_3$  catalyst is covered with  $\text{HC}$ . This  $\text{HC}$  coverage is proven to exist in section 4. 6. 6. 1. The  $\text{HC}$  is not only situated on the  $\text{Pt}$  particles but also on the alumina washcoat. This is established in section 4. 1. 1. 4 and section 4. 2. 2. 5. The  $\text{HC}$  effectively shields the  $\text{Pt}$  particles against  $\text{NO}$  adsorption. The promoting role of the oxygen in the  $\text{NO}_x$  reduction mechanism is that it removes the  $\text{HC}$  at least partly from the  $\text{Pt}$  by oxidation of the  $\text{HC}$ , proven in section 4. 6. 6. 2. Thus, at temperatures below  $\text{HC}$  light-off, it is oxygen, which removes the  $\text{HC}$  from the  $\text{Pt}$  and not vice versa as proposed by Burch et al.<sup>76</sup>. Now  $\text{NO}$  can be adsorbed on the  $\text{Pt}$  particle and react. There seem to exist at



least two reaction pathways. The first is the dissociation of the NO molecule and the subsequent reaction steps as proposed by Burch et al.<sup>76</sup> (see Background chapter, section 2. 5. 4. 1. 2. 4). However, in this thesis it is established (section 4. 2. 2. 5) that the value of maximum NO<sub>x</sub> conversion is dependent on the ratio of total support surface area (i.e. washcoat load times washcoat surface area) and active metal SA (targeted Pt particle size square). It is postulated that some sort of interaction between washcoat and active metal is of importance during the NO<sub>x</sub> reduction mechanism. It is proposed that NO<sub>x</sub> reduction occurs only on the edge of the metal particle where it meets the washcoat suggesting the spillover of one of the reacting species from the washcoat to the Pt or vice versa. Further evidence for this is given in section 4. 6. 6. 4. It is speculated that HC is pre-cracked on the washcoat and reacts as some sort of radical with the NO on the borderline between Pt particle and the washcoat. Further evidence for this is given by the observation that at under-stoichiometric conditions the NO<sub>x</sub> conversion achieves a constant value of 90% at temperatures above 400°C. This is attributed to a transport limitation of HC from the washcoat to the Pt particle border lines, where it reacts with the NO (section 4. 5. 2. 3).

As the temperature increases, the conversion of HC reaches 100%. It is assumed that from this temperature onward, HC which adsorbs on a Pt particle is immediately oxidised by oxygen. This assumption is based on the conclusions made in section 4. 6. 2. It is speculated that most of the Pt is now covered by oxygen, although this oxygen coverage is not established. The oxygen "layer" on the Pt makes it difficult for NO to become adsorbed on the Pt particles. If NO is not adsorbed, it can not dissociate and perform N, N recombination to form N<sub>2</sub>. Since the HC is removed by the oxygen as soon as it meets the platinum, NO reduction at this temperatures can only go through the reaction pathway adsorption - dissociation - N, N recombination. It is likely that adsorbed NO reacts with the co-adsorbed oxygen to form NO<sub>2</sub> before the NO can dissociate. This explains why the NO<sub>x</sub> conversion declines whereas NO<sub>2</sub> is formed at temperatures higher than those necessary for complete HC conversion. It is assumed that some of the NO oxidation may already take place even before HC light-off, since oxygen will always be at least partly present on the Pt.

## 6. Summary

Motor traffic is an important contributor to the pollution of earth's atmosphere. In order to reduce this pollution, laws have been enacted which require to keep the tailpipe emissions of motor vehicles below certain limits. These limits can not be met simply by modifying the engines to improve the combustion process. Hence, catalysts have to be applied, which reduce tailpipe emissions efficiently.

The removal of nitrogen oxides, commonly referred to as  $\text{NO}_x$ , from Diesel engine exhaust has been found a difficult challenge. Since a common three-way catalyst gets quickly deactivated by the high oxygen content in the Diesel exhaust gas, a new catalyst had to be developed: a  $\text{Pt}/\text{Al}_2\text{O}_3$  catalyst has been reported to be exceptionally active in the removal of  $\text{NO}_x$  from Diesel exhaust.

This thesis focuses on the characterisation and improvement of precious metal catalysts using alumina or zeolites as supports on honeycomb monoliths. Extensive activity tests, so-called Light-Off Tests (LOT), of catalytic samples are performed under model gas conditions. Additionally the samples are characterised by common BET- and CO chemisorption methods.

The thesis begins with a thorough literature review on the subject of catalytic detoxification of Diesel exhaust gases, with the main emphasis on  $\text{NO}_x$  removal.

The first experiments are performed with two so-called washcoat-only catalysts. These catalysts are honeycomb cordierite monoliths coated with an alumina and a zeolite washcoat respectively. They do not contain a precious metal.

Both catalysts show hydrocarbon (HC) oxidation. During HC oxidation, CO formation is observed. A high concentration of oxygen strongly favours the activity for HC oxidation. The HC oxidation activity is reduced by the presence of water in the gas mix. HC desorbs during temperature ramps from the washcoats of both catalysts. However, most HC desorbs from the zeolite-containing washcoat.

At temperatures higher than  $200^\circ\text{C}$ ,  $\text{NO}_x$  is reduced over both catalysts.  $\text{N}_2\text{O}$  as a product of the  $\text{NO}_x$  reduction reaction can not be ruled out but could not be

measured since no  $\text{N}_2\text{O}$  analyser was available. The reduction of NO is favoured by a high concentration of oxygen in the gas mix and by the absence of water.

The influences of four properties of a  $\text{Pt}/\text{Al}_2\text{O}_3$  catalyst on the conversion performance of this catalyst are extensively examined in this thesis: Pt load, Pt dispersion, washcoat load, and washcoat surface area.

BET and CO chemisorption measurements establish that large Pt particles on samples with low Pt dispersions are able to block washcoat pores. Any precious metal encapsulated inside such pores is unable to contribute to the catalyst's purpose.

A good catalyst features low HC and CO light-off, low formation of  $\text{SO}_3$  and  $\text{NO}_2$ , and a high maximum conversion of  $\text{NO}_x$  as well as a broad temperature-window of  $\text{NO}_x$  conversion. For easier comparison of the overall performance of catalyst samples with different formulations, the performance factor,  $P_c$ , is introduced.

The overall performance of samples with a high load of Pt exceeds the performance of samples with low Pt load. Isotope Transient Kinetics measurements reveal that a high dispersion benefits CO oxidation. The rate limiting factor for CO oxidation is identified as the number of active sites available for  $\text{O}_2$  adsorption and dissociation. No direct relation between maximum  $\text{NO}_x$  conversion and Pt dispersion is observed. Presenting the values of  $\text{NO}_x^{\text{max}}$  of high Pt load samples as a function of the ratio between total support area (washcoat load times washcoat surface area) and active metal area results in a curve with a minimum. This is interpreted as an indication for some sort of interaction between the washcoat and the Pt in the  $\text{NO}_x$  reduction mechanism.

Tests with  $\text{Pt}/\text{Al}_2\text{O}_3$  samples containing washcoat additives reveal that the use of a washcoat with silica in the alumina reduces  $\text{NO}_x$  conversion, while the incorporation of BaO or  $\text{La}_2\text{O}_3$  in an  $\text{Al}_2\text{O}_3$  washcoat gives a catalyst that performs with a wider  $\text{NO}_x$  conversion window without deteriorating the conversion performance for other gases. NO storage is identified as the reason for the broad  $\text{NO}_x$  conversion windows featured by these latter two samples.

HC desorption is not detected from non-zeolite-containing samples during SCAT rig temperature ramps, yet TPD studies reveal the formation of  $\text{CO}_2$  on these samples,

indicating the oxidation of adsorbed HC by co-adsorbed oxygen during the temperature ramp.

Zeolite-containing Pt/Al<sub>2</sub>O<sub>3</sub> samples feature higher P<sub>c</sub> factors than non-zeolite-containing samples

The addition of a small amount of ceria (2 wt.-%) to a zeolite-containing washcoat increases NO<sub>x</sub> conversion without affecting other conversion performances. The addition of manganese instead of CeO<sub>2</sub> has a cognate effect. Adding a high amount of ceria (20 wt.-%) causes a decrease of the NO<sub>x</sub> conversion. Increasing the weight percentage of ceria in a zeolite-containing washcoat reduces its HC storage capacity.

Pt/Al<sub>2</sub>O<sub>3</sub> catalysts loose Pt dispersion during hydrothermal ageing. The Pt dispersion is reduced more if the Pt clusters are closer to each other. In order to make the Pt dispersion of a catalyst less sensitive towards ageing, the Pt clusters must be kept apart from each other for a certain distance by using a high washcoat load on the sample.

The BET surface area of Pt/Al<sub>2</sub>O<sub>3</sub> samples decreases as well during the ageing process. This loss of BET surface area is assigned to a loss of pore structure in the Al<sub>2</sub>O<sub>3</sub> washcoat.

A high Pt load helps to maintain oxidation activity of the catalyst after ageing, while a high washcoat load helps to maintain a better NO<sub>x</sub> conversion efficiency of the same catalyst after ageing. It is postulated that a high washcoat load impedes the sintering of Pt particles. This is explained by thermoconductivity phenomena.

None of the washcoat-additives examined help exceptionally well to preserve the Pt dispersion or the BET surface area during an ageing treatment.

The conversion performances of various catalyst formulations including Ir are examined at two different oxygen levels: under-stoichiometric and highly oxidising.

Under highly oxidising conditions, the addition of Ir to a Pt/Al<sub>2</sub>O<sub>3</sub> catalyst reduced the THC(50) and the TCO(80) value compared to a plain Pt/Al<sub>2</sub>O<sub>3</sub> catalyst.

It is established that SO<sub>2</sub> and NO compete for adsorption sites on Pt/Al<sub>2</sub>O<sub>3</sub> catalysts and that in the absence of SO<sub>2</sub>, NO<sub>x</sub> is stored on sites otherwise occupied by SO<sub>2</sub>.

It is established that CO reduces NO<sub>x</sub>. However, only to a very limited extent.

During a LOT performed without CO in the feedgas, CO is detected at the outlet of the catalyst. It is proven that this CO originates from incomplete HC combustion. Propene may block active sites from CO adsorption and a high amount of HC in the feedgas inhibits its own oxidation.

The use of decane as HC during LOTs results in earlier HC and CO light-off compared with propene LOTs. A blocking of the catalyst's surface anticipated by the long chained decane is not observed. This is explained with the low concentrations of HCs used in these tests for economical reasons. Maximum NO<sub>x</sub> conversion is lower if decane is used in the LOT than if propene is the HC.

The use of NO<sub>2</sub> during LOTs reduces NO<sub>x</sub> conversion efficiency compared to the use of NO. NO<sub>2</sub> reacts with CO and forms CO<sub>2</sub> and NO. The HC conversion remains uninfluenced by a change from NO to NO<sub>2</sub>.

The rate for propene oxidation must be of negative order in propene. The catalyst can get choked by too much propene in the gas mix.

At a temperature below HC light-off, oxygen concentration must be high enough in order to avoid choking of the catalyst by HC.

NO<sub>x</sub> conversion increases at temperatures below HC light-off with increasing oxygen concentration in the feedgas. Oxygen "cleans" the catalyst's surface from HC deposits before NO<sub>x</sub> conversion can progress. This result is in contrast to a mechanism proposed by Burch et al.<sup>76</sup> and Ansell et al.<sup>56 85</sup>.

The rate for CO oxidation must be of negative order in CO.

If the NO<sub>x</sub> concentration in the gasfeed is high, the catalyst may "poison" itself due to dense NO<sub>x</sub> coverage. At temperatures above HC light-off an increase in NO<sub>x</sub> concentration above a certain value can choke the HC conversion.

This thesis provides a deeper understanding of the processes occurring on a precious metal based Diesel catalyst. It provides a plausible mechanism for the reduction of NO<sub>x</sub> over a Pt/Al<sub>2</sub>O<sub>3</sub> catalyst which is able to explain the positive influence of oxygen on NO<sub>x</sub> conversion. The weakness of NO<sub>x</sub> conversion mechanisms presented by other researchers is that they do not explain plausibly why an increasing oxygen concentration has a promoting effect on the NO<sub>x</sub> reduction at temperatures below ~200°C. In this thesis oxygen is identified as the species

which "cleans" the catalyst's surface from HCs which are deposited on the surface and obstruct NO<sub>x</sub> conversion.

A catalyst is presented which shows a maximum NO<sub>x</sub> conversion of 80,5%. This catalyst is the first of a new generation of multifunctional Diesel catalysts and is bound to trigger intensive future research.

## Catalyst Data

Note: Due to proprietary reasons the following data is restricted to the essential informations necessary for this thesis. Further data on the samples can not be given.

Catalyst Specification	Washcoat	Washcoat Load [g/l]	Washcoat Surface Area [m <sup>2</sup> /g]	2 <sup>nd</sup> Washcoat Type or Additives	2 <sup>nd</sup> Washcoat Load	2 <sup>nd</sup> Washcoat Surface Area [m <sup>2</sup> /g]	Metal Type	Metal Load [g/ft <sup>3</sup> ]	Metal Dispersion [%]	2 <sup>nd</sup> Metal Type	2 <sup>nd</sup> Metal Load [g/ft <sup>3</sup> ]	2 <sup>nd</sup> Metal Dispersion [%]
PP 41 WCO	Al <sub>2</sub> O <sub>3</sub>	160	160	-	-	-	-	-	-	-	-	-
DEV5 WCO	Zeolite/ Al <sub>2</sub> O <sub>3</sub>	160	270	-	-	-	-	-	-	-	-	-
PP 41 38	Al <sub>2</sub> O <sub>3</sub>	158	160	-	-	-	Pt	38	11,4	-	-	-
4093 a,b,c,d	Al <sub>2</sub> O <sub>3</sub>	100	140	-	-	-	Pt	40	50 (targeted)	-	-	-
4094 a,b,c,d	Al <sub>2</sub> O <sub>3</sub>	100	140	-	-	-	Pt	40	10 (targeted)	-	-	-
4095 a,b,c,d	Al <sub>2</sub> O <sub>3</sub>	100	140	-	-	-	Pt	100	50 (targeted)	-	-	-
4096 a,b,c,d	Al <sub>2</sub> O <sub>3</sub>	100	140	-	-	-	Pt	100	10 (targeted)	-	-	-
4097 a,b,c,d	Al <sub>2</sub> O <sub>3</sub>	100	230	-	-	-	Pt	40	50 (targeted)	-	-	-
4098 a,b,c,d	Al <sub>2</sub> O <sub>3</sub>	100	230	-	-	-	Pt	40	10 (targeted)	-	-	-
4099 a,b,c,d	Al <sub>2</sub> O <sub>3</sub>	100	230	-	-	-	Pt	100	50 (targeted)	-	-	-
4100 a,b,c,d	Al <sub>2</sub> O <sub>3</sub>	100	230	-	-	-	Pt	100	10 (targeted)	-	-	-
4101 a,b,c,d	Al <sub>2</sub> O <sub>3</sub>	200	140	-	-	-	Pt	40	50 (targeted)	-	-	-
4102 a,b,c,d	Al <sub>2</sub> O <sub>3</sub>	200	140	-	-	-	Pt	40	10 (targeted)	-	-	-
4103 a,b,c,d	Al <sub>2</sub> O <sub>3</sub>	200	140	-	-	-	Pt	100	50 (targeted)	-	-	-
4104 a,b,c,d	Al <sub>2</sub> O <sub>3</sub>	200	140	-	-	-	Pt	100	10 (targeted)	-	-	-
4105 a,b,c,d	Al <sub>2</sub> O <sub>3</sub>	200	230	-	-	-	Pt	40	50 (targeted)	-	-	-
4106 a,b,c,d	Al <sub>2</sub> O <sub>3</sub>	200	230	-	-	-	Pt	40	10 (targeted)	-	-	-
4107 a,b,c,d	Al <sub>2</sub> O <sub>3</sub>	200	230	-	-	-	Pt	100	50 (targeted)	-	-	-
4108 a,b,c,d	Al <sub>2</sub> O <sub>3</sub>	200	230	-	-	-	Pt	100	10 (targeted)	-	-	-
PP41	Al <sub>2</sub> O <sub>3</sub>	158	160	-	-	-	Pt	44,3	16,9	-	-	-
PP325	Al <sub>2</sub> O <sub>3</sub>	152	320	SiO <sub>2</sub>	5 wt.-%	-	Pt	40	13,3	-	-	-
PP422	Al <sub>2</sub> O <sub>3</sub>	140	200	BaO	3 wt.-%	-	Pt	39,4	17,8	-	-	-
PP428	Al <sub>2</sub> O <sub>3</sub>	158	170	La <sub>2</sub> O <sub>3</sub>	3 wt.-%	-	Pt	38,1	15,7	-	-	-
RD704	Al <sub>2</sub> O <sub>3</sub>	179	160	-	-	-	Pt	76,3	28,1	-	-	-
PP500	Al <sub>2</sub> O <sub>3</sub>	143	>350	SiO <sub>2</sub>	20 wt.-%	-	Pt	40,8	15,2	-	-	-

Catalyst Specification	wash coat type	wash coat load [g/l]	wash coat surface area [m <sup>2</sup> /g]	2 <sup>nd</sup> wash coat type or Additives	2 <sup>nd</sup> wash coat load	2 <sup>nd</sup> wash coat surface area [m <sup>2</sup> /g]	metal type	metal load [g/ft <sup>3</sup> ]	metal dispersion [%]	2 <sup>nd</sup> metal type	2 <sup>nd</sup> metal load [g/ft <sup>3</sup> ]	2 <sup>nd</sup> metal dispersion [%]
PP452	Zeolite/ Al <sub>2</sub> O <sub>3</sub>	confid. <sup>1</sup>	confid.	CeO <sub>2</sub>	2 wt.-%	-	Pt	38,8	12,3	-	-	-
PP454	Zeolite/ Al <sub>2</sub> O <sub>3</sub>	confid.	confid.	CeO <sub>2</sub>	20 wt.-%	-	Pt	40,8	17,7	-	-	-
RD763	Zeolite/ Al <sub>2</sub> O <sub>3</sub>	confid.	confid.	MnO <sub>2</sub>	confid	-	Pt	44,9	42,1	-	-	-
DEV 1	Al <sub>2</sub> O <sub>3</sub>	160	160	-	-	-	Ir	38	n.a.	-	-	-
DEV 2	Al <sub>2</sub> O <sub>3</sub>	160	160	-	-	-	Ir	70	n.a.	-	-	-
DEV 3	Al <sub>2</sub> O <sub>3</sub>	160	160	-	-	-	Ir	38	n.a.	Pt	38	n.a.
DEV 4	Al <sub>2</sub> O <sub>3</sub>	160	160	-	-	-	Ir	70	n.a.	BaO	400	n.a.
JJ1	Zeolite	confid.	confid.	Al <sub>2</sub> O <sub>3</sub>	confid.	confid.	Pt	confid.	confid.	Rh	confid.	confid.

<sup>1</sup> confidential



## Curriculum Vitae

**Name:** Jörgen Jochheim  
**Date of Birth:** 21. July 1968  
**Place of Birth:** Göteborg (Sweden)  
**Citizenship:** Swedish  
**Personal Status:** Unmarried, no children

**High-School Education:**  
1974 - 1978 Grundschule Laatzen, Germany  
1978 - 1980 Orientierungsstufe Ludwig-Windhorst-Schule Hannover, Germany  
1980 - 1984 St. Ursula Gymnasium Hannover, Germany  
1984 - 1985 Participant in the American Scandinavian Students Exchange Program with a high-school in Kentucky, USA  
1985 - 1988 St. Ursula Gymnasium Hannover, Germany

**University Education:**  
1988 - 1991 Basic studies of chemistry at the University of Hannover, Germany  
February 1991 First degree: Candidate of Chemistry  
1991 - 1994 Main studies of chemistry  
Special fields: technical chemistry, environmental chemistry  
September 1994 Diplom - Chemiker  
September 1994 - Writing Ph. D. in technical chemistry  
January 1998

**Additional Academic Activities:**  
Since June 1995 Scientific assistant at the University of Hannover for the supervision of students practical work

**Business Experience:**  
Since April 1995 Employee of Johnson Matthey CSD

**Languages:**  
German (native language)  
English (fluent)  
Swedish (fluent)

**Additional Qualifications:**  
Kuratorium Weinheim: Seminars: Rhetoric, Creativity, Moderation  
University of Hannover: Seminars: Business Administration, Marketing, Project Management, Taking Management Responsibility, Patent Data Base Research  
  
Basic knowledge of the German environmental law  
  
User knowledge of MS-Office and Internet programs

**Extracurricular Activities:**  
Since 1989 Member of the Corps Hannovera students association  
1991 - 1992 Vice President  
1992 Speaker to the Press  
1990 - 1993 PR and Recruiting Coordinator  
  
1997 Foundation member of the regional Jungchemikerforum of the German Chemists Association (GDCh)

**Hobbies:** Jeet Kune Do, Volleyball, Internet

---

<sup>1</sup> Korte, F.:

Lehrbuch der Ökologischen Chemie, Thieme, (1992)

<sup>2</sup> Cutting Vehicle Pollution Today & Tomorrow, Johnson Matthey, Plc. Brochure (1997)

<sup>3</sup> Hawker, P.N.:

Diesel Emission Control Technology: System Containing Platinum Catalyst and Filter Unit Removes Particulate from Diesel Exhaust

Platinum Metals Reviews, **39**, 1, (1995) 2-8

<sup>4</sup> Adams, K. M.; Cavataio, J. V.; Hammerle, R. H.:

Lean NO<sub>x</sub> Catalysis for Diesel Passenger Cars: Investigating Effects of Sulphur Dioxide and Space Velocity

Appl. Cat. B: Env., **10**, (1996) 157-181

<sup>5</sup> Jochheim, J.; Hesse, D.; Duesterdiek, T.; Engeler, W.; Neyer, D.; Warren, J. P.; Wilkins, A. J. J.;

Twigg, M.V.:

A Study of the Catalytic Reduction of NO<sub>x</sub> in Diesel Exhaust

SAE, **962042**, (1996) 11-17

<sup>6</sup> Bartsch, C.:

Ohne Diesel kein Drei-Liter-Auto

Frankfurter Allgemeine Zeitung, October 7 (1997) T3

<sup>7</sup> Beckmann, R.; Engeler, W.; Mueller, E.; Engler, B.H.; Leyrer, J.; Lox, E.S.; Ostgathe, K.:

A New Generation of Diesel Oxidation Catalysts

SAE, **922330**, (1992)

<sup>8</sup> Wyatt, M.; Manning, W.A.; Roth, S.A.; D'Aniello, M.J.; Andersson, E.S.; Fredholm, S.C.G.:

The Design of Flow-Through Diesel Oxidation Catalysts

SAE, **930130**, (1993)

<sup>9</sup> Hubbard, C.P.; Otto, K.; Gandhi, H.S.; Ng, K.Y.S.:

The Influence of Sulphur Dioxide on Propane Oxidation Activity over Supported Platinum and Palladium

Catalysis Letters, **30**, (1995) 41-51

<sup>10</sup> Stamatelos, A.M.:

On-line Regeneration Control for a Diesel Particulate Trap System

Automatica, **30**, 3, (1994) 513-520

<sup>11</sup> Yuan, S.; Mériaudeau, P.; Perrichon, V.:

Catalytic Combustion of Diesel Soot Particles on Copper Catalysts Supported on TiO<sub>2</sub>. Effect of Potassium Promoter on the Activity

Applied Catalysis B: Environmental, **3**, (1994) 319-333

<sup>12</sup> Grohe, H.:

Otto- und Dieselmotoren; 11<sup>th</sup> Edition, Vogel Buchverlag (1995)

<sup>13</sup> Neuendorf, S.:

Experimentelle Untersuchungen zur Minderung der Partikel- und Stick-oxidemissionen aus PKW-Dieselmotoren mit Oxidationskatalysatoren und selektiver katalytischer Reduktion

Ph. D. Thesis, Technische Universität Clausthal, (1994)

<sup>14</sup> Duesterdiek, T.:

Katalytische Stickoxidminderung im Abgas von Dieselmotoren

Ph. D. Thesis, Universität Hannover, (1996)

<sup>15</sup> Atkins, P. W.:

Physical Chemistry, 4<sup>th</sup> Edition, Oxford University Press, 1990

<sup>16</sup> Ullmann's Encyclopaedia of Industrial Chemistry:

Automobile Exhaust Control

---

Volume A3; 5th Edition, VCH Weinheim (1991) 189-200

<sup>17</sup> Levendis, Y.A.; Pavlatos, I.; Abrams, R.F.:

Control of Diesel Soot, Hydrocarbon and NO<sub>x</sub> Emissions with a Particulate Trap and EGR  
SAE, **940460**, (1994)

<sup>18</sup> Riedel, E.:

Anorganische Chemie

2nd Ed.; deGruyter, Berlin, New York; (1990) 441

<sup>19</sup> Majewski, W.A.; Ambs, J.L.; Bickel, K.:

Nitrogen Oxides Reactions in Diesel Oxidation Catalyst  
SAE, **950374**, (1995)

<sup>20</sup> Ullmann's Encyclopaedia of Industrial Chemistry:

Automobile Exhaust Control

Volume A17; 5th Edition, VCH Weinheim (1991) 300-339

<sup>21</sup> Muramatsu, G.; Abe, A.; Furuyama, M.; Yoshida, K.:

Catalytic Reduction of NO<sub>x</sub> in Diesel Exhaust

SAE, **930135**, (1993)

<sup>22</sup> Philips, P.:

Johnson Matthey CSD, Verbal Communication

<sup>23</sup> Düsterdiek, T.:

Volkswagen AG, Verbal Communication

<sup>24</sup> Zelenka, P.; Cartellieri, W.; Herzog, P.:

Worldwide Diesel Emission Standards, Current Experiences and Future Needs

Appl. Cat. B: Env., **10**, (1996) 3-28

<sup>25</sup> Bond, G. C.; Burch, R.:

Strong Metal Support Interactions

Catalysis (London), **6**, (1983) 27-60

<sup>26</sup> Stiles, A.B.; Klein, M.T.; Gauthier, P.; Schwarz, S.; Wang, J.:

Selective Catalytic Reduction of NO<sub>x</sub> in the Presence of Oxygen

Ind. Eng. Chem. Res., **33**, (1994) 2259-2264

<sup>27</sup> Cho, S.M.:

Properly Apply Selective Catalytic Reduction for NO<sub>x</sub> Removal

Chem. Eng. Prog., **90**, 1, (1994) 39-45

<sup>28</sup> Wood, S.C.:

Select the Right NO<sub>x</sub> Control Technology

Chem. Eng. Prog., **90**, 1, (1994) 32-38

<sup>29</sup> Hüthwohl, G.; Li, Q.; Lepperhoff, G.:

Untersuchung der NO<sub>x</sub>-Reduzierung im Abgas von Dieselmotoren durch SCR-Katalysatoren

MTZ, **54**, 6, (1993) 310-315

<sup>30</sup> Weisweiler, W., University of Karlsruhe

Lecture on De-NO<sub>x</sub>-ing of Diesel Exhaust at the University of Hannover

June 23, 1995

<sup>31</sup> Held, W.; König, A.; Richter, T.; Puppe, L.:

Catalytic NO<sub>x</sub> Reduction in Net Oxidising Exhaust Gas

SAE, **900496**, (1990)

<sup>32</sup> Truex, T.J.; Searles, R.A.; Sun, D.C.:

Catalysts for Nitrogen Oxides Control under Lean-Burn Conditions

Platinum Metals Review, **36**, 1, (1992) 2-11

<sup>33</sup> Shelef, M.:

Selective Catalytic Reduction of NO<sub>x</sub> with N-Free Reductants

Chem. Rev., **95**, (1995) 209-225

<sup>34</sup> Amiridis, M. D.; Zhang, T.; Farrauto, R. J.:

Selective Catalytic Reduction of Nitric Oxide by Hydrocarbons

Appl. Cat. B: Env., **10**, (1996) 203 - 227

<sup>35</sup> Reinoldsmann, P.; Gregor, K.H.:

---

Naßchemische Verfahren zur Entfernung von Stickoxiden aus Rauchgasen und Abgasen  
WLB Wasser, Luft und Boden, **5**, (1992) 72-

<sup>36</sup> Monatanaro, L.; Bachirri, A.:

Influence of Some Pollutants on the Durability of Cordierite Filters for Diesel Cars  
Ceramics International, **20**, (1994) 169-174

<sup>37</sup> Negro, A.; Montanaro, L.; Demaestri, P.P.; Giachello, A.; Bachiorri, A.:

Interaction between some Oxides and Cordierite  
J. Europ. Ceram. Soc., **12**, (1993) 493-498

<sup>38</sup> Chandran, R.G.; Patil, K.C.:

Combustion Synthesis, Characterisation, Sintering and Microstructure of Cordierite  
Br. Ceram. Trans., **92**, 6, (1993) 239-245

<sup>39</sup> Burch, R.; Millington, P.J.:

Role of Propene in the Selective Reduction of Nitrogen Monoxide in Copper-Exchanged Zeolites  
Applied Catalysis B: Environmental, **2**, (1993) 101-116

<sup>40</sup> Ansell, G.P.; Diwell, A.F.; Golunski, S.E.; Hayes, J.W.; Rajaram, R.R.; Truex, T.J.; Walker, A.P.:

Mechanism of the Lean NO<sub>x</sub> reaction over Cu/ZSM-5  
Applied Catalysis B: Environmental, **2**, (1993) 81-100

<sup>41</sup> Chajar, Z.; Primet, M.; Praliaud, H.; Chevrier, M.; Gauthier, C.; Mathis, F.:

Influence of the Preparation Method on the selective Reduction of Nitric Oxide over Cu-ZSM/5.  
Nature of active sites

Applied Catalysis B: Environmental, **4**, (1994) 199-211

<sup>42</sup> Yogo, K.; Ihara, M.; Terasaki, I.; Kikuchi, E.:

Gallium Ion-Exchanged Zeolite as a Selective Catalyst for Reduction of Nitric Oxide with  
Hydrocarbons under Oxygen-Rich Conditions

Catalysis Letters, **17**, (1993) 303-308

<sup>43</sup> Adelman, B.J.; Lei, G.-D.; Sachtler, W.M.H.:

Co-Adsorption of NO and NO<sub>2</sub> in Zeolitic De-NO<sub>x</sub> Catalysts  
Catalysis Letters, **28**, (1994) 119-130

<sup>44</sup> Li, Y.; Armor, J.N.:

Simultaneous, Catalytic Removal of Nitric Oxide and Nitrous Oxide  
Applied Catalysis B: Environmental, **3**, (1993) 55-60

<sup>45</sup> Bennett, C.J.; Bennett, P.S.; Golunski, S.E.; Hayes, J.W.; Walker, A.P.:

Selective Reduction of Nitrogen Oxides under Oxidising Exhaust-Gas Conditions  
Applied Catalysis A: General, **86**, (1992) L1-L6

<sup>46</sup> Grünert, W.; Hayes, N.W.; Joyner, R.W.; Shpiro, E.S.; Siddiqui, M.R.H.; Baeva, G.N.:

Structure, Chemistry, and Activity of Cu/ZSM-5 Catalysts for the Selective Reduction of NO<sub>x</sub> in the  
Presence of Oxygen

Journal of Physical Chemistry, **98**, (1994) 10832-10846

<sup>47</sup> Kripylo, P.; Wendlandt, K.-P.; Vogt, F.:

Heterogene Katalyse in der chemischen Technik  
1st Ed., Deutscher Verlag für Grundstoffindustrie, Leipzig, Stuttgart, (1993)

<sup>48</sup> Iwamoto, M.; Yahiro, H.; Yu-u, Y.; Shundo, S.; Mizuno, N.

Shokubai (Catalyst), **32**, (1990), 430

*Article is in Japanese cited in reference 67*

<sup>49</sup> Cho, B.K.:

Nitric Oxide Reduction by Hydrocarbons over Cu/ZSM-5 Monolith Catalyst under Lean Conditions:  
Steady-State Kinetics

Journal of Catalysis, **142**, (1993) 418-429

<sup>50</sup> Radtke, F.; Koepfel, R.A.; Baiker, A.:

Hydrogen Cyanide Formation in Selective Catalytic Reduction of Nitrogen oxides over Cu/ZSM-5  
Applied Catalysis A: General, **107**, (1994) L125-L132

<sup>51</sup> Spoto, G.; Bordiga, S.; Scarano, D.; Zecchina, A.:

Well Defined Cu<sup>I</sup>(NO), Cu<sup>I</sup>(NO)<sub>2</sub> and Cu<sup>II</sup>(NO)X (X=O<sup>-</sup> and/or NO<sub>2</sub><sup>-</sup>) Complexes in Cu<sup>I</sup>/ZSM-5  
Prepared by Interaction of H<sub>2</sub>/ZSM-5 with Gaseous CuCl  
Catalysis Letters, **13**, (1992) 39-44

- 
- <sup>52</sup> Moretti, G.  
Catalysis Letters, **23**, (1994) 135
- <sup>53</sup> Sepúlveda-Escribano, A.; Marquez-Alvarez, C.; Rodriguez-Ramos, I.; Guerrero-Ruiz, A.; Fierro, J.L.:  
Catalysis Today, **17**, (1993) 167
- <sup>54</sup> Miyamoto, A.; Himei, H.; Oka, Y.; Maruya, E.; Katagiri, M.; Vetrivel, R.; Kubo, M.:  
Computer-Aided Design of Active Catalysts for the Removal of Nitric Oxide  
Catalysis Today, **22**, (1994) 87-96
- <sup>55</sup> Grinsted, R.A.; Jen, H.-W.; Montreuil, C.N.; Rokosz, M.J.; Shelef, M.:  
The Relation between Deactivation of Cu/ZSM-5 in the Selective Reduction of NO and Dealumination of the Zeolite  
Zeolites, **13**, Nov/Dec, (1993) 602-606
- <sup>56</sup> Ansell, A.P.; Golunski, S.E.; Hayes, J.W.; Walker, A.P.; Burch, R.; Millington, P.J.:  
The mechanism of the lean NO<sub>x</sub> reaction over Pt-based catalysts  
Stud. Surf. Sci. Cat., **96** (1995) 577-590
- <sup>57</sup> Engler, B.H.; Leyrer, J.; Lox, E.S.; Ostgathe, K.:  
Catalytic Reduction of NO<sub>x</sub> with Hydrocarbons Under Lean Diesel Exhaust Conditions  
SAE, **930735**, (1993)
- <sup>58</sup> Kapteijn, F.; Marbán, G.; Rodriguez-Mirasol, J.; Moulijn, J. A.:  
Kinetic Analysis of the Decomposition of Nitrous Oxide over ZSM-5 Catalysts  
Journal of Catalysis, **167**, (1997) 256-265
- <sup>59</sup> Iwamoto, M.; Yahiro, H.; Shin, H.K.; Watanabe, M.; Guo, J.; Konno, M.; Chikahisa, T.; Murayama, T.:  
Performance and Durability of Pt-MFI Zeolite Catalyst for Selective Reduction of Nitrogen Monoxide in Actual Diesel Engine Exhaust  
Applied Catalysis B: Environmental, **5**, (1994) L1-L5
- <sup>60</sup> Hirabayashi, H.; Yahiro, H.; Mizuno, N.; Iwamoto, M.:  
High Catalytic Activity of Platinum/ZSM-5 Zeolite below 500K in Water Vapour for Reduction of Nitrogen Monoxide  
Chemistry Letters, (1992) 2235-2236
- <sup>61</sup> Dyer, A.:  
An Introduction to Zeolite Molecular Sieves  
J. Wiley & Sons, New York, (1988)
- <sup>62</sup> Cowan, A.D.; Dümpelmann, R.; Cant, N.W.:  
The Rate-Determining Step in the Selective Reduction of Nitric Oxide by Methane over a Co/ZSM-5 Catalyst in the Presence of Oxygen  
J. Cat., **151**, (1995) 356-363
- <sup>63</sup> Yogo, K.; Ihara, M.; Terasaki, I.; Kikuchi, E.:  
Selective Reduction of Nitrogen Monoxide with Methane or Ethane on Gallium Ion-Exchanged ZSM-5 in Oxygen-rich Atmosphere  
Chemistry Letters, (1993) 229-232
- <sup>64</sup> Greenwood, N.N.; Earnshaw, A.:  
Chemie der Elemente  
1<sup>st</sup> Edition, VCH, Weinheim, (1990)
- <sup>65</sup> Desai, R.; Hussain, M.; Ruthven, D.M.:  
Adsorption of Water Vapour on Activated Alumina. I - Equilibrium Behaviour  
Can. J. Chem. Eng., **70**, 8, (1992) 699-706
- <sup>66</sup> Kintaichi, Y.; Hamada, H.; Tabata, M.; Sasaki, M.; Ito, T.:  
Selective Reduction of Nitrogen Oxides with Hydrocarbons over Solid Acid Catalysts in Oxygen-Rich Atmospheres  
Catalysis Letters, **6**, (1990) 239-244
- <sup>67</sup> Sasaki, M.; Hamada, H.; Kintaichi, Y.; Ito, T.:  
Role of Oxygen in Selective Reduction of NO by Propane over Zeolite and Alumina-Based Catalysts  
Catalysis Letters, **15**, (1992) 297-304
- <sup>68</sup> Subramanian, S.; Kudla, R.J.; Chun, W.; Chattha, S.:

---

Removal of Nitric Oxide by Its Reduction with Hydrocarbons over Alumina under Lean Conditions  
Ind. Eng. Chem. Res., **32**, (1993) 1805-1810

<sup>69</sup> Tsuchida, H.; Tabata, M.; Miyamoto, K.; Yoshinari, T.; Yamazaki, H.; Hamada, H.; Kintaichi, Y.; Sasaki, M.; Ito, T.; Nakatsuji, T.; Yoshimoto, M.:  
Catalytic Performance of Alumina for NO<sub>x</sub> Control in Diesel Exhaust  
SAE, **940242**, (1994)

<sup>70</sup> Hamada, H.:  
Selective Reduction of NO by Hydrocarbons over Metal Oxide Catalysts  
Cat. Tdy., **22**, (1994) 21-40

<sup>71</sup> Hamada, H.; Kintaichi, Y.; Tabata, M.; Sasaki, M.; Ito, T.:  
Sulphate-Promoted Metal Oxide Catalysts for the Selective Reduction of NO by Propane in Oxygen-Rich Atmosphere  
Chemistry Letters, (1991) 2179-2182

<sup>72</sup> Masuda, K.; Sano, T.; Mizukami, F.; Takezaki, T.; Kuno, K.:  
Effects of Alumina Preparation Solvents on the Thermostability and Oxidation Activity of Alumina-Supported Palladium and Platinum Catalysts  
Applied Catalysis B: Environmental, **4**, (1994) 187-198

<sup>73</sup> Green, T. E.; Hinshelwood, C. N.:  
J. Chem. Soc., **129**, (1926) 1709

<sup>74</sup> Nellist, P. D.; Pennycook, S. J.:  
Direct Imaging of the Atomic Configuration of Ultradispersed Catalysts  
Science, **274**, 18 October (1996) 413-415

<sup>75</sup> Zhang, G.; Yamaguchi, T.; Kawakami, H.; Suzuki, T.:  
Selective Reduction of Nitric Oxide over Platinum Catalysts in the Presence of Sulphur Dioxide and Excess Oxygen  
Applied Catalysis B: Environmental, **1**, (1992) L15-L20

<sup>76</sup> Burch, R.; Millington, P.J.; Walker, A.P.:  
Mechanism of the selective reduction of NO on Pt-based catalysts in the presence of excess oxygen  
Applied Catalysis B : Environmental **4**, (1994) 65-94

<sup>77</sup> Löf, P.; Kasemo, B.; Andersson, S.; Frestad, A.:  
Influence of Ceria on the Interaction of CO and NO with Highly Dispersed Pt and Rh  
Journal of Catalysis, **130**, (1991) 181-191

<sup>78</sup> Obuchi, A.; Ohi, A.; Nakamura, M.; Ogata, A.; Mizuno, K.; Ohuchi, H.:  
Performance of Platinum-Group Metal catalysts for the Selective Reduction of Nitrogen Oxides by Hydrocarbons  
Applied Catalysis B: Environmental, **2**, (1993) 71-80

<sup>79</sup> Xue, E.; Seshan, K.; Ross, J.R.H.:  
Roles of supports, Pt loading and Pt dispersion in the oxidation of NO to NO<sub>2</sub> and of SO<sub>2</sub> to SO<sub>3</sub>  
Applied Catalysis B: Environmental, **11**, (1996) 65 - 79

<sup>80</sup> Vaarkamp, M.; Miller, J. T.; Modica, F. S.; Koningsberger, D.C. :  
On the Relation between Particle Morphology, Structure of the Metal-Support Interface, and Catalytic Properties of Pt/Al<sub>2</sub>O<sub>3</sub>  
J. Cat. **163** (1996) 294-305

<sup>81</sup> Burch, R.; Watling, T. C.:  
Kinetics and Mechanism of the Reduction of NO by C<sub>3</sub>H<sub>8</sub> over Pt/Al<sub>2</sub>O<sub>3</sub> under Lean-Burn Conditions  
J. Cat., **169**, (1997) 45 - 54

<sup>82</sup> Burch, R.; Watling, T.C.:  
Adsorbate-Assisted NO Decomposition in NO Reduction by C<sub>3</sub>H<sub>6</sub> over Pt/Al<sub>2</sub>O<sub>3</sub> Catalysts under Lean-Burn Conditions  
Cat. Let., **37**, (1996) 51-55

<sup>83</sup> Burch, R.; Watling, T.C.:  
The Difference Between Alkanes and Alkenes in the Reduction of NO by Hydrocarbons over Pt Catalysts under Lean-Burn Conditions  
Cat. Let., **43**, (1997) 19-23

<sup>84</sup> van Tillaart, J. A. A.; Leyrer, J.; Eckhoff, S.; Lox, E. S.:

---

Effect of Support Oxide and Noble Metal Precursor on the Activity of Automotive Diesel Catalysts  
Appl. Cat. B: Env., **10**, (1996) 53-68

<sup>85</sup> Ansell, G. P.; Bennett, P. S.; Cox, J. P.; Frost, J. C.; Gray, P. G.; Jones, A.-M.; Rajaram, R. R.; Walker, A. P.:

The Development of a Model Capable of Predicting Diesel Lean NO<sub>x</sub> Catalyst Performance Under Transient Conditions

Appl. Cat. B: Env., **10** (1996)

<sup>86</sup> Bourges, P.; Lunati, S.; Mabilon, G.:

NO<sub>2</sub> and NO<sub>2</sub> Formation During NO Reduction on Precious Metal Catalysts

Fourth Int. Congr. on Cat. and Automotive Pollution Control (Capoc)

Brussels, **09**, April 1997

<sup>87</sup> Eckhoff, S.; Hesse, D.; van den Tillaart, J. A. A.; Leyrer, J.; Lox, E. S.:

Mechanistic Investigation on the Selective Reduction of NO with Propene in the Presence of Oxygen over Supported Alumina

Fourth Int. Congr. on Cat. and Automotive Pollution Control (Capoc)

Brussels, **10**, April 1997

<sup>88</sup> Burch, R.; Watling, T. C.:

Kinetics of the Reduction of NO by C<sub>3</sub>H<sub>6</sub> and C<sub>3</sub>H<sub>8</sub> Over Pt Based Catalysts Under Lean-Burn Conditions

Fourth Int. Congr. on Cat. and Automotive Pollution Control (Capoc)

Brussels, **08**, April 1997

<sup>89</sup> Trautmann, S.:

Infrarotspektroskopische Untersuchungen zur Wechselwirkung kleiner Moleküle (CO, NO) an Edelmetallen (Pt, Pd, Rh)/Träger (SiO<sub>2</sub>, Al<sub>2</sub>O<sub>3</sub>, TiO<sub>2</sub>) - Katalysatoren

Ph. D. Thesis, Universität Bochum, (1994)

<sup>90</sup> Wahl, T.; Jacob, E.; Weisweiler, W.:

NO<sub>x</sub> Verminderung bei Dieselmotoren

Motortechnische Zeitschrift MTZ, **57**, 9, (1996) 506-514

<sup>91</sup> Burch, R.; Hayes, M. J.:

C-H Bond Activation in Hydrocarbon Oxidation on Solid Catalysts

J. Mol. Cat. A: Chem., **100**, (1995) 13-33

<sup>92</sup> Somorjai, G.A.:

Chemistry in Two Dimensions: Surfaces

Cornell University Press, 1981

<sup>93</sup> Cooper, B.J.; Roth, S.A.:

Flow-Through Catalysts for Diesel Engine Emissions Control:

Platinum Coated Monoliths Reduce Particulates

Platinum Metals Review, **35**, 4, (1991) 178-187

<sup>94</sup> Beretta, A.; Tronconi, E.; Alemany, L.J.; Svachule, J.; Forzatti, P.:

Effect of Morphology of Honeycomb SCR Catalysts on the Reduction of NO<sub>x</sub> and the Oxidation of SO<sub>2</sub>

Stud. Surf. Sci. Cat., **82**, (1994) 869-876

<sup>95</sup> Cooper, B.J.:

Challenges in Emission Control Catalysis for the Next Decade

Platinum Metals Review, **38**, (1), (1994) 2-10

<sup>96</sup> Pinkas, P.; Snita, D.; Kubíček, M.; Marek, M.:

Catalytic Honeycomb Reactors with Electrical Heating

Chem. Eng. Sci., **49**, 24B, (1994) 5347-5358

<sup>97</sup> Miyadera, T.:

Alumina-Supported Silver Catalysts for the Selective Reduction of NO with Propene and Oxygen-Containing Compounds

Applied Catalysis B: Environmental, **2**, (1993) 199-205

<sup>98</sup> Miyadera, T.; Yoshida, K.:

Alumina-Supported Catalysts for the Selective Reduction of Nitric Oxide by Propene

Chemistry Letters, (1993) 1483-1486

- 
- <sup>99</sup> Radtke, F.; Koepfel, R. A.; Minardi, E. G.; Baiker, A.:  
Catalytic Reduction of Nitrogen Oxides by Olefins in the Presence of Oxygen over Copper/Alumina: Influence of Copper Loading and Formation of Byproducts  
Journal of Catalysis, **167**, (1997) 127-141
- <sup>100</sup> Ukisu, Y.; Miyadera, T.; Abe, A.; Yoshida, K.:  
Infrared Study of Catalytic Reduction of Lean NO<sub>x</sub> with Alcohols Over Alumina-Supported Silver Catalyst  
Catalysis Letters, **39**, (1996) 265-267
- <sup>101</sup> Teraoka, Y.; Harada, T.; Iwasaki, T.; Ikeda, T.; Kagawa, S.:  
Selective Reduction of NO with Hydrocarbons over SnO<sub>2</sub> Catalysts  
Chemistry Letters, (1993) 773-776
- <sup>102</sup> Skoglundh, M.; Löwendahl, L.; Jansson, K.; Dahl, L.; Nygren, M.:  
Characterization and catalytic properties of perovskites with nominal compositions La(1-x)Sr(x)Al(1-2y)Cu(y)Ru(y)O<sub>3</sub>  
Appl. Cat. B: Env., **3**, (1994) 259-274
- <sup>103</sup> Congress of the Society of Automotive Engineers (SAE)  
Detroit, USA, 2702-020395  
Platinum Metals Review, **39**, (2), (1995) 73-74
- <sup>104</sup> Fridell, E.; Skoglundh, M.; Johansson, S.; Westerberg, B.; Törnroona, A.; Smedler, G.:  
Investigations of NO<sub>x</sub> Storage Catalysts  
Fourth Int. Congr. on Cat. and Automotive Pollution Control (Capoc)  
Brussels, **O 22**, April 1997
- <sup>105</sup> Haas, L.A.; Anderson, C.F.; Khalafalla, S.E.:  
Decomposition of Nitric Oxide in a Silent Discharge  
Ind. Eng. Chem. Process. Des. Dev., **18**, 1, (1979) 143-147
- <sup>106</sup> Tanagawa, T.; Inomata, T.; Takahashi, K.; Jinno, H.:  
Removal of NO<sub>x</sub> from Burned Gas by Electric Discharge  
Combust. Sci. and Tech., **97**, (1994) 237-242
- <sup>107</sup> Kubo, M.; Takahashi, K.; Inomata, T.; Moriwaki, T.; Okazaki, S.:  
Application of Silent Electric Discharge to Removal of NO<sub>x</sub>  
8th Int. Symp. Plasma Chem., **2**, (1987) 828-
- <sup>108</sup> Day, J. P.:  
Substrate Contributions to Automotive Catalytic Converter Performance: The Role of Channel Shape on Catalyst Efficiency  
Fourth Int. Congr. on Cat. and Automotive Pollution Control (Capoc)  
Brussels, **O 19**, April 1997
- <sup>109</sup> Chang, Y.; McCarty, J. G.:  
Isotopic Study of NO<sub>x</sub> Decomposition over Cu- or Co-Exchanged ZSM-5 Zeolite Catalysts  
Journal of Catalysis, **165**, (1997) 1-11
- <sup>110</sup> Biloen, P.; Helle, J. N.; van den Berg, F. G. A.; Sachtler, W. M. H.:  
J. Catalysis, **81**, (1983) 450
- <sup>111</sup> Frost, J. C.; Lafyatis, D. S.; Rajaram, R. R.; Walker, A. P.:  
The Use of Isotope Transient Kinetics Within Commercial Catalyst Development  
Fourth Int. Congr. on Cat. and Automotive Pollution Control (Capoc)  
Brussels, **O 14**, April 1997
- <sup>112</sup> Radtke, F.; Koepfel, R.; Baiker, A.:  
Harmful By-Products in Selective Catalytic Reduction of NO<sub>x</sub> by Olefins Over Alumina  
J. Cat., **28**, (1994) 131-142
- <sup>113</sup> Boudart, M.; Djéga-Mariadassou, G.:  
Kinetics of Heterogeneous Catalytic Reactions  
Princeton University Press, (1984) 26
- <sup>114</sup> Naito, S.; Tanimoto, M.:  
Chem. Lett. (1993) 1935
- <sup>115</sup> Tanaka, T.; Okuhara, T.; Misono, M.:  
Appl. Cat. B: Env., **4** (1994) L1



---

<sup>116</sup> Obuchi, A.; Ogata, A.; Takahashi, H.; Oi, J.; Bamweda, G. R.; Mizuno, K.:  
Cat. Td. **29** (1996) 103

<sup>117</sup> Bamwenda, G. R.; Obuchi, A.; Ogata, A.; Mizuno, K.:  
Chem. Lett. (1994) 2109